In special liquid-liquid, chemically stratified, micro-fluidic, lab-on-a-chip (LOC) systems, used in biological applications, rare bubble evolutions occur at temperatures far below the boiling point of the analyte solution, leading to erroneous analysis. The current, mainly experimental work, aims in providing a physical understanding to the above, and in closing, proposing solutions for the elimination/control of the same- for the overall betterment of such systems.

UNDERSTANDING BUBBLE DYNAMICS IN A CHEMICALLY STRATIFIED, BI-LIQUID, MICRO-DROPLET SYSTEM

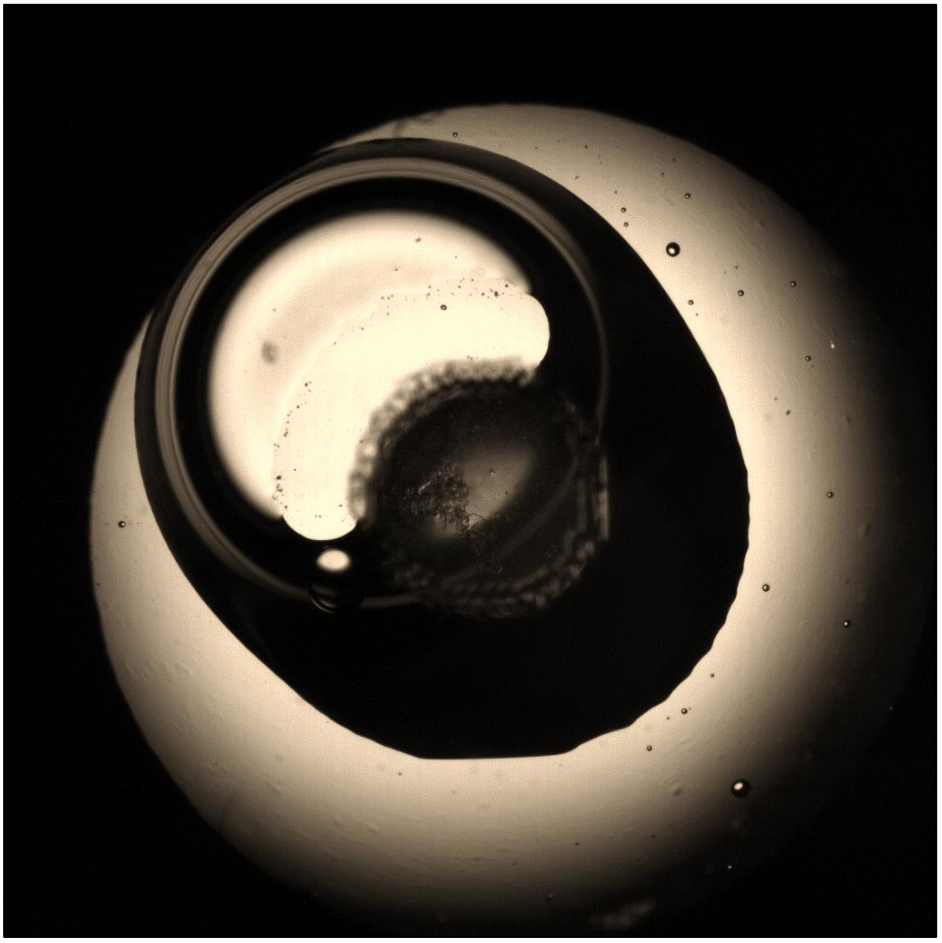

Neeti Phatak

UNDERSTANDING BUBBLE DYNAMICS IN A CHEMICALLY STRATIFIED, BI-LIQUID, MICRO-DROPLET SYSTEM

DISSERTATION

zur Erlangung des akademischen Grades
Dr. rer. nat.

eingereicht an der
Mathematisch-Naturwissenschaftlich-Technischen Fakultät
der Universität Augsburg

von

Neeti Phatak

Lehrstuhl für Experimentalphysik I
Institut für Physik
Universität Augsburg, Deutschland

Advalytix AG - part of Beckman Coulter Biomedical GmbH
München, Deutschland

May 2016

Erster Gutachter:	Prof.Dr.Achim Wixforth
Zweiter Gutachter:	Prof. Dr. Wolfgang Bruetting

Tag der Einreichnung :	30.05.2016
Tag der mündlichen Prüfung :	15.07.2016

ABSTRACT

In special liquid-liquid, chemically stratified, micro-fluidic, lab-on-a-chip (LOC) systems, used in biological applications, rare bubble evolutions occur at temperatures far below the boiling point of the analyte solution, leading to erroneous analysis. The current, mainly experimental work, aims in providing a physical understanding to the above, and in closing, proposing solutions for the elimination/control of the same- for the overall betterment of such systems.

Characterization of the amplification platform via various contact angle studies revealed freshly prepared surfaces to be the most homogeneous and reliable to work with, yielding consistent static contact angle values and lowest observed dynamic contact angle hysteresis (~30°). However, microscopic investigations revealed, chiefly on the hydrophobic regions of the chemically stratified surfaces (amplification platform), the presence of rare surface inhomogeneities in the form of crater like structures (diameter ~2-8 µm, depth ~2 nm, peak height~10-200 nm), possibly serving as potential sources of bubble formation(s). The above was supported by HD video recording nucleation studies, where laser engraved and lithographically etched micro cavities (with aspect ratios 1:1 and 4:5) were seen entrapping gas, in analogy with heterogeneous and crevice model of bubble nucleation. Further, nucleation sites were found to be more active when under water than oil- they being most active when in the vicinity of the water-oil interface. Particle Image Velocimetry (PIV) experiments as well showed greater flows/velocities at the water-oil interface, especially when in the locale of a bubble. Lower bubble growth rates were observed in oil (~2 µm/sec) than in water (~7 µm/sec), the rates almost exponentially increasing as the bubble approaches the liquid-liquid interface (~ > 70 µm/sec), thereby making the presence of this additional interface crucial to the system under consideration, in contrast to a single- liquid system. From mathematical calculations based on Henry's law and HD video recording bubble shrinkage experiments, the chief content of the bubbles came up as water-vapour; water being converted into its vapour rapidly at the liquid-liquid interface, feeding the bubble as it approaches this interfaces via diffusion (Marangoni/Thermo-capillary convection).

A well-calibrated heating platform, with optimum ramp rates (3°C/sec) and fresh, clean, highly degassed, carefully pipetted and loaded bi-liquid system was found to play no major in the evolution of bubbles howsoever.

Bubble nucleation was successfully supressed by increasing the pressure (minimum ~70 kPa) of the system as per pressure chamber experiments. Growth rates were to some extent seen lowered by the addition of surfactants (Tween 20) to the inner water mix- though surfactants proved not be highly successful in hindering the bubble growths. For the bubbles that escaped the nucleation and growth checks, merging of the adjacent droplets due to bubble bursts was attempted to be controlled by employing physical confinements (chambered PS/PDMS frames) and virtual confinements in the form of superhydrophobic rings and regions outside the reaction sites- the latter especially proving not be highly successful in achieving so- calling hence for more sophisticated techniques for the generation of superhydrophobic surfaces.

Keywords: water-oil interface, hydrophilic-hydrophobic interface, lab-on-a-chip, virtual reaction chamber, video recording, contact angle, bubble nucleation, bubble growth, surfactants, pressure chamber, superhydrophobicity.

ACKNOWLEDGMENTS

First and foremost, I would like to sincerely acknowledge my chief mentor, Prof. Dr. Achim Wixforth, for the immense faith that he had in me and for choosing me as a trustworthy candidate for the execution of this doctoral program. I just cannot thank him enough for the enormous support and invaluable guidance that he offered at all stages of this work. Time to time discussions with him not only facilitated me greatly in extending my knowledge in the field of microfluidics, but as well, groomed me significantly as a researcher. I feel highly indebted to him for providing such a fantabulous lab environment and a highly supportive team at the University, for all his patience and understanding, and most importantly- for never giving up on me! It was his confidence, that always kept me going and without which this dissertation would have never been possible.

Secondly, I would like to earnestly thank the Marie Curie Multiflow network for providing such an excellent organization and financial aid during the course of this work. The outstanding conferences and seminars arranged by the network not only provided great platforms for sharing and discussing research at an international level, but as well gave immense opportunities to visit places I had never been to and meet amazing people I never would have gotten the chance to meet otherwise.

My heartfelt acknowledgments to my industrial supervisors, Dr. Zeno Guttenberg and Dr. Heiko Habermueller at Beckman Coulter, Munich, for their priceless backing and constant support at all stages of this work. I just cannot thank them enough for all their time and efforts, for their irreplaceable feedback and suggestions, their positive criticism- immensely helping me throughout towards the betterment of my work. Particular thanks to Dr. Guttenberg for all his help regarding the financial aspects of the program, and for his active participation and support during various conferences organized by the network. A very sincere gratitude to Dr. Heiko Habermueller for his endless forbearance and his excellent

mentoring, that enabled an amateur like me in the field of microfluidic research, be able to finally pen down this thesis.

I feel deeply thankful to all my colleagues at Beckman Coulter, especially Dr. Reinhard Bittner and Dr. Maciek Domaniski for their manifold support during the execution of this work. Thank you Oezden and Ursula for all the help in the clean room, Mrs. Claudia Thanner for all your project regarding assistance, Dr. Marianna Alunni for making me understand the biological aspects of the study, and Claudia, Karina and Petra for all your friendliness and care. It all meant a lot to me!

My sincere thanks to the Experimental I Physics team at the University of Augsburg, primarily Dr. Thomas Franke and Andreas Spoerhasse for all their valuable suggestions and feedback during the course of this work. Thank you Alex, Lothar Schmidt and Sussane Bauermueller for all your cooperation and timely guidance. I feel predominantly thankful to Dr. Andreas Hoerner for taking out time in assisting me with the substrate preparations for DRIE nucleation studies. A very heartfelt thanks to Christopher Westerhausen and Dominik Bayer, for their immense co-operation regarding the AFM measurements.

I as well feel highly indebted to the expert technicians at University Manheim for their assistance with the RICM measurements. Sincere thanks to Dr. Frank Trixler and specially Klaus Knapp at the Deutsches Museum, LMU department, Munich, for their great co-operation and assistance with SEM measurements.

Many thanks to all my friends, in India and abroad, for all their love and constant support during the course of this work. Special thanks to Ranvir and Akash for their perpetual assistance in providing me with the inaccessible research articles in no time.

This work would not have been accomplished without the constant love and backing of my family, primarily my husband, Nishad Phatak. I cannot thank him enough for all his patience, his unconditional love, constant support, motivation, and for all the faith that he had in me, that always kept me going. Besides, I feel so blessed for having such affectionate parents and such a dear family, that stood always behind me and trusted me throughout in life. I would have not reached this milestone, had it not been for their love and support.

DISCLAIMER

This thesis includes part of the research that I intend to publish with my supervisors. The research reported in this document is original and the work of any other researcher has been appropriately referenced.

"…but I'd hate to see you close the book too soon and miss all the excitement that could happen to you on the next page—the page you're going to write.''

- The Other Side of Me, Sidney Sheldon

To my loving husband,

Nishad

CONTENTS

CHAPTER 1

INTRODUCTION

1.1 Motivation

Bubbles have always been an integral part of the fluidic systems- their presence at times desirable[1-4] , but often undesirable[1,5-7]- hence drawing the curiosity of the researchers towards comprehending them and their conduct in the concerned host systems. Till date, though tremendous research underwent into studying the occurrence of bubble(s) into various macro-fluidic systems[8-10], not much has been however accomplished towards understanding the same in micro-fluidic[11-12], especially in micro-droplet systems, particularly when bi-liquids at elevated system temperatures are involved.

Image 1.1: Bubble evolution in a bi-liquid (inner yellowish drop beneath the transparent outer drop), micro-droplet system

The current work, is thus a research oriented attempt, primarily an experimental one, towards the understanding of bubble dynamics in such micro-fluidic system(s)- hoping to provide solutions which might be beneficial for both academia as well as the industry.

1.2 Background

The principle components of present day micro-fluidics[13-17] are lab-on-a-chip[18-20] (LOC) devices: miniaturized analytical laboratories capable of transferring the work of an entire

clinical lab on a single, portable biochip[21]. Achieved by the integration of physics of fluid dynamics and the potential of micro-fabrication, these biochips have the ability to manipulate and characterize biological samples, being thus exceedingly in demand chiefly in biological sciences – owing to fluidics being the prime medium where biology operates at the cellular level[14].

One traditional laboratory process that has benefitted enormously from the reduced scale and integrated fluid management is the Polymerase Chain Reaction (PCR) [22-25] : an in-vitro, biological process incorporating repetitive synthetic reactions to make millions of copies of identical DNA sequences--- DNA amplification serving as an essential pre-requisite in many fields and applications, as in medicine for the detection and diagnosis of hereditary and infectious diseases, in forensic sciences, and paternity testing in the identification of genetic fingerprints, and so on [23-29].

Developed in 1983 by Kary Mullis[24], PCR largely relies on thermal cycling constituting of cycles of repeated, alternate heating and cooling of the reaction (mix) for DNA melting and its enzymatic replication[25]. Further, the PCR or the reaction mix mainly comprises of primers (short DNA fragments) containing sequences complementary to the target DNA region that is to be amplified, the DNA polymerase after which the method is named for synthesizing a DNA copy, de-oxy-nucleotide-tri-phosphates from which the DNA polymerase builds the new DNA, and a buffer solution providing suitable chemical environment for the optimal activity of the DNA polymerase. During the PCR run the generated DNA is itself used as a template for replication, setting in motion a chain reaction, thereby amplifying the DNA template exponentially [15,25].

Discussing various PCR stages briefly, the first step (I) is the 'Initialization' step in which the PCR mix is heated to a temperature of around 95°C for about 10 minutes- vital for the activation of the DNA polymerase requiring heat activation by hot start PCR[26,28]. Next is the 'Denaturation' step (II)- the first regular cycling event carried out at around 95°C again, but only for only 20-30 seconds this time. It is here that the hydrogen bonds between the complementary bases of the DNA get disrupted, causing the double helix to get physically separated into two single stranded DNA molecules [29]. Then comes the 'Annealing' step (III) carried out at comparatively lower temperatures of nearly 64°C for around 1 minute, during which the primers in the PCR mix anneal or bind to the targeted DNA sequence that is to be replicated [29]. 'Extension/elongation' (IV) step is carried out at around 72°C for about a minute, during which the DNA polymerase replicates the DNA strands by synthesizing new DNA strands complementary to the DNA template strands[15]. The DNA polymerase polymerizes a thousand bases per minute and under optimum conditions, as no dearth of substrates and reagents available, at each extension step the amount of DNA target is doubled, resulting in an exponential amplification of the specific DNA fragment [25]. Steps from II-IV are usually repeated 20-40 times resulting in an exponential amplification of the DNA. The final elongation step (V) at 72°C takes place for about 10 minutes to ensure the extension of any remaining single-stranded DNA [25]. Lastly comes the 'Final hold' step (VI) at 20°C, executed for an indefinite time for the short-term storage of the reaction [25] (refer figure 1.1).

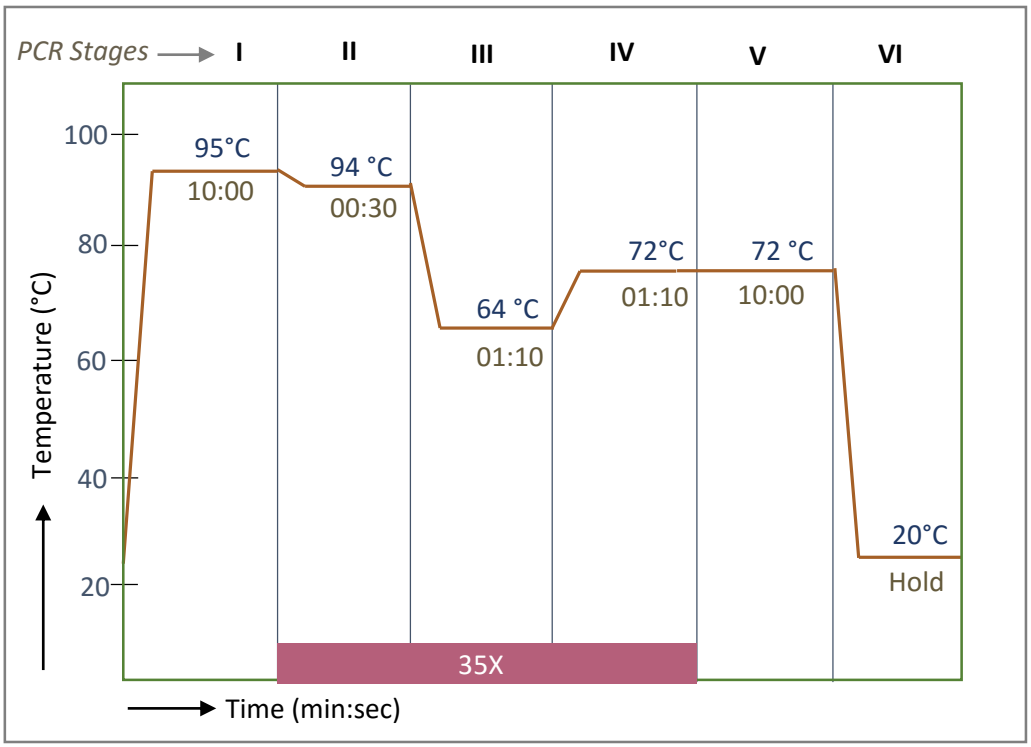

Figure 1.1: Various thermal cycling steps involved in a typical PCR run

Of the various systems developed for the conduction of PCR, initially came into limelight, based on continuous micro-fluidics [30-33] , continuous flow PCR systems, in which the sample was continuously pumped through a microfluidic channel during each temperature cycle[33]. For instance, Nakano et al.[33,34] introduced in 1994 continuous flow PCR concept by using a capillary passing through different temperature baths. Then in 1998 Kopp et al. reported a continuous-flow PCR chip using a serpentine channel passing through three thermostable copper blocks [33,35]. However, such continuous flow systems had several drawbacks as the easy generation of gas bubbles in the micro-channels adversely affecting the PCR amplification, difficulty in regulating the rate at which the PCR solution travels between different temperature zones thereby reducing the flexibility to regionally control fluid flow velocity in order to meet PCR requirements, high fabrication costs etc. [33]. Further, such conventional PCR instruments usually achieved a ramping rate of about 1-2°C/s in the temperature range relevant for PCR, where a complete PCR analysis needs approximately 1-2 hours. The resulting lower ramping rate was reported to be due to the high thermal capacity of the material of the PCR reaction system, which seemingly could not meet the need of fast DNA amplification[3,33].

The above limitations with continuous flow technology thus called for more sophisticated PCR systems- evolved next with the advent of digital micro- fluidics[15,16] as micro-fluidic digital PCR systems[34-37] . With their serial [38-40] or parallel[41-42] formats, this new technology allowed precise control of the sample volume and high throughput analysis - such systems nevertheless

suffering from their own limitations as cross contamination between samples, sample dispersion, etc., thus requiring appropriate two phase flow systems [33, 43-44].

An important digital/droplet architecture that followed was of stationary chamber based PCR amplification systems where the PCR mix was kept stationary and the temperature of the reaction chamber was cycled between different temperatures- the first such stationary chamber[40] architecture based PCR chip being developed by Northrup et al. in 1993. Stationary PCR systems were further classified as single -chamber[45-48] and multi-chamber [49-53] systems, as per the number of chambers employed for PCR conduction, as depicted in the figure 1.2.

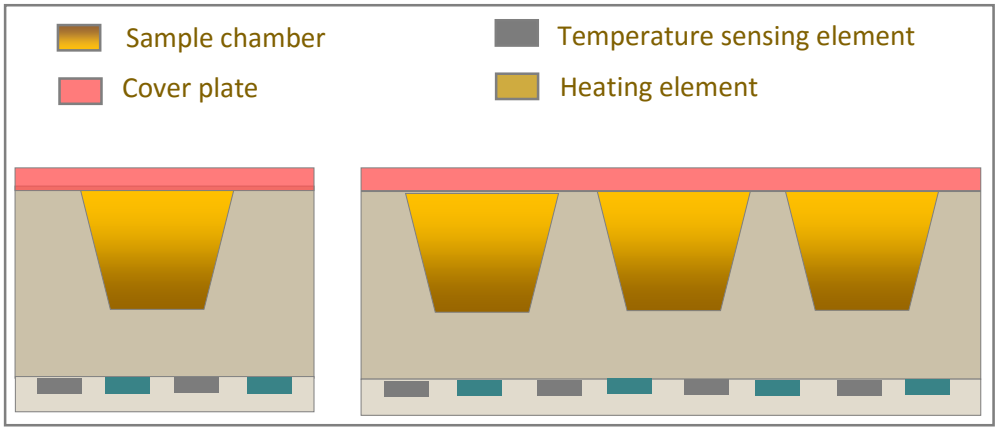

Figure 1.2: Schematic representation of (a) Single chamber, (b) Multiple chamber PCR amplification system[33,41]

Single-chamber stationary PCR systems though were a success in attaining good thermal and fluidic controls and reducing thermal and fluidic crosstalk between chambers, they however lacked high throughput and failed in single-cell gene expression analysis. Furthermore, with them was the risk of carry-over from experiment to experiment, enlarging the possibility of incomplete amplification or partial failure, especially for the cases when PCR amplifications were performed in the same PCR micro-fluidics. On the other hand, improvisation to multi -chamber stationary PCR systems though allowed greater generation of standard curves, use of multiple primer sets and optimization of micro-fluidic PCR, special care had to be however taken to achieve the thermal optimization of chamber array in order to obtain homogeneous temperature fields between chambers with this technology- precise handling and processing of sample micro-fluidic on such PCR chips still facing additional challenges [33,54-55].

In this regard, a novel approach was proposed by Guttenberg et al. to handle small scale sample volumes by incorporating a hydrophobic/oleophobic surface providing virtual fluid confinement [33, 56] to the liquids (droplets). The concept of virtual reaction chamber (VRC) was applied for the first time in 2005, in which each PCR sample droplet was covered with a drop of mineral oil, as can be seen in the figure 1.3 below:

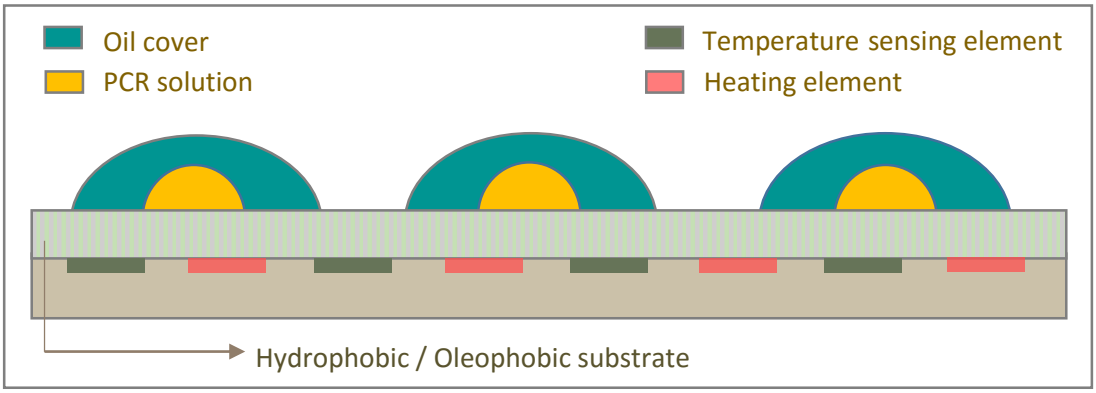

Figure 1.3: Schematic representation of Virtual Reaction Chamber (VRC) PCR amplification system [33,37]

The above architecture had many advantages over the standard chamber based PCR amplification systems as increased sensitivity and efficiency of the reaction, fast response time, low reagent and sample consumptions, reduced sample evaporation at elevated temperatures (required by biological reactions), reduced sample loss owing to liquid sticking to the sides of the chamber which diminishes to a great extent the adherence and adhesion problems, short heat and mass transfer times because of high surface –to-volume ratios at the micro-scale, increase in automation and parallelization opening a way to screening and systematic testing in the domain of drug discovery, etc. Finally, portability was a unique feature that permitted diagnostics and bio-analysis on the field[57].

Shortly after its invention, the VRC technology was adopted by the industry- Advalytix AG, part of Beckman Coulter Biomedical GmbH, in order to generate novel amplification platforms for carrying out of biological reactions, as the famous PCR. For commercial applications, the industry fabricated on a standard glass slide (75mm * 26mm * 1mm) an amplification platform based on the VRC architecture, as can be seen in the image 1.2 on the right.

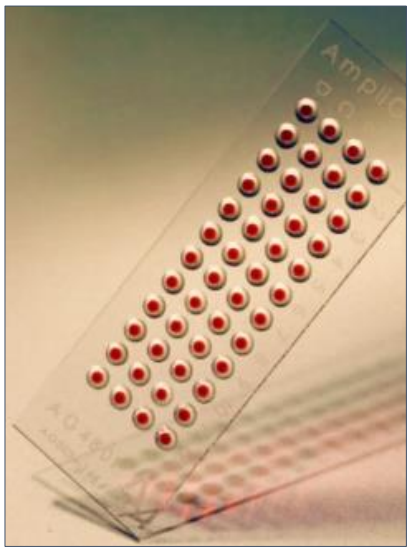

Image 1.2: Planar amplification platform with 48 reaction sites for the independent execution of various biological reactions[57]

Such platforms enabled faster DNA amplifications due to lower thermal capacities and larger heat transfer rates amid the PCR sample and the temperature controlled components- in addition to having other advantages as small sizes, fast ramping rates, low cost, high integration, and so on[57].

Normally, such systems proved to be a success- the only major limitation being the infrequent evolution of bubbles

within them at elevated working temperatures. The problem raises further when evolved bubbles are intense (of huge diameters) enough causing dropout of the respective sample solution(s), to an extent that it at times leads to the merging of the adjacent micro-droplets—a highly uncalled phenomenon resulting in loss of information, erroneous analysis, and reduced efficiency of the overall micro-fluidic systems.

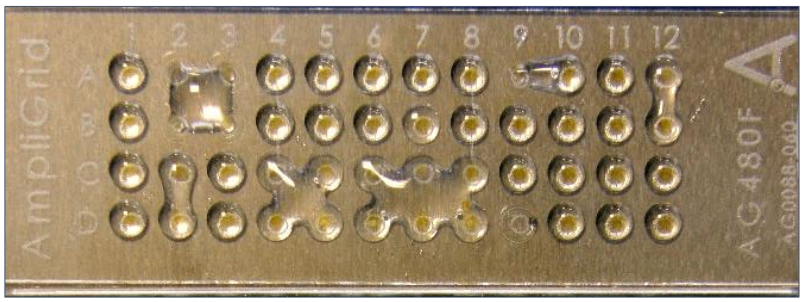

Image 1.3: End of PCR cycle- colossal bubble evolutions resulting in subsequent merging of the adjacent droplets

The above hence requires the comprehension of the concerned microfluidic system and the grasp of bubble dynamics in the same – such an analysis being the prime focus of the current, mainly experimental, work.

1.3 Organization of the thesis

The thesis is broadly organized into seven chapters. The present chapter, 'Introduction', highlights the motivation behind the work and provides a brief background to the study.

The 2nd chapter, titled 'System Specifications', aims to obtain an insight into the dealt with micro fluidic system – discussing the production, functional and technical details of the prime components of the system, viz. the reaction platform, the thermal/amplification cycler and the bi-liquid, micro-droplet duo, respectively.

The 3rd chapter, named as the 'Bubble evolution-*An overview*', focuses on obtaining an overall glimpse of bubble evolution and its aftermaths - by conducting a quantitative analysis of bubble occurrences, i.e. probability of bubble evolution, in the microfluidic system as under consideration.

Next, the 4th chapter, 'System characterization', investigates the prime components of the concerned microfluidic to find out if they encompass any imperfections that could possibly lead or aid in the generation of bubbles at elevated working temperatures. In this regard, the chapter puts forward various microscopic examinations and contact angle (static and dynamic) studies conducted to characterize the reaction platform, various calibration and

ramp rate related experiments to characterize the heating cycler and to study its role in bubble evolutions, and several contact angle studies for the single and bi-liquids, both independent and as a function of temperature, accompanied by surface tension and PIV analysis, to comprehend the behaviour of the bi-liquid, micro-droplet system and its possible contribution to the generation of bubbles at higher system temperatures.

Chapter 5, 'Bubble dynamics', discusses various stages in the lifespan of the bubble, viz. bubble nucleation, bubble growth, bubble burst, and bubble merge- various high definition video recording experiments being put forward in comprehending the same. In this respect, the chapter discusses the various microfabrication techniques, from fundamental laser engraving techniques to more sophisticated wet etching and deep reactive ion etching methods, adopted to understand the concept of bubble nucleation Next, from the video recordings, the chapter investigates the growth of bubbles, both primary and secondary, within single-liquid and bi-liquid systems. Additionally, the chapter presents studies conducted to determine the content of the evolved bubbles, the phenomenon of bubble burst, and the merging of adjacent droplets due to drastic bubble evolutions within the microfluidic system. Finally, the chapter talks about the various methods proposed that could be adopted to eliminate/ control the evolution of bubbles in such micro-fluidic systems- at the nucleation level (placing the system in a pressure chamber), at the growth level (addition of surfactants to the system), and at the merge level (fabricating superhydrophobic surfaces exterior to the micro drops).

Finally, the Epilogue being stated in Chapter 6, Chapter 7 provides the outlook to the work.

CHAPTER 2

SYSTEM SPECIFICATIONS

In analogy with the VRC concept design, the primary system requirements for carrying out the biological reactions as the PCR, are an amplification platform - a chemically modified substrate for holding the reaction liquids in place, a thermal cycler capable of providing the necessary heating and cooling cycles for say DNA amplification, and a set of bi-liquids acting as precursors for the execution of the concerned biological reactions.

However, the company, Advalytix AG[57] revised the above components and retitled them to be the Ampligrid (AG), the Ampli-Speed Cycler(ASC), and a sophisticated bi-liquid duo (inner reaction mix and outer sealing solution), respectively- the nomenclature being throughout referred to in the current work as and when the concerned micro-fluidic system is dealt with.

Further, chiefly, being an industrial project, the work incorporates the above as the fundamental system in which the bubble evolution phenomenon is comprehended and investigated- the system being detailed, as in the sub-sections below.

2.1 The Amplification Platform

An amplification platform, as stated, can be defined as a substrate holding the various liquids in place- attempting to integrate the various stages of the biological reactions on a single platform. Typically, being only a few millimeters to a few centimeters in dimensions, such platforms have been known to be usually biocompatible, heat resistant, and designed as to get easily incorporated into the overall micro-fluidic system[57] .Correspondingly, Ampligrid, the amplification platform being mainly used in this study, was developed-a big plus with such platforms being the possibility of amplification of low copy number DNA samples in minimal

volumes and at minimal DNA inputs (in the range of 30pg-1ng)- the prospect being of tremendous importance, particularly in the forensic community, where trace evidence or low copy number of sample volumes (lacking sufficient input material to allow for successful DNA testing) have always been a huge challenge [58-60].

The following sub-sections further detail the various production stages involved in the development of such amplification platforms- from the selection of a suitable substrate material, to their design, and to chip fabrication, as can be referred below.

2.1.1 Material

Good choice of a substrate material for PCR micro-chambers (or micro-channels)[61] marks as an essential and fundamental step for a successful micro-chip PCR. Various materials comprising the list in this regard, the most preferred choices however came out to be silicon [33,62-65] and/or glass [33,66-70] - chiefly due to the well-developed fabrication processes of standard photolithography and chemical (wet) etching that could be effectively used in the construction of refined micro-fluidic amplification platforms out of these materials (for instance enabling various metal heaters and sensors which could be easily patterned on such materials hence providing a high degree of integration [33,61]). Additionally, the superior thermal conductivity of silicon, about 160W/(m°C), has been reported to enable very fast ramping times[61], thereby allowing faster analysis. However, owing to disadvantages associated with silicon as the substrate material as the inhibition of PCR (lowering the overall amplification efficiency), bare silicon exhibiting no amplification at all in some cases, the high conductivity of silicon calling for thermal insulation in order to reduce the energy loss into the surroundings- where measures of thermal insulation in turn add to the high complexity of PCR microsystems, opacity of silicon limiting the application of real-time optical detection to the PCR microfluidic devices , and so on [33,61], hindered its complete assimilation as the substrate material for PCR chambers, thus calling for more sophisticated hybrid architectures and/or another substrate materials that could be deployed in this regard.

An alternative and a promising substrate, reported to be used since 1990's, that came out in this regard was glass- with an increasing number of PCR micro-fluidic systems being constructed out of glassy materials [33,66-70]. Prime advantages associated with glass being the achievement of well-defined surface chemistries, superior optical transparencies, and good Electro Osmotic Flow (EOF) characteristics- allowed for the integration of PCR and CE (Capillary Electrophoresis) separation on a single, monolithic glass chip or on a hybrid silicon/glass chip[61]. However, owing to the limitations with this material as the difficulty in disposing the glass (and/or silicon) chips owing to the higher costs of fabrications involved, and the persistence of problematic issues in the micro-fabrication of the above, their use at times gets hampered, especially in several commercial applications[61].

Other materials, on the other hand, that nevertheless came forward in this regard were polymer based PCR microchip materials as polydimethylsiloxane (PDMS) [33,71-75], polycarbonate (PC) [33,62,76-78], polymethylmethacrylate (PMMA) [33,79-81], polyimide (PI) [33,82-83],

polyethylene terephathalate (PET) [33,84-85], SU-8 [33,86-88], poly (cyclic olefin) [33,89-91], epoxy [33,92-93], and Gene Frame double-sided tape [33,94]-- polymers being reported to be being superior to silicon and glass in some cases [33,61]. In addition, the use of ceramics[95-96] , and even aluminium wells coated with Polytetrafluoroethylene(PTFE) [33,97] in some cases, were reported as good candidates as PCR micro-fluidics substrate materials. Further, were as well put to use many hybrid materials, chiefly being silicon/glass [33,98-101], polymer/silicon[33,] and polymers/glass[33,102-104] hybrids.

The current work however employs glass as the substrate material in the form of standard microscope glass slides- owing to their ease of availability, integration and transportation, not to mention ease of fabrication of glass as stated above, enabling rapid and handy PCR analysis- details into the design and fabrication of amplification platforms from glass slides being discussed as in the following sub-sections.

2.1.2 Design

The Ampligrid reaction platform, based on the Virtual Reaction Chamber architecture, was designed by fabricating 48 individual reaction sites, in a 12*4 matrix, on a standard glass slide (76 mm*25 mm *1mm)[57] , as can be referred to in the image 2. 1.1 below:

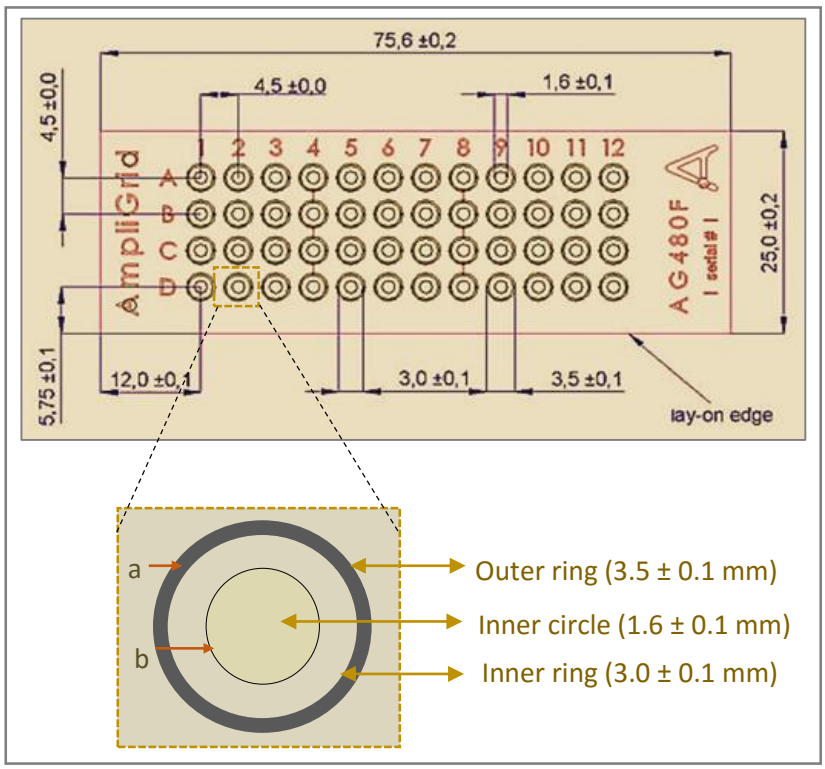

Image 2.1.1: Layout design of the AG slide (regions 'a' and 'b referred to as the outer and inner bands respectively)[57]

With the incorporation of adequate surface chemistry, alternate hydrophilic-hydrophobic (different wetting) character could be imparted to the above design (details into the generation of above surface chemistry being dealt with in the next section- fabrication).

As can be seen in the image 2.1.1, the inner hydrophilic region of 1.6 ± 0.1mm diameter was designed to hold the inner liquid (reaction mix) in place, followed by the outer hydrophobic region of 3.0 ± 0.1mm diameter surrounding by a hydrophilic ring of 3.5 ±0.1mm diameter (from center) for holding the outer liquid (oil) in place. Center-to-center spacing between the two adjacent reaction sites being kept as 4.5 mm to avoid any cross-contamination among the sample volumes, the above design successfully compartmentalized the bi-liquid, micro-droplets in place, thereby generating an urbane amplification platform [57].

2.1.3 Fabrication

Literature reports, as previously stated, chemical modification of the underlying surface as a successful and promising method for the attainment of virtual fluid confinement - the distribution of the fluid on the surface being controlled by the surface free energy. Depending on the nature and degree of chemical modification applied, (alternate) hydrophobic and hydrophilic regions could be generated on the selected surfaces (for the chosen substrate material)- droplets forming high contact with the surface on the hydrophobic regions and wetting the surface for hydrophilic regions, respectively-details into the phenomena being undertaken in the next chapter in the section contact angle studies.

Thus by imparting different wettabilities (chemical structuring) to the underlying surface, a chemically heterogeneous surface could be generated - an alternate patterning (hydrophilic-hydrophobic regions) enabling the exact confinement of the fluid (inner reaction mix) inside a hydrophilic region followed by a hydrophobic area (which in turn is further surrounded by a hydrophilic region(ring) for holding the outer cover liquid in place)[56].

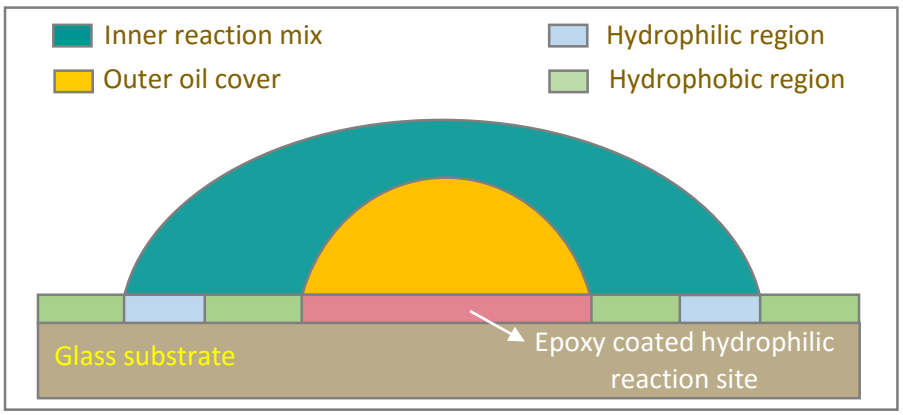

Figure 2.1.1: Cross-section of an Ampligrid slide depicting a chemically stratified reaction site generated using the concept of virtual fluid confinement

Further, depending on the kind of substrate used, chemical modification can be attained by coating the surface with silanes[33,105-108] , or thiols[33,109-110] -- the resulting organic films being structured via photolithography[33,111-113]. Usually with glass, researchers have adopted lithography (photolithography) or etching (Chemical Vapor Deposition (CVD)) [33,114-118], wet chemical etching[112-113,119-120], subtropical etching[33] and/or Reactive Ion Etching (RIE)[121-123] as the widely known techniques for chemical structuring of the underlying surfaces.

Nevertheless, based on the above, for the fabrication of Ampligrids used primarily in the current study, the chosen glass substrate was chemically structured using a well-defined sequence of cleaning/coating techniques- silane chemistry being chiefly employed for rendering appropriate (alternately varying) wettabilities to the targeted regions, which in turn is achieved mainly by employing photolithography (and/or more advanced mechanical coating (structured printing)) techniques, followed further by definite CVD process. All the above being carried out in a highly controlled, clean room environment, alternate hydrophilic-hydrophobic zones are fabricated, resulting in virtual confinement of the corresponding fluids (the glass slides having laser engraved 'reference rings' at the back in alignment with the upper inner reaction site- providing a guide to the eye for the virtual reaction chamber(s), and hence enabling ease in pipetting of the concerned liquids (refer images 2.3.1 and 2.3.2)).

In the above manner, 48 reaction sites were fabricated per slide surface – the technology aiming at multiple, parallel PCR analysis- the ease of integration of the glass slide with other systems as robotics, etc., further enabling full optimization of such systems[56,57].

In addition to the chemically structured surfaces as described above, worth mentioning are the chemically non-structured surfaces-- the glass substrates which have only being hydrophobically coated- being subsequently as well used (primarily for comparative studies) in the current work. Further, whereas the chemically structured surfaces have been usually referred to as the AG (Ampli-Grid) slides, the nomenclature for chemically non-structured surfaces has been as adopted as PFS- based on the homogenous silane coating applied in the generation of such surfaces.

2.2 The Heating cycler

After the amplification platform, the next vital component of the micro-fluidic system is the heating (or amplification) cycler- as dealt with in the current section. As stated previously, biological reactions as the PCR are a typical temperature controlled and enzyme catalyzed biochemical reactions, consisting of periodic repetition of primarily three different temperatures zones: melting, annealing and extension temperatures cycles (refer figure 1.1). Further, owing to the very high sensitivities involved with such reactions, a minor temperature difference may significantly affect the efficiency of the DNA amplification, especially in the PCR micro-fluidic systems[33]- which in turn could lead to flawed analysis, lowering the overall efficiencies of such systems Thus, to ensure high efficiencies, and to obtain faster ramping rates, the choice of an appropriate heating method marks as a step of

utmost importance. In addition, the heating stage should be such as to perform autonomous heating and cooling, over a number of times as desired, without a significant time lag. All the above is typically accomplished by employing PCR instruments or thermal cyclers- the DNA amplifiers regulating temperatures during such cyclic programs [33,57,280].

2.2.1 Literature review

Literature reports various heating methods adopted for PCR micro-fluidics- their choice chiefly dependent on the type of the material in use (different materials having different thermal masses requiring different heating methods). The methods further being broadly classified into contact and non-contact heating methods[33], are as discussed briefly in the sub-sections below.

a. Contact heating

As the name suggests, in this type of heating the thermal components embedding the heating element are in direct contact with the components of the PCR amplification system – the heating mainly employing the principle of electro-thermal conversion or the indirect utilization of joule heating to heat the corresponding PCR solution[33].

Moreover, among the contact heating method, the two main heating formats that have been widely reported have been the heating using the thin-film heating elements[124-125, 102,56] , and heating using the metal/other heating blocks[33,126-127]- the former concept being generally micro-machined, further utilizing film deposition techniques. Besides, the two primary materials being known to fabricate micro-heaters have been reported to be platinum (Pt)[128-130] and polysilicon[131-133]- the former nevertheless having an edge over the latter and other materials owing to its good temperature vs resistance relationship, its ability to withstand high temperatures, its chemical stability, its high oxidation, and purity and the ease with which it can be micro-machined[33]. Additionally, during Pt thin film deposition to fabricate micro-heaters and micro-sensors, a thin layer of titanium (Ti) is formed which often functions as an adhesion for Pt later[134-136]. However, the major drawback with Pt as the heating material on the other hand, is the high diffusion rate exhibited by this Ti layer, deteriorating Pt at high tempeartures[137]. Conversely, polysilicon, a polymer consisting of many single-crystal particles, has been reported to be compatible with high temperature processings, thereby interfacing very well with thermal silicon dioxide- widening its use for thin-film fabrication in PCR microfluidics[131-132]. However, in addition to the above materials, researchers have as well put forward some other metals, alloys or inorganic compounds that can be used as thin film heaters in PCR microfluidics such as aluminum[138-142], tungsten[143], gold[144-145], silver/graphite inks[146], silver/palladium[147-148], nickel/chromium[149], chromium/aluminum[150], Al_2NO_3[151] and Indium-Tin-Oxide (ITO)[152-155] . Coming to heating via metal/other heating blocks, the format employs insertion of the cartridge heater into the metal blocks or by utilizing the Peltier elements[156]. However, despite of the metal/other heating blocks having limitations as larger thermal mass, slower temperature ramping rates, difficulties in attaining fast thermal

transition from 55°C-95°C in the presence of a single Thermo-Electric (TE) device, and being non-transparent, metallic heating blocks and Peltier effect based TE ceramic heating blocks have been nevertheless reported to be widely in use along with the thin film heaters[157-164].

However, apart from the above, some other reliable heating solutions as well came into limelight as the commercial thin film resistance heaters[121-122], thermal component constructed using the single-sided Flexible Printed Circuit (FPC) technology[123], resistive heater coils[124-126], and even more convenient and commercial thermal cyclers[127-129]-- the methods have been proven to be efficient and robust for achieving faster PCR cycling in contrast to conventional PCR devices. Further, it is believed that more and more desirable contact heating methods for PCR microfluidics will be developed based on MEMS or non-MEMS techniques using electro-thermal Joule heating blocks in the future.

However, the above contact based heating methods suffered from various drawbacks – primarily being the large thermal mass[134-156], as stated, especially with the metal heating block contact heaters, limiting the thermal cycling rate of the heating element and of the whole PCR system. Moreover, in the case of an external contact heating devices, localized heating is ultimately restricted in the lateral resolution by the thermal conductivity of the substrate material for on-chip PCR microfluidics, making the fabrication of devices with multiple independent heating points not that feasible. Further, in the case of on-chip integrated heaters, these devices still need some tedious and complicated micromachining processes-hampering the flexibility to easily change the PCR microfluidic design[134.156]. Some researchers additionally have reported that when the integration of the PCR amplification with an electrophoresis microchip is taken into consideration, it becomes very difficult to regard the contact resource as part of the PCR chip and not as part of the electrophoresis chip itself on a single chip wafer in the presence of a contact-mediated heating method.

Owing to the above limitations associated with the contact based heating methods, great efforts were hence made to develop sophisticated non-contact or other heating methods, as detailed in the sub-sections below.

b. Non-contact heating

As the name suggests, in this case mode of heating, the heating part is not in direct contact with the PCR amplification components, but is remote from the microfluidic device [156]. Various non-contact heating modes have been reported to be utilized in the past as the non-contact heating based on hot air[165-169], based on IR light [170-172], based on laser-mediated heating[173-174], based on halogen lamp light source[175], based on induction heating[176], and based on microwave irradiation[177-179].

c. Other heating methods

In addition to the above mentioned contact and non-contact heating methods, literature as well reports heating methods based on convection (Rayleigh-Bénard convection cell)[180],

based on chemical and physical processes[181], and based on alternating electric current induced buffer joule heating[182,33].

The current work, however, employs the use of contact mode (based on Joule's heating) thin film heaters made out of polysilicon for the generation of sophisticate heating technology- being further detailed as following.

2.2.2 The Ampli-Speed Cycler (ASC)

For platforms as the Ampligrid, an ultra-compact heating unit was developed by Advalytix AG, based on resistive heating, named as the Ampli-Speed Cycler (ASC)[57]. The heating cycler integrates a superior heat transfer technology based on highly-planar silicon wafers, ensuring an optimal thermal coupling with the subsequent glass slide. Further, the technology was capable of accomplishing extremely homogenous surface temperatures with effective heating and cooling rates, which could be varied between 0.2°C/sec up to 3°C/sec. Additionally, ramp times as short as 40 seconds could be realized, thereby avoiding the formation of non-specific by-products and reducing thermal stress on the polymerase- essential for carrying out a successful PCR.

The cycler whereas achieves its heating performance by operation with minimized thermal loading of the heating system- its cooling performance has been based on dissipating the heat from the plate by means of a metal thermal energy buffer- being mechanically attached to the heating plate from below during the cooling phases. The buffer thereafter transfers its thermal energy to a larger heat sink, which as well acts as its rest position during the heating and idle phases of the cycler system. Besides, ASC can be used as a general purpose instrument for highly precise, programmable temperature control of any flat device as a microscope slide [57].

The ASC was designed to operate between the temperature range of ambient +15°C to + 99°C- heating/cooling cycles of the biological reactions usually falling within this range. However, to ensure that the right temperatures are worked with, calibration of the system marks as an essential step prior to any biological run or research oriented investigations. Further, an individual heating chamber unit providing thermal cycling to a single (Ampli-grid) slide was referred to as a *'bay'*- together with a possibility of multiple bays (up to 4) being coupled, allowing the parallel execution of various biological processes within few hours. Different versions of the ASC were additionally developed depending on the kind of heating platform

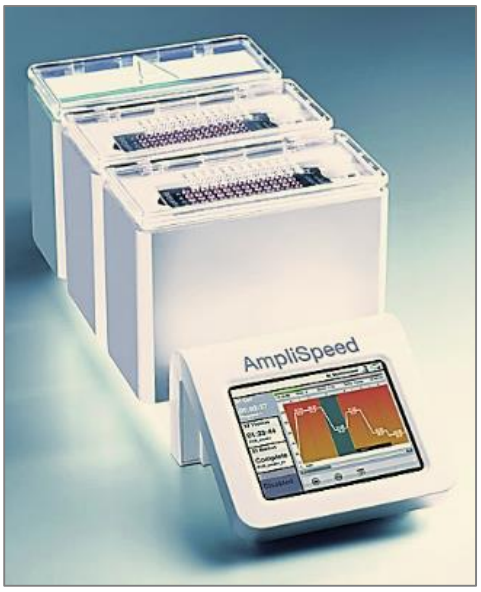

Image 2.2.1: A two-bay Ampli-speed cycler

employed: being available as lithographic heating plates as well as simple heating foils- in different thermal designs. Additionally, the ASC design came with a perforated lid preventing the blockage of the chamber from steam/vapour at elevated working temperature-enabling temperature control and for the clear visualization of the overall reaction process, especially during research oriented investigations. Further, controlling and definition of thermal cycling profiles was carried out using the new 640*480 pixel VGA (Video Graphics Array) touch screen display via an innovative graphical user interface (GUI) for bench top programming, configured in front of the ASC (refer image 2.2.1[57]).

2.3 The Bi-liquid, Micro-droplet System

On a reaction platform as the Ampligrid, as previously stated, virtual reaction chambers are realized from a set of overlapping bi- liquids, dispensed as micro droplets on the chemically modified substrate[56]. The inner liquid being the biological sample or the reaction mix, on top of it is dispensed an outer liquid, usually an oil cover, to circumvent its evaporation at elevated system/reaction temperatures.

Further, a microfluidic device demands movement/positioning of the droplets in order to bring the reagents in contact for the biological reactions to effectively take place. Literature reports different approaches that have been applied for the actuation of droplets on the solid surfaces, as electro-wetting, usage of light sensitive materials that change their surface energy during illumination, employing diamagnetic levitation, concept of Surface Acoustic Waves (SAW), and so on[56]. Another promising possibility in this regard has been the deployment of surface chemistry for chemical modification of the substrate itself for the actuation/guiding of droplets, as previously stated- on a gradient of surface free energy[56] a small amount of liquid (drop) having the tendency to move in the direction of increasing hydrophilicity. The latter technique being utilized for the actuation of droplets on the Ampligrid platform as under consideration, the droplets dispensed either via manual (pipetting) or automated means- the details into the bi-liquids employed being as discussed in the sub-sections below.

2.3.1 The Inner Liquid

As stated, the inner liquid is usually the biological solution- PCR or the reaction mix- the primary fluid where the biological reactions take place. It comprises of small volumes of various biological components, master mix (magnesium salts, pH buffer, and potassium salts), DNA substrate(s), oligonucleotide primers, polymerase enzyme, and dNTPs ^{3}- all diluted in a major volume, ~ 90%, of degassed, deionized water, thereby making water as the primary component of this inner mix. Tiny volumes of DNA, which normally are included in this mix for biological and industrial purposes, being however expensive, are usually skipped for research oriented purposes and a ‘dummy’ PCR solution devoid of DNA is used instead.

The inner liquid is held in place by the inner hydrophilic ring (reaction site) of 1.6 ± 0.1 mm diameter (refer image 2.3.1)[57] on a chemically stratified surface, as the AG slide. To achieve complete wetting and to attain a spherical cap configuration in analogy with the VRC concept design, volumes of ~ 1 µL were chosen for this inner drop.

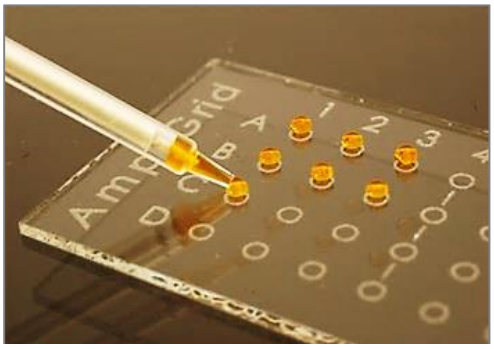

Image 2.3.1: Manual pipetting of 1µL of the inner PCR mix on the inner hydrophilic region of the AG slide (the backside engraved reference rings facilitating dispensing of the droplet(s); the droplets being guided automatically by the underlying surface chemistry)[57]

Further, biological inert dyes which impart slightly yellowish (Adva-Gold) or slightly bluish (Adva-Blue) tinge are added (~0.1% in volume) to the otherwise transparent inner droplet. This differentiates it from the transparent outer oil cover, thereby facilitating pipetting of the liquids and their clear visualization, especially for research oriented experimental investigations.

Additionally, all the components of the inner liquid are stored at low temperatures (-4°C) in a dry, dust free environment. Around half an hour prior to loading, the components are taken out (of the storage/freezer) and once at room temperature, are mixed in the definite ratios and the inner liquid pipetted on the targeted/desired regions of the slide surface.

2.3.2 The Outer Liquid

Low volumes or greater surface-to-volume ratio of the inner aqueous micro-droplet makes it easily prone to rapid evaporation if left by itself-- the effect becoming more prominent at high denaturation temperatures (~ 95°C). This, if left unchecked, could possibly result in the drying up of the (inner) sample mix, leading to flawed overall analysis and DNA amplification[33,56].

To circumvent the above, often a liquid cover is employed- the liquid selected being such as having a high boiling point (>>100°C), less viscosity (to facilitate easy pipetting), biological inertness, and free from DNA/RNA, so as not to interfere with the reaction mix at any stage.

All these requirements are generally met by oils- mineral oil being typically being the preferred choice in this regard, owing to its ease of availability, high boiling point (far above 100°C), and density of 0.8 g/cm^3 (slightly below 1.0 g/cm^3 of water. However, in analogy with the inner reaction mix and the VRC based architecture, Advalytix AG developed a special oil, which they named as the Sealing solution.

Sealing solution is a mix of several oils, prime constituents being mineral (90%) and silicon oils. Having a high boiling point (>> 100°C), and at ambient temperatures (~20°C) with a density of 0.833 g/cm^3, dynamic viscosity of 27.617 mPa*s, and surface tension of 27mN/m[57],

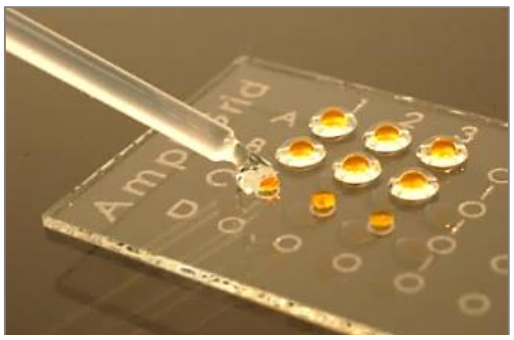

Image 2.3.2: Outer liquid being (manually) pipetted on the inner liquid, creating a bi-liquid micro-droplet system[57]

sealing solution was developed as to serves as an appropriate outer liquid covering the inner droplet- experimental checks further proving it successful enough for providing ideal evaporation protection for water-based biological reaction buffers. As for the AG slides, after production, this liquid was packed in a light-protective aluminum foil under an inert gas, and stored in a clean, dust-free environment at room temperatures; the pack being opened just prior to use. Manual pipetting or automated pipetting using electronic multi-step pipette(s) is employed for loading of this outer liquid, as other pipettes might cause generation of satellite droplets. Further, owing to high viscosities associated with this outer(oil) liquid, usually, slow pipetting speeds are adapted during its loading as compared to when loading the inner (aqueous) liquid. Once dispensed above the inner drop, this cover liquid is held in place by the outer hydrophilic band of 0.5mm diameter on the chemically structured AG slide surfaces- as can be seen in the image 2.3.2.

Further, in accordance with the Ampli -grid (VRC) architecture, to completely cover the inner drop (usually 1µL of dummy PCR solution or water), volumes of approximately 5 µL's were chosen (as per calculations) as the dispensing volumes for this outer liquid (sealing solution).

2.4 Final Conclusions

The current chapter hence outline the primary system components that have been fundamentally used in the current work. Other set –ups/ systems designed for detailed experimental purposes, however, will be discussed alongside as the work proceeds.

CHAPTER 3

BUBBLE EVOLUTION - *AN OVERVIEW*

The previous chapter effectively described in detail the micro-fluidic system, especially the one considered within the scope of the current work, and the key components comprising it.

In order to next comprehend the occurrence of bubbles in such systems- which, as said, serves as a major limitation in the efficient functioning of the same, the fundamental step was to get a feel of 'what is happening?' – both in terms of bubble evolution and the behavior of the system itself, while the biological reactions at varying temperature cycles within the fluids proceed. This was chiefly attempted by conducting few preliminary quantitative experimental investigations, as detailed in the following sub-sections.

3.1 Quantitative analysis: The Probability of bubble evolution

As stated, to begin with, a series of quantitative experimentations were carried out, in order to primarily determine the probability of bubble evolutions in the concerned microfluidic systems, at varying temperature cycles of the PCR run.

In this regard, several surfaces, both chemically structured (AG) and chemically non-structured (PFS coated) glass slides, arbitrarily chosen from different production lots, were selected. The slides were then loaded with the respective liquids (in the standard manner, as detailed in the previous chapter) and carefully placed on the heating plate of the Ampli-Speed Cycler. Typically, four slide surfaces being considered at a time (placed in parallel on a 4- bay ASC), around 40 such surfaces with 48 reaction sites per surface were investigated, especially for the phenomenon of bubble evolution, during the proceeding of the entire PCR cycle.

Both naked eye and video recording observations were made in this regard- the latter employing the set-up as depicted in the figure 3.1 below. The set-up primarily comprised of two upright microscopes- being arranged in parallel above and at the side of the reaction site, for top and side view investigations, respectively.

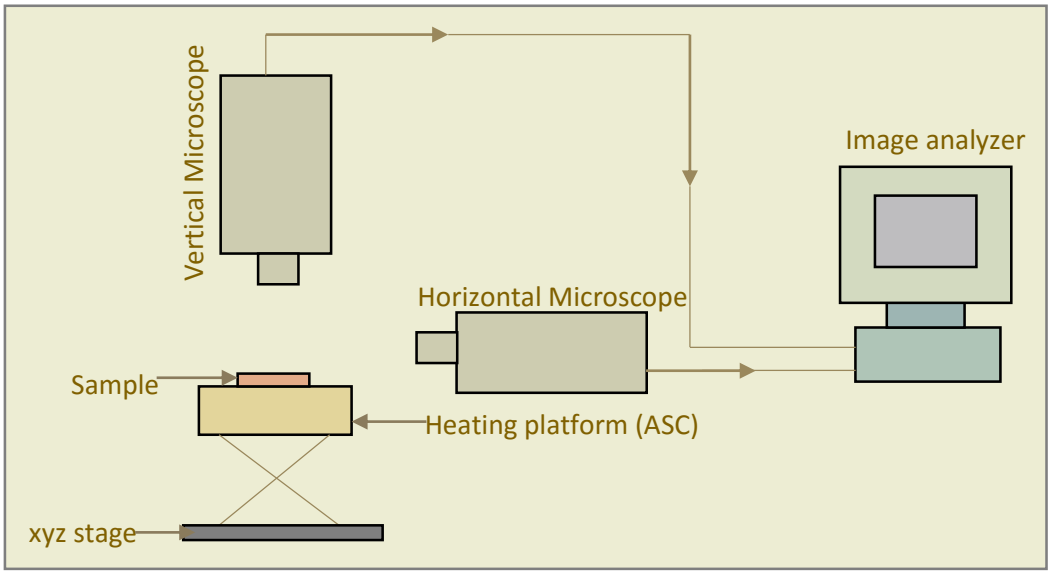

Figure 3.1: Pictorial representation of the video-recording experimental set-up to evaluate probability of bubble evolutions /qualitative analysis

Further, for the case of video recordings, the experimental data was later evaluated using appropriate image analyzing software as Paint.Net and Windows Media Player Classic for appropriate assessments.

The key observations that came forward from the above introductory experimentations were:

- Not all the reaction sites exhibited bubble evolutions, making it hence a very random and arbitrary phenomenon, occurring on few unpredictable regions on some of the slide surfaces- the probability of bubble evolutions being estimated to be less than 1%.
- Bubbles, if and when they evolved, mostly occurred during the initial stage of the PCR cycle, i.e. at 95°C for the early 10 minutes of heating. In some cases, the evolutions were seen occurring during the initial ramp time as well (within 40 seconds of heating)- the minimum evolution temperatures, however, observed to be around 77°C. Further, the bubble occurrences and their growths were observed to be strongly temperature dependent- the bubble growths seen to get suddenly hampered as soon as the temperatures were stopped or lowered from 95°C (say as and when the PCR shifts to its third stage and so on).
- Observations additionally revealed not all bubble evolutions to be similar in nature, meeting comparable destinies. While some bubbles were seen evolving and popping out

in no time, others were observed to grow to ample sizes before getting burst. Also, among the latter cases, not all big bubble bursts led to drop out of the sample solution (reaction droplet), while for some of the other cases, bubble bursts were found intense enough spilling the reaction mix all over– so much so that in some instances the merging of the adjacent droplets took place. Merging, on the other hand, was observed to be more obvious and enhanced if simultaneous big bubbles (tending to cause drop out the sample solution) occurred in the adjacent bi-liquid drops. However, the above observations were very absurd in nature, providing no clear relation between an evolved bubble and the kind of destiny it would eventually face, within the micro-fluidic system as under consideration.

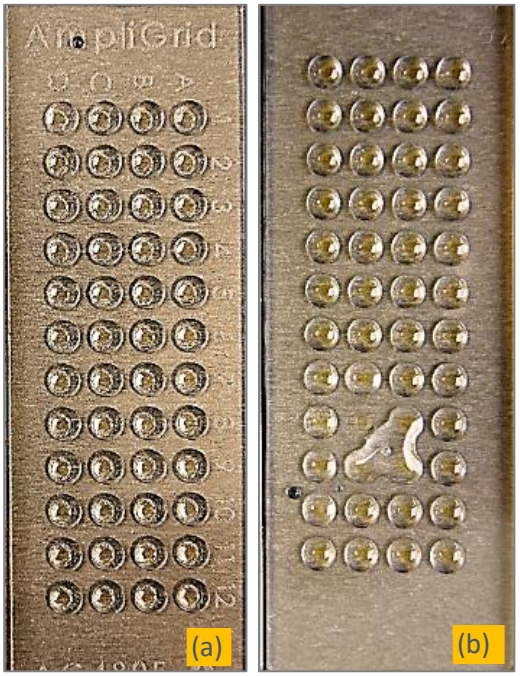

Image 3.1: Slide surface at the end of PCR (a) no bubble occurrences, (b) bubble occurrences

- In addition, it was prominently observed, that an initial/parent bubble after its burst usually led to a cascade of secondary/daughter bubbles within the system-for the same conditions of temperature and pressure.

- Again, keeping in mind the probability of overall bubble evolution in a system (generally approved by the quality control tests) to be less than 1%, observations further revealed no remarkable difference in the above findings as far as chemically structured or chemically non-structured surfaces (glass slides) were concerned, or when dummy PCR solution was substituted with water and/or sealing solution with other (ventana or diesel) oils.

3.2 Summary

The above preliminary experimentations, hence aided in providing an initial glimpse of the bubble evolution phenomenon – primarily concluding the phenomenon to be highly rare, random and unpredictable in nature. This therefore calls for detailed investigations, as in 'What is the source of bubbles if and when they occur? ', 'How and if the micro-fluidic system (the amplification platform, the heating cycler and the bi-liquid micro droplets) contributes to their evolution and/or growth? ', 'Why some bubbles pop off quickly while others grow big enough- at times resulting in the merging of adjacent droplets?', and 'How is the micro-fluidic system (as the one dealt with the current work) with an additional liquid-liquid interface behaves differently than a single-liquid system , especially in regard to bubble dynamics?' – all the queries being stepwise and in detail undertaken in the upcoming chapters, as discussed next.

CHAPTER 4

SYSTEM CHARACTERIZATION

Based on the findings of the quantitative analysis as conducted in the previous chapter, for a detailed comprehension of the 'knows-and -hows' of the bubble evolution phenomenon, the foremost step was characterizing the microfluidic system, as the one dealt with in the current work. As no system is ideal in nature, despite of the extreme care taken in its production and handling, the system might still encompass some flaws- possibly leading to or aiding in the evolution of bubbles at elevated working temperatures. In this regard, three prime components of the system (detailed in chapter 2) were analyzed, viz. the reaction platform, the heating cycler, and the bi-liquid, micro -droplet duo-- as detailed in the following sub-sections.

4.1 The Amplification Platform

The previous chapter put forward the bubble evolution phenomenon to be extremely rare and random in nature, occurring on few unpredictable regions of some of the slide surfaces. A potential source to the above, that could be thought upon, might be some local, 'missed-out' surface imperfections/inhomogeneities, that crept in the system say either during improper production or handling of the surfaces- in turn perhaps acting as sites for bubble formations at elevated system temperatures. In order to hence investigate the above, the resultant surfaces were characterized using various surface characterization techniques- from numerous microscopic investigations to multiple contact angle and surface energy measurements, as discussed next.

4.1.1 Microscopic Investigations

Microscopy has been known as one of the significant surface characterization techniques, being widely developed and used over the years for the investigation of surfaces at the microscopic scale[184-185]. Various microscopic techniques have been established in this regard, successfully enabling the comprehension of different surface types- thus making it an important technique for the study of surface (topologies) in use.

However, the selection of surfaces for microscopic analysis (to investigate the nature and source of surface imperfections) became a highly challenging task, as far as the surfaces as dealt with in the current work (chemically structured AG glass slides) were concerned. This was initially due to the fact that not all the surfaces were 'infected' and exhibited the bubble evolution phenomenon (it being very rare and random in nature, as previously discussed), and secondly owing to the reason that the surfaces which (if and when) showed such occurrences, could not be directly taken at the end of PCR for microscopic examinations - microscopy requiring clean and inclusion free surfaces as possible for a successful analysis (whereas the surfaces in this case being now contaminated by the biological liquids -bubble bursts leading to the dropouts of the sample solutions and perhaps the merging of the adjacent droplets, making the surfaces further messy) .Though the above residues could be to some extent washed off by cleaning the surfaces say using hexane (especially for oil residues) and then rising the surfaces under water and drying with nitrogen gas, chances could be that in the process the surface coatings or the inclusions be moderated too.

Hence, in this regard, a detour that was adopted was by choosing surfaces adjacent to the ones that exhibited (greater number of) bubble evolutions/ droplet incidences (at the end of PCR) from production lot(s)—assuming the selected surfaces to be possibly as 'infected' as their blemished neighbors. The picked up surfaces were then taken for various microscopic investigations, as detailed in the following sub-sections.

Standard Optical (light) microscopy[186]

To begin with, the opted surfaces (chemically structured AG glass slides) were examined under a standard upright microscope (Olympus CX23) for the presence of any surface defects. Nearly 20 such surfaces being investigated, examinations revealed, the presence of ring like surface inhomogeneities of varying diameters on some of the surfaces - such inhomogeneities further being prominently observed on the hydrophobic regions of the chemically structured surfaces (refer micrographs in the image 4.1.1).

Such imperfections presumably being thought upon to be the source of bubble evolutions at elevated system temperatures, the above were nevertheless very fundamental findings, calling for more detailed surface investigations using sophisticated microscopic techniques, as attempted using atomic force and electron microscopy subsequently.

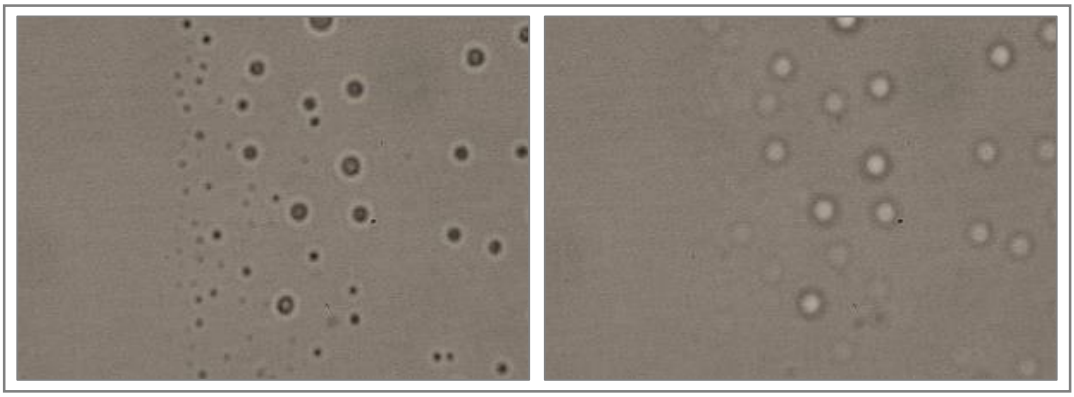

Image 4.1.1: Optical photomicrographs of hydrophobic regions of chemically structured slide surfaces revealing ring like structures

Scanning probe microscopy: Atomic force microscopy[187-188]

For a more comprehensive analysis, scanning probe microscopy or the Atomic Force Microscopy (AFM) was opted as the next characterization technique. The technique being capable of analyzing non-conductive surfaces, AFM characterization allowed samples (chemically structured AG glass slides) to be directly taken for analysis without the need of them to be coated with a conductive material prior to investigations. Additionally, as compared to the standard light microscopy, scanning probe microscopy has been reported to have far greater resolution (of the order of fraction of nanometers which is around 1000 times better than the optical diffraction limit), thereby enabling and aiming at a considerable in-depth analysis of the subsequent surfaces.

For examinations, as discussed, the selected ('thought to be infected') surfaces (chemically structured glass slides) were taken for AFM scans- the studies being carried out the University Augsburg's Experimental Physics II Lab, using AFM from JPK instruments. Calibrating the system using force spectroscopy, contact mode measurements were made to determine any surface inhomogeneities possibly associated with the analyzed surfaces.

Surface scans being made for nearly 20 such surfaces (fresh, clean but potentially infected), investigations revealed the presence of distinct crater like surface inhomogeneities, found again primarily on the hydrophobic regions of the chemically structured glass slides, as can be seen in the image 4.1.2 on the next page.

Utilizing a graphics editor program as Paint.Net, calculations revealed the above crater like inhomogeneities to be having diameters between 2-7 micrometers, peak heights between 10-200 nanometers, and inner depths varying between 2-4 nanometers.

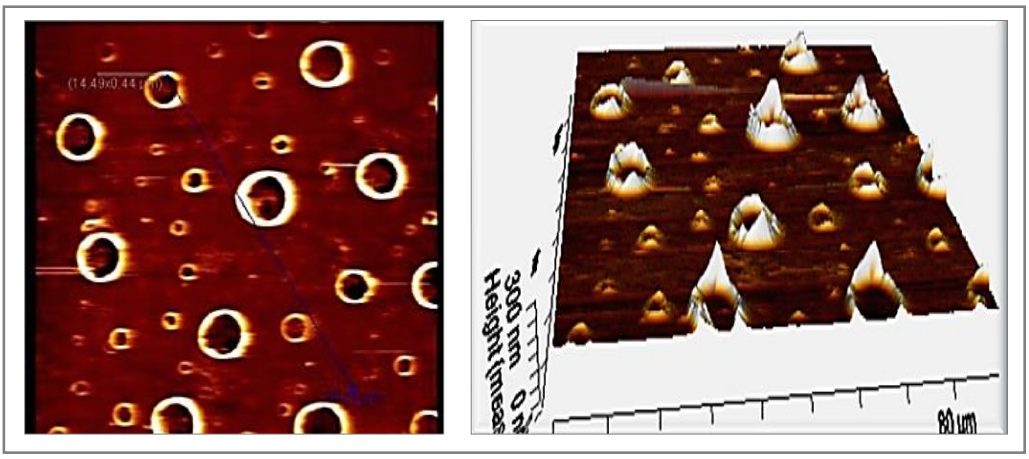

Image 4.1.2: AFM surface characterizations revealing crater like surface imperfections primarily on the hydrophobic regions of the chemically structured slide surfaces: (left) 2D view, (right) 3D view: craters with peak like projections at their edges

Additionally, the surfaces were scanned to determine the presence of any distinct step at the hydrophobic-hydrophilic interface (of the chemically structures surfaces), which if present might presumably serve as a region for gas (bubble) entrapment leading to bubble evolutions at elevated system temperatures. AFM scans however revealed no distinct step at this juncture, as can be referred to the images 4.1.3 below, hinting in turn strongly towards the homogeneity of the surfaces (cleanings/coatings applied).

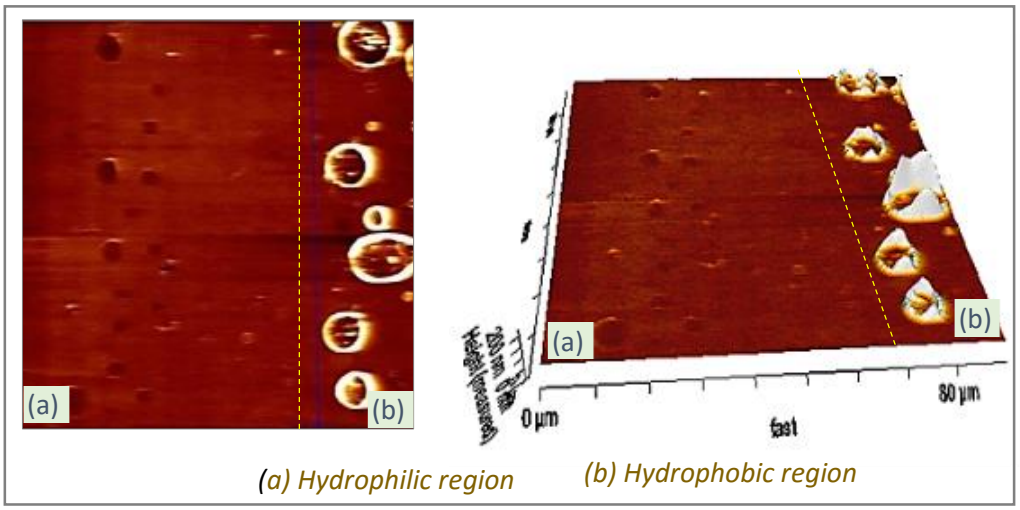

Image 4.1.3: AFM scans revealing presence of crater like structures on the hydrophobic regions than on the hydrophilic regions on the chemically structured slide surface, (left) 2D view, (right) 3D view

Electron microscopy: Scanning electron microscopy (SEM)[189-190]

To further confirm the above findings, the 'thought to be infected' surfaces were characterized using Scanning Electron Microscopy (SEM)-the technique known to be capable of revealing details less than 1nm in size. However, unlike AFM, SEM has been reported to work best for conductive rather than non-conductive surfaces- thereby hindering glass slides (non-conductive) to be directly taken for such investigations. Besides, conductive coating of the to be investigated chemically structured surfaces might alter/ layer their surface chemistries, potentially leading to an inappropriate analysis- thus making it not to be a very effective measure to be employed for such examinations.

Hence, in this regard, silane wafers were utilized- the conductive surfaces being chemically structured (fabricate with alternate hydrophobic/hydrophilic regions) by employing adequate surface chemistries, in a similar fashion as for the production of the chemically structured (AG) glass slides. For various of such surfaces produced, some of them when examined under standard upright microscope, showed, accidentally, the presence of surface inhomogeneities- such surfaces being then later selected/taken for detailed SEM investigations.

Studies being conducted at the Deutsches Museum SEM Lab, Munich, Germany (using LEO 440i SEM from Zeiss), scans of the opted surfaces (potentially infected, chemically structured, silane wafers) revealed, as previously in the AFM investigations, the presence of crater like inhomogeneities, being particularly yet again observed on the hydrophobic regions of the chemically structured silane wafers. Additionally, anew, no distinct step at the hydrophobic-hydrophilic interface was identified, excluding it to be the possible prime contributor to the bubble evolution phenomenon- not to mention the findings once again confirming the homogeneity of surfaces and the cleaning/coatings applied (refer image 4.1.4).

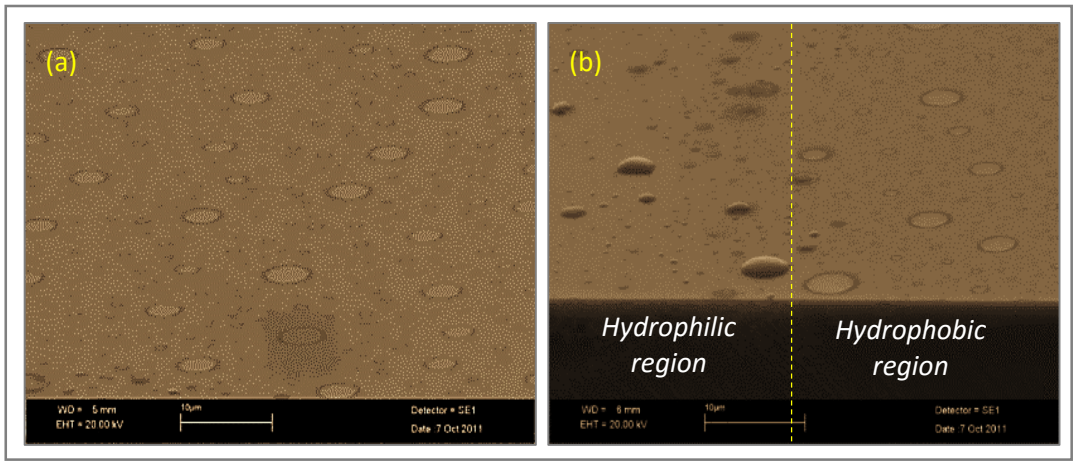

Image 4.1.4: SEM surface characterization of chemically stratified silicon surfaces, revealing (a) crater like structures on hydrophobic regions (appearing slightly flattened owing to 67° tilt between the sample and the sample holder), (b) absence of such structures (not to be confused with water residues) on the hydrophilic regions

Further, as for the AFM images, analysis of the SEM scans using appropriate graphics editor program as Paint.Net, yielded the diameters of the observed structured to be in the range of 2-8 microns— the values being in analogy with the AFM outcomes.

Optical microscopy: Reflection Interference Contrast Microscopy (RICM)[191-192]

On similar lines as the above, the opted, 'thought to be infected' surfaces (chemically structured glass slides in this case) were finally characterized using Reflection Interference Contrast Microscopy (RICM) - the technique based on the utilization of polarized light to form an image of an object on the glass surfaces (from the interference pattern produced by light reflecting from both the object and the surface).

Investigations in this regard were conducted at the University of medicine Mannheim, Experimental Dermatology Medical Faculty, Heidelberg University, Mannheim; the studies conducted using the microscope: Zeiss Axio Observed Z.1 equipped with 63-fold/1, 25 Plan-Neofluar Antiflex objective and Colibri LED system capable of performing (fluorescence) and RICM investigations. Image acquisition and analysis was further performed using MrM AxioCam and Axio Vision softwares respectively (both at Carl Zeiss AG, Oberkochen, Germany).

Again, nearly 10 of such surfaces being investigated, RICM results synced with the earlier findings: the presence of crater like surface inhomogeneities observed mainly on the hydrophobic regions of the tested, chemically stratified slide surfaces -as can be seen in the image 4.1.5 on the right.

Calculations (using image analysis software as Paint.Net) further revealed typical dimeters of these structures to be in the range of 3-4 µm, though some having diameters in the range of 7-10 µm were as well detected --the values being however in sync with the ones obtained from the previous microscopic analyses.

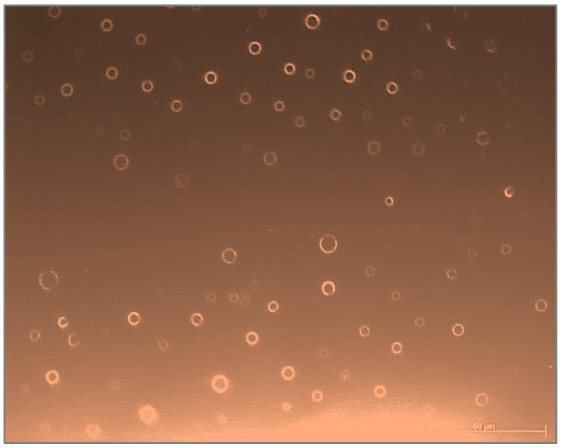

Image 4.1.5: RICM surface characterization of chemically structured surfaces revealing similar crater like structures of average diameters between 3-4 microns.

Microscopic Investigations: Conclusions

From the above microscopic investigations, it can be hence primarily concluded that the potential source of bubble formations (at elevated system temperatures) could be some surface inhomogeneities, identified as crater like imperfections on some of the (rare, random) slide surfaces. However, such inhomogeneities being largely detected on the hydrophobic regions of the chemically structured surfaces, a possible origin to such imperfections, could

be some left over coating (silane) residues– which probably were accidentally missed out being washed away, say in the second cleaning (post-coating) of such surfaces.

Further, to check on the above and to determine the exact production step (if) responsible to be causing such defects, microscopic (AFM) investigations were done where the slide surfaces were examined after each cleaning/coating fabrication stage. With minimum of ten, randomly selected surfaces being selected (from the production lots) and tested per case, studies nevertheless failed in filtering out a distinct fabrication step being potentially responsible in the generation of such surface imperfections. However, acknowledging that possibly 'unflawed' surfaces were tested (keeping in mind the rarity of bubble evolutions in general), the above called for further similar and/or other investigations for the determination of the source of such rare surface defects. In any case, the above further confirmed the good quality of coatings/cleanings applied, and of the surfaces produced.

Additionally, for the surface inhomogeneities detected by the microscopic investigations on the 'possibly infected', rare surfaces, calculations (via Paint.Net on the scans) revealed such structures to typically have diameters between 2-10 μm, inner depths between 2-4 nm, and heights (of the distinct peak like projections at their edges) in the range between 10-200 nm. However, in-depth examinations of a surface inhomogeneity of above dimensions trapping gas and the conditions of bubble formation from it, will be dealt with in the next chapter, titled, bubble dynamics.

4.1.2 Contact angle studies

Apart from the microscopic investigations, as discussed above, to further determine the degree of wettabilities and homogeneities associated with the produced surfaces and possibly the exact source (say a particular fabrication stage) of the rare surface inhomogeneities detected, the surfaces were further analyzed using an important characterization technique -the contact angle (CA) investigations. The technique being basically based on the utilization of the contact angle information of the liquid on the surface under scrutiny, enables in determining the character of the latter – details into it being as discussed in the sub-sections below.

Introduction

Wettability, the ability to which the surface can be covered with water or other liquid(s), has been reported to mark as an important property in defining the underlying solid. A dispensed drop might bead up or spread depending on its interaction with the underlying surface and the balance of forces acting upon it-- for the magnitude of cohesive forces (forces between the liquid-liquid (like) molecules) greater than the adhesive forces (forces between the liquid-solid (unlike) molecules) beading of the droplets taking place, whereas their spreading for the other way around [15,193-196].

Mathematically, for a drop resting on a solid surface, if a tangent be drawn at the triple contact point where the three phases viz. the solid phase, the liquid phase, and the gas phase meet, wetting or contact angle (θ) can be defined as the angle (measured through the denser phase) the tangents to the planes of two intersecting interfaces make at their interesting line. For zero CA, the droplet is said to completely wet the surface, while for θ=180° complete non-wetting is said to take place. These cases being typically hard to realize, CA has been reported to usually belong to any of the partial wetting regimes between the above two extremes. Normally, for θ > 90°, the contact is classified as hydrophobic (liquid-liquid cohesive forces being dominant) and as hydrophilic for θ < 90° (solid-liquid adhesive forces being dominant)[15].

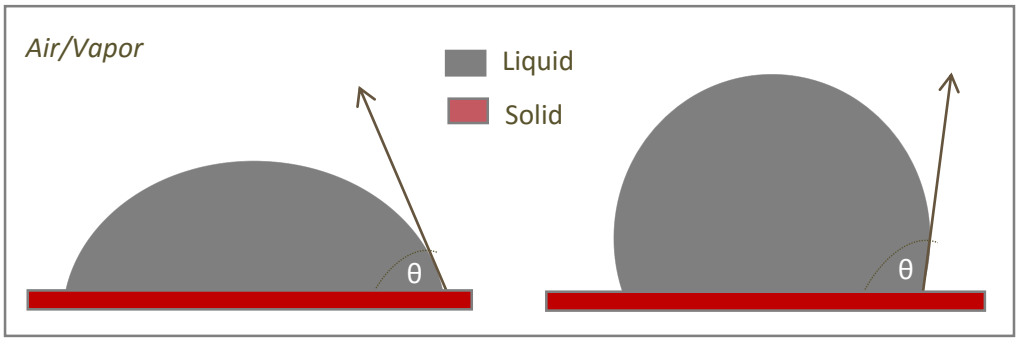

Figure 4.1.1: (a) Hydrophilic behaviour of liquid (water) droplet for CA < 90° (b) Hydrophobic behaviour of liquid (water) droplet for CA > 90°

Thermodynamic considerations

T. Young was the first to describe CA equilibrium in 1805 [15] - CA being thermodynamically defined by the well-known Young-Laplace equation. A drop resting on a solid surface in thermodynamic equilibrium is said to be subjected to various surface tension or surface energy forces, typically being the solid-liquid surface tension (γ_{SL}), the solid-vapour surface tension (γ_{SV}), and the liquid-vapour surface tension (γ_{LV}), as depicted in the figure 4.1.2. below.

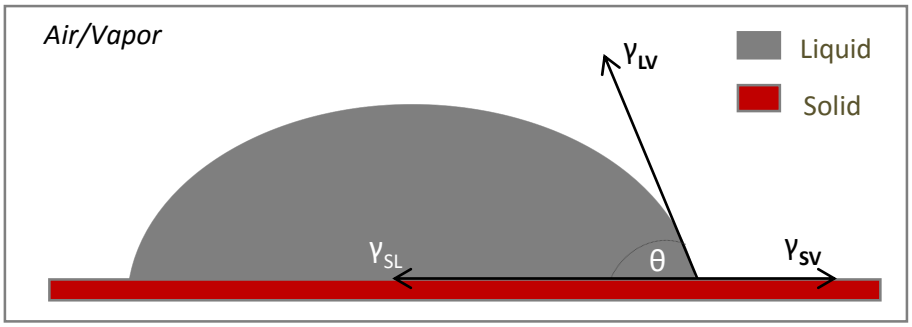

Figure 4.1.2: Image depicting various forces acting on a liquid drop resting on a solid surface

Since in equilibrium, the resultant forces must be zero, using appropriate co-ordinate system, the Young-Laplace equation[15,196] was developed, as depicted in equation 4.1.1 below:

$$\text{Cos } \theta = \frac{\gamma_{SG} - \gamma_{SL}}{\gamma_{LG}} \qquad (4.1.1)$$

where γ_{LG}, $\gamma_{SG,}$ and γ_{SL} are the liquid-gas, solid-gas, and solid-liquid surface tensions respectively. The equation 4.1.1. marks as an important relation in the contact angle studies, enabling the determination of any of the associated parameters, provided the other three variables are known.

Furthermore, CA investigations can be broadly categorized into static and dynamic contact angle studies- measurements being made on the liquid drop at rest (on the solid surface) or in the static state for the former case, and on the liquid in motion (advancing/receding on the solid surface) or in the dynamic state for the latter case- as detailed next.

Static contact angle: Introduction[193,196]

As the name suggests, static contact angle refers to the angle made by the liquid drop resting on a solid surface in an equilibrium or a non-moving state- such droplets being as well referred to as sessile droplets (adhering to the solid surface forming a spherical cap geometry) sometimes. For static drops, ideally the drop's volume and size do not alter during the measurements, though the values might fluctuate due to effects such as evaporation of the droplet with time, migration of substances dissolved within the drop to the solid surface (or in the opposite direction) in some cases, chemical reactions between the solid and the liquid, and/or the solid being dissolved/swollen by the liquid- leading to an increase or decrease of the contact angle with time. Of the above, micro-droplets have been reported to be the most vulnerable to evaporation effects- such effects being predominant for aqueous liquids with comparative lower boiling points than for say organic liquids (like oils) with boiling points typically greater than 200°C. Thus, as can be seen in the figure 4.1.3., evaporation, if left unchecked, could lead to inaccurate contact angle measurements- 'θ_2' being measured instead of 'θ_1', thereby raising the likelihood of erroneous analysis.

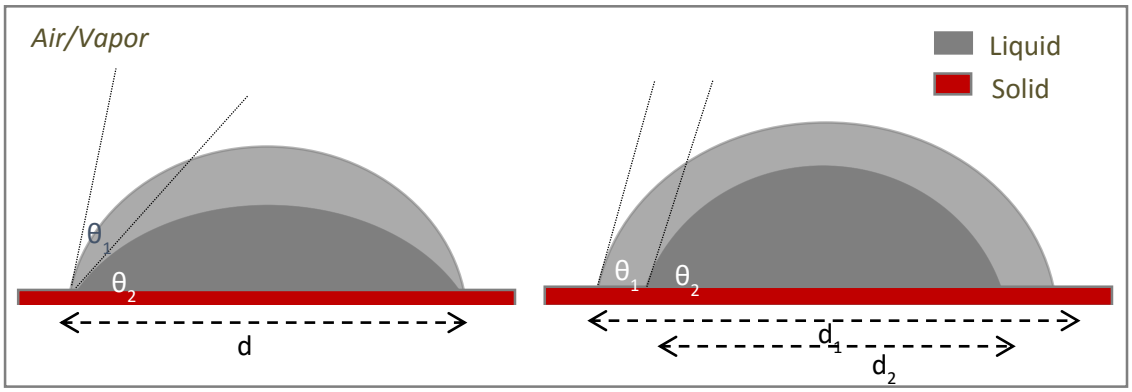

Figure 4.1.3: The two schemes for sessile droplet evaporation depending on the wettability of the underlying surface (a) droplet pinned on a chemically structured surface (as AG slide), (b) droplet on a chemically homogenous (as PFS slide)[15]

One way of minimizing evaporation effects, especially for say static contact angle studies of the aqueous liquids, could be by analyzing the 'frozen' state of the droplet instead of the live drop- details into it being taken up in the next sub-sections.

Literature further reports various methods for the measurement of static contact angles- of them primarily adopted being the drop shape analysis method, the Wilhelmy plate method, the Washburn method, and the top-view distance method. The current work, however, among all of the above, employs the drop shape analysis method for static contact angle measurements- principally owing to its ease of availability and operation-- the method being essentially based on the utilization of the sessile drop's image at the three phase contact (point of intersection between the drop contour and the projection of the surface (baseline)) for contact angle measurements.

Static contact angle: Measuring technique[193,196]

The prime system requirement for conducting static contact angle measurements employing the drop shape analysis method is usually a video based optical measuring device- as the OCA measuring device from Dataphysics[197] used in the current work. Reportedly have been known to be the most versatile instrument for the measurement and analysis of contact angles and the drop shapes, the OCA measuring set-up marked with its primary components, can be as referred to in the image 4.1.6. below.

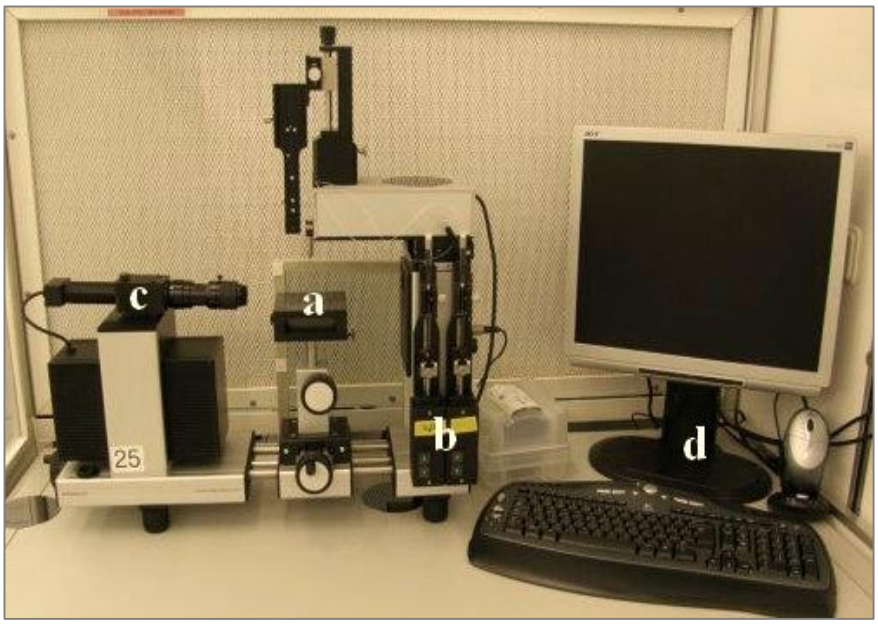

*Image 4.1.6: Contact angle (OCA) measuring set from DataPhysics [197] (a) measuring stage (100*100mm) adjustable in three axes for accurate sample positioning and drop pick up from the dosing unit, (b) dosing bay for installation of the optical manual syringe units and single or multiple (max.4) needle support with a vertical and horizontal fine adjustment, (c) goniometer attached to the CCD camera, and (d) a PC connected to the system to analyze the results*

In addition to the above, few other components that the set-up comprised of, were: a lens mount with an adjustable tilt, a high speed video system with an adapter and a CCD camera, a high performance six-fold power zoom lens with an integrated continuous focus, and a halogen light source with continuously adjustable intensity without hysteresis for a homogeneous back lighting.

Coming next to the measuring technique, to begin with, the OCA system was turned on and the position of the measuring table and the camera adjusted so as to be exactly in a horizontal plane with respect to each other. A sample surface was then placed on the measuring table, atop of which was dispensed, either via automated (say using dosing syringes of OCA's dosing system) or by manual (say using Eppendorf multi-pipettes) means, a test drop (usually 1µL of water being typically opted), whose contact angle has to be measured. Automated dispensing being generally chosen for aqueous liquids and manual pipetting being typically preferred for more viscous fluids (as oils), in any case, the syringes while loading of the liquids were filled slowly as to ensure no air withdrawal, which otherwise might inject unwanted air bubbles into the system-possibly serving as 'seeds' for bubble nucleations at elevated working temperatures. Further, the syringes internal diameter was fed to the software for the calibration of the pump, and dosing rates usually in the range of 0.3-0.5µL/s adopted (except for more viscous fluids requiring comparatively much slower pumping rates to accommodate the pressure drop across the needle). Additionally, it was made sure that while being dispensed, the droplets fall as little as possible as to avoid their spread by kinetic energy[279]. This was typically achieved by positioning the droplets tip above the underlying solid surface at such a height that the growing pendant drop touched the surface and detached itself before it fell free of its own weight (image 4.1.7 (a)). Once dispensed, the dosing needle was drawn out, forming a sessile drop (image 4.1.7. (b).

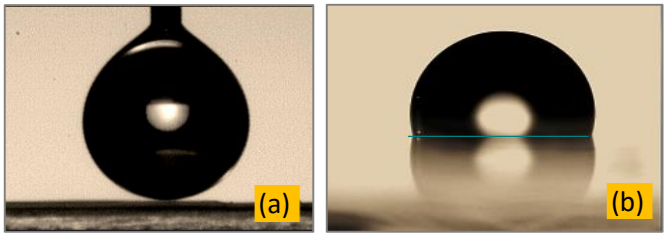

Image 4.1.7: (a) Droplets tip positioned above the solid surface such that it detaches itself before falling of its own weight (forming a sessile droplet); (b) 'Frozen' drops image with baseline (blue line) adjusted correctly for accurate static CA measurements[279]

By focusing the droplet and adjusting the back lightening, the system was subsequently calibrated using the optical magnification of the lens – the overall set-up being finally ready for the measurements[197,279].

After the above initial preparations, without disturbing the rest of the set-up, the dummy (sample) test slide was replaced by the to be investigated surface with a new drop of test liquid (1µL DI water) dispensed (typically by automated means) above it. However, as previously stated, to minimize evaporation effects and hence inaccurate static contact angle measurements, a quick snapshot of the drop's profile as soon as it was formed was captured (via the OCA's software)- static CA being measured on this 'frozen' image instead of on the live drop. Besides, another criterion important for these measurements was the right

adjustment of the baseline to the drops image, marking the position to which the software draws a tangent for contact angle measurements (refer image 4.1.7 (b))-which if misaligned could lead to 'false' contact angle values and hence erroneous results [197,279].

After the drop's image is captured and a baseline to it adjusted, the static contact angle was calculated by the measuring software by fitting a mathematical expression to the drop's contour- the mathematical fitting computing the slope of the tangent at the liquid-solid-vapor (LSV) line interface. Further, depending on the choice of the mathematical model adopted (from a variety of models available), various fitting methods can be defined, primarily as the Young-Laplace (Y-L) fitting method, the tangent fitting method, the height-width fitting method, the elliptical fitting method, and the circle fitting method. The methods compute either the complete drop´s shape or a part of it or only the area of the phase contact- all the methods nevertheless calculating contact angle as 'tan θ' at the intersection of the drop's contour line with the solid surface (or the base line) [194,197].

The selection of the fitting method further depending largely on the nature of measurements, the type of solid and liquids opted, and the volumes of the liquids selected[194], initial experimental investigations revealed Young-Laplace fitting to be the most reliable method in calculating static contact angles on drops for the solid-liquid combinations and the volumetric range of test liquids as opted in the current work (refer Appendix D for further details).

Static contact angle: Experimental investigations

Using the experimental set-up and the measuring technique as described in the sections above, a number of static contact angle related experimental studies were carried out to determine the degree of wettabilities and homogeneities associated with the various surfaces-produced say using different substrate materials, different coating techniques, different cleaning methods, and being stored under different conditions post-production-- in addition during the course of investigations to possibly determine the production stage (if) responsible for contaminating the surfaces with the rare defects (as observed under microscopic examinations).

a. Study of surfaces with varying wettabilities

As modification of surfaces to generate (alternate) hydrophobic/hydrophilic regions serves as an integral part of the surface fabrication process in the current work, static contact angle studies were conducted to determine the degree of wettabilities and homogeneities associated with the chemically treated surfaces –CA's < 90°, as stated, implying hydrophilic character of the surfaces, whereas surfaces said to be exhibiting a hydrophilic character for > 90° CA values. Additionally, greater the consistency and reliability in the contact angle data, higher can be said to be the degree of homogeneity associated with the tested surface /region - the surfaces in such cases being devoid of any prominent pinning centers possibly altering the shape of the dispensed droplet and hence the corresponding CA's.

In this regard, various surfaces were examined- static CA's being measured anywhere on the chemically non- structured (PFS coated glass slides) surfaces, and on the hydrophobic regions (between four reaction sites) and the hydrophilic regions (top and bottom slide edges) for the chemically structured (AG) slide surfaces. Minimum of six surfaces being examined per case, with CA's of at least ten droplets (DI water) being measured per surface, the data was analyzed for evaluating the averages and standard deviations of the contact angles collected (via Microsoft Excel 2016) - results depicted as in the respective graphs 4.1.1 and 4.1.2 below:

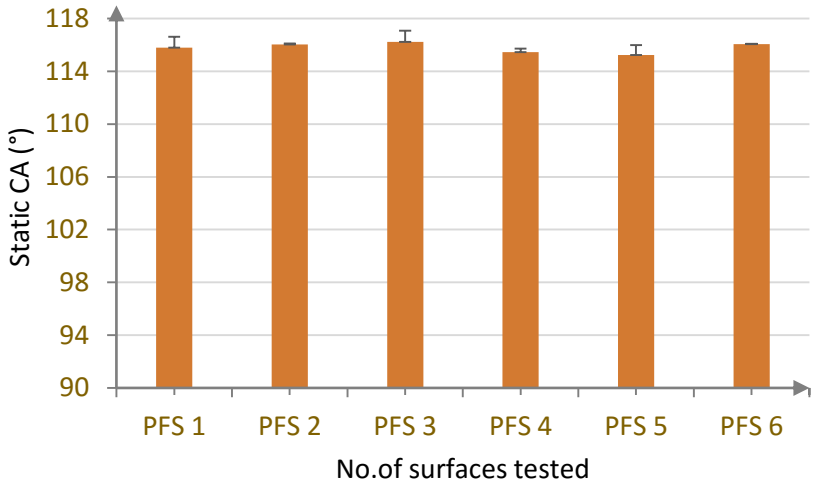

Graph 4.1.1: Static CA measurements on the chemically non-structured (hydrophobically coated, PFS) slide surfaces

As can be seen in the graphs 4.1.1 and 4.1.2, the hydrophobic regions, be it on the chemically non-stratified PFS slide or on the structured AG slide surfaces (for the same typing of coating procedure applied), yielded average static CA's to be approx. 115°- the values being greater than 90° signifying the hydrophobic character associated with such surfaces/regions. Measurements further gave standard deviations to be less than 2° for the CA data obtained per case (surface tested) on these regions- low values thus indicating the consistency and reliability of the measurements and hence good homogeneity of the surfaces produced/coatings applied.

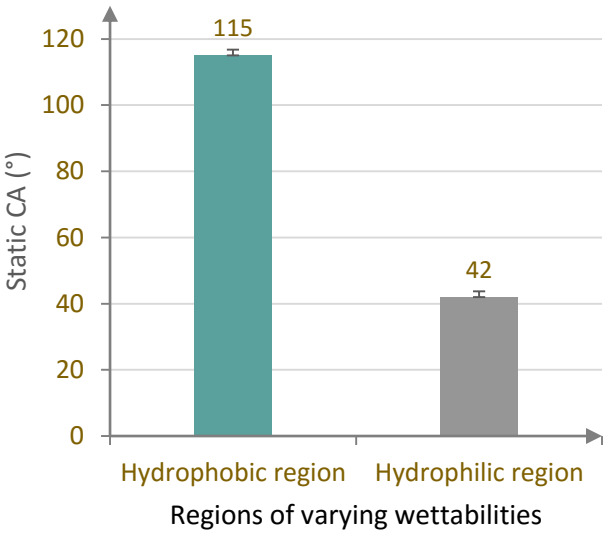

Graph 4.1.2: Static CA measurements on the chemically structured (AG) glass slides

On similar lines, measurements yielded static CA's of ~42° (with standard deviations<2°) for the hydrophilic regions of the chemically stratified (AG) slide surfaces- the values indicating the hydrophilicity associated with such regions and the homogeneity of the surfaces, respectively.

Hence, from all of the above, it can be said that the surfaces produced, as the chemically-structured AG glass slides usually dealt with in the current work, have in general good wettabilities and homogeneities associated with them - the surfaces being typically devoid of any prominent inhomogeneities (pining centers modifying the drop shapes and hence the static contact angles), which possibly might act as gas entrapment sites leading to bubble evolutions at elevated working temperatures.

b. Study of surfaces generated using different coating techniques

Another investigation that was done was by testing surfaces produced using different (hydrophobic) coating techniques- to determine if a particular technique generates surfaces with superior wettabilities and/or homogeneities as compared to the other.

In this regard, the hydrophobic surfaces, primarily produced using the conventional chemical (lithography or gas phase silanization (GPS)) technique and the state- of -the -art mechanical printing technique were examined; static CA's being measured in the manner as described earlier using 1µL of DI water as the test liquid dispensed on the subsequent surfaces.

Chiefly hydrophobic surfaces (PFS coated glass slides and hydrophobic regions for the chemically structured AG glass slides) being tested, with at least six surfaces being examined per case, measurements revealed (refer graph 4.1.3 on the right) average static CA's of nearly 116° (s. d~1.2°) on the chemically coated surfaces and of nearly120° (s. d~1.8°) on the mechanically coated surfaces- thereby indicating higher hydrophobicities associated with the surfaces generated using the latter coating technique. Additionally, lower standard deviations for the CA's obtained per case pointed out to the reliability and consistency in the measurements, revealing the absence of any prominent pinning centers (possibly altering the shape of the measured drop) and hence good homogeneities associated with the examined surfaces.

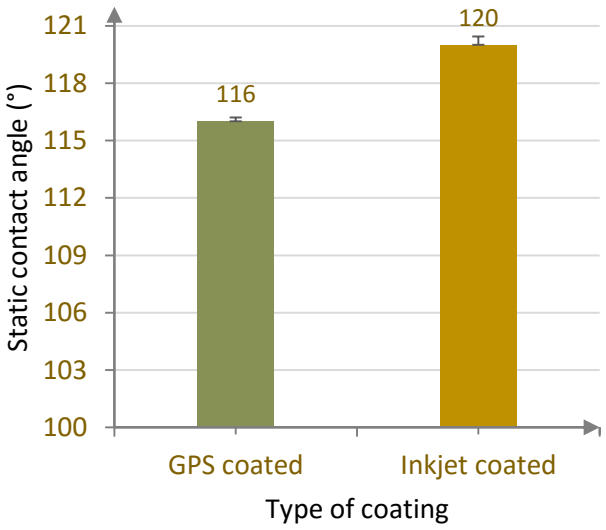

Graph 4.1.3: Static CA measurements for (chemically non-structured) surfaces produced using different coating techniques

Nevertheless, despite of not so much differences in the wettabilities and homogeneities of the surfaces generated using the above techniques, mechanical coating is typically employed for the production of chemically treated surfaces- both for industrial as well as research oriented applications (as in the current work). This can be primarily attributed to the faster coating speeds associated with the mechanical printing- with the potential to coat the entire production lot in one go, within few hours. However, for instances, where (when and if) lithography has been employed as the coating technique, will be explicitly mentioned as the work proceeds.

c. Study of surfaces generated using different substrate materials

Apart from the above, static CA studies were conducted to examine and compare the wettabilities and homogeneities associated with the surfaces generated using different substrate(base) materials- glass slides and silicon wafers being mainly opted in this regard.

The surfaces being fabricated in the standard manner as described in the earlier sections, measurements revealed slightly lower static CA's for the generated hydrophobic and hydrophilic regions on the silicon wafers than on glass slides (refer graph 4.1.4).

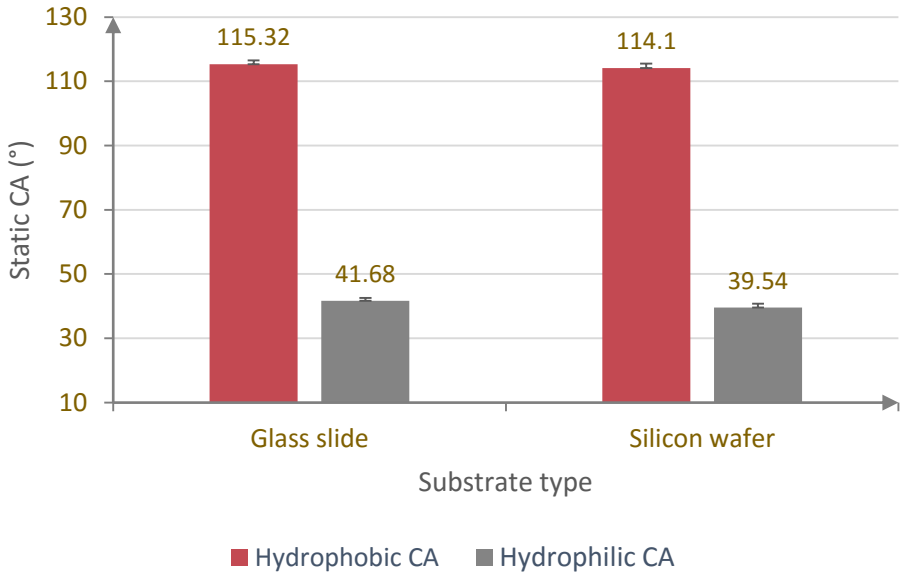

Graph 4.1.4: Static CA studies on the hydrophilic, hydrophobic regions of surfaces generated using different substrate material

Nevertheless, lower standard deviations obtained for the average of CA's for the cases studied, further indicated good homogeneities and wettabilities associated with the fabricated surfaces- the finding in turn referring to the efficacy of the fabrication techniques employed, and to no prominent role of the (otherwise good quality) base material itself in the generation of surface defects.

However, glass slides, owing to their ease of availability and low purchasing costs, are typically preferred as the substrate materials- both for industrial and research based applications, as in the current work.

d. Study of surfaces subjected to different cleanings

A vital step in the generation of the chemically fabricated surfaces is their second cleaning - employed to ensure the removal of any left-over coating residues, post-coating of the resultant surfaces. Typically, being done by dipping the ensuing surfaces in an ultrasonic bath, for around 30 minutes, this cleaning usually utilizes reagents that are milder in nature and concentrations (as to be not harsh on the surface coatings), as compared to the chemicals used for first cleaning (pre-coating) purposes.

In order to determine the efficacy of the above production stage and to check if it contributes to the occurrence of any surface defects (due to say missed out washing of some of the coating residues), the subsequent surfaces (hydrophobic and hydrophilic regions of the chemically structured glass slides) were examined for their homogeneities and wettabilities via static CA studies (using 1µL of DI water as the test liquid). Further, apart from the ultrasonic cleaning, other cleaning methods were as well tried out as the plasma and HCl-methanol (in volumetric ratio of 1:1) cleaning- the surfaces being dipped in the respective cleaning chambers (in a clean room environment) again for around 30 minutes and next examined and compared for their topologies via static contact angle measurements.

With minimum of ten measurements being made per surface, and nearly ten surfaces being examined per case, analysis revealed:

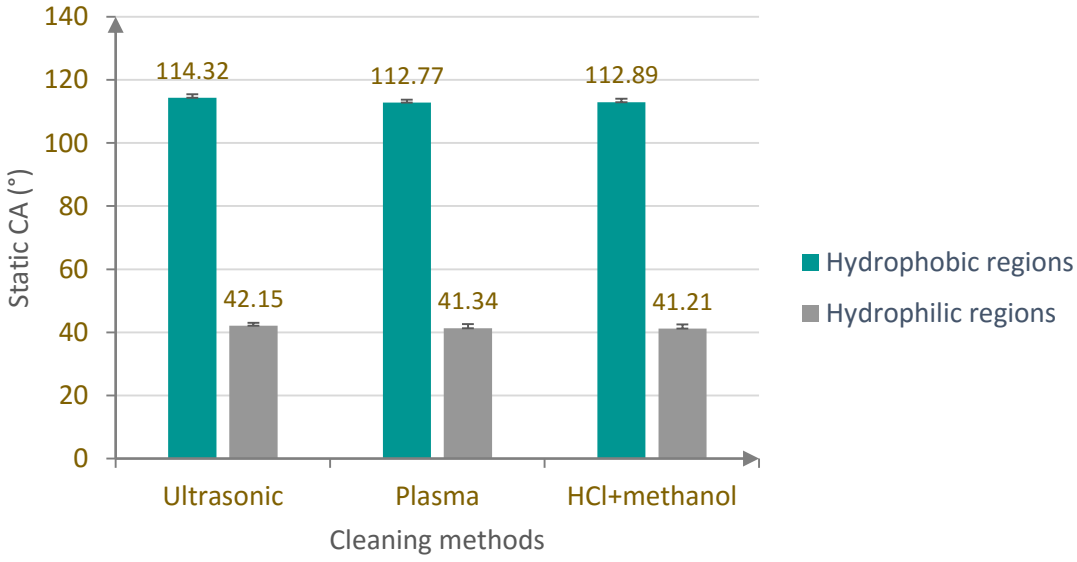

Graph 4.1.5: Static CA studies of surfaces (PFS coated) generated via various surface cleaning techniques (pre- coating)

As can be seen in the graph 4.1.5 above, examinations revealed no drastic differences in the (average) static CA's for the surfaces cleaned via the above cleaning procedures- ultrasonic cleaning nevertheless yielding (hydrophobic) surfaces with slightly higher CA's as compared to the other tested techniques.

The above findings, together with the lower standard deviations observed (per case), further pointed towards the good wettabilities and homogeneities associated with the fabricated surfaces- indicating in turn the good quality of cleanings applied in general. However, ultrasonic cleaning, owing to it being the commonly used technique in the industrial production of the slide surfaces, as for the chemically structured AG slides under consideration, has been adopted as the generally used method for research based applications too, as preferred in the current work.

e. Study of surfaces subjected to different storage conditions

The surfaces, post-production and pre-delivery, are generally stored in an air tight, dust-free, environment- being placed in clean plastic boxes and kept further under vacuum in aluminum packets. However, despite of the extreme care taken in protecting the sensitive surfaces from any contaminations, chances might be that storage alters their surface chemistries, possibly modifying the homogeneities and wettabilities associated with them.

Hence, in this regard, static CA studies (using 1µL of DI water) were conducted to determine the topologies of various surfaces (hydrophobic and hydrophilic regions of the chemically stratified glass slides) stored over say a 'n' number of days. Further, each of the above examinations were tailed by analyzing the subsequent surfaces after having them cleaned gently using a tissue dipped in Isopropyl Alcohol (IPA), followed by a good rinse in water and drying off the water residues via a nitrogen gas- comparative studies being made by analyzing freshly prepared surfaces in addition.

With minimum of ten measurements being made per region, and nearly ten surfaces being examined per case, results revealed, as can be seen in the graph 4.1.6 on the next page, freshly prepared surfaces to be exhibiting the most consistent and reliable static CA values as compared to the data observed for the stored surfaces – especially for the ones stored over a period of six or more months. Further, gentle cleaning (using IPA, water, and nitrogen) of the surfaces prior to examinations, as expected, seemingly improved their homogeneities- seen as slightly improved wettabilities (especially for the hydrophobic regions) and reduced standard deviations in the average of measurements for such cases.

Hence, from the above it can be said that though freshly produced surfaces are the best to work with, storing of the surfaces, however, generally does not affect their topologies, unless done for say a period of more than six months or so (in some of the cases). In any case, especially for research oriented applications, it is always good to do a gentle cleaning (using IPA, water and nitrogen as discussed before), prior to the surfaces being taken for examinations/used.

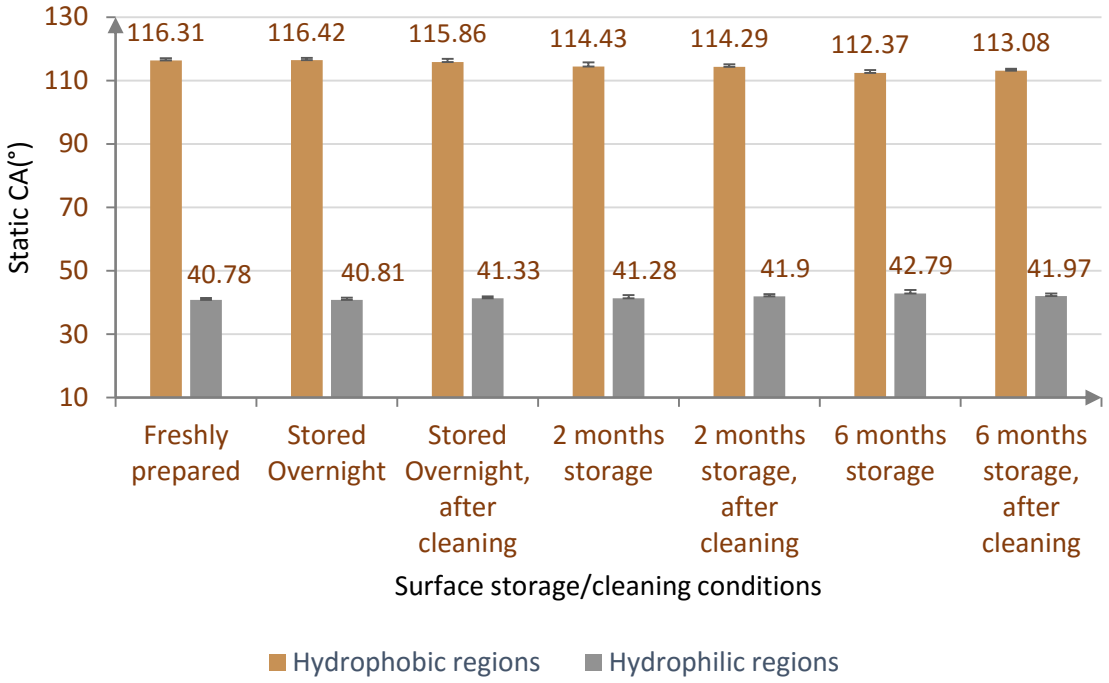

Graph 4.1.6: Static CA measurements on regions of varying wettabilities for surfaces stored for 'n' number of days, pre and post their cleaning

Static contact angle: Conclusions

Thus from the above static CA investigations, it can be said that the surfaces produced are generally homogeneous in nature with good degrees of wettabilities associated with them, thereby indicating the effectiveness of the coatings and cleanings applied in the fabrication of the same. Further, no production or post-production (storage) step could be particularly filtered out, potentially leaving the surfaces 'flawed' or infected (in terms of say the crater like inhomogeneities as detected on the hydrophobic regions for some of the slide surfaces in microscopic investigations).

Nevertheless, in regard to having greater homogeneities and wettabilities, freshly prepared surfaces came out as the most promising candidates- preferred hence largely for research oriented purposes, as in the current work. Yet surfaces, stored in a clean, air-tight environment proved to be not flawed either (except they being more vulnerable to contaminations if stored for say more than six months or so), thereby being equally successful in usage when coming to industrial applications.

However, in in order to complement the above investigations, equally important was the investigation of surfaces via dynamic CA studies- aimed to provide a better, overall insight into the surface topologies, as discussed next.

Dynamic contact angle: Introduction

Dynamic contact angle studies, together with the static CA measurements, mark as an important characterization technique for the comprehensive analysis of the underlying surfaces. Whereas static CA measurements help in determining the wetting properties of the solid by a certain liquid, it's the dynamic CA studies which have been known to better provide a detailed information on the homogeneity of the underlying solid substrate(s).

Further, as the name suggests, dynamic contact angle measurements are 'dynamic' in nature where the liquid drop is first made to fall or advance on the solid substrate, and withdrawn or receded subsequently. Hence, dynamic CA's are better measured 'live' as the liquid falls/recedes, in contrary to on the 'frozen' state of droplets, as for the static CA studies, as previously discussed [193,196,197].

Next, for the falling and receding droplet cases, dynamic contact angle measurements are characterized typically by two contact angle values, known as the advancing and receding contact angles respectively. Describing the former, the liquid once fully advanced on the solid surface, a part of it still attached to the dispensing unit, forms an angle between the tangent drawn to the liquid drop and the solid surface- for the maximum possible contact between the above two phases, the angle known as the advancing contact angle, denoted by 'θ_a'. However, for the latter case, after the advancing contact angle is formed and its value noted, with the needle still in the drop, the liquid is withdrawn back into the dispensing unit, till a minimum limit is reached where the liquid just contacts the minimum surface area possible without being completely sucked back- the angle formed at this stage then known as the receding contact angle, denoted by 'θ_r' –- the cases as depicted in the figure 4.1.4 below:

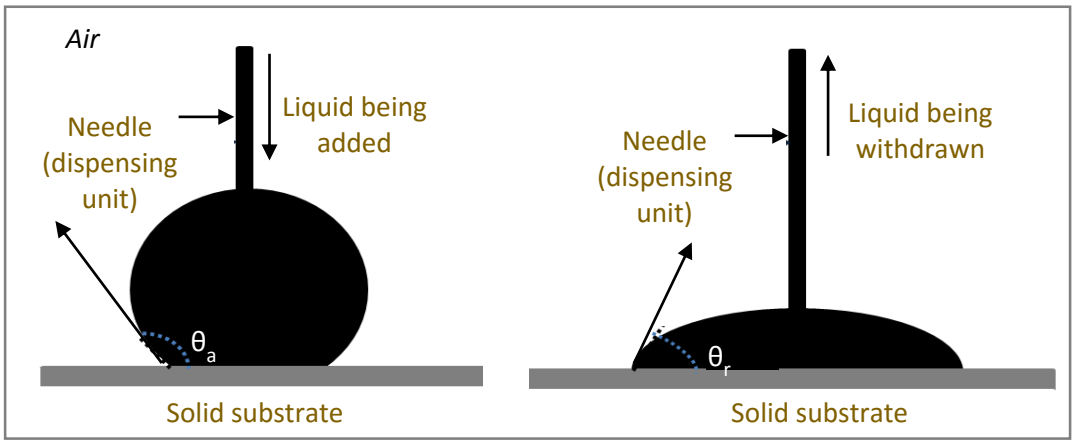

Figure 4.1.4: Illustrative representation of advancing and receding CA's [195](images not up to scale)

Additionally, the difference between the advancing and the receding CA is known as the contact angle hysteresis (δ)[193,281], serving as in important parameter in determining the degree of homogeneity associated with the underlying solid surfaces. Literature reports the occurrence of this hysteresis owing to the system under investigation not meeting ideal

conditions, as being chemically homogenous, rigid and flat at an atomic scale, and say not perturbed by chemical interaction or by vapour or liquid adsorption[199]. For such an 'ideal' surface wet by a 'pure' liquid, contact angle theory predicts typically one and only one thermodynamically stable value of contact angle. However, in reality, such an, 'ideal' surface is rarely found and there exists generally a wide range of 'metastable states' which can be observed as the liquid meniscus scans the surface at the solid-liquid-vapour interface. Due to the presence of free energy barriers that exist between these metastable states, thus a true 'equilibrium contact angle' is typically impossible to be measured in the real time. Therefore, the complete characterization of any solid surface necessitates the measurement of both advancing and receding contact angles and computing the difference as contact angle hysteresis[199]. Literature reports, on practical or non-ideal surfaces, the presence of contact angle hysteresis usually to be in the range of 10°-20°; values of and 50° or more being as well observed for some of the cases. Besides, higher the value of the hysteresis, greater is said to be the degree of roughness associated with the underlying surface- hence indicating the surfaces having lower hysteresis values to be more homogenous in nature.

Literature further reports six known sources of contact angle hysteresis, broadly categorized as the thermodynamic and kinetic hysteresis[199]. To qualify as 'true' or classical thermodynamic contact angle hysteresis, both advancing and receding contact angles must be stable (reproducible), i.e. regardless of time (time independent) or the number of measurements undertaken. Additionally, surface roughness and surface heterogeneity have been reported to be the two main causes of thermodynamic hysteresis, as summarized in the table 4.1.1 below:

General assumption	Specific assumption	Effect on hysteresis	Time dependent
Surface is smooth	Surface must be smooth at 0.1-0.5µm level	‚δ' increases with increasing roughness (θ_a increases and θ_r decreases with increasing roughness)	No
Surface is homogeneous	Surface must be homogenous at the 0.1µm level	θ_a dependent on low energy phase; θ_r dependent on high energy phase	No

Table 4.1.1: Sources of thermodynamic contact angle hysteresis[199-200]

In addition, as the Cassie-Baxter equation[193,196], helps in determining the degree of heterogeneity associated with a chemically structured surface, an important relation that describes the effect of surface roughness on contact angle hysteresis is the Wenzel equation[193,196] - which takes into account the influence of an increased 'effective' surface area on the contact angle, as stated in the equation 4.1.2 :

$$\text{Cos } \theta_w = r \cos \theta_y \qquad (4.1.2)$$

where 'r' is the roughness factor representing the ratio of effective area to the geometric area, 'θ_w' the Wenzel angle- the actual measured CA on rough surface, and 'θ_y' the stable or equilibrium Young angle as measured on a corresponding 'smooth' surface. The value of 'r' being typically always ≥ 1, the presence of surface roughness tends to increase the CA for 'θ_y' > 90° (i.e. for non-wettable, smooth surfaces), whereas decreasing the CA value for 'θ_y' < 90° (i.e. for wettable, smooth surfaces) [193,196].

From the Cassie –Baxter and Wenzel laws, it can be hence said that the surface under investigation may indeed exhibit a wide range of CA's, making it thus impossible to measure 'θ_w' and 'θ_c' different from any other 'θ'. However, a surface that exhibits CA hysteresis due to roughness or heterogeneity can be characterized by measuring the highest (advancing) and lowest (receding) CA values. Besides, keeping in mind the model of a heterogeneous surface, literature reports that whereas the advancing angle reflects the characteristics of the low-energy portion of the surface, the receding angle reflects the characteristics of the high-energy portion of the surface[193,194,196].

Additionally, apart from the surface roughness and surface heterogeneity, another commonly observed source of hysteresis that has been reported has been hysteresis due to surface contamination[196,199]. Solid surfaces usually tend to be contaminated with foreign substances during their formation or production. Even the liquids used for drop formations (test liquids) might as well contain foreign substances, possibly contaminating the underlying surface(s). Hence, the surfaces if not rigorously cleaned and/or the test liquids not properly purified before contact angle measurements, could lead to a larger hysteresis (an oily contaminant might lead to smaller receding contact angle owing to spreading of oil on the water surface). Thus, in order to minimize any hysteresis due to surface contaminations, it is made sure that the surfaces, especially if not fresh, are washed off properly with suitable solvents (which do not dissolve the solid but dissolve the possible contaminating materials), prior to any use[199].

Besides the above mentioned thermodynamic classification of contact angle hysteresis, literature as well reports its kinetic classification- distinguished from the former by time or cycle dependent changes in the contact angle values. Kinetic hysteresis, further, has been reported to be mainly caused by surface reorientation, surface deformation, liquid penetration, and surface mobility[199]. However, since rigid, solid surfaces are mainly dealt with in the current work, the work neglects the kinetic aspects and generally considers the thermodynamic aspects of the contact angle hysteresis[196,199].

Dynamic contact angle: Measuring technique[193,194,196,197]

For the measurement of dynamic CA's, various methods have been reported, commonly used being the optical tensiometry (goniometry) and/or the force tensiometry (Wilhelmy plate or the Du Noüy ring or the Washburn) methods [194]. The current work, however, employs the

former, the optical tensiometry or goniometry technique, chiefly owing to its ease of use and availability, and the possibility of dynamic contact angles to be measured via it using the same measuring device as for the static CA measurements-OCA from DataPhysics. Further, the basic principle behind the measurements (employing optical tensiometry) remaining the same: the shape of the drop determined and the corresponding contact angles calculated by assessing the angle formed between the solid and the tangent to the drops surface[197,198], the advancing and receding contact angles were evaluated in the manner, as described next.

For the advancing contact angle measurements, the liquid was first made to advance with the needle (of the dispensing unit) placed at a height sufficient enough for the free fall of the drop on the to be investigated solid surface(s). Via automated means and with a pre-defined advancing rate, the droplet was made to advance until it hit the solid surface- after this point additional liquid added till the droplets contact line got pinned and further advancing or increase in volume lead to distortion of its shape (bulging effect). At this point, the needle of the dispensing unit inside the droplet tending to distort it more at the apex, the advancing contact angle (θ_a) was hence measured (on the live drop by the high speed image capturing and analysing OCA instrument) before this point was reached[279].

Next, the droplet with the needle still inside it, was retreated with a selected receding rate- the receding rates opted being usually lower than the advancing rates for smooth withdrawing of the droplet (generally, if advancing rates selected were around 0.5µL/sec, receding rates of approx. 0.3µL/sec were adopted). Again while retreating, at the point where further suction of the liquid by the needle distorts the drops shape such that the contact angle cannot be measured, the minimum receding contact angle, θ_r, was measured.

Further, thin needles having comparatively lower (internal) diameters have been reported to be better suited for dynamic CA studies- as was experimentally tested and proven (refer Appendix C for further details).

Dynamic contact angle: Experimental investigations

Employing the measuring technique as discussed above, using DI water as the test liquid, various surfaces, as with static CA studies, were characterized to further determine their wettabilities and homogeneities using the dynamic CA studies. Additionally, owing to greater volumes of the test liquid used for dynamic CA measurements (as compared to nearly 1µL of DI water employed for static CA measurements), the hydrophilic regions of the chemically structured glass slides were skipped (greater volumes of water nearly spreading on such surfaces), and dynamic CA studies typically made on the hydrophobic surfaces (chemically non-structured, PFS coated) and/or the hydrophobic regions of the chemically structured (AG glass slides) surfaces.

With minimum of ten measurements being made per surface, and nearly ten surfaces being analysed per case, the data (advancing and receding CA values) were next analysed for the corresponding CA hysteresis using Microsoft Excel 2016- surfaces exhibiting lower and

consistent CA hysteresis were generally tagged to have higher degrees of surface homogeneities and vice-versa.

a. Study of surfaces having varying wettabilities

Dynamic CA measurements revealed, the hydrophobic regions/surfaces for the produced surfaces to be having (average) advancing CA's of nearly 120° and receding CA's of nearly 86°; dynamic CA hysteresis calculated to be around 34° for the various hydrophobically coated regions/surface tested. Further, the values observed were highly consistent and reliable in nature, with lower standard deviations (< 2°) being observed per case- as can be seen in the graph 4.1.7 below:

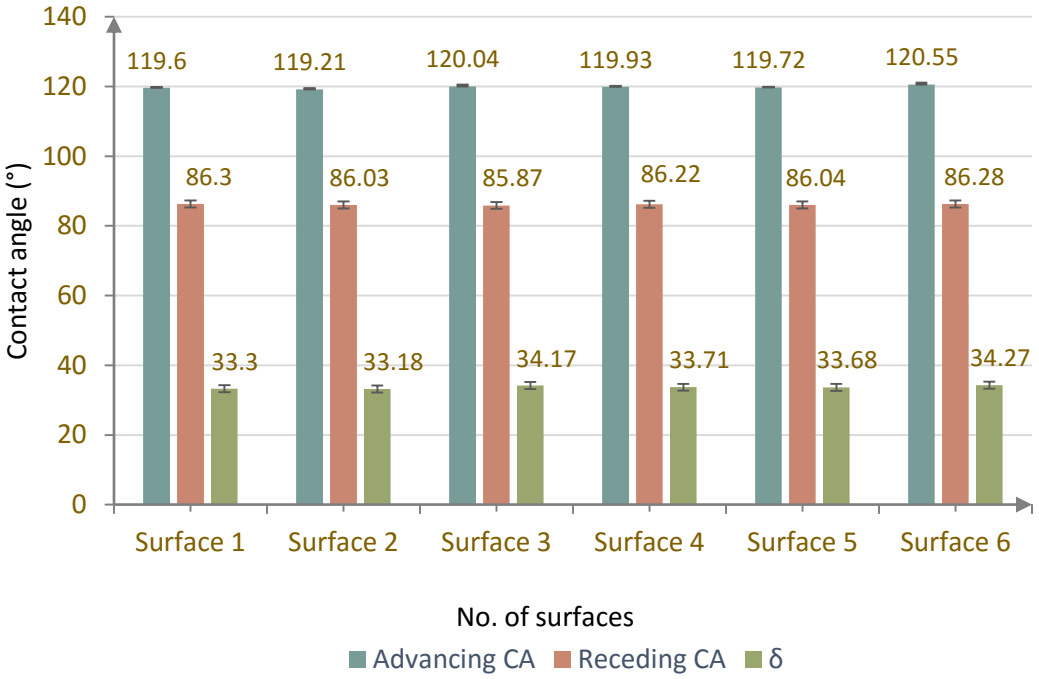

Graph 4.1.7: Dynamic CA measurements for chemically non-structured surfaces (hydrophobically coated PFS glass slides)

Hence, from the above it can be said that the surfaces generated are largely homogeneous in nature- the consistency in the measurements (lower standard deviations) further signifying no prominent pinning centres present, distorting the free movement of the advancing and receding liquid during measurements. This, in turn, indicates the efficiency of the fabrication(cleaning/coatings) applied in the production of such surfaces (as dealt with in the current work), further confirming the decent quality of surfaces generated on an average, and the rare occurrence of any surface defects (if and when present).

b. Study of surfaces generated using different coating techniques

Dynamic contact angle investigations, as with the static contact angle studies, were further conducted to determine the degrees of homogeneities associated with the surfaces, produced using different coating techniques.

In this regard, as previously discussed, surfaces primarily generated via the conventional, lithographic technique (chemical coating) and the contemporary, mechanical printing technique were tested – again chiefly hydrophobic surfaces/regions being analysed using DI water as the test liquid.

As can be seen in the graph 4.1.8, results revealed lower dynamic CA hysteresis (~30°) being observed for the mechanically coated surfaces, as compared to the hysteresis values obtained for the chemically coated surfaces (δ~34°). This, along with the lower standard deviations observed per case, indicated the greater proficiency of the former technique (relatively) over the latter in generating surfaces with better homogeneities- the results being in analogy with the findings of the static contact angle studies in this regard.

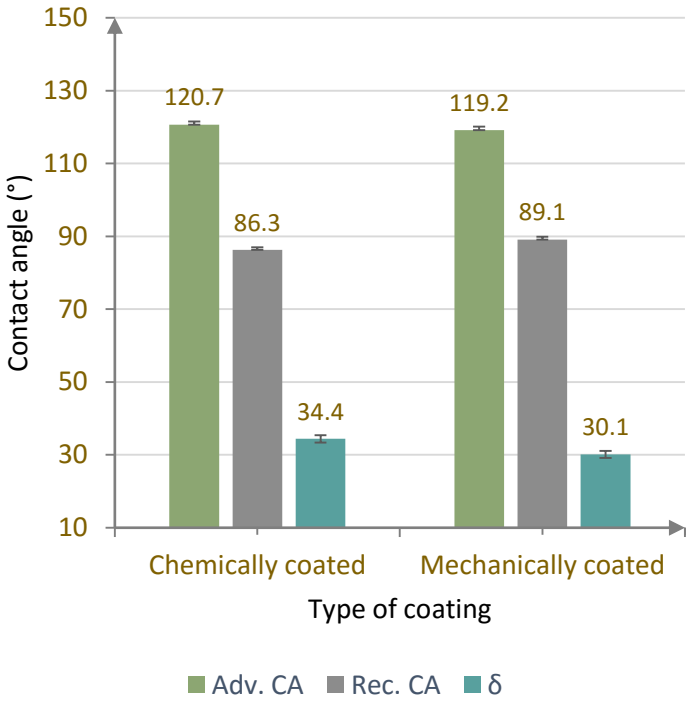

Graph 4.1.8: Dynamic CA studies for surfaces generated via various coating techniques

Nevertheless, the above analysis further confirmed the effectiveness of the coatings applied and the good quality of the surfaces fabricated on the whole- with no detectible contribution of this production stage in the introduction of any surface defects, in general.

c. Study of surfaces fabricated using different base materials

Again as with the static CA studies, dynamic CA investigations were done to analyse the surfaces for their homogeneities, produced using different base (substrate) materials.

Chemically treated glass slides and silicon wafers being chiefly opted in this regard, for their hydrophobic regions tested (using DI water), results revealed relatively lower dynamic CA

hysteresis for such regions on silicon wafers (δ~27°) than for when on the glass slides (δ~34°), as can be referred to in the graph 4.1.9.

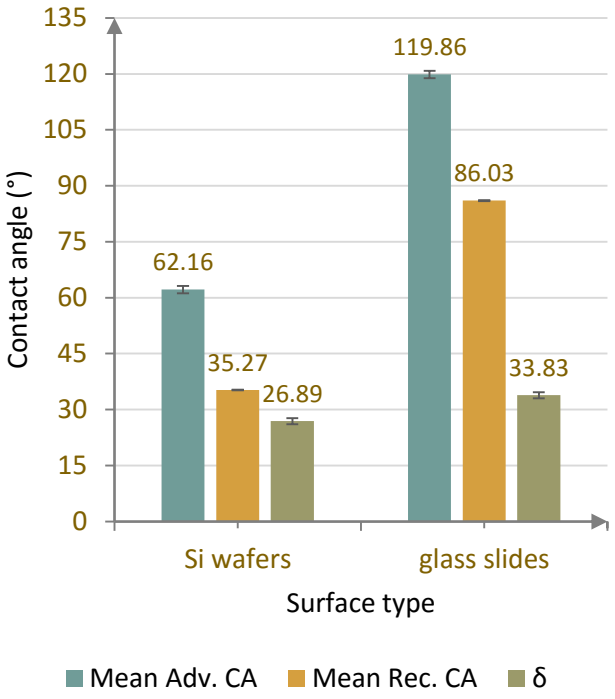

Graph 4.1.9: Dynamic CA measurements for surfaces (PFS coated) generated using different substrate materials

This though indicated (relatively) slightly greater homogeneities associated with the chemical treatments when on silicon wafers than on glass slides, lower standard deviations observed for both the cases, nevertheless, (further) pointed to the absence of any prominent pinning centres on such surfaces (hindering the free movement of the advancing/receding liquids during measurements).

Additionally, although the above once again confirmed the good quality of the surfaces produced (cleanings/coatings applied), it however excluded the choice of the base material contributing largely to the presence of any surface defects (considering the base material selected to be not majorly flawed in itself)—the occurrence of surface inhomogeneities/imperfections (if and when they occur) being presumably dependent on the nature of the fabrication process (surface treatments adapted).

The dynamic contact angle studies in this regard syncing with the static contact angle findings, glass slides, owing to their ease of availability, low buying costs, and the multiple advantages associated with glass as the substrate material (as discussed in chapter 2), continues to be the first preference in this regard.

d. Study of surfaces generated using different cleaning methods

Further, in analogy with the static contact angle measurements, dynamic contact angle studies were conducted to analyse the surfaces (hydrophobic) fabricated using different cleaning (post-coating) procedures for their homogeneities. As detailed in the corresponding static contact analysis, surfaces subjected to primarily three different cleaning methods: the ultrasonic leaning, the plasma cleaning, and the HCl-methanol cleaning, were tested- results as depicted in the graph 4.1.10.

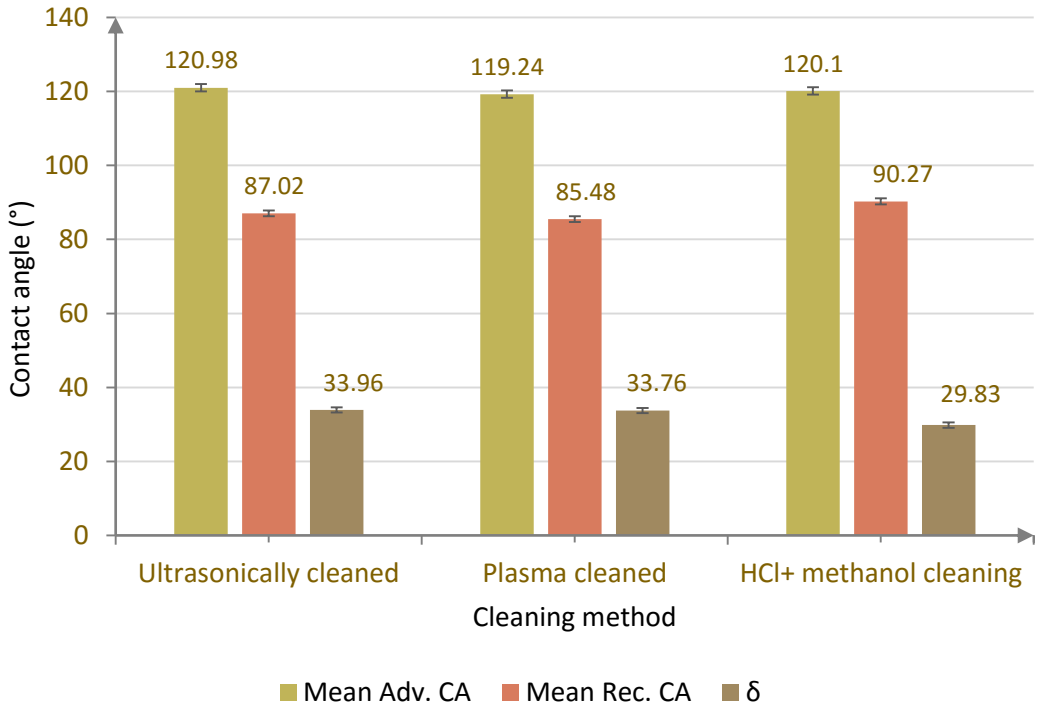

Graph 4.1.10: Dynamic contact angle studies for surfaces(hydrophobic) generated using different cleaning methods (pre-coating)

As can be seen in the graph above, cleaning using HCl +methanol yielded surfaces having comparatively lower dynamic contact angle hysteresis values (δ~30°), thereby concluding it to be the better method in generating surfaces with higher homogeneities. However, no drastic difference in the hysteresis for all the three cleaning methods tested was observed, as with the static contact angle studies- the typically used ultrasonic cleaning method being nevertheless preferred for the production of the chemically treated surfaces.

e. Study of surface subjected to different storage conditions

As detailed in the static contact angle studies, storage of the surfaces post-production (and pre-delivery) marks as an integral part of the supply chain. However, storing the surfaces (as the chemically structured, AG, glass slides dealt with in the current work), despite of opting a highly clean and an air tight storage environment, might modify their surface chemistries and thus the degree of wettabilities and/or homogeneities associated with them.

Though the static contact angle measurements (being previously done in this regard) revealed freshly prepared surfaces to be having comparatively greater homogeneities and wettabilities as compared to the stored ones (especially for the ones stored over a period of say six or more months), the surfaces were examined additionally via dynamic contact angle studies to put further light on the above findings.

In this respect, as with the earlier studies, usually hydrophobic regions of the fabricated surfaces were tested (using DI water as the test liquid)- investigations being done for various freshly prepared surfaces and for the ones being stored for say overnight, over a period of two months, and over a period of six months. Additionally, studies were conducted where the subsequent surfaces were cleaned (gently wiping them with a tissue dipped in Isopropanol, followed by a good rinse under water and drying the water residues using nitrogen gas)- to determine the effect of mild cleaning on the homogeneities of the (stored) surfaces.

Minimum of six surfaces being examined per case, with nearly ten measurements being conducted per surfaces, results revealed, as can be seen in the graph 4.1.11, freshly prepared surfaces exhibiting most consistent and reliable advancing and receding contact angle values with a (relatively) lower contact angle hysteresis (δ~33°). This hence indicated the greater homogeneities associated with the such surfaces as compared to their stored counterparts- freshly prepared surfaces hence being the preferred choices especially for research oriented applications (as in the current work). Further, though storage, especially for months/years, raises the vulnerability of the surfaces to any local contaminations, not so huge differences in the hysteresis values observed for the surfaces stored for six months or less, however makes them the acceptable candidates in the industrial applications.

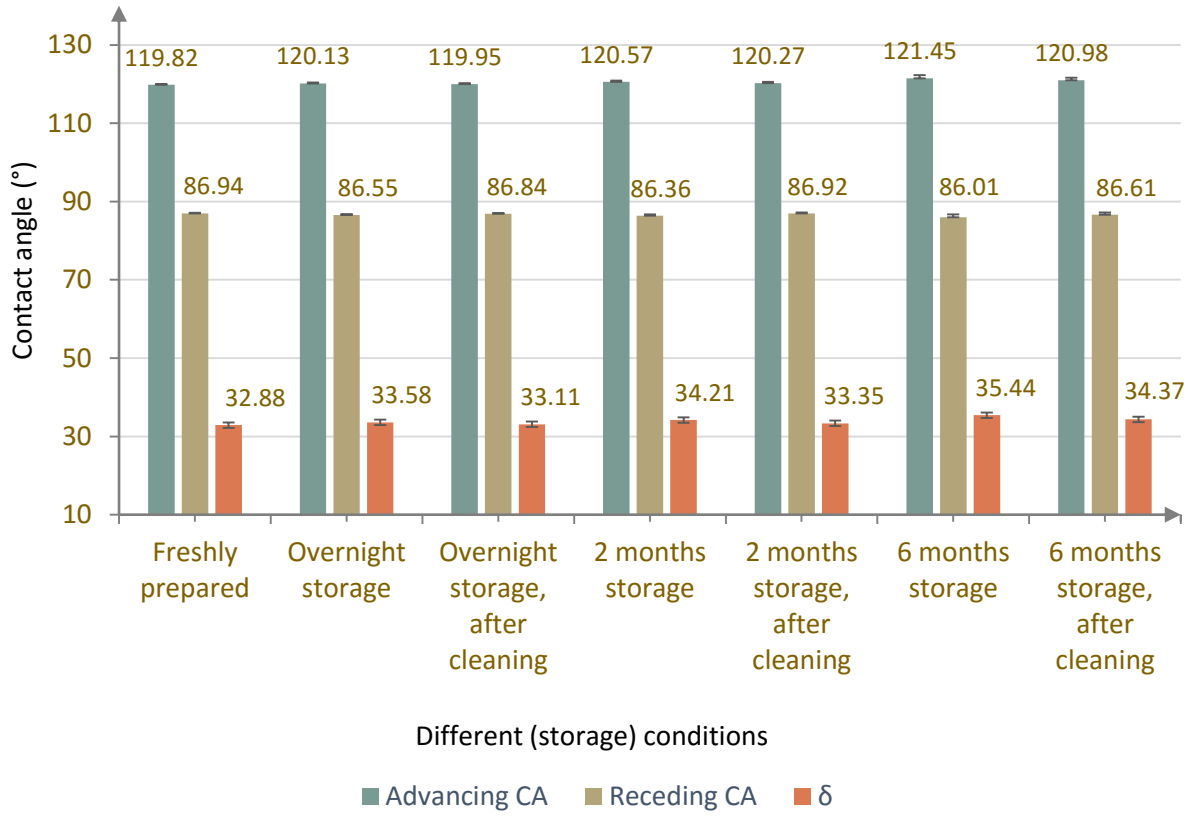

Graph 4.1.11: Dynamic CA studies for surfaces subjected to different storage conditions

Further, mild cleaning of the surfaces, as described above, was observed to improve their homogeneities—the results in sync with the outcomes of the static contact angle studies.

Dynamic contact angle: Conclusions

Hence, from the above dynamic contact angle studies, it can be concluded that the surfaces fabricated are largely homogenous in nature with good degrees of wettabilities associated with the chemical structuring applied. This in turn signified, as with with the static contact angle studies, the efficiency of the cleaning/coatings applied in the generation of such surfaces- ultrasonic cleaning and coating using the mechanical printing technique nevertheless ruled out to be having greater competences in this regard.

Additionally, freshly prepared surfaces were observed to have better surface homogeneities than the ones stored or cleaned (after storage) prior to use; surfaces stored for more than half a year being most vulnerable to surface imperfections

However, the analysis could not filter out a particular production stage that could be potentially responsible for the insertion of any surface (rare) defects- as detected in the microscopic examinations, calling for detailed similar or other investigations in this regard.

4.1.3 Surface energy measurements[193,194,196]

As surface tension is for liquids (as detailed in section 4.3.2 later), it's the solid's surface energy that aids in determining the amount of energy associated with a given surface. Greater the surface energy, greater can be said to be the wettability or the hydrophilic character of a particular surface, whereas surfaces associated with lower surface energies can be said to possess reduced wettabilities or their hydrophobic nature.

Thus while the contact angle studies (based on solid-liquid interactions) provide information on the relative hydrophobicity and/or hydrophilicity of a given surface, it is the surface energy (solely the property of the surface), that helps better in determining the degree of wettability linked with a particular surface.

Mathematically, surface energy can be successfully defined by the Young´s Law, as mentioned previously in the contact angle studies (refer figure 4.2), according to which a drop resting on a solid surface is chiefly balanced by the ratio of three interfacial energies (forces): the solid-liquid interfacial energy, the solid-gas interfacial energy, and the liquid-gas interfacial energy. The shape (or contact angle) of the drop reflecting in turn the prime contribution of a specific energy at that point- drops(aqueous) having lower contact angles on higher energy surfaces and vice-versa.

Some authors have as well defined the solid-gas or solid-vapour interfacial energy or the surface energy (σ_S) as the amount of work expended in order to increase the size of a phase, as energy per unit area- having the units of mJ/m^2, or the more frequently used mN/m.

Literature however reports various theoretical difficulties in the evaluation of surface energy, chiefly due to the deviations from ideality of the surface, owing to say immobility of the surface atoms/molecules, and/or due to the presence of surface defects as dislocations (missing atom or molecules and the presence of extra atom (adatoms) or molecules, formation of kinks, edge and/or screw dislocations), and so on[196]. This hence makes the surface energy of solids largely a function of their history of formation, thus calling for indirect experimental methods for its determination. Of the various methods known, the current work employs the determination of surface energy from the corresponding contact angle data, as per the Young´s relation[194]:

$$\sigma_S = \gamma_{SL} + \sigma_l \,.\, \cos\theta \qquad (4.1.3)$$

where `$\sigma_S$´ is the surface free energy of the solid, `θ´ the static contact angle, `$\sigma_l$´ the surface tension of the liquid, and `γ_{SL}´ the solid-liquid interfacial tension. Further number of models have been proposed for the calculation of free energy from the contact angle data-the methods typically relying on a second equation for calculations, having the general form as[194]:

$$\gamma_{SL} = \sigma_S + \sigma_l - (\text{interactions between phases}) \qquad (4.1.4)$$

The proposed models differ in the way in which these 'interactions between the phases´ is interpreted and as which interaction component(s) of the individual phases is made responsible for producing the surface tension or surface free energy (for further details into the models, refer appendix I at the end of the work)[194].

Experimental investigations

Based on the above, for the (indirect) determination of surface energy from the contact angle data, static contact angles were measured using minimum of two test liquids (usually DI water and DIM being opted in this regard), on the hydrophobic and hydrophilic regions of the chemically stratified surfaces (AG glass slides) respectively. For at least of six measurements made per solid-liquid combination selected, the data collected was fed next to the OCA surface energy measuring software-automatically calculating the energies associated with the corresponding surfaces.

Initial studies revealed (refer graph 4.1.12), the hydrophobic surfaces generated by both the mechanical and chemical coating techniques to be exhibiting surface energies of approximately 11mN/m- nearly similar values indicating not much difference in the wettabilities of the surfaces produced using the above coating methods- lower surface energies obtained further pointing towards the good hydrophobic character associated with

such surfaces. Also, studies revealed higher surface energies with the corresponding hydrophilic regions- thereby additionally revealing efficiency of the coating/cleaning techniques in generating surfaces with good/desired wettabilities.

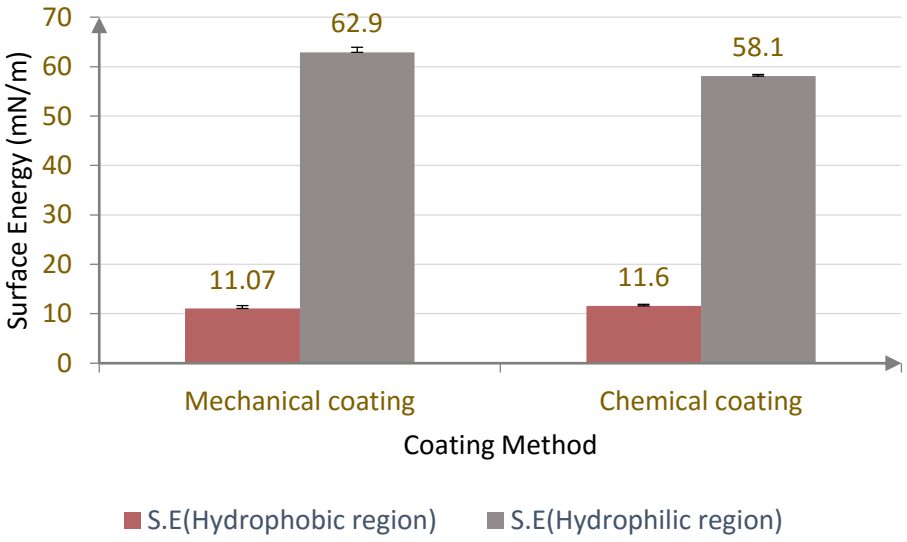

Graph 4.1.12: Surface energies for hydrophobic (generated using mechanical and chemical coating techniques) and hydrophilic regions of the chemically structured surfaces

Further, to determine the contribution of various components to the surface energy[194,197], as of the dispersive part, the polar part, and of the H-H part, surface energy measurements were conducted using different liquids as water, Di-iodomethane, and a set of alkane's viz. Decane, Do-decane, Octane, Tetradecane, Un-decane, Penta-decane, and Nonane – on the homogeneous, hydrophobically coated surfaces as chemically non-structured (PFS) glass slides. In this respect, measurements for comparative and detailed studies were made using various methods as the Fowkes (Geometric mean approach), extended Fowkes, Wu (harmonic mean approach), O.W.R.K, Zisman, Schultz, and the Acid-base theory (refer Appendix I for further details in to each of the above methods).

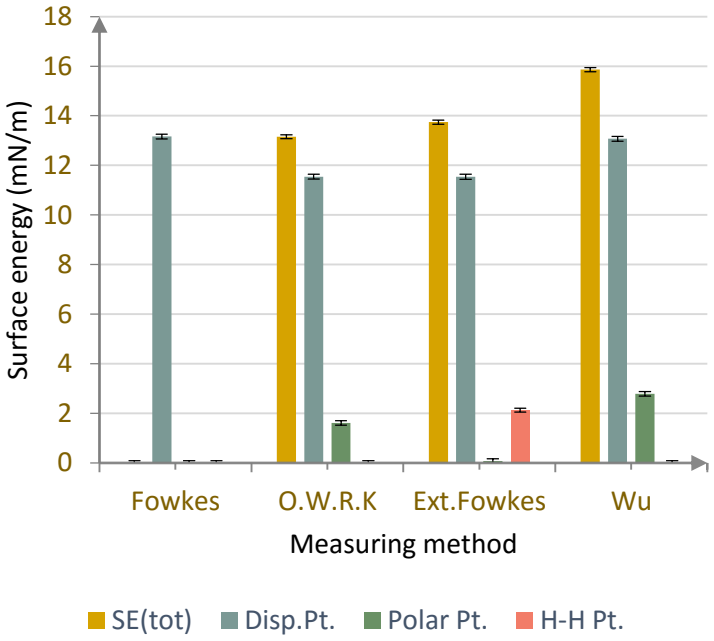

Graph 4.1.13: Comparison of different S.E methods for the evaluation of dispersive, polar, and hydrogen parts of the surface free energy

Results revealed, as can be seen in the graph 4.1.13 on the right,

average surface energy on such surfaces, from all the above methods, calculated to be nearly 14.25mN/m – lower values further putting forward the lower wettabilities (good hydrophobic character) associated with such surfaces. This in addition to the contact angle studies, hence, established the good quality of fabrication steps involved (cleaning/coatings applied) in the generation of the subsequent surfaces.

Further, results revealed the dispersive component of the surface energy for the hydrophobic surfaces/ regions to be in the range of 11.5-13.2 mN/m, its polar part in the range of 0-2.8 mN/m, and its H-H part in the range of 2.13 mN/m, thereby giving for such surfaces the contribution of:

Dispersive Component > Polar Component > H-H component

The above outcome was in analogy with as expected for the hydrophobic surfaces- such surfaces having in general higher dispersive parts than polar parts of surface energies [hydrocarbons present making such surfaces not mixing in water (polar) owing to the high (London) dispersive interactions associated with them] [194,197,251,252.]

4.1.4 Summary

From the various surface characterization investigations conducted, it can be hence summarized that the chemically treated surfaces, as the AG structured glass slides dealt with in the current work, typically exhibit good surface wettabilities with significant homogeneities- in turn implying the efficiency of the fabrication techniques (cleaning/coatings) applied in the generation of same.

However, as no system is ideal in nature, chances might be that some (rare) surface inhomogeneities get associated with some of the surfaces - as the crater like surface imperfections detected in the microscopic investigations. Such defects being further primarily obtained on the hydrophobic regions of the chemically structured surfaces, brought to the mind their possible source being some coating residues, which perhaps have been missed out being cleaned in the later cleaning procedures in the production of such surfaces. Various microscopic and contact angle investigations being done in this respect however could not successfully filter out a particular fabrication stage responsible for the above – contact angle studies additionally ruling out the storage of the surfaces, in general, potentially contaminating the surfaces in any way (except for the surfaces stored for say a period of serval months/ a year showing greater vulnerabilities in this regard).

The contact angle surface characterization studies further revealed the independence of the selection of the base material in the fabrication of such surfaces- glass being nevertheless preferred as the first choice in this respect, primarily owing to its ease of availability, and low purchasing and fabrication costs involved. The studies further sifted out mechanical printing and ultrasonic cleaning to be the promising methods in generating surfaces with greater

homogeneities and/or wettabilities- freshly prepared surfaces in addition preferred over their stored counterparts in this respect.

Various surface energy measurements additionally synced with the above findings- chemical treatments applied generating surfaces of good wettabilities in general- surface energies for the hydrophobically coated regions (low energy/wettability) observed to be as low as ~11mN/m in value. Additionally, dispersive component, as expected, came out to be the prime contributor to the surface energy for the hydrophobic surfaces- indicating the higher dispersive interactions associated with them.

Keeping in mind all of the above, the surfaces, nevertheless were briefly tested under a standard upright microscope for any prominent surface inhomogeneities (if present) prior to especially research oriented applications. In any case, the surfaces which failed the above test, together with the immediate neighbours of the ones which showed drastic bubble evolutions in the biological (PCR) runs, were better rejected/not preferred.

4.2 The Heating Platform

Other than the amplification platform (chemically structured AG glass slides), the other major component of the micro-fluidic system that required investigation for its optimum operation and functionality was the heating cycler- The Ampli Speed Cycler (ASC) as used in the current work. Again, despite of the extreme care taken in its production, handling, and its well-calibration prior to use, some ‘flaws’ or local imperfections might be present, causing inhomogeneous heating (of its heating plate)-possibly leading to or aiding in the evolution of bubbles at elevated working temperatures.

Hence, to comprehend the above, appropriate experimental investigations were conducted, as detailed in the sub-sections below.

4.2.1 Study of homogeneity of the heating plate of the cycler

As stated in chapter 2, a good heating platform is the one capable of providing the desired temperatures in a minimum possible time and being able to generate highly consistent and accurate thermal profiles. This can be further said to be dependent on the heating provided by the cyclers heating plate-overall homogenous heating implying the absence of any local ‘hot-spots’ which might otherwise lead to local bubble nucleations/evolutions at elevated working temperatures (of say 95°C -particularly sensitive for the inner aqueous drop).

In order to hence determine the thermal homogeneity of the heating plate of the cycler (ASC, as under consideration), and that the right temperatures are worked with, experimental studies were conducted where a dummy (chemically structured, AG) glass slide, with four PT 100 sensors (four terminal sensing) attached nearly to its middle, was placed on the heating plate of the subsequent cycler. Further, with no liquids pipetted on the dummy slide for these measurements, in order to mimic the actual working conditions, a steel, ‘three-legged’ stand

having weight of ~20 grams (nearly equal to the weight of the 48 bi-liquid micro-droplets when pipetted) was placed on the slide surface, as can be seen in the image 4.2.1. below:

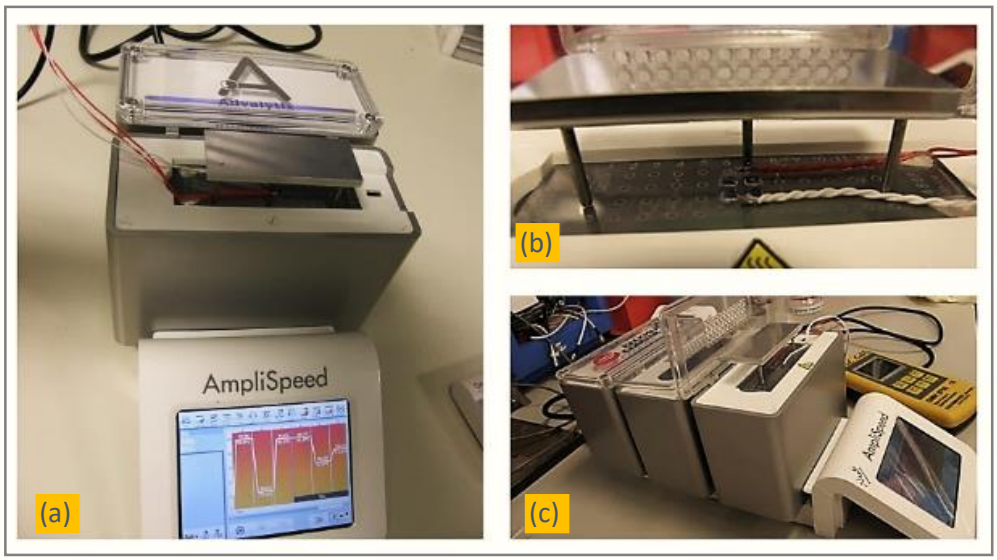

Image 4.2.1: (a) Experimental set-up for manual calibration of the heating plate of the ASC, (b) top view: close up of dummy slide with PT 100 sensors and a steel stand on above, (c) edge-view of the set-up

The other end of PT100 sensors attached to a resistance thermometer, investigations were made where for a particular set temperature, temperatures attained on the glass slide (recorded by the PT100 sensors) in a given time interval were measured.

Examinations being done usually for the initial 10 minutes of heating (ramp rate of ASC= 3°C/sec) and at a set temperatures of 95°C (temperature associated with the 1st stage of the PCR where most of the bubbles evolutions were observed to take place), studies revealed approximately within 40 seconds of heating, the resistance thermometer showing a reading of 95°C—the value remaining consistent for the rest of the measurement's time interval (refer graph 4.2.1).

This above hence indicated the effectiveness of the heating cycler(ASC) in providing faster and accurate heating profiles; no major inconsistencies in the attained values (95°C, after of 40 seconds of heating) for an average time interval of

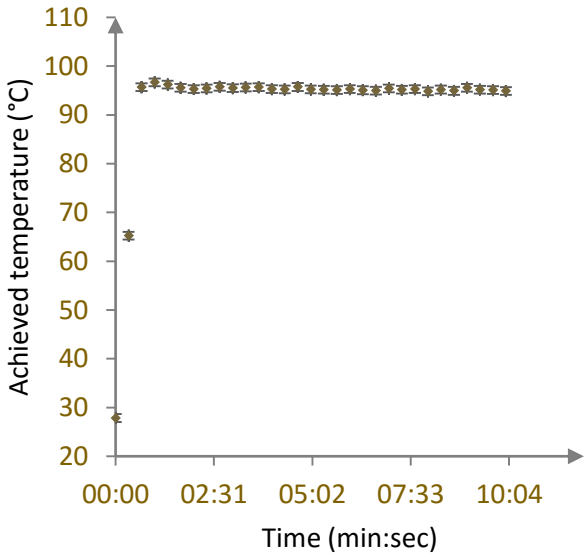

Graph 4.2.1: Set temperature (95°C of the ASC) vs. attained temperature (as measured by the PT 100 sensor on the glass slide -atop the heating plate of the ASC cycler), for a time interval of 10 minutes

10 minutes, further reflecting the thermal homogeneity provided the heating plate of the cycler, in general.

Additionally, experimental investigations were conducted where the PT100 sensors were attached, instead of all in the middle, at different positions on the glass slide: at its top edge (referred as position A), its bottom edge (referred as position B), its right edge (referred as position C), and in its middle (referred as position D)- as can be seen in the image 4.2.2 on the right- the sensors individually attached to four resistance thermometers at their other ends.

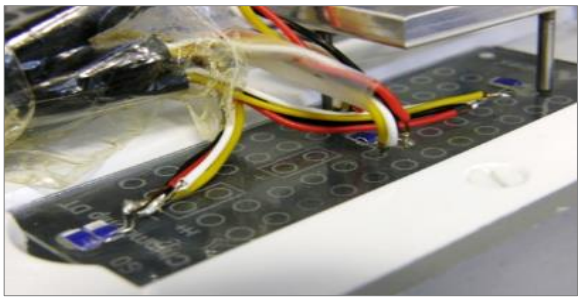

Image 4.2.2: Four PT100 sensors attached on different locations of the glass slide (placed on the heating plate of the cycler)

Rest of the experimental set-up being the same as for the earlier studies (PT100 sensor only in the middle of the glass slide), measurements were made where for the set temperature of 95°C, the temperature attained on the various locations of the slide surface were evaluated (anew for the initial 10 minutes of heating).

As can be seen in the graph(s) 4.2.2 below, results revealed almost similar set vs. attained heating profiles for the different positions on the slide surface tested- the surface achieving within ~40 seconds of heating the set temperature (95°C) - the value remaining consistent for the rest of the observed time interval (10 minutes).

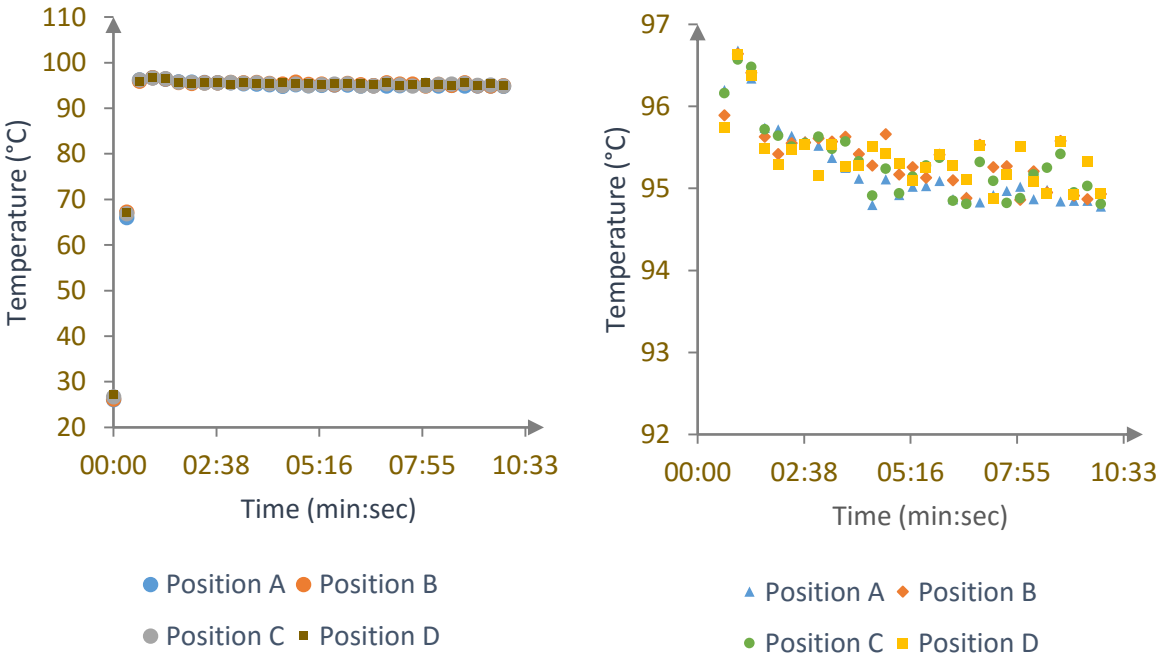

Graph 4.2.2: (left) For a given set temperature of 95°C and for initial 10 minutes of heating, attained temperature vs time plots for different positions on the tested slide surface, (right) zoomed in view depicting almost similar heating profiles for different locations tested on a given surface

The above, hence, further pointed towards the overall (thermal) homogeneity provided the ASC's heating plate- the heating of the glass slide atop being uniform with no prominent thermal fluctuations detected. This, in turn excluded the contribution of the heating cycler (ASC) in say unevenly heating the bi-liquids during biological runs, which might otherwise lead to or aid in the evolution of bubbles (especially at elevated working temperatures, particularly sensitive for the inner aqueous drop), resulting in erroneous analysis.

However, as can be seen in the graphs above, a slight shoot up in temperature (of ~1.5° C) at the start of the heating was observed. Though this occurred for a short time interval (around 40 seconds), after which the system attaining the set temperature (95°C) instantaneously (for the rest of the observed time interval), experiments were conducted to determine the effect (if) of this brief thermal 'shoot-up' on the bubble evolution phenomenon. For this, investigations were done by pipetting various combinations of rows and columns (different regions) on the chemically structured glass slide (placed on the heating plate of the cycler), and observing the occurrence of bubbles again at 95°C for initial 10 minutes of heating. Minimum of 10 slide surfaces being investigated per case, results, in analogy with the quantitative analysis as conducted in the previous chapter, revealed the probability of bubble evolution to be < 1% per case.

This hence indicated no prime contribution of the little temperature 'shoot-up' or slight thermal fluctuation during the initial heating in the evolution of bubbles- the outcomes further revealing the higher thermal homogeneities associated with the heating plate of the subsequent cycler (uniformly heating all the regions(pipetted) on the slide surfaces in general). Also, the successful execution of the biological reactions as the PCR, utilizing heating platforms as the ASC, further specified their overall efficiencies and widespread use in industrial applications.

4.2.2 Effect of ramp rate of the heating cycler on bubble evolutions

Another important characteristic defining a good heating platform, as stated in chapter2, is its ability to provide autonomous heating/cooling at appropriate ramp rates- ramping rate reported to be an essential feature to a successful PCR[30]. Too high or too low ramp rates, might influence the desired heating profiles, possibly interfering with the effective execution of the biological reactions. Especially too high ramp rates, might result in transitory temperature 'shoot-ups', resulting in the sudden heating of the subsequent micro-droplets. Further, such thermal non-uniformities if present, raise the vulnerability of particularly the inner aqueous drop to increased evaporation effects- the droplet possibly reaching its boiling point (during say the 1st stage of the PCR which operates at 95°C) for greater degrees of fluctuations, if present. This might, in turn, alter the behaviour of the overall micro-droplet system, possibly leading to or aiding in the evolution of bubbles at elevated system temperatures.

Thus, in order to study the effect of ramp rate of the heating cycler on the bubble evolution phenomenon, experimental investigations were conducted, where, as with the quantitative analysis made in the previous chapter, around 40 surfaces were tested for bubble evolutions- ASC ramp rates selected to be 0.2°C/sec, 1°C/sec, 2°C/sec and 3°C/sec, per case.

Naked eye observations and top and side view video recordings (refer figure 3.1) made in this respect revealed no major dependence of bubble evolutions on the ramp rate of the ASC selected – the probability of bubble evolutions per case calculated to be again <1%. Nevertheless, owing to the comparatively lower ramp times associated with higher ramp rates, typically ramp rates of 3°C/sec (ramp time ~40 seconds) are usually adopted- both for industrial and research oriented purposes.

4.2.3 Summary

From the above characterization of the heating cycler studies, it can be hence summarized that a well-calibrated heating cycler (as ASC), typically, provides quick, optimum, homogenous, and consistent heating- indicating no significant contribution of the heating cycler to the bubble evolution phenomenon. Further, the bubble occurrences were found to be independent of the cyclers ramp rates –ramp rates of 3°C/sec, owing to their comparatively faster ramp timings (~40 seconds), being nevertheless preferred in this regard.

4.3 The Bi-liquid, Micro-droplet system

After the amplification platform and the heating cycler, the other vital component of the micro-fluidic system that was characterized was the bi-liquid, micro-droplet duo (as previously detailed in chapter 2) - to determine the role (if) of the involved liquids in the bubble evolution phenomenon, and to study their behaviour, for the comprehension of the dealt with micro-fluidic system in general.

The liquids, despite of being produced and handled in a highly clean, dust-free environment, might still hold some unwanted contaminations, possibly serving as nucleation sites for bubble formations. Besides, the liquids might contain sufficient volumes of air, regardless of they being highly degassed and carefully pipetted /loaded – the dissolved air degassing as (air) bubbles at elevated system temperatures.

Thus, to investigate the above, various experimental investigations were conducted, as detailed in the sub-sections below.

4.3.1 Estimation of drop(s) profiles: Contact angle studies

For the comprehension of the bi-liquid system, to begin with, primarily static CA investigations, as described in section 4.2, were made. The drop profiles (geometries) for the single- liquids and for the bi-liquids (for the outer drop above the inner drop and for the inner

drop beneath the outer drop) on chemically non-structured (PFS) and chemically structured (AG) glass slides were studied in this respect -both at room and elevated temperatures, as discussed next.

4.3.1.1 Drop's profiles at ambient temperatures

- For the single-liquid system

Initially, to determine the behaviour of the droplets at room temperatures, for a particular surface type selected (either chemically structured or non-structured), static CA's were measured for varying volumes of liquids - dummy PCR solution, DI water, and sealing solution being typically chosen as the test liquids in this regard.

Whereas for chemically non-structured surfaces (homogeneous, hydrophobically coated PFS glass slides) measurements were made by pipetting the liquids anywhere on the subsequent surface ('true' CA's), for chemically structured surfaces (as AG glass slides), the values were measured by pipetting liquids on the confined reaction sites ('modified' CA's), to study the profiles of the droplets as in the actual cases. Nearly 10 surfaces being examined per case, with around 10 measurements being made per surface (/per liquid), analysis revealed (refer graph 4.3.1 below) increase in CA with increase in volume of the dispensed liquids- greater variations being witnessed especially for the chemically stratified surfaces in this regard.

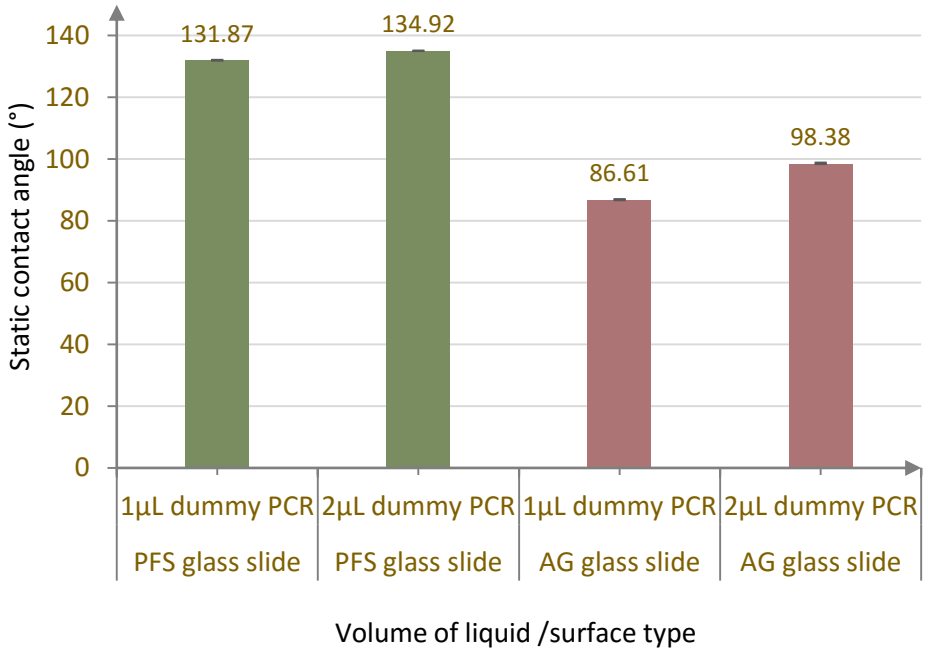

Graph 4.3.1: Variation of static CA with drop's volume (dummy PCR solution), on chemically non-stratified (PFS) and stratified (AG) slide surfaces

Further, the droplets were seen to exhibit higher CA's when dispensed on 'pure' (hydrophobic) surfaces, than when on the 'mixed' surfaces (as on the inner hydrophilic reaction site bounded by a hydrophobic exterior, as for the AG slides as used mainly in the current work).

Also, similar observations were made when DI water was opted as the test liquid (refer graphs 4.3.2 and 4.3.3) – DI water, however, exhibiting slightly greater static CA's than the dummy PCR solution for a particular surface type.

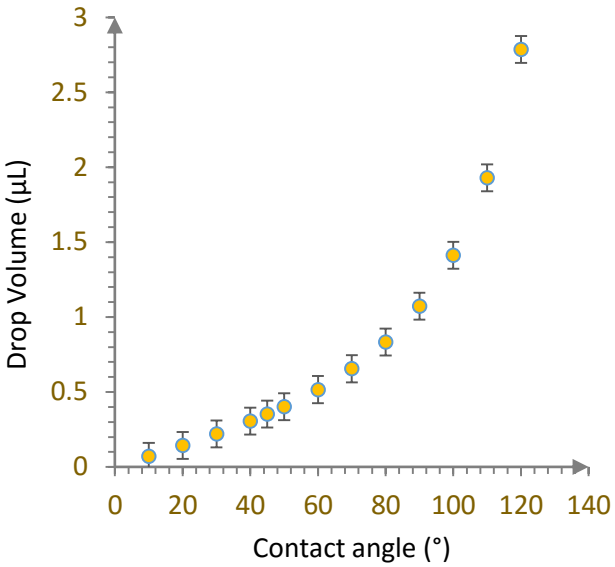

Graph 4.3.2: Static CA as a function of drop´s volume (DI water) on a chemically stratified surface

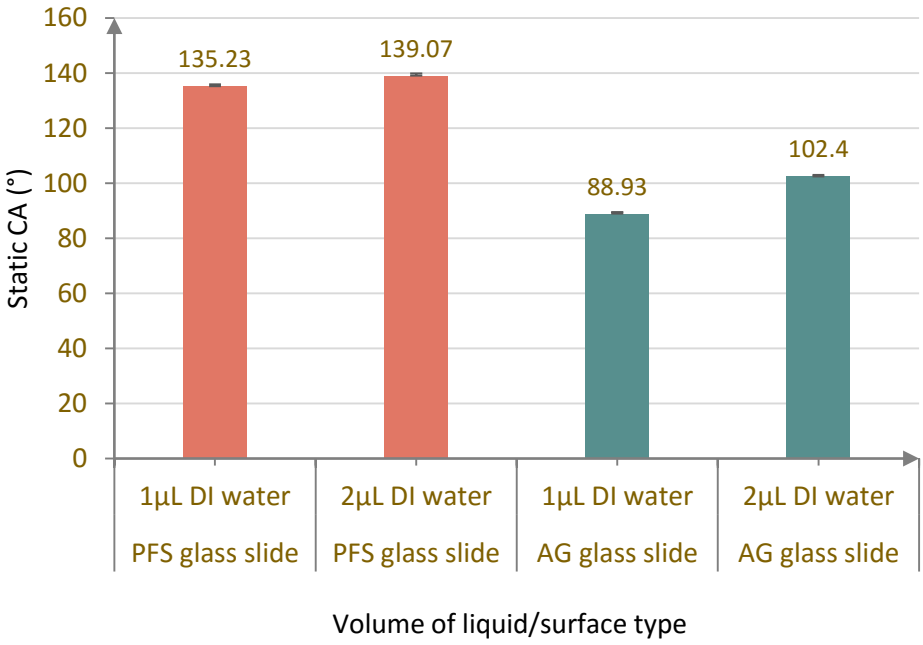

Graph 4.3.3: Variation of static CA with drop's volume (DI water) on chemically non-stratified (PFS) and stratified (AG) slide surfaces (liquid pipetted on the inner hydrophilic ring for the structured surfaces)

Measurements made on similar lines revealed, static CA's of ~ 85°, and of ~58°, for 'pure' (homogeneous PFS coated glass slides) and 'mixed' (reaction site of AG glass slides) surfaces

respectively, when sealing solution (5µL, as used in the actual work) was employed as the test liquid, as can be seen in the graph 4.3.4 on the right.

Additionally, both for the chemically non-structured and structured surfaces, along with contact angles, the corresponding base diameters and heights of the droplets were estimated (via the OCA measuring software)- values for 1µL of DI water and 5µL of sealing solution (i.e. for standard liquids and their volumes as used in the current work) summarized as in the table 4.3.1 below.

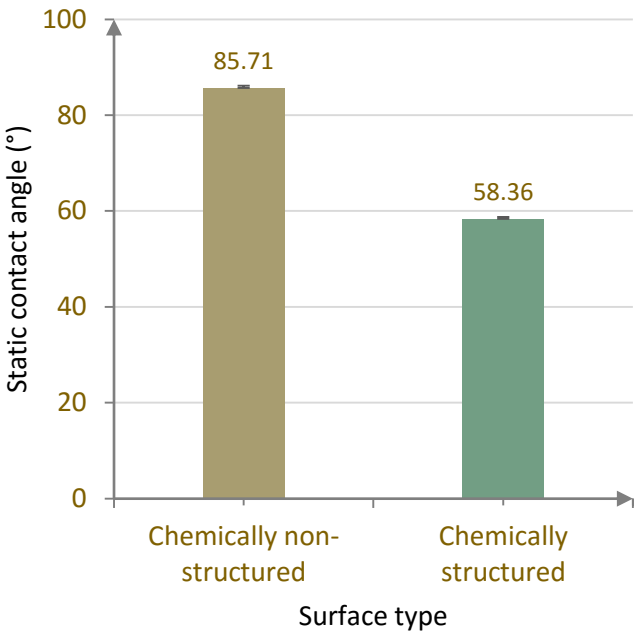

Graph 4.3.4: Static CA measurements for 5µL of sealing solution- on chemically non-structured (PFS) and chemically structured (reaction site of AG glass slide) surfaces

Parameter	Liquid			
	1µL DI water		5µL sealing solution	
	PFS	AG	PFS	AG
Base Radius (mm)	*0.57*	*0.80*	*1.50*	*1.75*
Height (mm)	*1.06*	*0.78*	*1.18*	*0.95*

Table 4.3.1: Base radius and height of droplets when pipetted on the chemically non-structured (PFS) and structured (AG) glass slides- for the latter case, 1µL of DI water being pipetted on the inner hydrophilic region and 5µL of sealing solution being pipetted on the outer hydrophilic ring of the slide surface. Standard deviations observed per case < 0.2°

Studies further revealed, for chemically structured AG glass slides (providing fixed base diameters to the drops), an increase in the height of the droplets with an increase in their volumes – results as can be seen in the graph 4.3.5 on the right (for DI water as the test liquid).

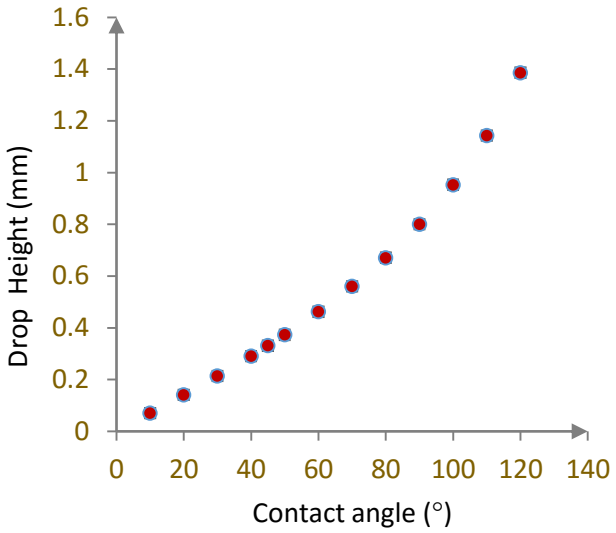

Graph 4.3.5: Variation of drop's height (DI water) with its volume on a chemically structured surface (fixed base diameter)

The above dependence complemented with the earlier findings where an increase in contact angle of the drop with an increase of its volume was observed (refer graph 4.3.5)—the outcomes overall indicating, for the chemically stratified surfaces, the volume sensitivity of the micro-drop profiles, and thus the need of right volumes to be dispensed to obtain the desired drop configurations on such surfaces.

However, from the above studies, the shape (geometries) of the droplets- as of 1µL of DI water and 5µL of sealing solution (liquids and their volumes being typically used in the current work), at room temperatures, and on chemically non-stratified and stratified surfaces, can be interpreted as depicted in the figures 4.3.1 and 4.3.2 below:

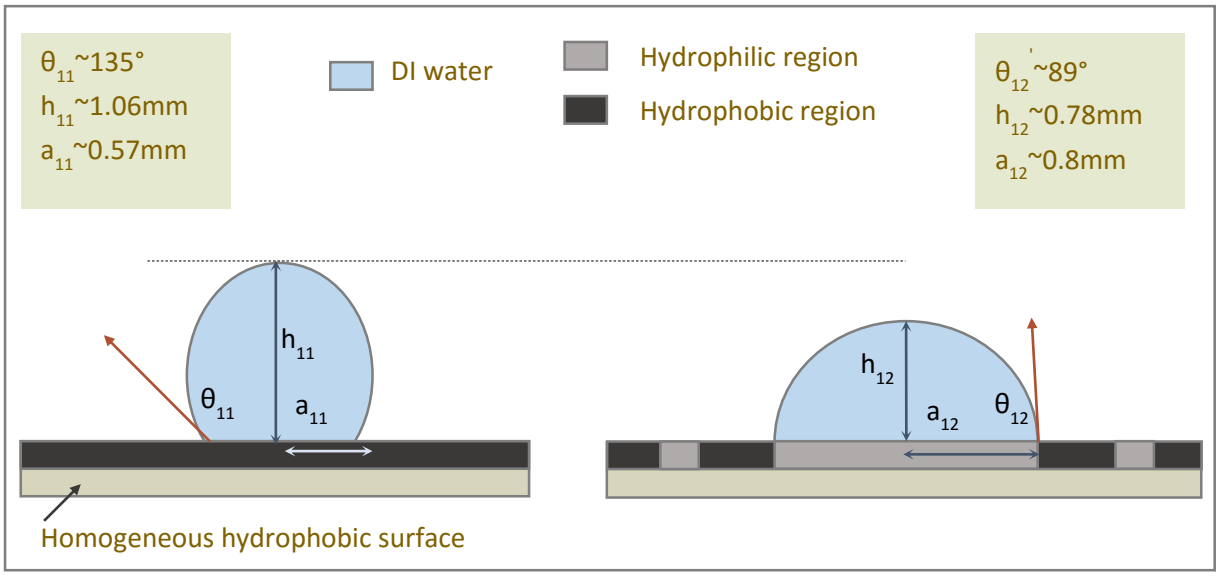

Figure 4.3.1: Configuration of 1µL of DI water droplet(s) resting on (left) chemically non-structured surface, (right) chemically structured surface

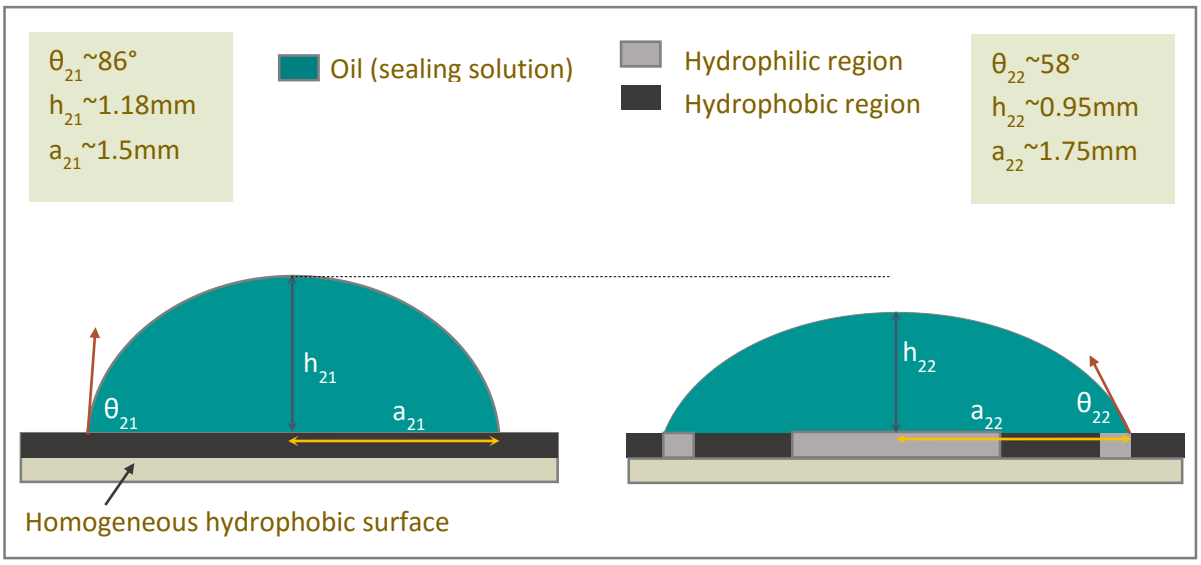

Figure 4.3.2: Configuration of 5µL of oil (sealing solution) droplet(s) resting on (left) chemically non-structured surface, (right) chemically structured surface

The above drop configurations, based on the experimental data, further synced with the mathematical interpretations made in this respect, where according to literature, the shape of a microscopic droplet residing on a solid surface is said to be solely governed by the surface tension forces, whereas the balance of surface tension and gravitational forces is said to determine the shape of larger droplets[15]. A key parameter that helps in evaluating the balance between the above two forces is the Bond number (B_o), defined as:

$$B_o = \frac{\rho g R^2}{\gamma} \qquad (4.3.1)$$

where 'ρ' is the density of the liquid, 'ϒ' its surface tension, 'g' the acceleration due to gravity, and 'R' of the order of drop´s radius.

For B_o < 1, the drop is usually said to attain a spherical shape, dominated by the surface tension forces, whereas it attains a somewhat flattened spherical cap geometry, dominated by the gravitational forces, for Bo >1[15].

Further, for (1µL) of aqueous droplets (water or water based PCR mix) dispensed on chemically non- structured surfaces (hydrophobic PFS slides), calculations gave Bo to be ~0.04 - the value being much less than 1, indicating a little elongated shape of the drop. Similar calculations when done for such drops on chemically structured surfaces (as AG glass slide with inner base radius of 0.8mm), yielded B_o to be ~0.87 – the value being slightly less than 1 indicating nearly spherical shape of the drop—calculation being in sync with the configurations as observed experimentally (figure 4.3.1).

Additionally, for B_o< 1, the drop's height can be calculated via the formula[15]:

$$V(a, h) = \frac{\pi}{6} h (3a^2 + h^2) \quad (4.3.2)$$

where `V´ is the volume of the drop, `a´ the base radius, and `h´ the corresponding height. Calculations give for water droplets (1µL) on chemically structured surfaces, h~1.063 mm and for chemically non -structured surfaces, h~0.8mm – the values being similar to ones observed experimentally, thereby validating the correctness of the obtained results.

On similar lines, literature reports another important parameter known as the "capillary length" [15,] defined as the ratio of the Laplace pressure characterizing the size of the microscopic drop to the hydrostatic pressure[15]. Comparing the two pressures, the following relation can be obtained:

$$\frac{\Delta P\ laplace}{\Delta P\ hydrostatic} \approx \frac{\gamma / l}{\rho g l} \quad (4.3.3)$$

where 'Υ' is the surface tension, 'ρ' the density, and 'g' the acceleration due to gravity. The two pressures are said to be of the same order when:

$$l \approx \sqrt{\frac{\Upsilon}{\rho g}} \quad (4.3.4)$$

`l' being the capillary length in the above equation. Again, a drop having dimensions (generally horizontal radius being considered) smaller than the capillary length is said to have a spherical cap geometry or a surface of minimum energy, whereas a drop having proportions greater than the capillary length is said to be flattened by gravity.

For aqueous droplets (say 1µL of DI water), calculations gave, l ~ 2mm – the value being greater than the drop's dimensions (of ~0.55mm for chemically non- structured and ~ 0.8mm for the chemically structured surfaces), further indicated the domination of surface tension forces over the gravitational forces in determining the shape of these droplets.

In similar respects, for oil drops (sealing solution, 5µL), calculations revealed:

Chemically non-structured surfaces	Chemically structured surfaces
B_o ~ 0.6 (<1)	B_o ~ 0.92 (close to 1)
l ~ 1.81 (<1.5 mm - drop's radius)	l ~ 1.81 (close to 1.75 mm- drop's radius)

Table 4.3.2: Bond number and capillary length calculations for 5µL of sealing solution on chemically non-structured and chemically structured surfaces (reaction site of AG slide)

As stated in table 4.3.2, the data hence indicated the close to spherical cap configuration for 5µL of oil drops on the chemically structured surfaces (pipetted on the reaction site-outer hydrophilic ring of AG slide), and their somewhat flattened configurations on the chemically non-structured, homogeneous (PFS) surfaces. Besides, from equation (4.3.2), heights of 5µL of sealing solution, for both the surface types, were again calculated to be in analogy with the values obtained experimentally- further approving the droplet's configurations as experimentally interpreted (figure's 4. 3.1 and 4.3.2).

Conclusions

From the above contact angle studies for single-liquids at room temperatures, it can be hence concluded that low volumes (~1µL) of aqueous drops, typically form nearly spherical cap configurations (dominant by surface tension forces), whereas as the volume of the drop increases, its tendency to acquire a flattened spherical cap shape raises (in this case drop being dominant by gravitational forces)- as usually observed for 5µL of oil drops.

Further, the above behaviour was seen to largely depend on the nature of surface in use - shape of the drops on homogeneous, chemically non-stratified (PFS) surfaces, owing to the absence of any surface structuring, being customarily independent of the drop's volume, whereas, profiles acquired by the droplets being largely volume dependent for the chemically stratified surfaces -the surface structuring constraining the drop's movement in this case.

Additionally, for a given volume of the liquid, and a particular surface type selected, the shape of the drops was found to as well depend on the nature of the liquids– liquids having more cohesive interactions or greater surface tensions (as for water) tending to attain a more spherical shape, whereas liquids having lower cohesive interactions or smaller surface tensions (as for oils) tending to have a slightly flattened spherical configuration. The above behaviour being again largely dependent on the volume of liquid opted, micro-droplets (usually ≤ 1µL in volumes), however, typically were seen to exhibit spherical configurations.

Lastly, the consistency and reliability in the contact angles observed for the various solid-liquid combinations examined, further pointed towards the absence of any prominent pinning centres in the form of surface and/or liquid contaminations, which if present, might have altered the drops shapes and hence their contact angle values. This hence proved, apart from the homogeneity and good quality of the in use surfaces, the pureness of the liquids opted- leaving in general no inhomogeneities into the system which might lead to bubble evolutions at elevated working temperatures.

- Drop's profiles at ambient temperatures: For the bi –liquid system

Though the above examinations successfully explained, at room temperatures, the configuration of single -liquids on a given surface, for the overall analysis of the micro-droplet system, investigations were additionally done to determine the configuration of the bi-liquids:

of the outer drop with the inner drop beneath it, and of the inner drop with the outer drop above it.

For the former case, analysis was done where static CA's were measured for 5µL of sealing solution above 1µL of DI water- both for the chemically non-structured surfaces (liquids pipetted anywhere on the homogeneous, PFS glass slides), and for the chemically structured surfaces (liquids pipetted on the reaction sites of the virtually stratified AG glass slides), as with the previous studies.

Again, minimum of ten surfaces being examined per case, with at least ten measurements being made per surface, investigations revealed, as compared to for a single oil drop (refer earlier graph 4.3.4), a slight increase in the CA of the (oil) drop with the inner water drop beneath it. Further, similar behaviours as above were observed for the liquids when dispensed on chemically non-structured and structured surfaces - results as can be seen in the graph 4.3.6 on the right.

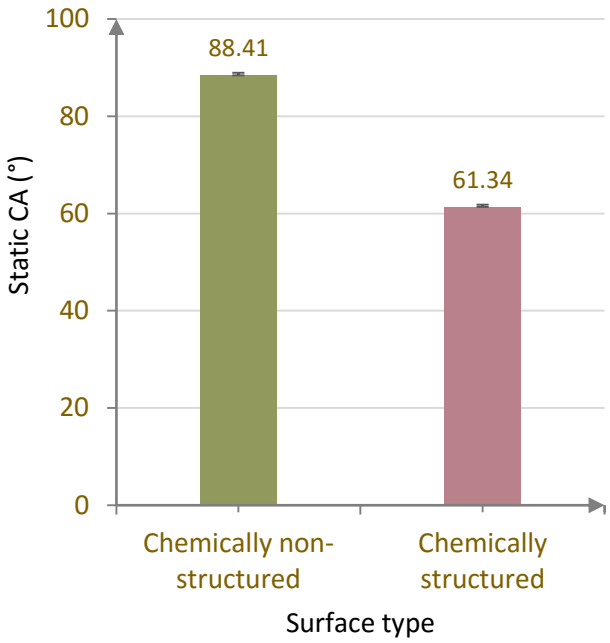

Graph 4.3.6: Static CA of the outer drop (sealing solution, 5µL) with the inner drop (1µL, DI water) beneath it—both for the chemically non-structured and structured surfaces

The above CA data was further complemented by the base diameter and height values calculated for such bi-liquid system—results revealing, as compared to for a single-liquid(oil) system (refer figure 4.3.2), for the oil (above water) drop, a slight decrease in its base diameter(ΔB.D ~ -0.32mm) and a slight increase in its height (ΔH ~+0.06mm) for chemically non-stratified surfaces, and a slight increase in its height (ΔH~ +0.15mm) for chemically stratified surfaces (droplets having fixed base diameters in this case).

On similar lines, studies were done to determine the behaviour of the inner drop (1µL water) when beneath the outer droplet. However, in order to work upon the profile of just the inner droplet and not the outer one, the contact angle measuring set-up was a bit modified: the bi-liquids (on the glass slide) placed in a glass cuvette (inner dimensions: 20*10*10mm), the cuvette further sited on the sample stage of the measuring device (OCA), as can be seen in the image 4.3.1 on the next page.

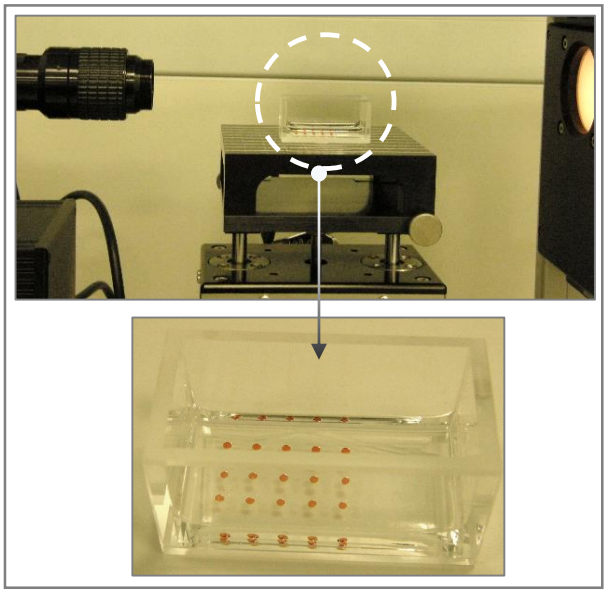

Image 4.3.1: Experimental set-up for bi-liquid static CA measurements (aquarium technique)

For this, using a diamond cutter, the surfaces (PFS and AG glass slides) were cut into parts- the cut parts having base dimensions analogous to that of the cuvette's base area for their easy placement into it for the experiments. However, the extracted surfaces, prior to being positioned in the glass cuvette(s), were properly cleaned for any leftover glass residues- cleaning done by wiping the surfaces gently with a tissue dipped in IPA, followed by a subsequent rinse under water, and drying using nitrogen.

After the above cut part(s) carefully slid into the glass cuvette, placed next on the sample stage of the OCA measuring device, and the experimental set-up calibrated (as previously described in the static contact angle studies), 1µL of DI water was pipetted almost in the centre of the (cut) slide surface, and immediately above it was dispensed 5µL of sealing solution (to minimize any evaporation of the inner droplet, as stated previously). However, the above volume (standard of 5µL) of the outer liquid was seen not be sufficient for the clear and whole visualization of the inner droplet's profile, thereby requiring its greater volumes to be dispensed to achieve the same. Initial quick experiments made in this regard revealed that for the outer droplet (oil) volumes of ~ 900µL, the profile of the inner droplet (1µL DI water) could be clearly detected by the measuring software- experiments nevertheless revealed no distinct dependence of the contact angle of the inner liquid on the volume of the outer liquid pipetted (refer Appendix A for further details).

Thus, for sufficient volumes of the outer liquid(oil) pipetted, once the profile of the inner liquid (DI water) was clearly visible, static contact angles of the latter were measured – comparative studies being made again for varying inner drop volumes, both for the chemically non-structured and structured surfaces (cut slide parts). In this regard, minimum of ten measurements were made per (volume of the inner) liquid selected, with minimum of ten

surfaces being analysed per case - a fresh, cleaned cut part of the subsequent slide surface being opted per study. The measurement data analysed using Microsoft Excel 2016, revealed:

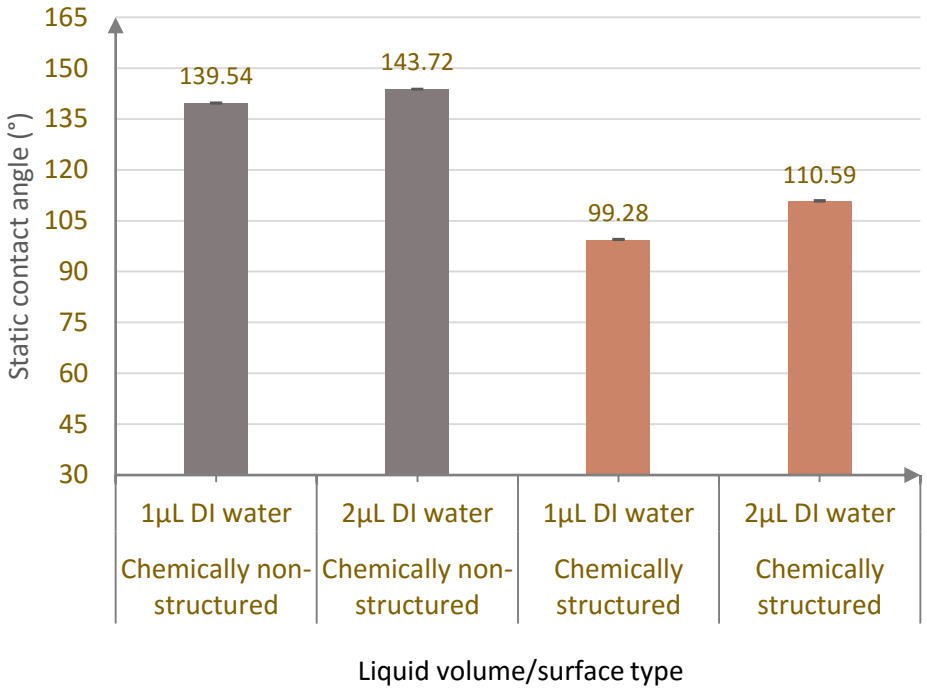

Graph 4.3.7: Static contact angle of the inner liquid (water) beneath the outer liquid (oil) on chemically structured surfaces (as AG glass slides)

As can be seen in the graph 4.3.7 above, contact angles of the (inner) drops were seen to increase with an increase in their volumes- the effect being again more evident for the 'virtually confined' surfaces- observations being in analogy with the behaviour of single-liquid systems as previously discussed.

However, the contact angles of the inner, DI water drops, when beneath the outer, oil drop (bi-liquid system) were observed to be greater in values as compared to the values obtained for the same volumes of equivalent liquids without the oil cover (single-liquid system) (comparing graphs 4.3.3. and 4.3.7)—the effect again being more prominent for the chemically stratified surfaces (ΔCA's ~10°).

The above contact angle data was further complemented by the base diameter and height values calculated for such bi-liquid system—results revealing, as compared to for a single-liquid (DI water drop) system (refer figure 4.3.3), for water drop (beneath the oil drop), a slight decrease in its base diameter (ΔB.D ~ -0.08mm) and a slight increase in its height (ΔH ~ +0.06mm) for chemically non-stratified surfaces, and a slight increase in its height (ΔH~ +Δ0.32mm) for chemically stratified surfaces (droplets having fixed base diameters in this case).

Based on the above parameters, the configuration of the bi-liquid droplets on chemically non-structured and structured surfaces can be hence represented as:

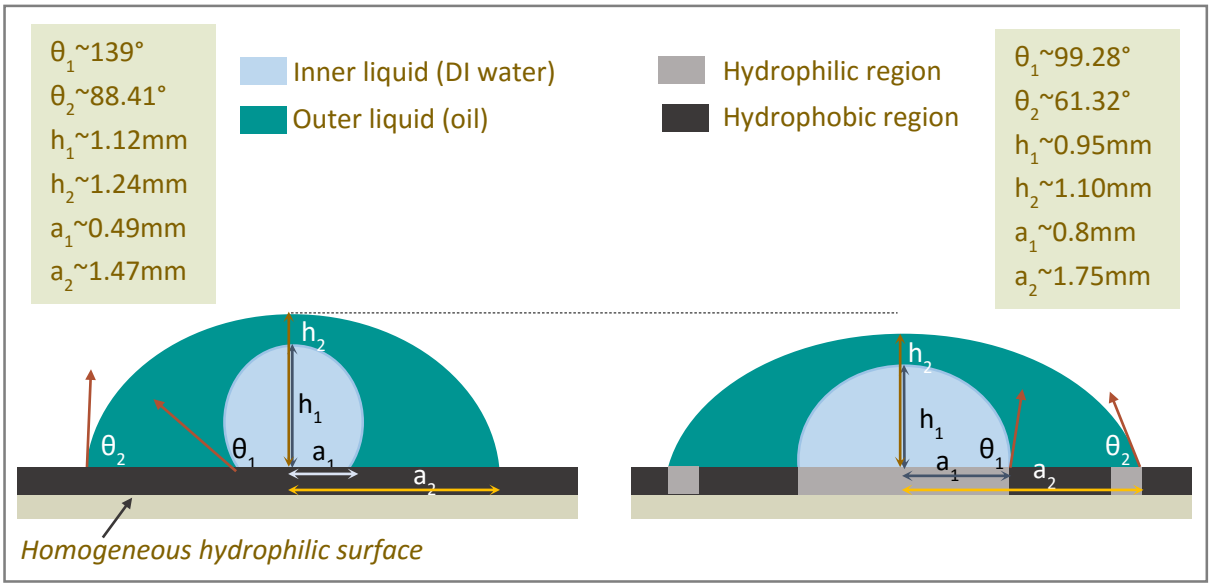

Figure 4.3.3: Configuration of the bi-liquid, micro-droplet system on the chemically non-structured surfaces (left), and on the chemically structured surfaces(right)

Conclusions

From the above analysis, it can thus be concluded that the geometries of droplets get modified when in the vicinity of an another liquid- the droplets exhibiting higher CA's for this case, as compared to for a single-liquid system. This was further accompanied by an equivalent increase in heights and decrease in base diameters for the bi-liquid drops – the effect being more prominent for chemically stratified surfaces where fixed base diameters pin the droplets making them bulge more as compared to when on homogenous, chemically non-structured surfaces.

The above behaviour can possibly be attributed to the greater water-oil (liquid-liquid) interactions than liquid-solid interactions- the homogenous, hydrophobic (chemically non-stratified) surfaces already repelling, particularly the aqueous drops. To it, potentially, as well contributes the lower liquid-air interactions [13q] than the subsequent liquid-liquid interactions (lower water-oil surface tension than water-air surface tension), as will be in detailed discussed in the section 4.3.3). The above hence overall results in slight elongation of the inner water droplet with the outer oil droplet above it. Also, this modified behaviour of the inner droplet effects the profile of the outer oil droplet- slightly raising the contact angle of the latter as well- again on similar lines as previously discussed, the effect being greater for the chemically stratified substrates.

Further, the consistency and reliability of the above measurements, indicted apart from the greater homogeneities associated with the underlying surfaces, pureness of the concerned liquids- the liquids possessing no prominent 'contaminations' (say in the form of a suspended solid particle or an already present air bubble) which could otherwise disrupt/pin the drops motion during analysis, resulting in disrupted geometries. This, in turn, as well excludes any major the role of the bi-liquid system, in general, in providing nucleation sites for bubbles formations at elevated working temperatures.

Nevertheless, moving from the study of the concerned micro-drops at room temperatures, next interesting aspect was to determine their behaviours at elevated temperatures- especially during the 1st stage of the PCR cycler (i.e. at 95°C for initial 10 minutes of heating), where most of the bubbles (when and if) were found to take place- as being taken up in the sections below.

4.3.1.2 Drop's profiles as a function of temperature

Temperature playing a vital role in the current work, an important analysis that demanded attention was determining the behaviour of the involved micro-droplets (liquids) as a function of temperature.

Literature reports, both experimentally and theoretically, a decrease in the CA of a liquids with an increase in the system´s temperature[15]. Though no details into the nature (degree of wettability's) of the associated surfaces was provided, statistics however claimed that for solid surface term assumed to be more or less independent of temperature, i.e. the ($\gamma_{SV} - \gamma_{SL}$) term to be approximately constant, according to Young-Laplace law (refer section 4.1.2.1), the cos θ term decreases with an increase in temperature, thereby yielding negative temperature coefficient of CA's ($d\theta/dT$)[196]. Conversely, some authors reported minimal effect of temperature on the CA- increase rates reported to be around 0.1°/K [196].

However, to determine the effect of temperature on the CA's and hence the droplets profiles for the system as under consideration, sophisticated experimental investigations were conducted, using the same (CA) measuring set up as described in section 4.2 before.

Such measurements nevertheless required the incorporation of a heating platform into the set-up; ASC, as typically being used in the current work, being not a very promising candidate in this regard owing to its dimensional incompatibility with the OCA static CA measuring assemble. For this, hence, a heating set-up (based on Peltier effect) was specially designed, such that the corresponding heating platform could be placed directly on the OCA sample stage for temperature dependence measurements- the altered set-up as can be seen in the image 4.3.2 on the next page.

The Peltier heater was, in turn, backed with an appropriate software control system capable of providing temperatures in the range of -20°C to 100°C (with ramp rates of 3°/sec).

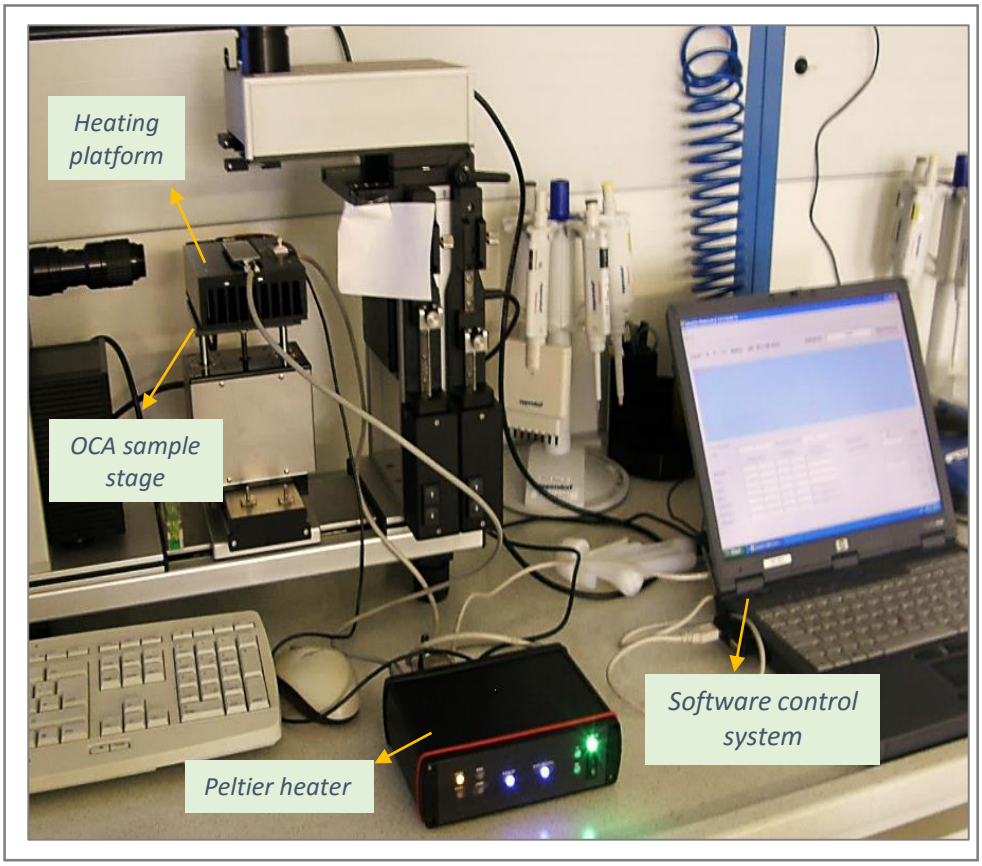

Image 4.3.2: Experimental set-up for temperature dependence of CA studies

Besides, another important system requirement owing to the high temperature sensitivities of the micro-droplets (especially of the inner aqueous drop) was the utilization of a glass aquarium- the to be investigated drops being enclosed inside a glass cuvette (10*10*10mm) for the measurements, as can be seen in the image 4.3.3 below:

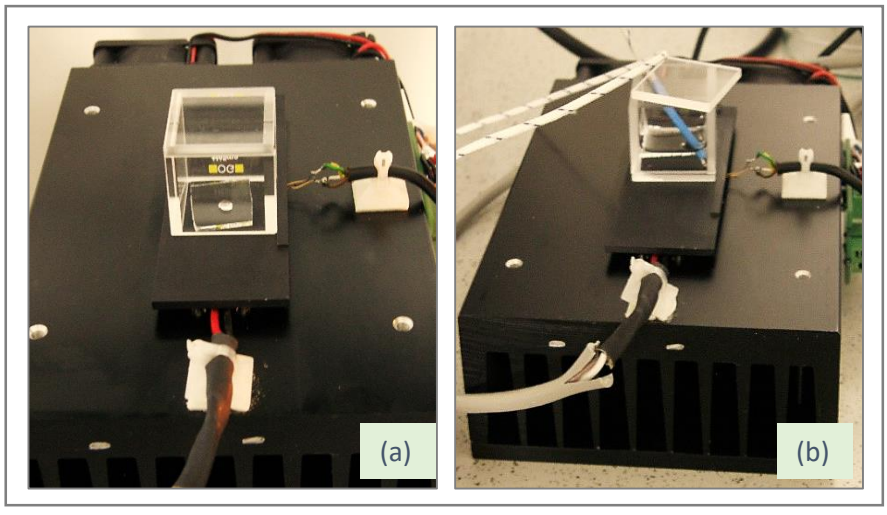

Image 4.3.3: Temperature dependence of static CA's for bi-liquid system - (a) glass cuvette containing the cut slide part placed on the specially constructed (Peltier) heater (b) set-up for calibration of the set-up prior to measurements

As with the study of bi-liquids at ambient temperatures, for their temperature dependences studies using the 'aquarium technique', the subsequent surfaces (glass slides) were cut using a diamond cutter into parts- the parts having base dimensions analogous to the base area of the cuvette for their easy placement into it. The cut surfaces after being properly cleaned for any leftover glass residues (using IPA, rinse in water, and drying with nitrogen), were next carefully slid into the cuvette- sited further atop the heater (on the sample stage of the OCA measuring (refer image 4.3.3)

Prior to measurements, the system was calibrated by inserting a PT100 sensor into the glass cuvette (refer image 4.3.3 (b)) - the sensor attached to a resistance thermometer at its other end for temperature readings. With the lid of the cuvette atop (for the maximum stabilization of the temperature inside it), using a standard stop watch, the time in which the (cut) slide surface (inside the cuvette) showed a particular set temperature was measured, and time vs. attained temperatures plotted (refer graph 4.3.8).

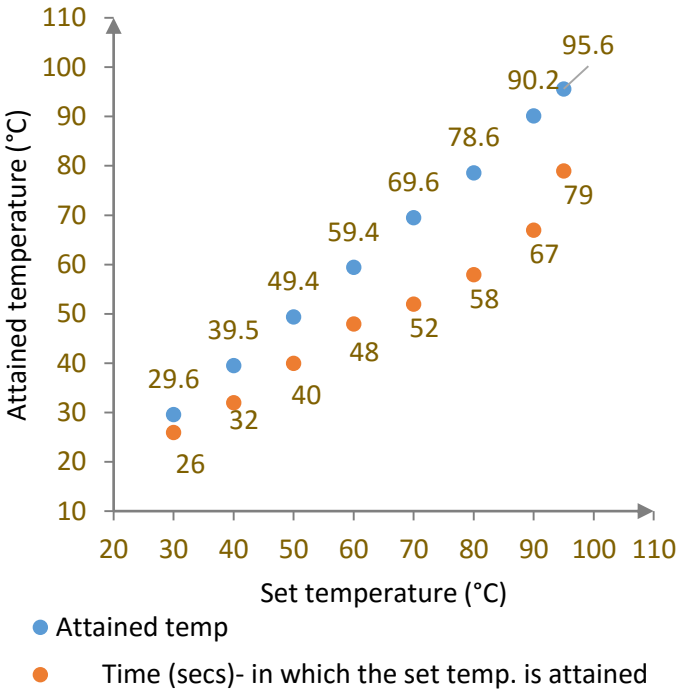

Graph 4.3.8: Calibration of the heating set-up for temperature dependence of CA studies

After the system was properly calibrated, and a desired temperature inside the cuvette stabilized (as measured by the PT100 sensor), the to be investigated micro-droplet(s) were dispensed on the cut part of the slide surface (placed inside the cuvette). Static CA's were measured on the instantaneously taken frozen image of the drop –studies being made both for the chemically non-stratified and stratified surfaces (their cut parts inside the cuvette) for comparative studies. Again, minimum of ten droplets being measured per temperature step, at least ten surfaces were analysed per study (opting a new solid (cut part of slide) surface and liquid combination per study).

In the similar manner as above, static CA's were measured and hence the drop profiles evaluated (both for single-liquid and bi-liquid systems) as a function of temperature – for the set temperatures of 23°C, 40°C, 60°C, 80°C and 95°C, as detailed in the following sub-sections.

- Temperature dependence of CA: For the single –liquid system

To study the behaviour of single-liquid systems as a function of temperature, typically oil droplets (standard 5µL of sealing solution), owing to their high boiling points (usually >200°C), were opted; aqueous micro-droplets due to their high temperature sensitivities rapidly evaporating, especially at higher temperatures, leading to false analysis, if used. The PT100 sensor inside the glass cuvette (with its lid on) throughout the measurements ensuring that the right temperatures are worked with, as with the previous RT studies, the drop's CA, its base diameter, and its height was studied as a function of temperature. Further, comparative studies were made for the droplets when dispensed on the chemically non-structured and structured surfaces.

For the **chemically non-structured** surfaces (PFS coated glass slides), results revealed (graph 4.3.9) an overall decrease in the CA of the oil drop with an increase in temperature – decrease rates observed to be comparatively smaller at lower measuring temperatures and greater as the temperatures were increased.

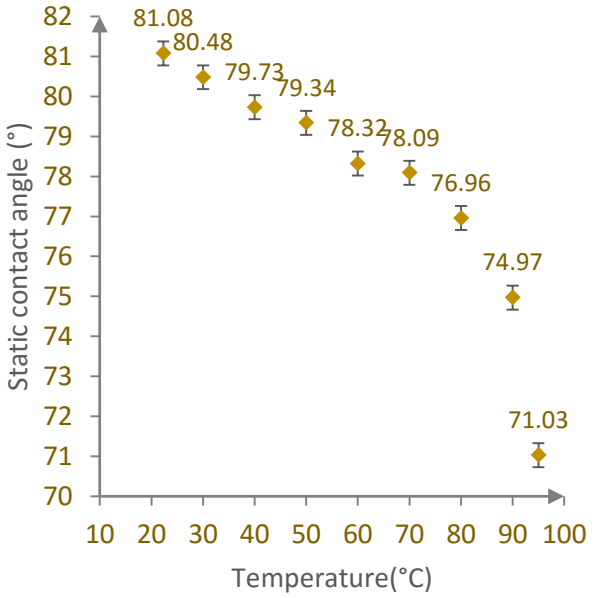

Graph 4.3.9: Temperature variation of CA for single -liquid system (5µL sealing solution) on chemically non-structured surfaces

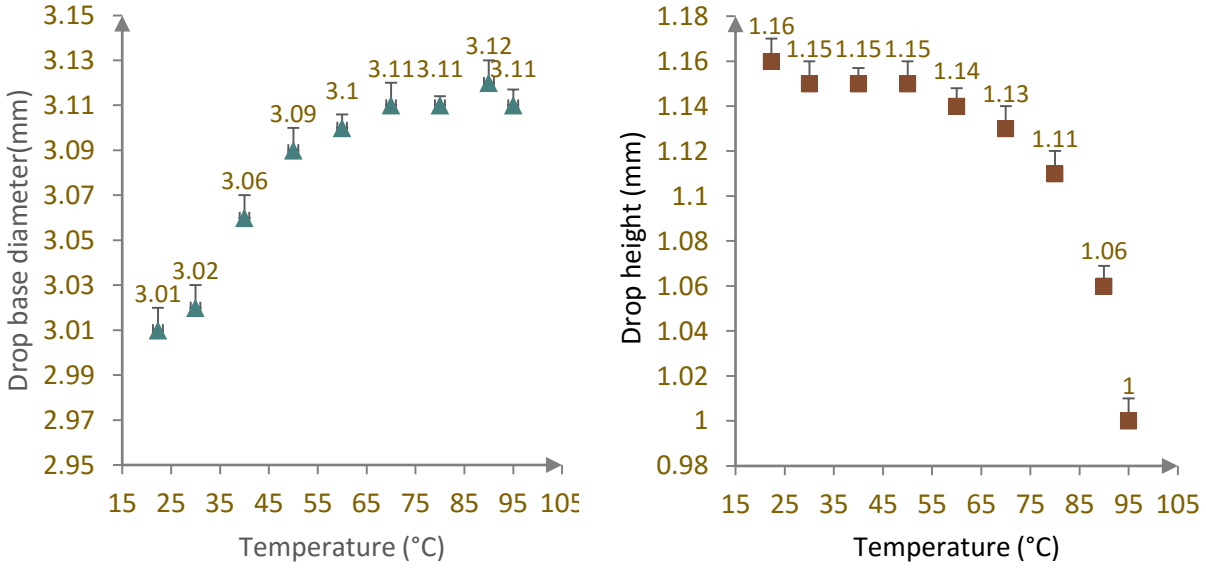

Graph 4.3.10: Temperature variation of base diameter(left) and height (right) for a single -liquid system (5µL sealing solution) on chemically non-structured surfaces

This was further complemented by a general increase in the base diameter (~0.01mm/10°C) and decrease in height (from RT-80°C to be ~0.01mm/10°C and from 80-95°C to be ~0.06mm/10°C) of the oil droplet with temperature for the chemically non-structured surfaces- as can be seen in the graphs 4.3.10 on the previous page.

However, analysis of the above single-liquid system (5µL sealing solution) on **chemically stratified substrates** (the liquid dispensed on the outer hydrophilic ring of 3.5mm diameter for the AG glass slides as used in the current work), results revealed two regimes in study of the variation of CA with temperature.

In the 1st regime, as can be seen in the graph 4.3.11 on the right, the CA of the drop was seen to increase with an increase in temperature- with a rate of ~0.15°/10°C from RT to around 70°C. However, beyond this temperature, in the second regime, the CA of the drop was seen to decrease with an increase in temperature: with a rate of ~ 1.6°/10°C from 70-80°C, and with a rate of 2.5°/10°C from 80-95°C ~ 2.5°/10°C.

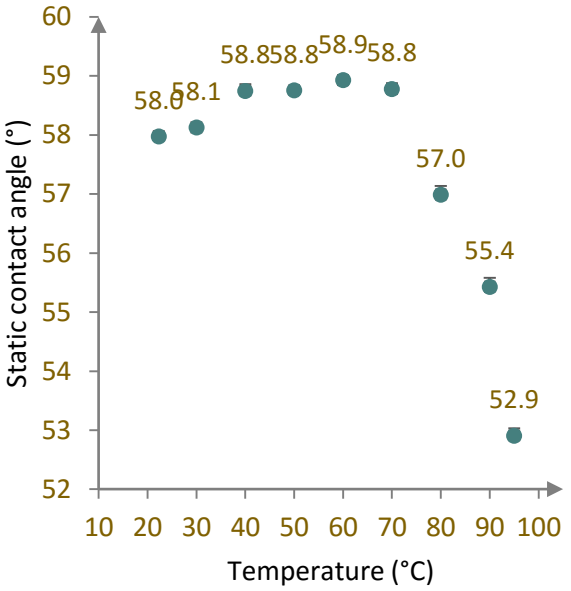

Graph 4.3.11: Temperature variation of CA for 5µL of sealing solution on chemically structured surfaces

The droplet being pinned by the surface chemistry on the chemically stratified slide surfaces, i.e. having fixed base diameters (of 3.5mm for the 5µL oil drop dispensed on the outer hydrophilic ring of the AG glass slides), the variation of heights of such droplets as a function of temperature complemented the above contact angle analysis: from RT to 70°C the droplets height calculated to increase (slightly) with an increase in temperature (ΔH ~ 0.01mm/40°C), whereas its height decreasing as the temperatures were increased further (from 70-80°C rate of decrease being ~0.03mm/10°C and from 80-95°C, rate of decrease being ~ 0.05mm/°C), as can be seen in the graph 4.3.12 on the right.

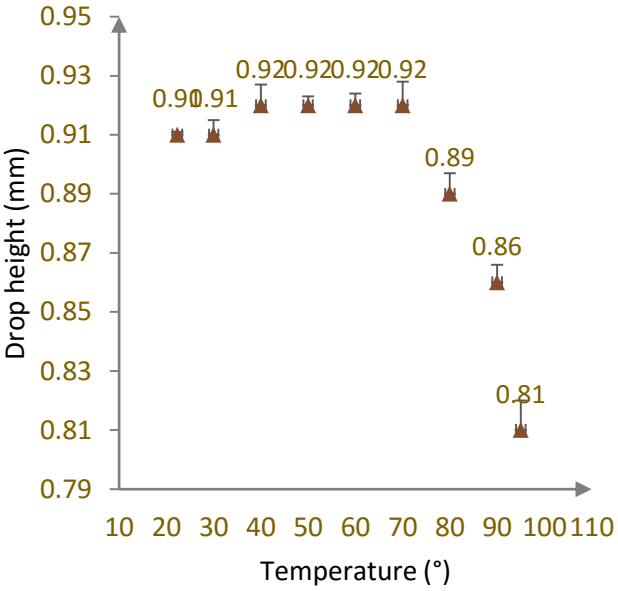

Graph 4.3.12: Variation of height of single - liquid (5µL sealing solution) on chemically structured surfaces with temperature

Conclusions

From the above analysis it can be hence concluded that increase in the temperature of the system modifies the profiles of the micro-droplets - the variations differing for the droplets when dispensed on the chemically non-structured than on the chemically structured surfaces.

The micro-droplets, owing to their low volumes are highly sensitive to evaporation effects, as previously discussed. Even though oils (with much higher boiling points) have been used to study the behaviour of single-liquids as a function of temperature, and despite of opting a highly temperature controlled measurement technique (with the OCA software capturing the image of the drop at a particular temperature as soon as it is formed), evaporation of the micro-droplets cannot be completely minimized, especially at higher system temperatures.

However, as the temperature of liquid increases, it's density decreases (refer Appendix B for the variation of density with temperature for sealing solution) – leading to an increase in the volume of the subsequent liquid (drop).

Thus, at higher temperatures, the profile of the droplet can be said to be determined by the balance of the evaporation and the (local) density effects- the evaporation effects nevertheless surpassing the density effects at higher temperatures.

Further, for the chemically non-structured surfaces (as the homogeneous, hydrophobically coated(PFS) glass slides), the initial (local) increase in the volume of the drop doesn't get highlighted owing to non-pinning of the droplet at a particular position on the slide surface— evaporation effects dominating the complete drops(free to move) behaviour- as reflected in an overall decrease in the CA , complemented by an equivalent decrease in the base diameter and increase in the height of the subsequent drop(s).

However, the droplets when dispensed on the chemically structured surfaces (as the AG glass slides), owing to they now being pinned by the surface chemistries, cause the initial (local) increase in their volumes with temperature dominate over the (early) evaporation effects - reflected in a slight increase in the CA, complemented by an equivalent increase in heights of the subsequent drops (for fixed base diameters) in this initial regime. But as the temperature of the system further increases (from say 70°C to 95°C), strong evaporation effects, as previously discussed, dominate the drop completely, resulting in a decrease in its CA (and its height) in this second regime.

Nevertheless, the variation of CA of a drop with temperature has been calculated to be very low in value (< 1°/ 10°C), in analogy with the literature- the temperature effects hence taken to be not very prominent in largely modifying the shape of the concerned micro-droplets, especially in a manner that would generate bubbles in an otherwise non-contaminated micro-fluidic system.

However, for a detailed analysis, interesting was to as well determine the behaviour of the bi-liquid system as a function of temperature- as detailed next.

-Temperature dependence of CA: For the bi-liquid system

Using the experimental set-up as described in the section above (refer images 4.3.2 and 4.3.3), for the complete comprehension of the micro-fluidic system, investigations were next done to determine the behaviour of the bi-liquid system as a function of temperature.

In this regard, mainly the behaviour of the inner water droplet (1µL) beneath the outer oil droplet as a function of temperature was studied (considering a slight increase in the CA of the oil droplet with the water droplet below it than without it- the effect prominent for the chemically structured surfaces, as with the RT studies).

The measurement technique for the clear visualization of the inner drop beneath the outer drop being same as for such studies at RT (section 4.3.1.1), with minimum of ten drops being analysed per surface, and at least ten surfaces being opted for a particular temperature measurement, studies revealed for the **chemically non-structured surfaces** (as PFS coated glass slides), CA of the inner water drop (beneath oil drop) to increase with an increase in the temperature- rates being ~1°/17°C from RT-70°C and ~ 0.2°/17°C from 70-90°C, (refer graph 4.3.13 on the right).

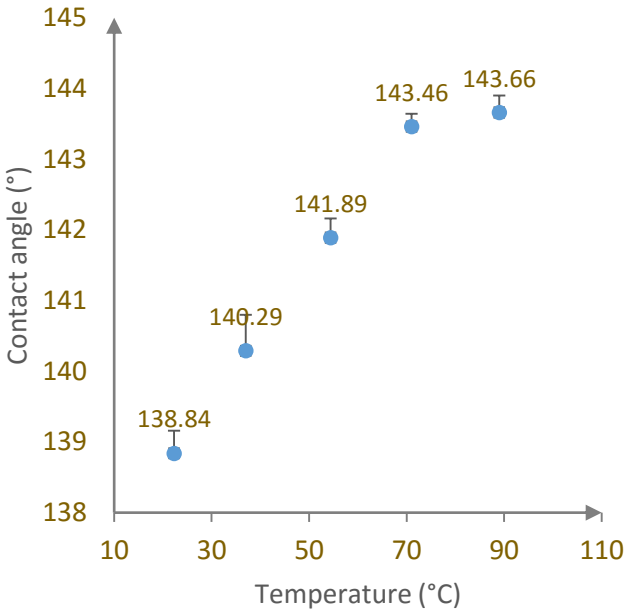

Graph 4.3.13: Temperature variation of CA for 1µL of DI beneath 5µL of sealing solution, on chemically non-structured surfaces

The above variation of contact angle of the inner water drop beneath the outer oil drop was further complemented by an overall decrease in the base diameter with increase in temperature of such (inner) droplets- decrease rates being ~0.01mm/17°C below 40°C, and ~ 0.06mm/17°C from 40°C- 95°C (refer (left) graph 4.3.15) , and an increase in the heights of (inner water) drops (beneath the outer oil drop) with an increase in temperature- increase rates being ~ 0.01mm/17°C from RT- 40°C and ~ 0.06mm from 40-95°C, as can be seen in the (right) graphs 4.3. 14 on the next page.

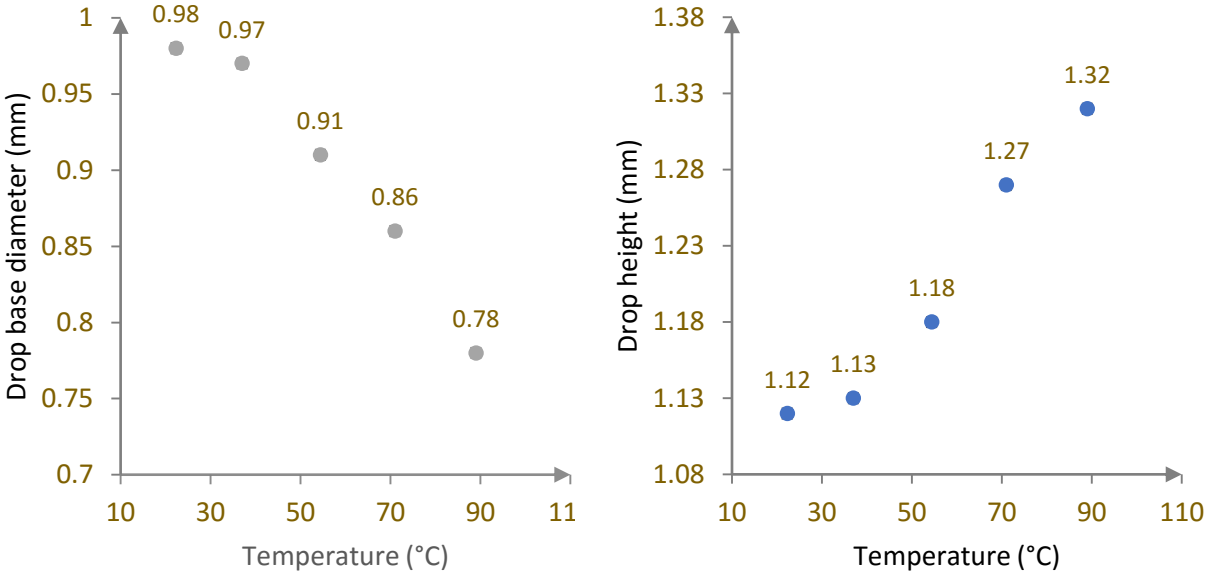

Graph 4.3.14: Temperature variation of base diameter (left) and height (right) for 1µL of DI beneath 5µL of sealing solution, on chemically non-structured surfaces

The above when compared to **chemically structured surfaces** with fixed base diameters (as=1.6mm for inner hydrophilic ring holding the inner liquid in place on the AG glass slides), measurements revealed two major regimes: CA increasing from RT-37°C with a rate of ~0.04°/°17°C and from 37°C-54°C with a rate of ~0.3°/17°C in the first regime, and CA decreasing from 54°C-95°C with a rate of ~2°/17°C in the second regime (refer graph 4.3.15).

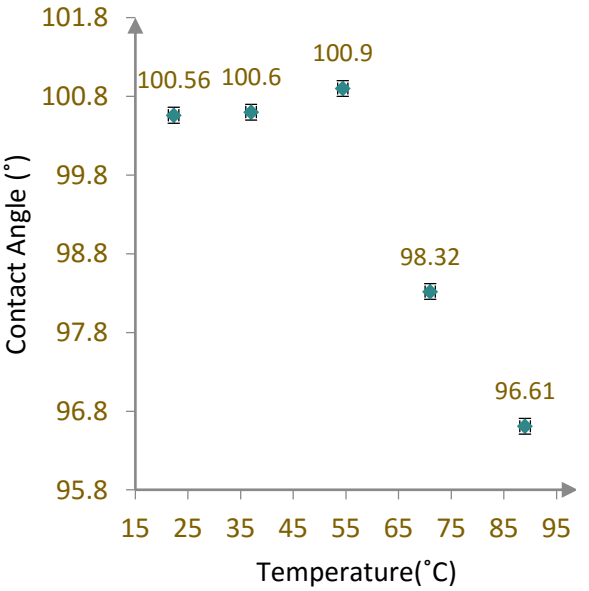

Graph 4.3.15: Temperature variation of CA for 1µL of DI beneath 5µL of sealing solution, on chemically structured surfaces

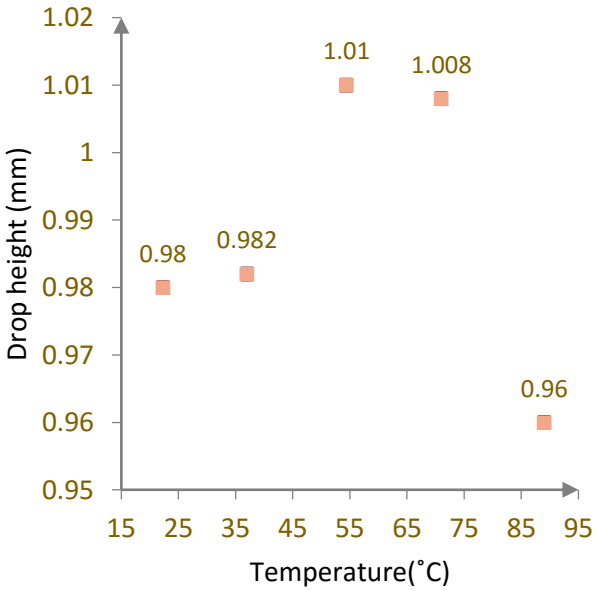

Graph 4.3.16: Temperature variation of height for 1µL of DI beneath 5µL of sealing solution, on chemically structured surfaces

This was again complemented by the temperature dependence of height measurements for the above system: the height of the (inner water) droplet beneath oil on chemically stratified substrates calculated to increase in the first regime: from RT-54°C with a rate of ~0.002mm/10°C, and decrease in the second regime: from 54-70°C with a rate of ~0002mm/16°C and from 70-95°C with a rate of ~0.004mm/25°C (refer graph 4.3.16).

Conclusions

From the above studies it can be hence concluded that as for the single-liquid system, the behaviour of the bi-liquid system (of the inner water drop beneath oil) with temperature is largely dependent on the type/nature of surface in use. For the chemically non-stratified surfaces, as the homogenous, hydrophobic coated PFS glass slides, with an increase in the system's temperature, the CA of the inner water drop increases (slightly) in value, complemented by an equivalent decrease in its base diameter and an increase in its height. This could possibly be attributed to the greater liquid-liquid interactions [surface tension of water-oil interface (~42 mN/m) lesser than the surface tension at the water-air interface (~72 mN/m), as will be dealt with in the next section] as compared to the liquid-solid interactions (the hydrophobic surface already repelling the (aqueous) liquid)- making the inner droplet 'shift-up' a bit with the outer liquid(oil) above it. The effect seems further enhanced at elevated temperatures apparently owing to greater repellency of the inner water drop by the hydrophobic surface (hydrophobicity reported to increase with an increase in the system's temperatures [q]), and not so prominent evaporation of the inner shielded water drop – making it elongate a bit more at higher temperatures, as can be seen in the image 4.3.4 on the right.

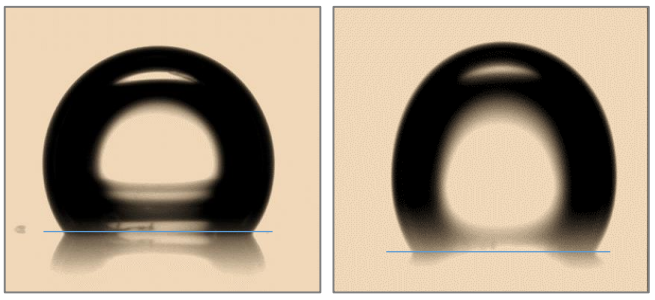

Image 4.3.4: Profile of the inner droplet (beneath the outer) on a chemically non-structured surface at (left) RT, (right) 80°C

The behaviour of the above bi-liquid system was however different from that of a single-liquid system (say just the oil drop) with temperature- the overall CA of the drop for the latter case decreasing (rather than increasing) with an increase in temperature. This was attributed to the dominance of evaporation effects on the oil drop at the liquid-air interface, complemented by non-pinning of the underlying hydrophobic (PFS) surfaces, making the droplet slightly spread out or flatten as the temperature of the system increased. Hence, for an in-depth understanding of the discrepancies in the behaviour of the single-liquid (focus: outer oil drop) and bi-liquid system (focus: inner water drop) with temperature, on the similar surface type (hydrophobic glass slides in this case), essential is to comprehend how the hydrophobicity changes with temperature for the non-polar liquids (as oil) and for the polar

liquids (as water)- the analysis serving as a promising outlook for further studies for the system as under consideration.

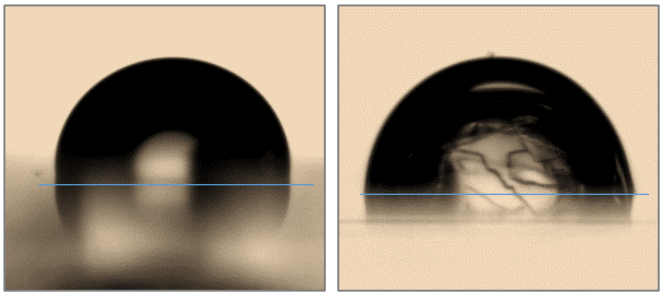

Image 4.3.5: Profile of the inner droplet (beneath the outer) on chemically structured surface, at (left) RT, (right) 80°C

However, for the chemically structured surfaces, as the AG glass slides, the behaviour of the bi-liquid system (inner water drop dispensed on the inner hydrophilic ring of the slide surface, beneath oil) as a function of temperature came out to be in analogy with as for the single-liquid system (just oil drop) : density effects dominating the drop's profile at lower temperatures (leading to small local decrease in volume and hence its CA), whereas evaporation effects dominating the drop's profile at higher temperatures, resulting in decrease in their CA with temperature—the behaviour being therefore different from when on a chemically non-structured surface (compare images 4.3.4 and 4.3.5).

4.3.1.3 Summary

From the above studies, it can hence be summarized that the profile attained by a liquid drop on a given surface depends largely on the nature of the liquid (say polar or non-polar), nature of the underlying surface (say chemically non-stratified or stratified), and on the measurement conditions (say at room or elevated temperatures) opted. Also, the studies successfully enabled in comprehending at room temperatures the behaviour of the dealt with bi-liquid system on chemically stratified AG glass slides (standard substrates): the 1µL inner exhibiting nearly spherical cap geometry with the outer, 5µL oil drop sitting slightly flattened above it.

However, the bi-liquid system when studied as a function of temperature, showed slight variations (measured in terms of CA's, base diameters and heights of the respective droplets), dependent again on the kind of liquid-solid combination opted- the disparities being nevertheless too low in values to greatly influence the overall micro-fluidic system, apparently- especially to an extent to effect the occurrence of bubbles in such systems.

Thus, it can be said that in the absence of any prominent nucleation sites (for the substrates fresh & clean, liquids clean, degassed and carefully pipetted/loaded, and the heating platform homogeneous and well-calibrated being opted), the above variations in the profiles of the bi-liquid system with temperature are not prominent enough to lead to or aid in the evolution of bubbles at elevated system temperatures (the statement further being in sync with the quantitative analysis conducted in the previous chapter where in the absence of any major nucleation sites, no bubbles occurrences were observed to take place).

However, it could be that the variation in the profile of the droplets with temperature, even though minimal, might influence the growth/rise/burst of the already nucleated bubbles - the area requiring in-depth experimental analysis say backed up with an appropriate numerical simulation/mathematical modelling of the concerned bi-liquid system- serving as another promising outlook for the detailed comprehension of the such micro-fluidic systems.

4.3.2 Surface tension studies

Apart from the CA studies, to further investigate the behaviour of the concerned bi-liquid system, surface tension at the liquid-air interface (for single-liquid system) and at the liquid-liquid interface (for bi-liquid system) was measured- both at RT and as at elevated system temperatures.

Whereas CA measurements are based primarily on the solid-liquid interactions, an important property that solely defines a liquid in the micro-scale regime has been reported to be its surface tension. For a freely dispensed liquid drop, its shape is largely determined by the degree of cohesiveness among the liquid molecules, which in turn is determined by the knowledge of surface tension for the corresponding liquid[15]. Since fluid systems always tend to minimize their surfaces, as larger the surfaces, larger are the number of molecules at the interface and hence greater the cohesive energy imbalance. In order to equilibrate their interactions, molecules at the interface thus always look for other molecules, in the process of which and in the absence of other forces, interfaces tend to adopt a flat profile- which when becomes difficult owing to the capillary constraints at the contact of solids, interfaces take a convex rounded shape as close as possible to that of a sphere[193,196,201-203].

Besides explaining the phenomena at the liquid-gas interface, the concept of surface tension equally holds true for liquid-liquid interfaces- the term being referred to as 'interfacial surface tension' in the latter case[193]. Also as compared to liquid-air interface, liquid-liquid interactions have been reported to be more energetic in nature (less dissymmetry)- thus explaining lower surface tension values for this interface (e.g. 50mN/m at water-oil interface) than at the corresponding liquid-gas interface (e.g. 72mN/m at water-air interface)[193].

4.3.2.1 Surface tension and Young-Laplace pressure[196]

An important equation in the study of interfaces and micro droplets is the Young-Laplace or the Laplace law, defining the relationship between the surface tension (γ) and the Laplace pressure (ΔP)- the pressure difference between the inside and the outside of a curved surface. For an interface locally defined by two (principal) radii of curvatures R_1 and R_2, Laplace law can be defined as:

$$\Delta P = P_{inside} - P_{outside} = \gamma \left(\frac{1}{R_1} + \frac{1}{R_2}\right) \quad (4.3.5)$$

For spherical shapes as bubbles or droplets, the radii of curvature being equal (R_1=R_2), yields:

$$\Delta P = \frac{2\gamma}{R} \qquad (4.3.6)$$

The above mark as significant relations in describing the behaviour of bubbles and droplets, and helps in determining the extra pressure (Laplace pressure) inside the bubble(s) or droplet(s) if the corresponding surface tension value is known, and vice-versa.

4.3.2.2 Measuring surface tension of liquids[193,196]

Literature reports various methods for measuring surface tension of the liquids-the measurements being usually based on taking surface tension as a force (as gravity in the pendant drop method, pressure in the bubble pressure method, capillary force in the Wilhelmy plate method, and fluid stress as in the drop deformation method) and calculating it by comparison with an another known force. However, owing to the ease of use, accuracy and availability, pendant drop method was utilized as the measuring method in the current work, as detailed in the sub-sections below:

The pendant drop method: using gravity[194,197,198]

Pendant drop, also sometimes known as the hanging drop, can be defined as a drop suspended from a fixed solid surface, say a needles tip, as can be seen in the image 4.3.6.

Such a drop is said to be chiefly balanced by the ratio of gravitational and surface tension forces- the ratio being scaled by a dimensionless number, the Bond number[15], as mentioned again in the equation 4.3.3 below:

$$B_o = \frac{\Delta\rho g R^2}{\gamma} \qquad (4.3.3)$$

where `Δρ´ is the density difference between the liquid and the surrounding fluid, 'g' the gravitational constant, 'R' a typical dimension of the hanging droplet taken as the maximum horizontal radius of the pendant drop in the current study, and 'γ' the associated surface tension. Whereas gravity tending to elongate the drop vertically and surface tension trying to minimize its interface to keep it as spherical as possible- the balance of the above two determines the shape of the droplet – the shape being evaluated via a suitable image analysing software on which the corresponding surface tension is determined.

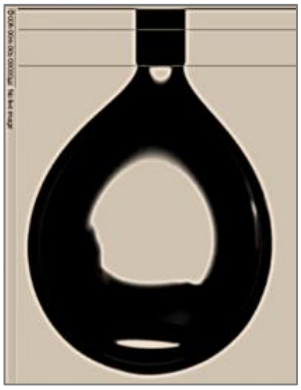

Image 4.3.6: Pendant or hanging drop suspended from a needles tip

Surface tension studies: Experimental investigations

For surface tension measurements, the same measuring device as used for the CA studies (OCA from Dataphysics) was employed- except for a few modifications that were made to the set-up -to analyse the shape of hanging droplets than of sessile droplets for the former studies. In this regard, first, the automated standard dosing unit for dispensing droplets for CA measurements was replaced by a third dosing unit -attached vertically upwards for the formation of pendant droplets, as can be seen in the image 4.3.7 below:

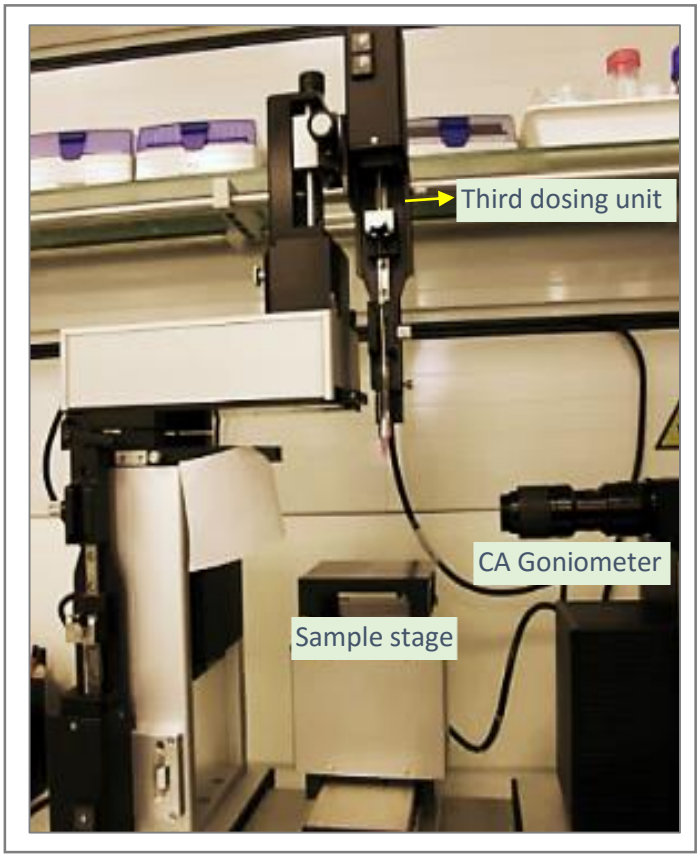

Image 4.3.7: Experimental set-up for surface tension measurements

The above dosing unit carefully holds the syringe loaded with the liquid whose surface tension is to be measured; the tip of the syringe needle being adjusted in alignment with the goniometer so as to view the formed hanging drop correctly.

Second, for liquid-air surface tension measurements, requiring no solid-liquid interface and to provide ample room for the pendant drop to freely form, the sample stage, an otherwise important component in contact angle studies, was significantly lowered as not to interfere with the surface tension measurements at any stage—the sample stage being only indirectly employed for liquid-liquid surface tension measurements as will be discussed later. In any case due to no direct usage of the sample stage in pendant drop method, no special care in cleaning of the stage was required- in contrast to other measuring methods as the Wilhelmy plate method where cleanliness plays a major role[2].

In accordance with literature, which reports the use of needles with large diameters to avoid the formation of too spherical but pear shaped drops elongated by gravity for accurate surface tension measurements, steel syringes with internal diameters 1.6 mm (largest ones available) with volumetric capacity of up to 28µL were used. Initial quick measurements at the water-air interface using needles having the above diameters, yielded values in close proximity with the available literature values, i.e. 72mN/m, thereby confirming their measurement accuracy.

Post needle selection, the OCA system was calibrated using the optical magnification of the camera lens, the software fed with the density of the respective test liquids for high accuracy measurements, and the pump calibrated using the internal diameter of the syringe (1.65mm). A hanging drop, as big as possible of the test liquid was then then dispensed from the needles tip and its snapshot taken around 1 minute after its formation- surface tension measurements best performed on the 'frozen' droplets image as with sessile droplet measurements. This was done to avoid any vibrational effects (caused by the surrounding medium) which might not let the drop instantaneously stabilize after its formation thereby significantly affecting its shape, and to capture the drop (shape) just prior to its fall (greater volumes associated with the hanging droplets raising their chances to fall off as soon as they are formed owing to domination of gravitational forces). Besides for high viscous fluids, viscous forces might creep in interfering with the required balance of primarily surface tension and gravitational forces- thereby avoiding live-in measurements to eliminate effects of inertial and viscous forces. The baseline to this frozen image rightly adjusted, surface tension was calculated by the fitting the drops profile (L-Y fitting method) by the measuring software. Surface tensions were calculated for the liquid-air and liquid-liquid interfaces, both at RT and as a function of temperature- for minimum of ten autonomous measurements being made per case.

Surface tension studies at room temperature:
At the liquid-air interface

Surface tension measurements for the liquid-air interface were made by dispensing drop of the test liquid (higher density) in air (lower density); dispense rates chosen as per the different viscosities of the measured liquids.

Measurements revealed, as can be seen in the graph 4.3.17 on the right, average surface tension for the **water-air interface** to be **72.04 mN/m** (with standard deviation of 0.3 mN/m) and average surface tension for the **oil (sealing solution) -air interface** to be **27.75mN/m** (with a standard deviation of 0.4 mN/m).

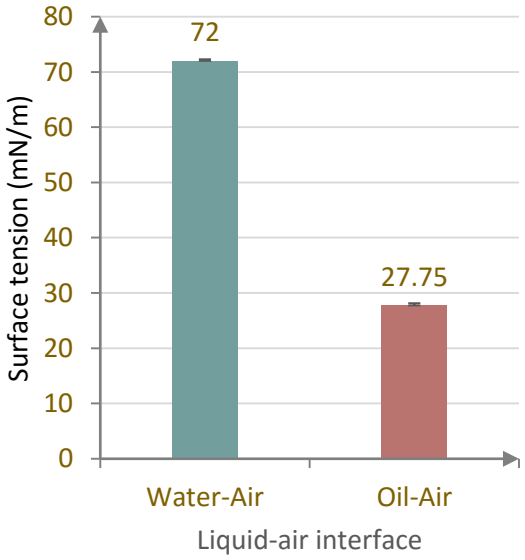

Graph 4.3.17: Surface tension at the liquid-air interface

Surface tension studies at room temperatures: At the liquid-liquid interface

Measuring surface tension for the bi-liquid system, i.e. at the water-oil interface required dispensing droplet of higher density (water) in the lower density (oil) liquid, for which the experimental set-up was briefly further modified. The measuring table was incorporated, above which was placed a glass cuvette containing oil (sealing solution), into which was dispensed the water-droplet, as depicted in the image 4.3.8 on the right.

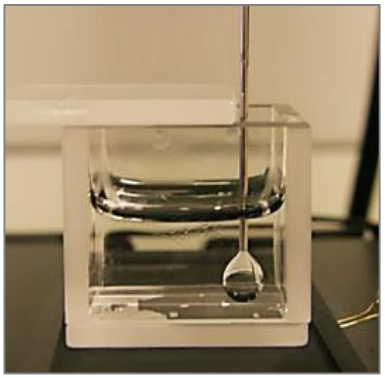

Image 4.3.8: Experimental procedure for surface tension measurement at the liquid-liquid interface

The average interfacial tension at the **water-oil interface** was measured to be **43mN/m** with a standard deviation of 0.13 (graph 4.3.18). Experiments further revealed the surface tension at the water-oil interface to be independent of the height of the oil in the cuvette.

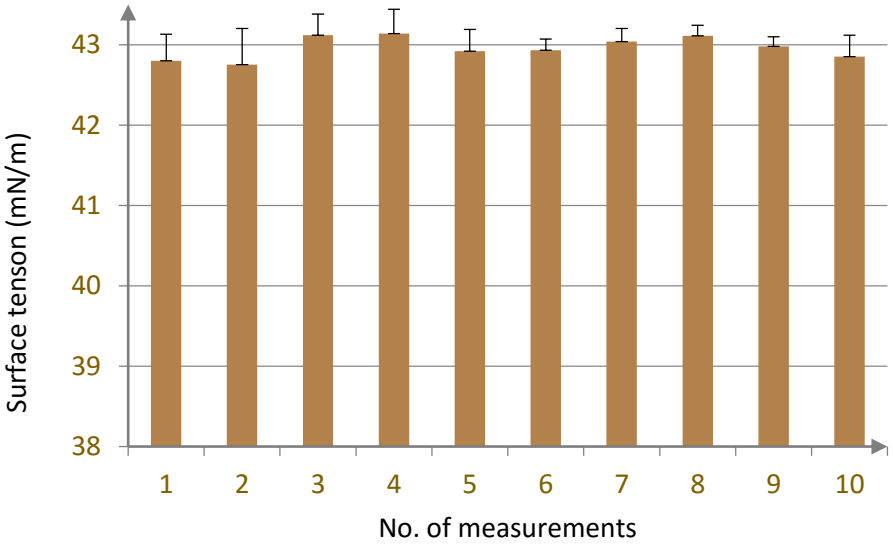

Graph 4.3.18: Surface tension measured at the water-oil interface

Dependence of surface tension on temperature

Temperature playing a vital role in the current work, an important analysis worth making was investigating the surface tension of the respective liquids as a function of temperature.

Literature reports the surface tension of liquids to linearly decrease with an increase in temperature in accordance with the relations[193]:

$$\Upsilon=\Upsilon^{*}(1+\alpha T) \qquad (4.3.7)$$

$$\Upsilon=\Upsilon_o\,(1+\beta(T-T_o)) \qquad (4.3.8)$$

where 'Υ^*' is constant for each liquid, 'α' and 'β' constants, and 'Υ_o' and 'T_o' the measured reference values.

However, to study the above for the liquids involved in the current work, sophisticated experimental investigations were conducted using the basic experimental set-up same as described in the section above. However, owing to the dimensional incompatibility of the heating cycler (ASC) with the OCA set-up, for temperature dependence studies, a specially designed (Peltier based) heating platform was used, as detailed in section 4.3.1.2 previously.

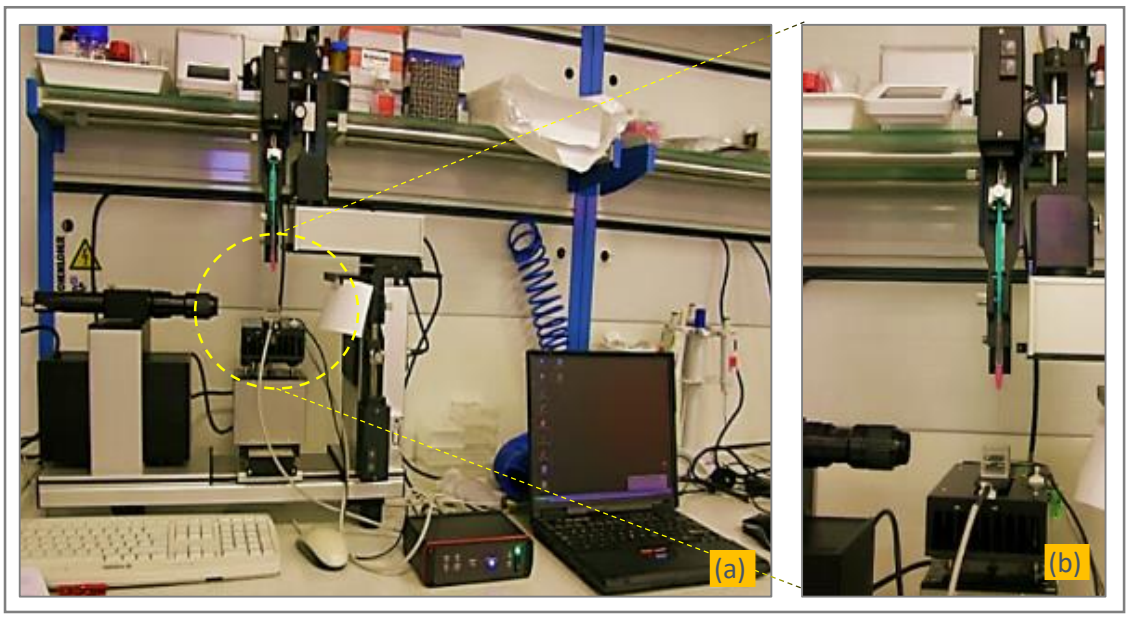

Image 4.3.9: Experimental set-up for temperature dependence of surface tension studies

Additionally, the sample stage of the OCA was utilized for these measurements, on top of which was placed the heating stage along with the glass cuvette with the liquid whose surface tension is to be measured (liquid-air system) and the lower density liquid (for liquid-liquid system). A PT100 sensor was inserted into the liquid bath connected to a digital thermometer at its other end, for calibration of the set-up (refer calibration graph 4.3.19), for the set temperature (of the heater) vs. attained temperature (of liquid in the glass cuvette with its lid on) after 10 minutes of heating, on the right).

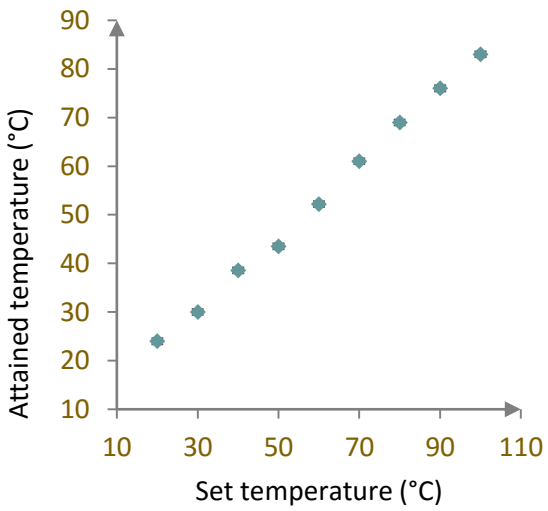

Graph 4.3.19: Calibration of set-up for temperature dependence of surface tension measurements

In order to study the temperature dependence of surface tension for liquid-air system (water-air or oil-air), 'bubble rising method' was adopted in which the glass cuvette was filled with the liquid whose surface tension was to measured, and an air bubble (lower density) was dispensed (rising up) using an inverted U-shaped syringe into the heated liquid.

However, for studying the effect of temperature on the surface tension of the liquid-liquid (water-oil) system, standard needles as used for room temperature measurements were taken- a drop of high density liquid (water) suspended into the lower density liquid (oil in the glass cuvette) for measurements. The liquid in the glass cuvette was heated to the desired temperature- measurements being made in steps of 10°C on the range of 25-95°C. A PT100 sensor was placed in the cuvette containing the liquid for measuring the temperature and calibration of the set-up (refer image 4.3.10).

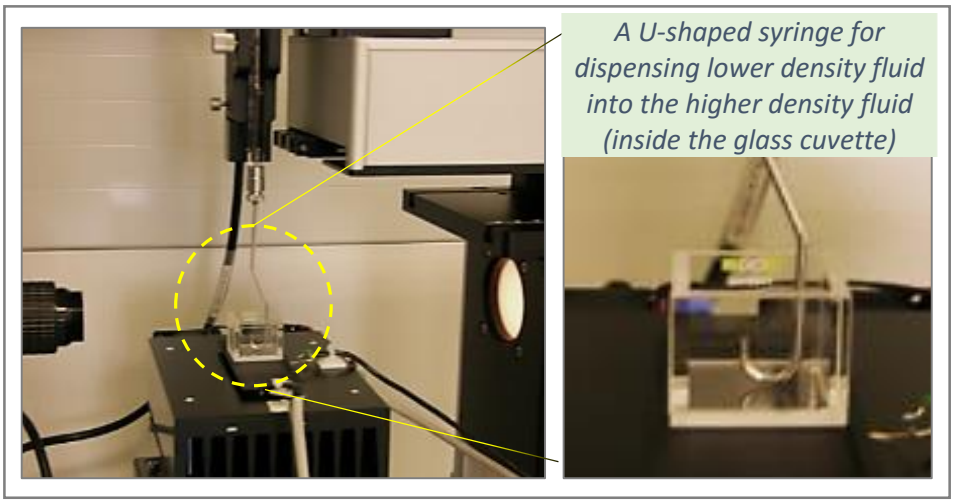

Image 4.3.10: Temperature dependence of surface tension studies at the liquid/air interface using rising bubble method[22q]- modified pendant drop method

For each measurement, a new liquid drop was dispensed, with minimum of ten measurements being made per case and the resulting data analysed in Excel 2013 for the corresponding averages and standard deviations.

Measurements revealed an overall, almost linear decrease in the surface tension with temperature- both at the liquid-air and at the liquid-liquid interfaces: rates of decrease being around **1.8(mN/m) /10(°C) for the water-air interface** (refer graph 4.3.20 on the right), around **0.8(mN/m)/10(°C) for the oil-air interface** (refer graph 4.3.21 below), and around **1.5(mN/m)/ 10(°C) for the water-oil interface** (refer graph 4.3.22 below).

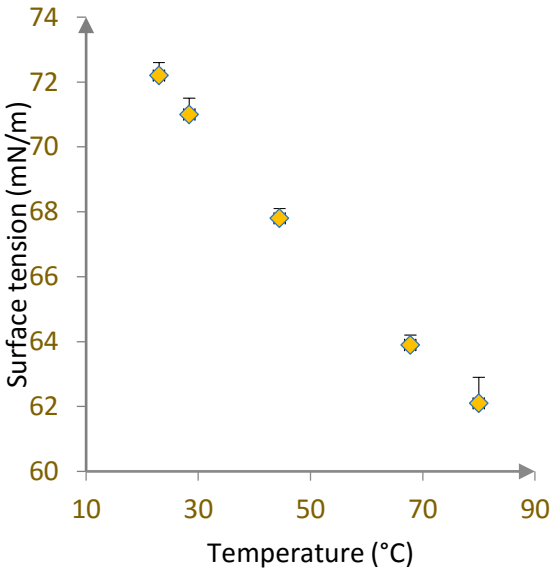

Graph 4.3.20: Variation of S.T with temperature at the water-air interface

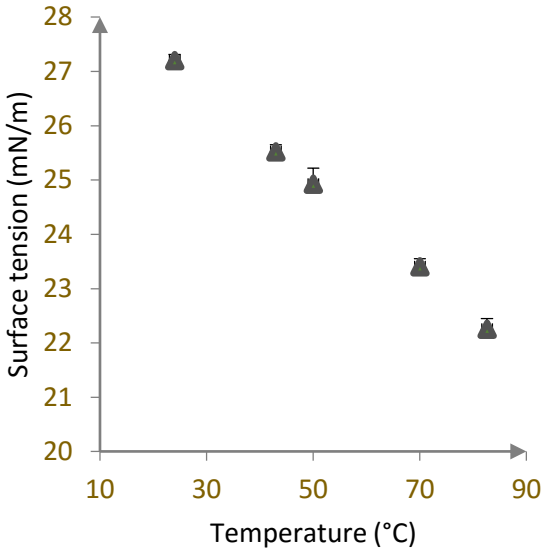

Graph 4.3.21: Variation of surface tension with temperature at the oil-air interface

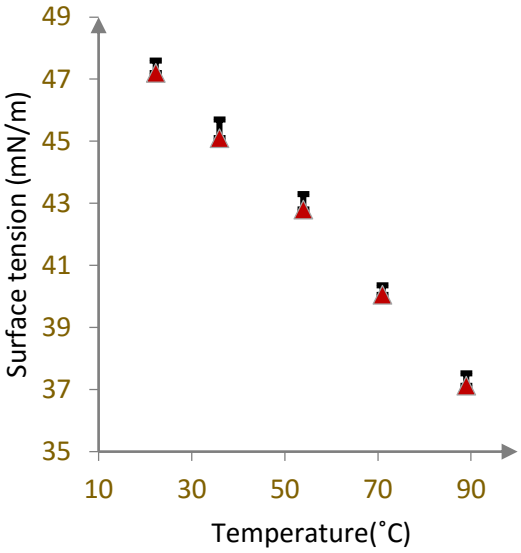

Graph 4.3.22: Variation of surface tension with temperature at the water-oil interface

Conclusions

The surface tension studies hence put forward, at room temperatures, the water-air interface to have much greater surface tension (~72 mN/m) than the oil-air interface (~27 mN/m)- the surface tension of the water-oil interface (~43 mN/m) lying somewhere in between the above two values. This hence further explains the beading up of the water droplets and spreading of the oil droplet on a homogeneous surface- the findings being in sync with the CA studies which figured out the inner water droplet to have nearly spherical cap geometry and the outer oil drop with a slightly flattened spherical cap shape sitting above it. Additionally, the results explain the slight 'lifting' up of the inner water droplet as the oil droplet is dispensed above it (i.e. for the bi-liquid system)- such an effect being more prominent for the chemically stratified substrates, holding the droplets in place and pinning their free motion.

Further, in analogy with the literature data, the experimental studies showed a nearly linear decrease of surface tension with an increase of temperature: the rates being ~1.8mN/m /10°C for the water-air interface, ~ 0.8mN/m/10°C for the oil-air interface, and ~ 1.5mN/m/ 10°C for the water-oil interface - the studies further explaining the slight spreading (decrease in CA) of the droplets (single-liquid systems) on a homogenous surface with an increase in the temperature.

Hence, while the surface tension studies complemented the CA data in explaining the behaviour of the micro-droplets at room- and elevated temperatures, the analogy of the experimental data with that in the literature signified the efficiency of the pendant drop method for successful surface tension measurements.

4.3.3 Liquid flows/convection profiles

Apart from the CA and surface tension studies, the bi-liquid system was further characterized to determine the nature of flows or the convection profiles in the respective liquids, especially at elevated working temperatures of 95°C. This was accomplished using Particle Image Velocimetry (PIV) – an optical method of flow visualization for obtaining instantaneous velocity measurements within the fluids[204].

PIV analysis usually requires seeding of the fluid whose velocity profile is to be measured with tracer particles, which for sufficiently small particles, are assumed to faithfully follow the flow dynamics (of the liquids). The degree to which the above occurs is represented by Stoke´s number[205-206]- a dimensionless number characterizing the behaviour of particles suspended within a fluid and defined as the ratio of the characteristic time of a particle (or droplet) to the characteristic time of the flow or of an obstacle, represented as:

$$Stk = \frac{t_0 u_0}{l_0} \tag{4.3.9}$$

where 't_0' is the relaxation time of the particle (the time constant in the exponential decay of the particle velocity due to drag), 'u_0' is the fluid velocity of the flow well away from the obstacle, and 'l_0' the characteristic dimension of the obstacle (typically its diameter). Particles with low Stokes number are said to follow the fluid streamlines (perfect advection), whereas particles with higher Stokes number are said to be dominated by its inertia and hence continue along their initial trajectories. Next, the concerned liquid is illuminated for the visibility of the entrained particles; the speed and direction (velocity field) of the flow calculated from the motion of the seeding.

In accordance with the above, for the determination of flows within the respective liquids (water and oil), both with and without the presence of a bubble, and at working temperatures of 95°C, initially sophisticated, HD, bottom view video recordings were conducted, using the experimental set-up as depicted in the image 4.3.11 on the next page.

The basic experimental set-up being the same as with the previous studies: the liquid droplet(s) placed on an AG glass slide above the heating platform investigated for the nature of flows within them, slight modifications were however made to the standard components of the micro-fluidic system for such investigations. In this regard, primarily, the direct incorporation of the typically used heating platform-the ASC, was skipped, owing to its dimensional incompatibility with the sample stage of the bottom view microscope. Instead, a new heating plate was constructed which could be placed straight away on the sample stage of the concerned microscope – the heating plate, in turn, attached via appropriate connections to the ASC at its another end. The heating plate was further secured onto an aluminium frame with clamps for holding the to be investigated slide/region in place. Additionally, the assembly was given a cut-out (a window of diameter ~4.5mm), to facilitate

easy and direct visualization of the to be investigated droplets, with one droplet examined at a time (refer image 4.3.12).

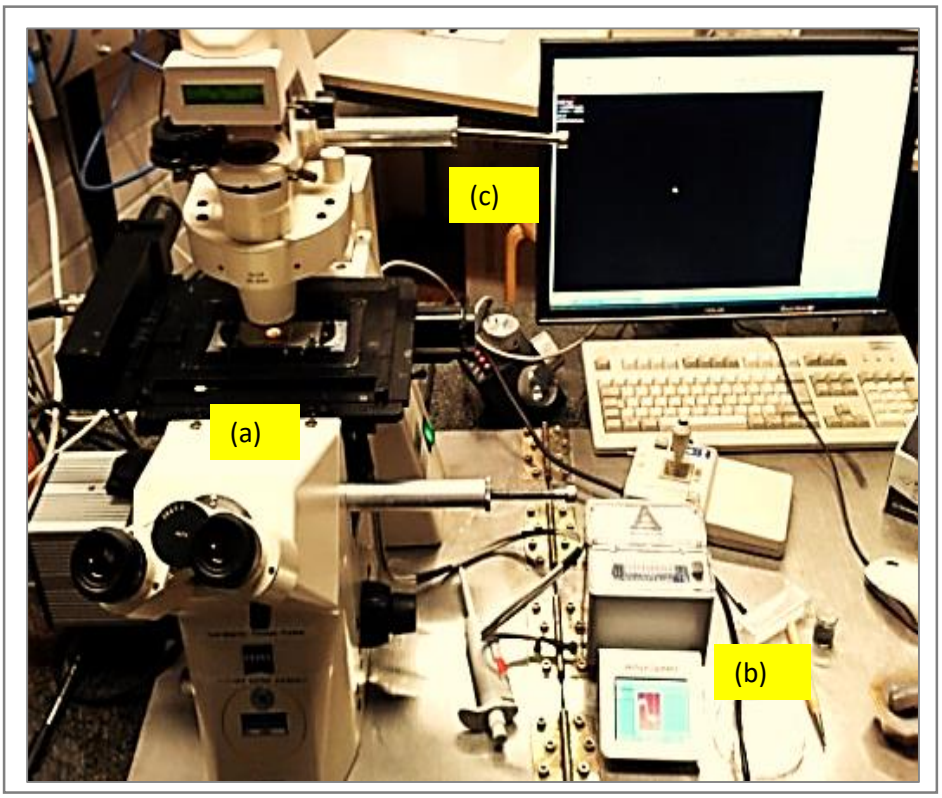

Image 4.3.11: HD bottom view recording experimental set-up for PIV analysis- (a) sample stage of the optical inverted microscope (Carl Zeiss) equipped with a high speed camera (Photron FastCam 1024 PCI), (b) ASC coupled with the heating foil (placed further on the sample stage of the microscope) to provide the necessary working temperatures, (c) attachment for image/video acquisition of the recordings

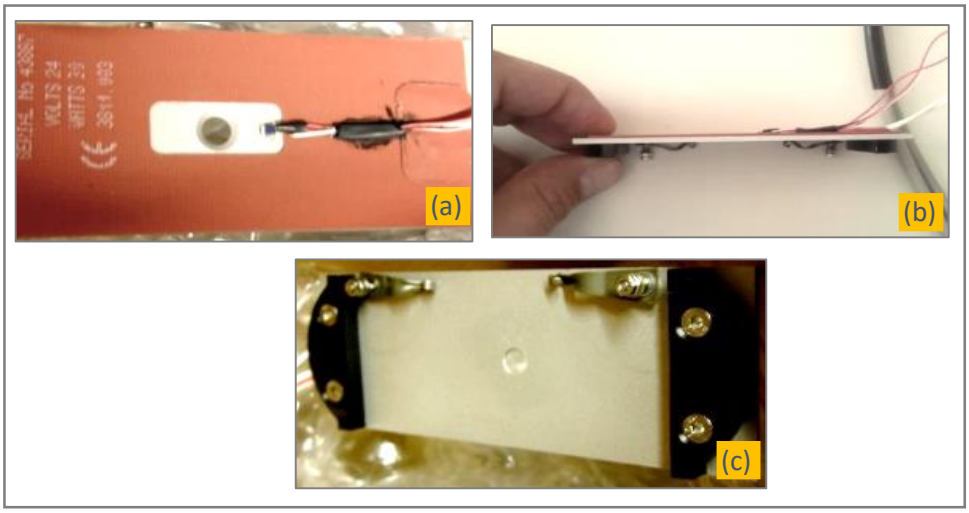

Image 4.3.12: (a) Heating foil top view, (b) side view: fixed onto an aluminium base, (c) back clamps to the Al base for holding the to be investigated slide in place

Using a dummy glass slide with a PT100 attached to it, the system was well-calibrated prior to use- refer calibration graph 4.3.23 on the right.

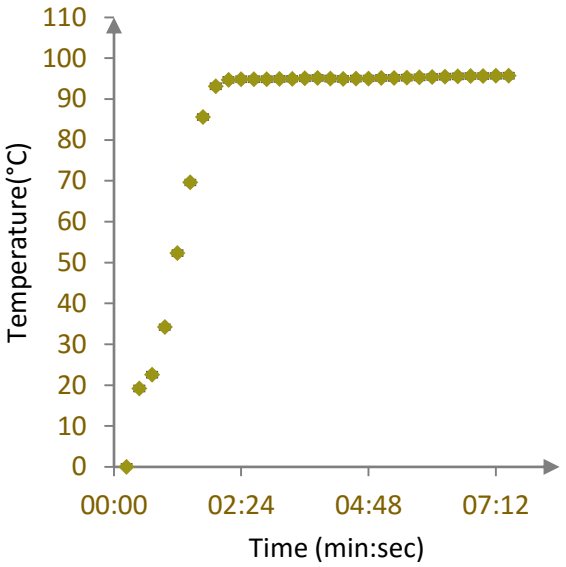

Graph 4.3.23: Calibration of experimental set-up for PIV analysis - for set temperature of 95°C, attained temperature (on the slide surface) vs time

Once done, a fresh, clean, glass slide (AG) was clamped to the aluminium frame below the heating plate-placed further on the sample stage of the inverted microscope. The to be examined liquid was monodispersed with biocompatible polystyrene (PS) particles via centrifugal technique- another important modification made to the micro-fluidic system for the PIV analysis- the drop of this prepared liquid next dispensed on the targeted region (reaction site) of the chemically structured glass slide. In some cases, experiments were as well done by dispensing as tracer particles thermos-labile polymer beads (2µm size) in water and diamond particles of 3µm size in oil.

As stated, with a single drop being examined at a time, studies were conducted to determine the flows at 95°C in 1µL of DI water (inner liquid) and in 5µL of sealing solution (outer liquid)- with minimum of ten drops being investigated per case. The video recordings were later analysed using appropriate video and image analysing software's as windows media player classic and Paint.Net; software's as ImageJ further employed for PIV analysis* (to estimate the corresponding velocity profiles) on the extracted image files.

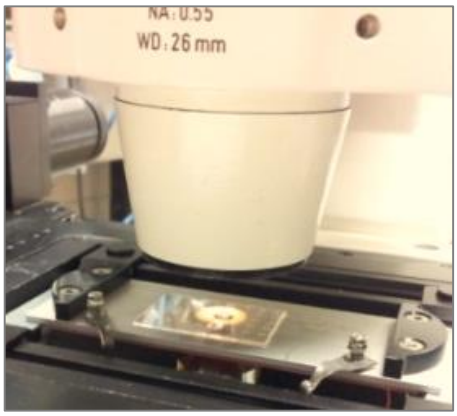

Image 4.3.13: Slide placed on the (specially designed) heating plate of the bottom -up set-up for PIV analysis, with the concerned micro droplet in focus

Initial quick experiments however revealed, for an underlying surface as fresh and clean as possible, for the liquids clean, properly degassed, and carefully pipetted/loaded, and for the heating plate homogeneous and well-calibrated, the mono-dispersed tracer particles not serving as nucleation sites for bubble formations at elevated temperatures- the probability of bubble evolution remaining <1% throughout.

The PIV analysis, on the other hand, showed clear motion of the tracer particles following the liquid

* *Data analysis courtesy: Dr Maciek Domansiki*

trajectories – the flows observed to be more prominent at the liquid-liquid interface especially when in the vicinity of a (rare) bubble.

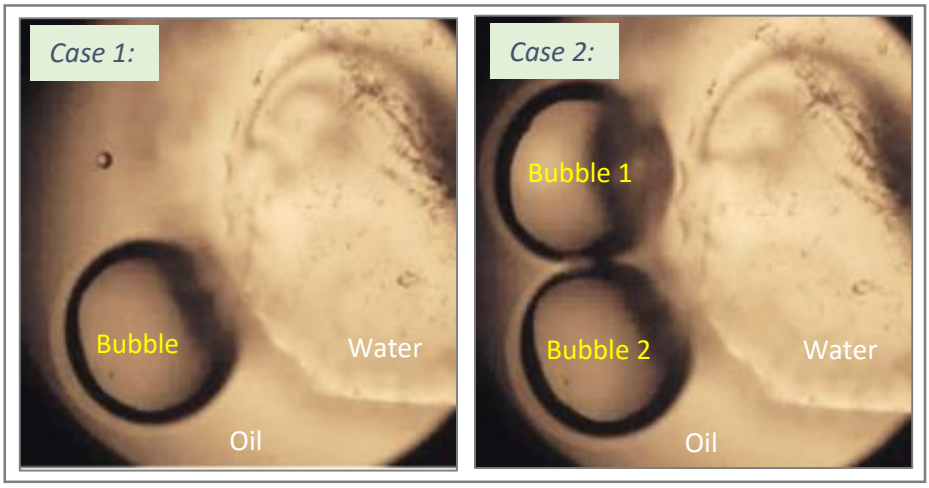

Image 4.3.14: Clear visualization of flow patterns traced by the polymer beads in water, at elevated temperatures of 95°C

Further, the ImageJ analysis revealed:

- The average velocity in oil *(in the absence of any bubble)* taken over ten measurements (n=10) to be ~1377±139 µm s^{-1}
- The average velocity in water *(in the absence of any bubble)* taken over six measurements (n=6) to be~ 24±13µm s^{-1}
- The average velocity of water *(in the presence of bubble)* taken over six measurements (n=6) to be~ 1040 ± 99 µm s^{-1}.

Thus, the PIV studies put forward, for the standard bi-liquid, micro-droplet system as under consideration, at 95°C, the velocity of the inner liquid (water) to be much lower than the velocity of the outer liquid (oil) – greater flow fields being nevertheless observed within the liquids when encompassing an emerging bubble.

Further, an important parameter that was estimated from the above results was the Reynolds number (R_e) – a number which helps in determining if the flow associated with the liquids is laminar or turbulent in nature. Liquids characterized by low values of R_e are said to be usually Newtonian or having a laminar character, whereas liquids having greater R_e values are said to be typically non-Newtonian or having a turbulent character[193,206-208].

Further being a dimensionless quantity, Reynolds number can be defined by the ratio of inertial to the viscous forces, as:

$$R_e = \frac{\text{inertial forces}}{\text{viscous forces}} = \frac{\rho v^2 L^2}{\mu v L} = \frac{\rho v L}{\mu} = \frac{v L}{\vartheta} \qquad (4.3.10)$$

where 'ρ' is the density of the fluid (kg/m^3), 'v' the mean velocity of the object relative to the fluid (m/s), 'L' the characteristic linear dimension (travelled length of the fluid) (m), 'μ' the dynamic viscosity of the fluid (N.s/m^2), and 'ϑ' the kinematic viscosity (m^2/s) of the fluid.

As can be seen from the equation 4.3.10, for fluids having low Reynolds number, viscous forces dominate their behaviour making them have a smooth constant motion, whereas fluids tend to exhibit turbulent flows for higher values of Reynolds numbers where the flow is mainly subjugated by the inertial forces- these forces having a tendency to produce eddies, vortices and other flow instabilities within the fluid. In the micro-fluidic regime, however, usually low Reynolds numbers are encountered, thereby characterizing laminar flow of the concerned liquids[193,206-208].

Estimating R_e for the micro-fluidic (water-oil) system as under consideration [for sealing solution taking its velocity to be 1377±139 um s^{-1} , length scale=1.75mm (radius of the outer drop holding the oil), density=0.78 g/cm^2 and dynamic viscosity=3.4 mPa*sec, for water taking its velocity without a bubble =24±13 um sec^{-1} and in the presence of bubble(s) =1040±99 um sec^{-1}, length scale =0.8 mm (radius of the inner drop holding the water), density= 961.62kg/m^3 and dynamic viscosity =0.000298 kg/m *s, calculations at 95°C revealed:

R_e (oil, without bubble) ~ 0.553 (I)

R_e (water, without bubble) = 0.0645 (II)

R_e (water, with bubble) =2.8 (III)

(I) and (II) being < 1 indicate the laminar flow or Newtonian nature of the concerned micro-fluids; (III) being > 1, on the other hand, directing to slight turbulent character of the liquids when incorporating an evolving bubble.

The above studies hence successfully helped determine the nature/degree of flows within the micro-droplets; the fluids exhibiting typically laminar flows, except for the turbulent regimes detected when a bubble evolves/grows within the system (as in the vicinity of the water-oil interface as shown in the image 4.3.14). Further, the average velocity within the inner droplet (water) was estimated to be way too less than that of the outer droplet (oil) – the outcome probably attributed to the shielding of the inner (1μL) water drop by the outer (5μL) oil drop (closed system) as compared to the direct exposure of the outer droplet to the atmosphere (open system). In any case, the outcomes of the PIV analysis might be additionally useful for the numerical simulation/mathematical modelling of the concerned micro-fluidic system (where the inner drop can be taken to almost stationary w.r.t to the outer counterpart) – for

a detailed study into the behaviour of the liquids, both with and without a bubble, and hence for the better comprehension of bubble dynamics in the same.

4.3.4 Summary

The above characterization of the bi-liquid system, initially in terms of CA and surface tension studies, hence successfully enabled the comprehension of the micro-fluidic system, both at room and at elevated system temperatures, and on chemically non-stratified and stratified substrates. Though the above studies revealed slight variations in the profiles/behaviour of the fluidic system especially with an increase of the system's temperature, for a fresh, clean substrate, an un-contaminated, degassed, and carefully pipetted/loaded liquid system, and a homogeneous, well-calibrated heating platform, the detected disparities came out as not sufficient enough to lead to or aid in the evolution of bubbles in such systems. This synced further with the findings of the quantitative analysis done in the previous chapter where for a system devoid of any prominent nucleation centres, the behaviour of say the micro-fluids with temperature, does not by itself result in the generation of any bubbles.

The PIV analysis, additionally revealed the presence of flows within the micro-droplets (at 95°C of working temperatures) -the flows typically being laminar in nature, except for the slight turbulences that creeps in for the system when encompassing an evolved bubble.

Thought the studies revealed no prime role of an un-contaminated liquid system in the nucleation of bubbles, how and if the system would influence the conduct of an emerging(nucleated) bubble, say its growth/rise, calls for a further detailed analysis- the experimental studies complemented by equivalent numerical simulations and/or mathematical modelling – serving as another promising outlook in this regard.

4.4 Final conclusions

The system characterization studies hence helped in gaining a better insight into the dealt with micro-fluidic system, primarily concluding:

- The surfaces produced are, on an average, greatly homogeneous in nature with high degrees of wettability's, thereby indicating the effectiveness and quality of the production techniques employed in generating the same. Nevertheless, for few of the exceptional cases, some surfaces exhibited rare surface imperfections (in the form of crater like structures)- potentially serving as sites for bubble formations at elevated working temperatures. The above inhomogeneities mainly detected on the hydrophobic regions of the fabricated surfaces, further indicated some left over coating residues, not being properly cleaned, perhaps being the source of such inhomogeneities. This hence calls for extreme care taken in the production of the concerned surfaces, to avoid such discrepancies- in any case, for the surfaces detected exhibiting such regions being

discarded prior to use. However, detailed understanding on how a site having dimensions analogous to the ones detected by say microscopic investigations leads to the nucleation of bubbles and the conditions of gas entrapment will be attempted in the next chapter- tilted as Bubble Dynamics.

- Characterization of the heating cycler (ASC) revealed homogenous and consistent overall heating provided by the heating plate of the cycler- with no prominent fluctuations in the heating profiles that could aid to lead in the evolution of bubbles, especially at the vulnerable 1st stage of the PCR cycle (i.e. at 95°C). Further, the thermal profiles generated were found independent of the ramp rates opted- higher ramp rates (3°C/sec) being nevertheless employed owing to faster ramp timings (~40 seconds) associated with them.
- Lastly, the characterization of the bi-liquid system revealed slight variations in the profiles of the micro-droplets with temperature- the variations nevertheless being not significant enough to hugely modify the system so as to lead to or aid in the evolution of a bubble. Typically, an un-contaminated, highly degassed, and well loaded/pipetted bi-liquid system was found to be superior enough not to generate any nucleation sites for bubble formations. PIV experiments further revealed greater velocities in water (inner liquid) than in oil (outer liquid); greater turbulences being observed within the liquids when encompassing an evolved bubble. The studies, however, called for detailed numerical simulations/mathematical modelling in this regard, for a better comprehension of the micro-fluidic system and to understand the concept of bubble dynamics in the same.

Thus, the chapter successfully helped in the comprehension of the dealt with micro-fluidic system- details into the understanding of dynamics of a bubble (when and if evolved in the concerned system) being taken up in the next chapter.

CHAPTER 5

BUBBLE DYNAMICS

5.1 Introduction

Bubble dynamics can be defined, in a broader sense, as a term encompassing the various physical phenomenon governing the different stages in the lifetime of a bubble- from its nucleation to its growth and/or rise, and finally to its burst. Thus, in order to comprehend the concept of bubble evolution in any system and to subsequently put forward methods for the control or elimination of the same, investigation of the above mentioned facets, both independently and coherently, marks as an elementary and a significant analysis step.

The chapter hence aims in providing an in-depth grasping to the above, by initially offering the relevant research carried out (so far) in comprehending the above facets, with subsequently stating the various experimental investigations conducted in understanding of the same. In closing, the chapter proposes various experimentally tried out solutions, that could be possibly adopted for the elimination or suppression of bubbles in such systems.

5.2 Bubble nucleation

The previous chapter hinted, that the solid-liquid interface, either in the form of surface imperfections (as crater like structures) in the vicinity of the liquids, or as suspended solid inhomogeneity's within the bi-liquid system, could serve as potential sites for bubble nucleations. Further, the crater like surface inhomogeneities detected (mainly on the hydrophobic regions of the chemically structured surfaces), were observed to have diameters in the range of 2-10 μm, inner depths between 2-4 nm, and heights (of the distinct peak like projections at their edges) in the range of 10-200 nm. However, the studies, owing to the

extreme rarity and randomness of the above structures, could not exactly spot a site having above dimensions nucleating bubbles. This hence calls for more sophisticated, say experimental proceedings, to confirm the above findings- done primarily in the current chapter by mimicking the above structures (say via refined surface fabrication techniques) and investigating the criterion of bubble evolutions from them. Besides, queries as: 'What is the physical phenomena governing nucleation?', 'What is the mechanism and condition for a solid-liquid interface to act as a gas entrapping site?', 'What is the effect of temperature on bubble nucleation?', and 'How and if the nucleation varies for the nucleation sites present at different positions (say under water, under oil, or at the water-oil interface) in the concerned micro-fluidic system?', seek detailed understanding- being the prime focus of the current section.

However, before proceeding to the various experimental investigations done in this regard, a brief literature review into the nucleation phenomenon is put forward, as stated in the following sub-sections.

5.2.1 Literature review

Literature reports tremendous work that underwent into studying the phenomenon of bubble nucleation, especially in superheated liquid systems- covering largely the realms of bubble cavitation and nucleate boiling[209-216]. Additionally, though much has been accomplished regarding the same in single-liquid systems, not much has been reported to have been achieved in understanding the evolution of bubbles in bi-liquid systems- that too in the micro-scale regime.

However, talking of nucleation in general, researchers have defined it broadly as the localized budding of a distinct thermodynamic phase -- the onset of a phase transition in a small region of a medium- the phase transition being either in the form of a tiny bubble in a liquid or a droplet in a saturated vapor[216-218]. Depending on the rate of super-saturation in the system, nucleation has been further reported to have been classified into various categories[219], as discussed next.

Nucleation: Classification

Researchers have largely classified nucleation into four categories: the classical homogeneous nucleation (type I), the classical heterogeneous nucleation (type II), the pseudo classical nucleation (type III), and the non-classical nucleation (type IV)- the classification being primarily based on the rate of super-saturation in the system- highest rates being required for the type I and lowest for the type IV nucleation. Talking of super-saturation, a supersaturated solution can be referred to a solution containing more of the dissolved material than that could be dissolved by the solvent under normal circumstances. Further, supersaturation has been reported to be highly temperature and pressure dependent- different levels of supersaturation possible by increasing the temperature or by decreasing the pressure of the concerned system(s)[219].

Beginning with classical homogenous or type I nucleation, this type of nucleation has been reported to require very high levels of system supersaturation to occur, within a supersaturated liquid. Such a nucleation could take place without the presence of any gas cavities on a molecularly smooth surface in a perfectly degassed system, i.e. the nucleation being able to take place in the liquid phase without the prior presence of any additional phases. The nuclei responsible for bubble formations in this case are also at times referred to as cavitation nuclei- the cavity formation in a homogenous nucleation requiring sufficiently large stress, known as the tensile strength of the liquid at that temperature, to rupture the host liquid. Additionally, some authors have as well reported that for this type of nucleation, once a bubble is incepted, it rises to the surface of the liquid- it being unlikely that additional bubbles form at the same location in the system[218-219].

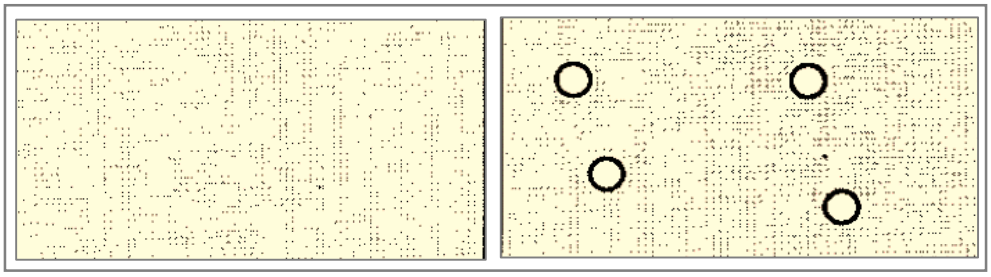

Image 5.2.1: Pictorial representation of type I or classical homogeneous nucleation-producing gas bubbles in the bulk of the liquid at high levels (of 100 or more) of system super -saturation. System before super saturation(left), system after super saturation (right) [219]

In contrast to the above comes the classical heterogeneous nucleation (type II), requiring comparatively lower levels of system super-saturation. This type of nucleation has been reported to usually occurs at the interface between a contacting metastable phase and another (usually solid) phase. In a system initially devoid of any gas cavities in the bulk or on the solid surface, a bubble may be formed by the diffusion of gases from the supersaturated liquid (high pressure region) to the pit (low pressure region) on the solid surface (as per Laplace law), on an otherwise molecularly smooth surface, or on a particle suspended in the bulk of the liquid. This incepted bubble then grows, sufficiently enough to a point where the buoyancy forces dominate the gravitational forces, resulting in the eventual detachment of the bubble from its nucleation site – in turn leaving behind a low pressure region (pit), thereby forming a (new) gas filled cavity. Hence, for type II nucleation, in contrast to type I nucleation, detachment of bubble from a nucleation site, leads to further generation (cascade) of bubbles from the same site till the system's supersaturation (system's pressure/temperature) is unaltered. Further, in respect to the size of the nucleation cavities some authors have reported that the nanometer sized cavities are usually not potential sites for gas entrapment for type II nucleation's to occur- owing to the high pressure difference between the bubble and the vapor in the surrounding liquid- resulting in quick collapse of the bubbles upon formation[215,219-222]. Besides, though some authors reported that for surfaces having varying wettabilities (different hydrophobic/hydrophilic character), the amount of super-saturation required for heterogeneous nucleation to occur on a hydrophobic and a hydrophilic smooth

particles is about the same, others, on the other hand ,concluded that small pockets of gas stabilized at the bottom of the cracks or crevices exist chiefly on the hydrophobic solid impurities in the liquid or on the solid surface – thereby deducing such a nucleation to occur more likely on the hydrophobic surfaces than on the hydrophilic ones[219-222].

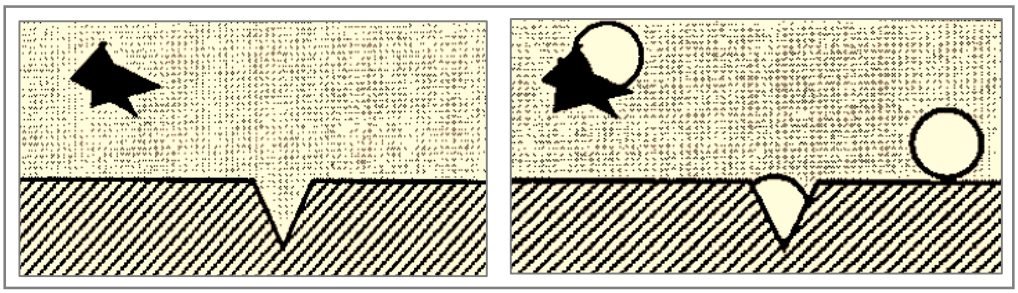

Image 5.2.2: Pictorial representation of Type II or classical heterogeneous nucleation- catalysed by the presence of another material in the bulk liquid. System before super saturation (left), system after super saturation(right)

Moving next, the third type of nucleation, the pseudo-classical nucleation, was reported to require further lower levels of system super-saturation as compared to type I and type II nucleation. Presence of gas cavities in the system, either at the solid surface, at the surface of suspended particles or at the metastable micro-bubbles in the bulk solution, serve as 'seeds' for bubble nucleation; the presence of participating interfaces affecting the nucleation process by decreasing the energy barrier to nucleation[219].

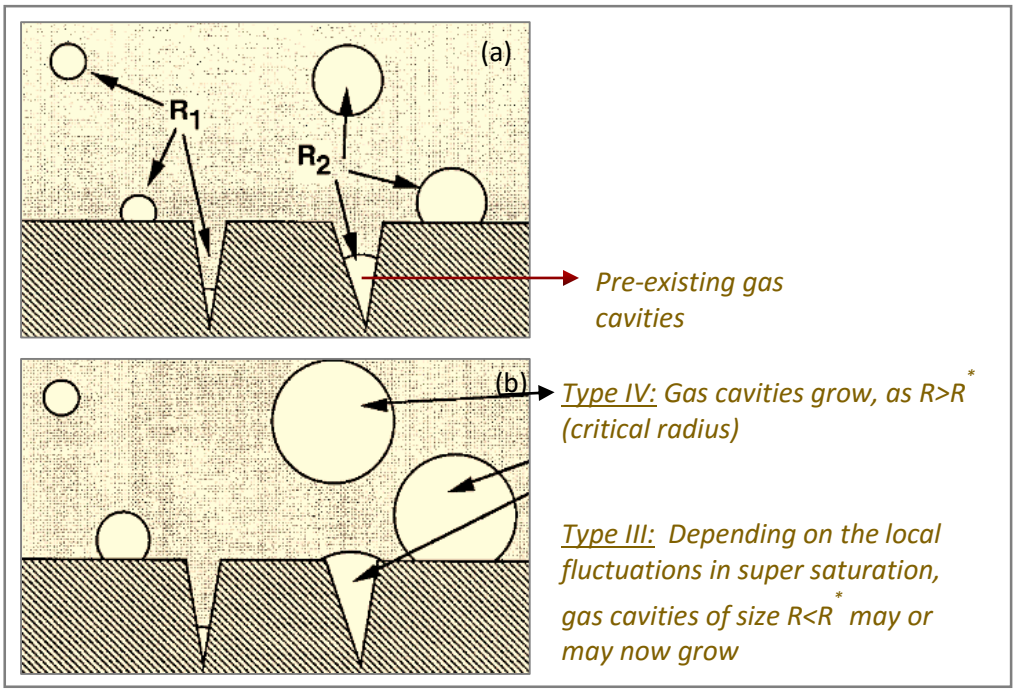

Image 5.2.3: Pictorial representation of Pseudo –classical (type III) and non-classical (type IV) nucleation [A] (a) system before super saturation (pre-existing gas cavities) (b)system after super saturation

The fourth type, the non- classical nucleation, on the other hand, requires comparatively very low levels of super-saturation, and as the name suggests, necessitating no nucleation (energy) barrier for bubble nucleation to take place. This type of nucleation has been reported to take place usually on the pre-existing gas cavities at the solid surface or elsewhere in the bulk liquid and may subsequently follow type II or type III nucleation events. Over time, as the super-saturation decreases, the critical nucleation radius increases to a value equal to the radius of the given cavity meniscus, resulting in the cease of the bubble production from the cavity[219].

However, as far as the micro-fluidic system, as dealt with in the current work is concerned, for maximum working temperatures of 95°C (at atmospheric pressures), and considering the liquids to be highly clean and degassed, the system can be said to not have very extreme levels of supersaturations. To this, adds the findings of the previous chapter, where bubble evolutions(rare) were seen to occur on substrates potentially being 'infected' by the crater like surface inhomogeneities – hence indicating the heterogeneous or type II nucleation to be the prime mode of nucleation, if and when it takes place in the dealt with fluidic system.

In this regard, an important model, that successfully explains the phenomenon of especially heterogeneous bubble nucleation, is the crevice model of bubble nucleation, as briefly discussed next.

The crevice model of bubble nucleation[6,223]

Originally proposed by Atchley and Prosperreti (1989), the crevice model is based on two prime assumptions: one, that the crevice or the nucleation cavity assumed for the study is conical in shape with a half angle aperture 'β ', and two, that the model ignores the phenomenon of diffusion of gas in or out of the nucleus, i.e. the gas content in the cavity is taken to be constant. According to the model, when the liquid flows over the solid surface having such conical shaped cavities, gas filled sites can be readily generated while pipetting or filling of the container, depending on the relation between the advancing CA (θ_A) of the flowing liquid and the crevice half angle (β), as can be seen in the figure 5.2.1 below.

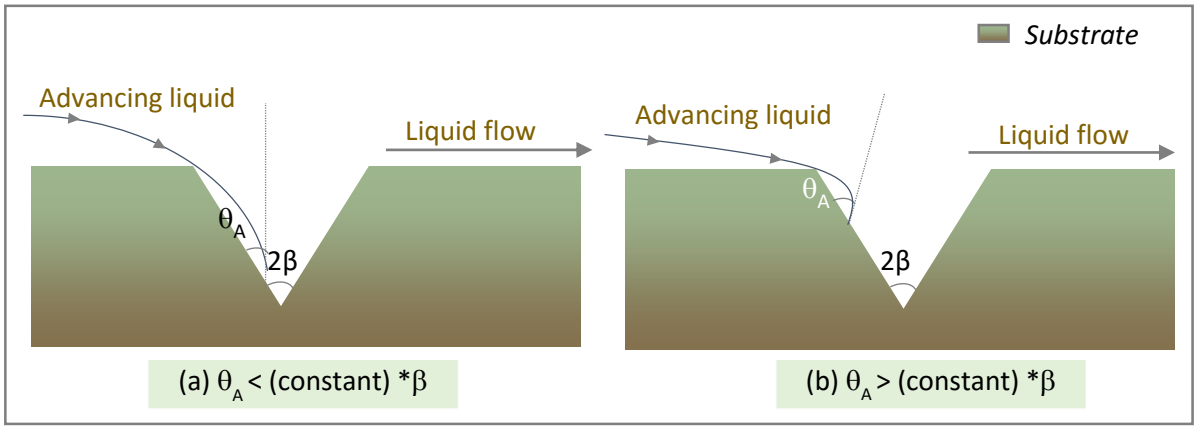

Figure 5.2.1: (a) No gas trapped cavity on a surface inhomogeneity, (b) Gas trapped cavity on a surface inhomogeneity

For $\theta_A <$ (constant) $*\beta$, as the liquid passes over the groove it advances down the front wall, thus expelling the gas in the cavity and fully wetting the conical grove. In this case no gas filled cavity is formed. However, for $\theta_A >$ (constant) $*\beta$, the liquid should advance across the cavity before the portion of a liquid scan reach the base, thereby forming a gas filled cavity. Usually for a wedge shaped crevice, it has been reported, that the 'constant' in the above relations equals to 2, and can be expected to be of order 1 for more complicated conical shapes.

Further, the model states, that at equilibrium, the free (liquid) surface forms with the solid an angle 'θ', which cannot exceed the advancing CA 'θ_A' nor be smaller than the receding CA 'θ_R- the condition as expressed by the equation 5.2.1 below:

$$\theta_R \leq \theta \leq \theta_A \qquad (5.2.1)$$

Now, as per the crevice model of bubble nucleation, for a saturated liquid, the interface must be flat so that $\theta = \beta + \pi/2$, and 'β' be such that, that the equation (5.2.1) is satisfied. However, in a saturated or an under-saturated liquid, if $\theta < \beta + \pi/2$, the interface will spontaneously move towards the bottom of the crevice resulting in the complete dissolution of the gas. Such a nucleus can be stable however in a super-saturated liquid- in this case if the inequality (5.2.1) is violated and $\theta_R > \beta + \pi/2$, the interface will spontaneously recede drawing gas from the solution into the nucleus, which will then slowly evolve into a gas bubble.

Additionally, researchers studied that the radius of curvature of the meniscus formed as a result of an advancing sheet of liquid depends on the height of the liquid wall, the diameter of the cavity mouth, the static and dynamic advancing CA's and the half angle of the groove; the curvature of the meniscus being defined as C=2/R, where R is the radius of curvature. If the free surface of the liquid trapping the gas is convex towards the liquid, C is positive, and vice versa (refer fig. 5.2.2 on the right).

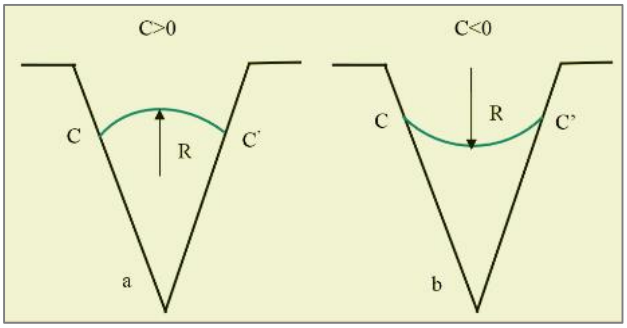

Figure 5.2.2: A bubble in a crevice may have an interface with a radius with respect to the gas inside that is either (a) positive or (b) negative. CC'=line of contac[6,223]

Initially when the liquid is under-saturated, the interface is convex towards the gas. As the liquid pressure falls, the curvature decreases while the contact line (CC′) maintains its position. A point comes when Laplace pressure inside the cavity is equal to the saturation pressure, and the interface is plane. A further decrease of the liquid pressure causes the interface to become concave towards the gas- the sign of the curvature being reversed and a new equilibrium established. Thus as the Laplace pressure inside the cavity is decreased, the equilibrium value of 'θ 'shifts, finally reaching 'θ_R' (receding contact angle value of the

surrounding liquid). Only at this point, the gas-solid- liquid contact line becomes free to move. Further if at this point, if the radius of curvature is less than the critical radius(R^*), the equilibrium is stable and the interface recedes from the bottom of the crevice following the continuous increase of Laplace pressure inside the cavity. In this case, if the decline of Laplace pressure were arrested, the interface motion would stop and no bubble would appear. An unstable growth would occur only in a crevice sufficiently deep that as the Laplace pressure decreases further, the radius of the receding interface would reach the value of critical radius.

Contrary, for the radius at the receding point greater than the critical radius, the interface attains unstable equilibrium as soon as the line of contact becomes free to move. The ensuing growth of the nucleus is then triggered by a mechanical instability and would persist even if the decline of the liquid pressure were to stop- the only case of unstable growth where true nucleation occurs.

Summary

From the above, it can be hence summarized that depending on the nature (say the dimensions) of the nucleation sites and the rate of super-saturation in the system, bubble nucleation can vary from that of classical homogeneous to non-classical type of nucleation. However, as previously stated, in the microfluidic system as dealt with in the current work, owing to moderate working temperatures (far below the boiling points of the liquids concerned), and keeping in mind the highly clean and degassed liquids used generally, the system can be said to have not very extreme levels of super-saturation. Additionally, bubble evolutions(rare) occurring on substrates, potentially being 'infected' by the crater like surface inhomogeneities, indicate the heterogeneous or type II nucleation to be the prime nucleation type event- for the nucleation, if and when occurring in the dealt with micro-fluidic system.

However, for a much detailed understanding as per the crevice model and heterogeneous model of bubble nucleation, as to verify the findings of the previous chapter that surface inhomogeneities entrap gas, detect the dimensions of a nucleation site that nucleates bubbles and thus establish conditions of gas entrapment, and to determine the prime interface (among the various solid-liquid, liquid-liquid, and liquid-gas interfaces present in the dealt with micro-fluidic system), sophisticated experimental investigations were conducted, as discussed in the following sections.

5.2.2 Experimental investigations

To analyze the nucleation phenomenon in the micro-fluidic system as dealt with in the current work experimentally, the preliminary system requirement was surfaces with surface inhomogeneities capable of emitting bubbles -so that such regions could be precisely focused for in-depth investigations. However, as previously discussed, owing to the extreme rarity and randomness of the bubble evolution phenomena in the system's as under consideration, the selection of such a surface/region became quite a cumbersome task. Besides, for the 'thought

to be infected' surfaces (say chosen adjacent to the surfaces that showed tremendous droplet incidences at the end of PCR), since not all regions exhibited bubble evolutions or similar nature of bubble evolutions, choosing a specific, potential nucleation spot remained to be a big challenge. Also, the 'infected' surfaces that led to several bubble evolutions during the biological runs, owing to them now being contaminated with the concerned liquids (say their spilling/dropout), in turn potentially modifying the nature/behavior of the original nucleation sites, could not be re-used for such experimental investigations as well.

Hence, in this regard, in analogy with the crevice model of bubble nucleation, using sophisticated micro-fabrication techniques, artificial nucleation sites (having dimensions analogous to that detected in the microscopic investigations in the surface characterization studies in the previous chapter) were fabricated on the desired regions of the slide surfaces. This idea behind this approach was to study in detail an exact nucleation site, of a known dimension, and thus to establish the criterion of bubble nucleation from it, for the micro-fluidic system as under consideration. Various crude engraving and sophisticated micro-fabrication techniques were employed in this regard- as detailed next.

Nucleation study I- Diamond cutter

In order to confirm the functionality of the approach of `forced´ or 'artificial' nucleation sites, the initial, rough experimental investigations were conducted by manually engraving (via diamond cutter) random scratches, deep enough not to break the slide, on the to be examined regions of the slide surfaces (refer image 5.2.4 below).

Image 5.2.4: Rough scratches (crosses) made on the reaction sites of the AG slide surfaces. Note: the abrasions made were very crude with no two marking being similar in nature, as was seen under a standard, top down microscope

The surfaces after being scratched were thoroughly cleaned off for any leftover glass residues by a gentle wipe using IPA, a rinse in water, and a subsequent drying using compressed nitrogen gas. Next being pipetted with the regular liquids in the standard manner, the subsequent slide was placed on the heating plate of the cycler (ASC), and naked eye and top and side view video recording observations (refer experimental set-up as depicted in the image 5.2.5) for bubble evolutions made for the 1st stage of the PCR cycle.

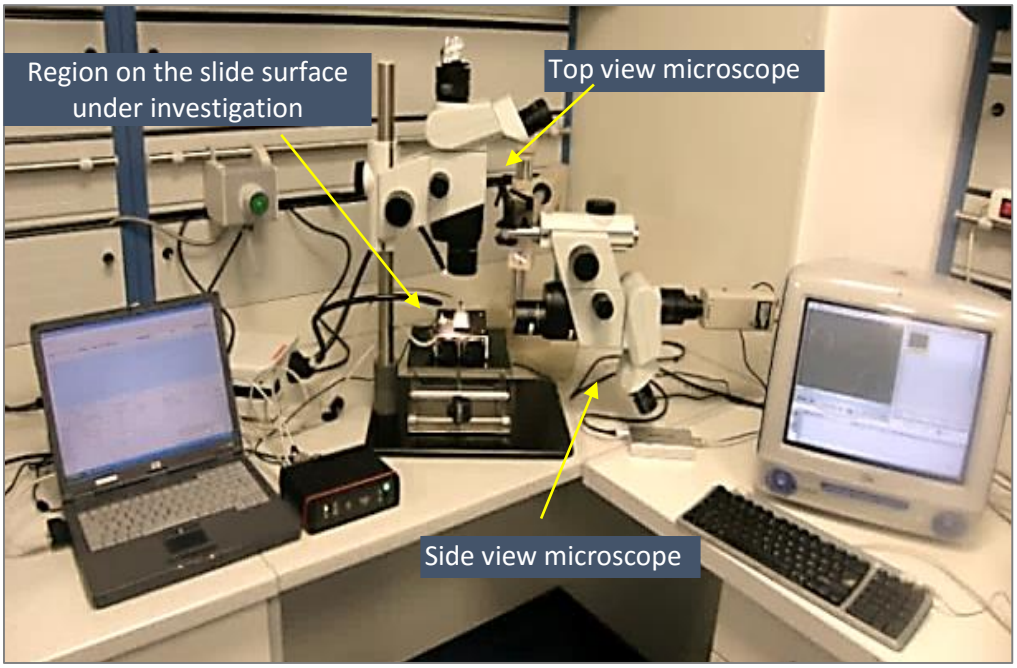

Image 5.2.5: Top and side view Olympus microscopes for parallel video recordings

For nearly 30 arbitrary chosen surfaces, both chemically structured and non-structured, with and without the marked artificial nucleation sites, around 15 randomly selected regions were investigated per case. Further, the naked eye observations were documented in Microsoft Excel 2016 (for the number of active sites, number of dropouts, and number of merges), and the video files analyzed using software's as Windows Media Player classic and Paint.Net.

In this regard, naked eye observations clearly revealed the evolution of bubbles from the scratched regions than from the unscratched ones- the findings being independent of the chemical structuring of the underlying surfaces. Further the bubbles, if and when they occurred, were seen evolving within nearly 10 seconds of heating- minimum evolution temperatures observed to be ~77°C. Also, for most of the cases, observations revealed continuous (cascaded) bubble emissions from a site once active, till the systems temperature was lowered or stopped. Many a times, multiple sites were seen active from a single scratch; a scratched region thereby emitting numerous bubbles- evolving, growing, popping, and bursting, all at the same time. Further since no two sets of experimentations could be directly compared owing to the inconsistency in the nature of the artificial nucleation sites created by the above method, the probability and intensity of the bubble evolutions per site was observed to be highly diverse and unrelated in nature, thereby making the overall analysis quite cumbersome and challenging.

However, in this respect, top and side view video recordings helped gained a better insight into the bubble evolution phenomena- snapshots of a case (recording) as depicted in the images 5.2.6 and 5.2.7 below:

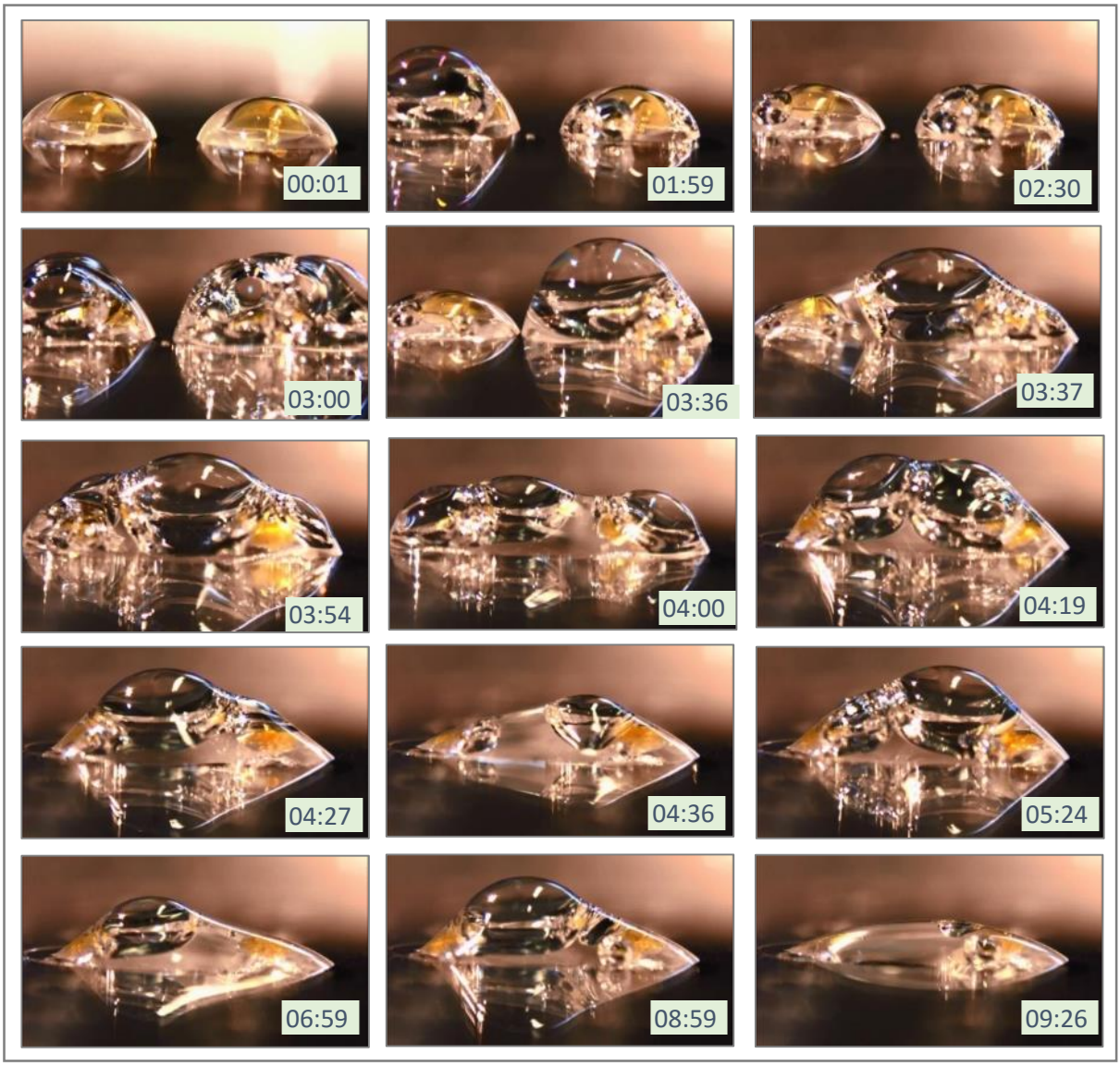

Image 5.2.6: Top-view video recording snapshots depicting the phenomenon of bubble evolution, at 95°C, from two adjacent reaction sites with artificial nucleation sites (marked with diamond cutter). Total recording time =10:00 (min:sec)

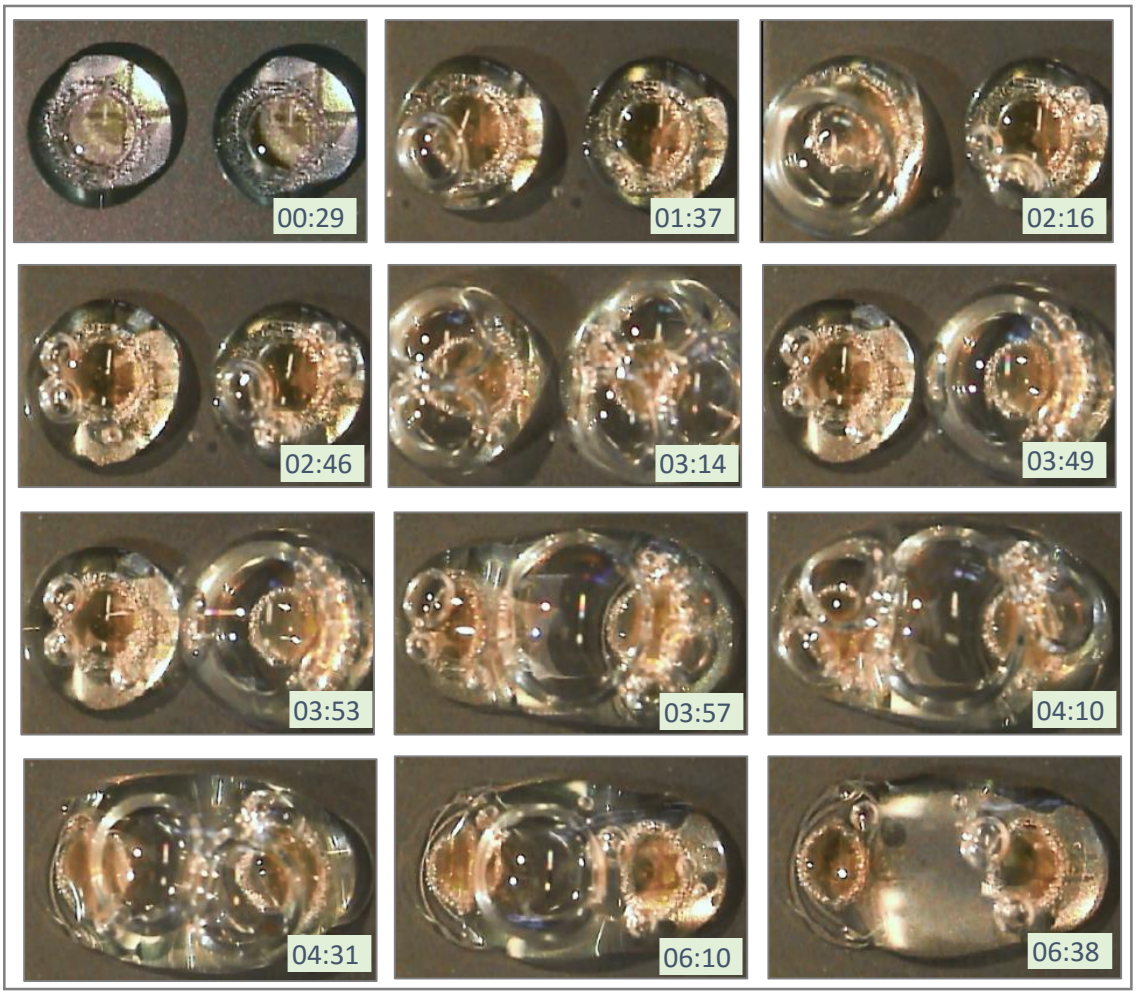

Image 5.2.7: Side-view video recording snapshots depicting the phenomenon of bubble evolution, at 95°C, from two adjacent reaction sites with artificial nucleation sites (marked with diamond cutter). Total recording time =10:00 (min:sec)

As can be seen in the images above, video recording analysis revealed:

- Most of the artificial nucleation sites (marked via a diamond cutter) to be active.
- A site once active, continues to remain active (emit bubbles) till temperature of the system is lowered or stopped.
- The activity of a site to be independent of the wettability of the underlying solid surface, i.e. if the surface is chemically structured or non-structured.
- The intensity and the frequency of the bubble evolutions apparently to be directly proportional to the nature of nucleation sites- penetrating scratches observed yielding more intense and greater number of evolutions, and vice-versa.
- For a number of cases, the burst of a parent bubble, causing spilling/dropout of the reaction liquids, scatters multiple daughter bubbles in the system-they serving as independent 'seeds' for further bubble evolutions, under the same conditions of temperature and pressure.

- The bubbles, especially the ones growing continuously to ample diameters, potentially lead to the merging of the adjacent droplets at some point or the other- the probability of merging being higher for cases where big bubbles in all of the neighboring droplets are encountered.

Further, comparable observations as above were made when DI water was substituted for the dummy PCR solution as the inner liquid, or when chemically structured (or non-structured) glass slides or silicon wafers were tested as the substrate materials.

Thus, though the generation of the artificial nucleation sites via diamond cutter was a very preliminary and a crude attempt, the above studies proved surface inhomogeneities to be the potential sites for bubble formations- in analogy with the heterogeneous model of bubble nucleation. However, owing to the inconsistency and imprecision of the artificial nucleation sites created in the above study, no two experimental cases could be directly compared, and hence no clear criterion for a site to act as gas entrapment site (in analogy with the crevice model of bubble nucleation) could be established. Furthermore, the activation of multiple sites from a single scratched region, causing bubbles to simultaneously evolve, grow, pop, burst, and making the adjacent droplets merge, made the overall nucleation analysis quite cumbersome and challenging; thereby calling for more sophisticated and precise fabrication techniques for an in-depth study of the (bubble) nucleation phenomenon.

Nucleation study II –Laser engraver

In reference to the above, a second attempt that was made to study more closely the nucleation phenomenon, was by laser engraving the 'artificial' nucleation sites on the to be investigated regions of the subsequent slide surfaces- laser engraver from Trotec [309] being used in this respect. The engraving technique being far more refined than the previously employed surface scratching endeavour, the idea was to have greater, specific control over the nucleation sites created, and hence determine say the dimensional range of the cavities that usually lead to bubble evolutions.

Again, as with the previous studies, comparative analysis was made by engraving artificial nucleation sites on the chemically structured and non-structured surfaces- both for glass slides and silicon wafers opted as the substrate materials. Further, by varying the engraving technique, and hence the nature of engravings made, and the type of experimental set-up employed, two cases were tried out, as detailed in the following sub-sections.

Laser engraving: Case 1

In this case, artificial nucleation sites of 0.5 mm diameter using various laser powers (P) (in the range of: 50-100%), and laser velocities(V) (in the range of: 10-70%), and with a constant laser frequency of 100 kHz were engraved on the to be investigated regions of the subsequent slide surfaces- various nucleations sites engraved as can be seen in the image 5.2.8 below:

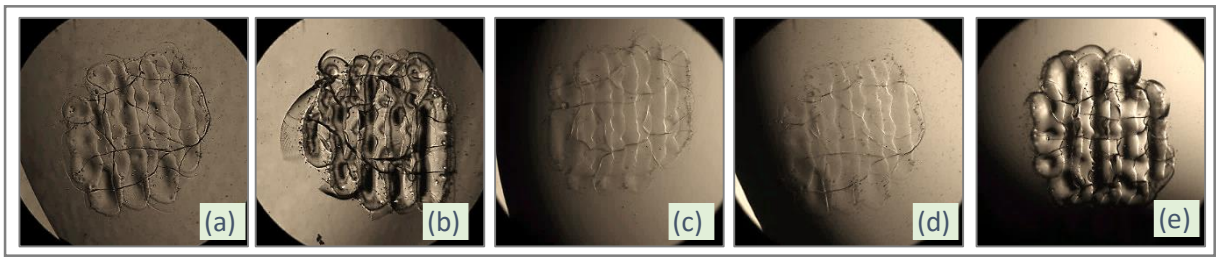

Image 5.2.8: HD bottom view pictures (refer set-up image 4.3.4 of inverted microscope in the previous chapter) of artificial nucleation sites (0.5mm dimeter) laser engraved using laser frequency= 100kHz, and varying laser powers (P) and velocities(V)---(a) P=40%, V= 30%, (b) P= 70%, V=30%, (c) P=100%, V=60%, (d) P=30%, V=50%, and (e) P=30%, V=70%

Experimental investigations at elevated temperatures (95°C) were conducted to determine and compare the activity of each of the above nucleation sites – when engraved beneath the inner liquid (as on the inner hydrophilic region of the chemically structured surfaces), when beneath the outer liquid (as on the outer hydrophobic region of the chemically structured surfaces), and when at/ in the vicinity of the water-oil interface (overlapped by the inner hydrophilic-hydrophobic interface for the chemically structured surfaces)- engravings on different locations of the micro-fluidic system as can be seen in image 5.2.9 below:

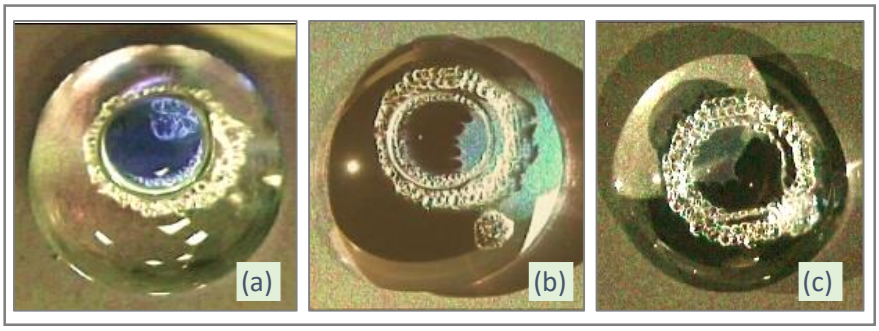

Image 5.2.9: Laser engraved artificial nucleation sites (0.5mm diameter) on chemically structured surfaces (a) on the inner hydrophilic region, (b) on the outer hydrophobic region, (c) at the inner hydrophilic-hydrophobic interface

The surfaces, after being engraved, were properly cleaned to get rid of any leftover (glass) residues, by a gentle wipe with a tissue dipped in isopropanol, and a subsequent rinse in water and their drying using compressed nitrogen, as with the previous studies. Next, loading the to be investigated regions on the slide surface with the standard liquids (except for the slight color imparted to the inner DI water using biocompatible Adva Blue (0.1 vol%) dye, to ease visualization of the inner and outer transparent liquids during experimental runs), the slides were placed on the heating plate of the ASC, and the surfaces/regions investigated for bubble evolutions at 95°C for the initial 10 minutes of heating (1st stage of PCR cycle). The analysis chiefly conducted via sophisticated top view HD video recordings- the image 5.2.10 depicts the overall experimental set-up employed in this regard.

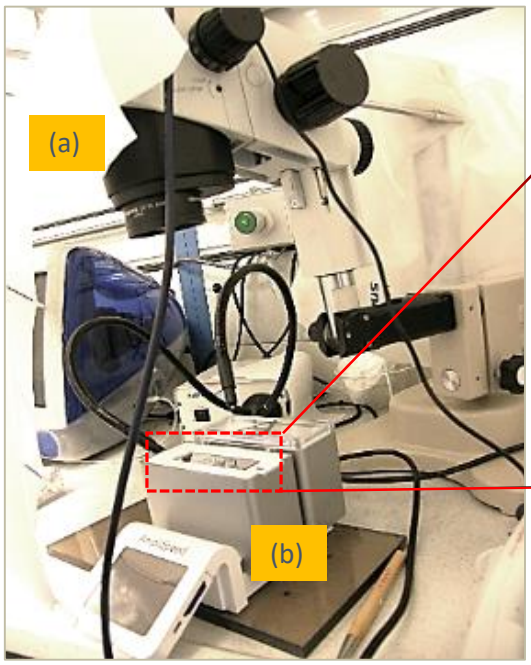

Close-up of the experimental set-up depicting 15 reaction sites investigated on a slide surface

Image 5.2.10: Top down experimental set-up for bubble nucleation (II) studies- (a) Top down microscope, (b) to be investigated slide surface (with micro droplets atop) placed on the heating plate of the ASC

With minimum of 10 surfaces (with and without artificial nucleation sites, and for different positions of nucleation sites in the system) being tested per case, and at least 15 engraved regions being investigated per surface, the corresponding video recordings were analyzed later using appropriate video and image editing software's as windows media player classic and Paint.Net.

Results revealed, as with the previous studies, clear evolution of bubbles from the engraved regions than from the non-engraved ones. Further, for most of the cases, bubbles, when and if they appeared, were seen evolving within 10 seconds of the start of the heating; the minimum temperatures for bubble activity again measured to be ~77°C. Also, as with the previous nucleation I studies, for this case too, a site once active, was seen evolving cascading bubbles, for the same conditions of pressure and temperature.

Observations for this case additionally revealed, as compared to the artificial nucleation sites generated using lower laser power and higher velocities, the ones engraved with 100% laser powers and 10% laser velocities to be the most active- such sites hence being preferred for further nucleation II case studies. However, no direct correlation in terms of number of bubbles evolving from a particular site could be clearly made – the quantity and frequency of evolutions observed to be largely dependent on the position of the site within the system, as will be discussed next.

For the micro-fluidic, bi-liquid system as dealt with in the current work, for the engraved sites when under water (on the inner hydrophilic region of the chemically structured surfaces),

observations revealed evolution of bubbles generally form an engraved site. However, not all nucleated bubbles were seen growing big enough to be distinctly detected - the probability of prominently visible bubble evolutions under water being around 80%.

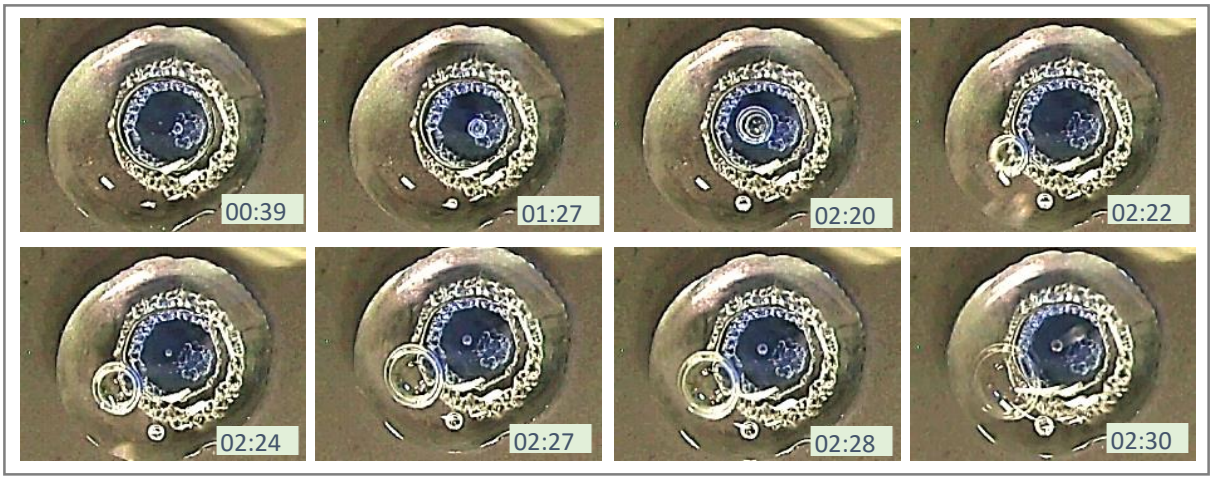

Image 5.2.11: Snapshots of video recordings for a study with artificial nucleation site under water in the micro-fluidic system. Working temperatures=95°C. Total recording time=10:00 (min:sec)

Furthermore, the nucleated bubbles were seen instantaneously growing to ample diameters as and when they approached the liquid-liquid interface (overlapped by the bottom hydrophilic-hydrophobic interface on the chemically structured surfaces)—detailed investigations on bubble growths and the role of an individual interface in the nucleation and growth of bubbles being taken up in sections 5.3 and 5.4, respectively.

For the engraved nucleation sites when under oil (i.e. on the hydrophobic region surrounding the inner hydrophilic region on a chemically structured surface), though the studies, for most of the observed cases, revealed the sites to entrap gas (/air), however, no prominent bubble growths were detected of these nucleated bubbles, as can be seen for the case in the image 5.2.12 below.

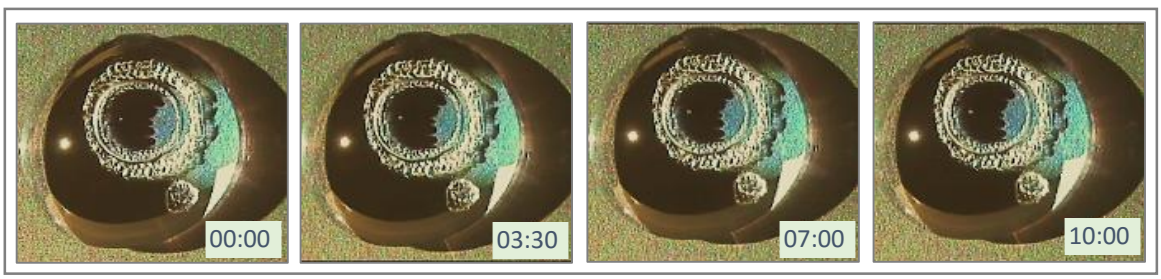

Image 5.2.12: Artificial nucleation site under oil. Though some bubbles were seen nucleating from the engraved sites, no prominent growths/evolutions of these nucleated bubbles were observed throughout the experimental run. Total recording time = 10:00 (min:sec)

Similar observations as above were made for the cases when only oil (single-liquid), instead of oil with water below it (bi-liquids), was dispensed atop the engraved nucleation sites (refer image 5.2.13 below for such a case).

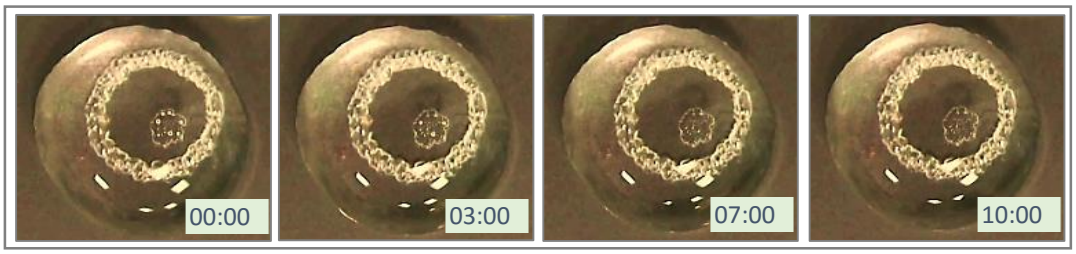

Image 5.2.13: No prominent bubble growths/ evolution from the engraved site when under solely under oil throughout the experimental run. Total recording time=10:00 (min:sec)

However, when studies were made for the engraved site at the inner hydrophilic-hydrophobic interface for the chemically structured surfaces (which owing to the design of the virtually confined micro-fluidic system is overlapped by the water-oil interface), observations revealed, for most of the cases (around 90%), bubbles not only nucleating from these sites, but growing rapidly too--generally big enough leading to huge bursts and subsequent merging of the adjacent droplets.

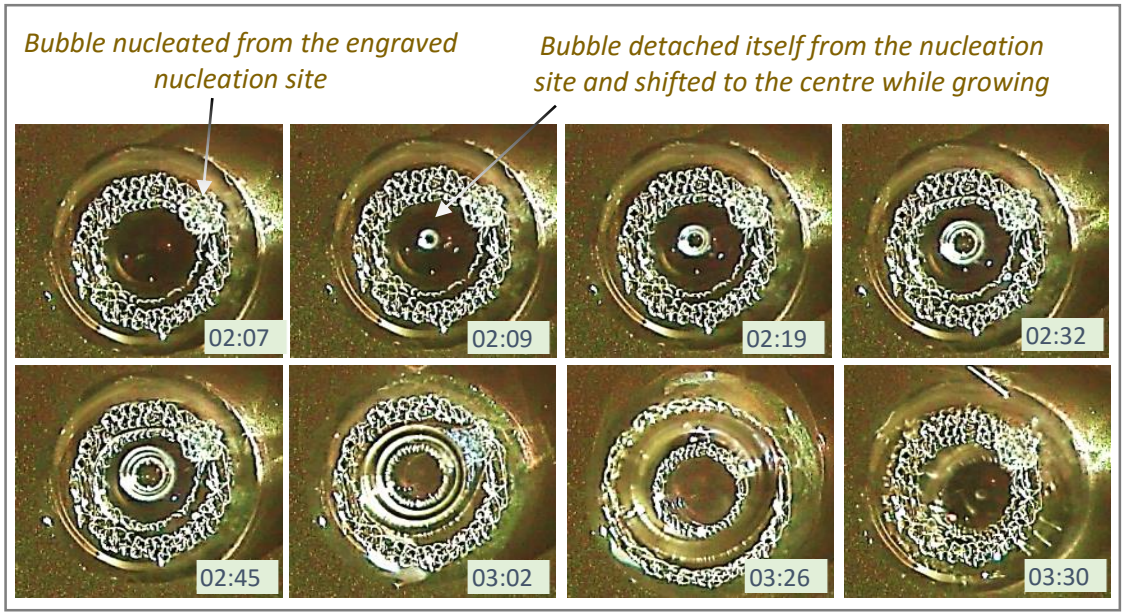

Image 5.2.14: Huge bubble evolutions observed for cases with artificial nucleation site at the hydrophilic-hydrophobic interface of the chemically stratified substrates (the interface overlapped by the water-oil interface owing to design of such micro-fluidic systems). Total recording time= 10:00 (min:sec)

From all the above analysis, it can be hence concluded that though the engraved sites generally trapped gas, not all the nucleated bubbles grew big enough diameters, leading to huge bursts, and the potential merging of the adjacent droplets. The sites when under water were found to be more active in this regard than for the sites when under oil—the nucleation sites being most active when at or in the close vicinity of the liquid-liquid (water-oil) interface. With an in-depth study done into the bubble growth in the next section, the above nucleation studies hence primarily concluded the bubbles at or in the locale of the hydrophilic-hydrophobic(water-oil) interface to be the dubious ones- growing to immense diameters, causing huge bursts, and potential merging of the neighboring droplets. This hence calls for the policing of the system for nucleation sites at say in the vicinity of the hydrophilic-hydrophobic interface- the slide surfaces properly characterized prior to use for such defects, which if present, necessitating the discarding of such surfaces- to minimize failure of equivalent micro-fluidic systems owing to bubble evolutions.

However, though the above laser engraving technique provided sufficient control in generating nearly reproducible structures (artificial nucleation sites) with a good precision, the approach proved to be not every effective in fabricating well-defined nucleation sites, so that conditions of gas entrapment (say for what dimensions a site traps gas, as per the crevice model of bubble nucleation) could be established. A single 0.5mm laser engraved site was found to comprise of multiple smaller sites, and hence it could not be really determined which of the sub-sites and having what specifications had higher probabilities of nucleating bubbles. This as well limited the understanding of the finding that the crater like surface inhomogeneities, as detected in the microscopic, surface characterization studies in the previous chapter, serve as potential sites for bubble formations.

Thus, a detailed study in regard to the above, calls for the generation of single, definite sites, which could be examined for bubble nucleations using more sophisticated experimental techniques—as attempted next.

Laser engraving: Case 2

Playing with different laser parameters revealed, that besides altering the laser power, its velocity and frequency, choosing a timed laser shot, could help generate specific, definitive structures. In this regard, by selecting different laser intensities (8-12%) and shot times (between 2-5 seconds), various artificial nucleation sites were generated on the to be investigated surfaces, as can be seen in the image 5.2.15 on the right.

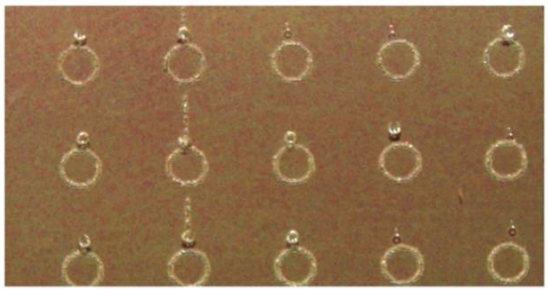

Image 5.2.15: Top view (using experimental set-up in the image 5.2.16) of surfaces engraved with timed laser shots (3 sec. shot of 12% laser intensity for the shown case)

Again, as with the previous studies, artificial nucleation sites were created at different

locations of the slide surfaces, so that when the liquids are pipetted, the sites lie under water, under oil, and at or in the vicinity of the water-oil interface- both chemically structured and non-structured, glass and silicon wafers being tested in this regard. For minimum of 10 surfaces being investigated per case, and with at least 15 regions tested per surface, experiments were conducted to investigate if and for what dimensions (laser parameters) a site trapped gas, using the top and subsequent bottom view experimental set-up's as depicted in the images 5.2.16 and 5.2.17 below:

Image 5.2.16: Top-view experimental set-up to study the phenomenon of bubble nucleation: (a) Sony HD camera backed with Olympus top down microscope for more detailed investigations, (b) close up of the investigated regions being recorded, (c) surfaces marked with single laser shots (three seconds, 12% intensity) Olympus SZX9 (12X magnification)

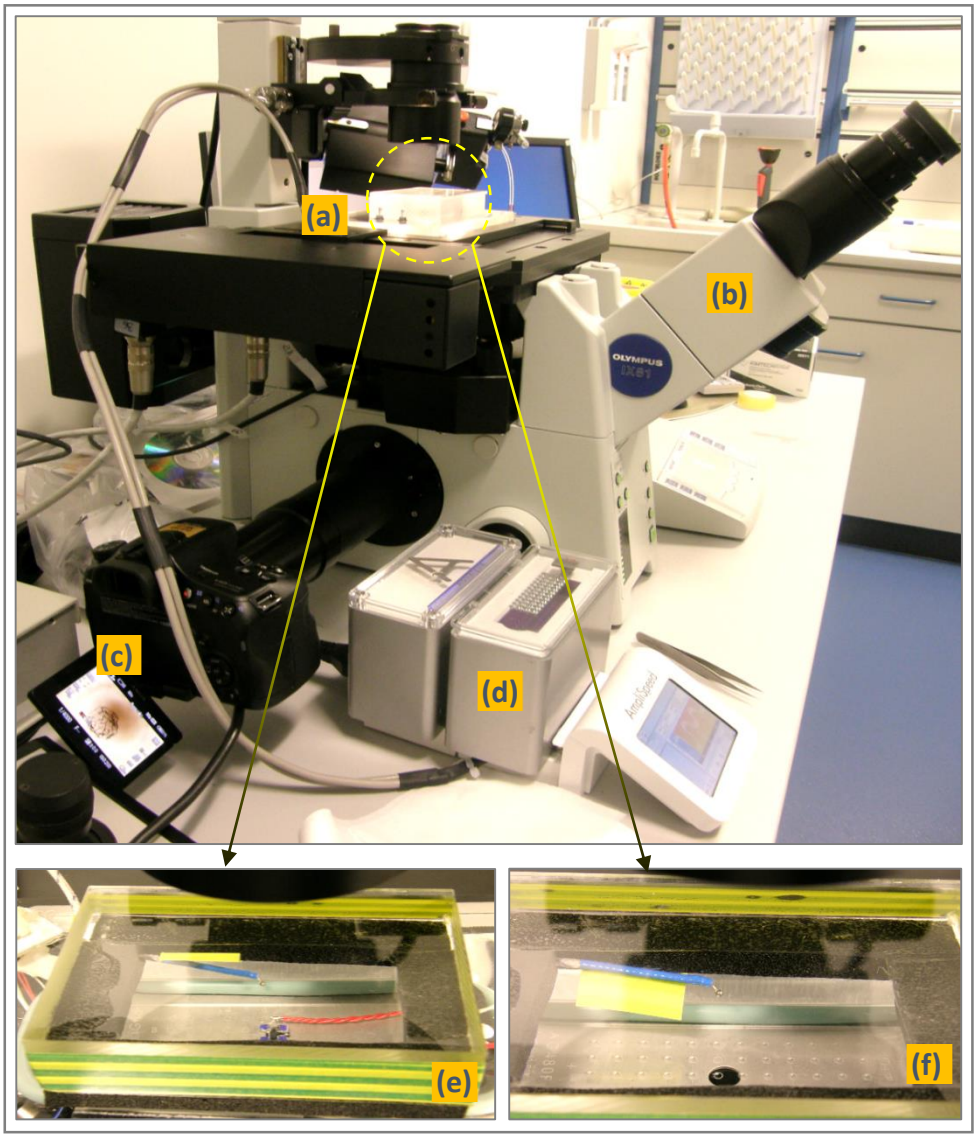

Image 5.2.17: Bottom-view experimental set-up to study the phenomenon of bubble nucleation: (a) the to be investigated slide surface, (b) Motorized inverted research microscope- Olympus IX81, (c) the inverted microscope backed with Sony HD camera (for bottom view HD recordings), (d) well calibration of set-up with ASC prior to use), (e) calibration of the set-up prior to use (using dummy glass slide with PT100 sensors), (f) a specific engraved region on the glass slide focused for bottom-view examinations

For the various artificial nucleation sites generated using different intensities and time of the laser shot, top and bottom view recordings revealed no major bubble evolutions (at 95°C) from majority of the engraved sites. However, for rare sites engraved using 12% laser intensity for 3 seconds, especially for such sites when at or in the vicinity of the hydrophilic-hydrophobic interface, bottom view experiments showed some bubble evolutions, as can be seen in the image 5.2.18 below:

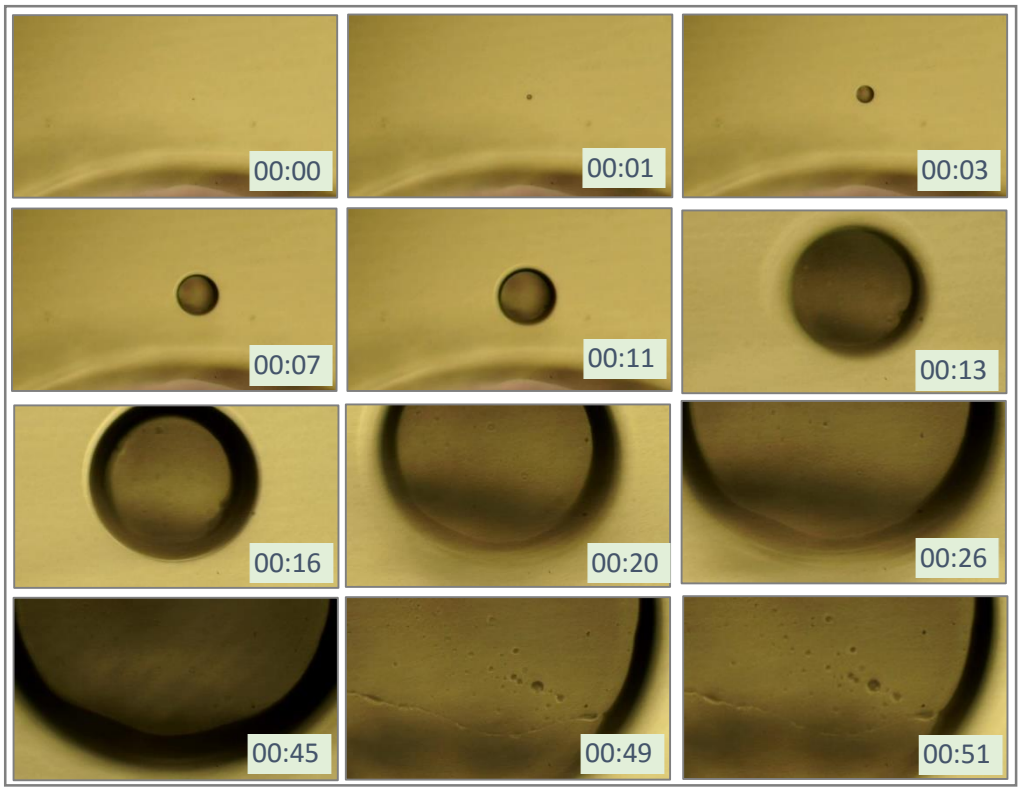

Image 5.2.18: Bottom-view experiments showing some rare bubble evolutions from laser engraved sites using 12%laser intensity, shot for 3seconds. Bubble for the depicted case growing primarily in oil, but in close proximity of the water-oil interface (intersecting the bottom hydrophilic-hydrophobic interface of the chemically engraved slide). Bubble growing big enough within 51 seconds during the experimental run.

Bottom view analysis further revealed that the sites engraved using 12% laser velocity (shot time=3 seconds), had diameters in the range of 70-120 microns (calculated on the highly magnified bottom view snapshots of such sites using image analyzing software as Paint.Net), and depth of ~ 150 microns (measured via adjusting the bottom and top focal plane distances of the motorized bottom view microscope), as can be seen in the image 5.2.19 below:

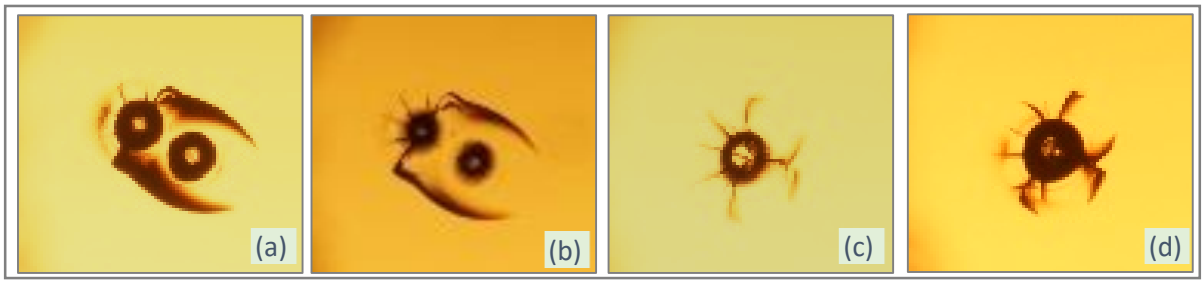

Image 5.2.19: Bottom view snapshots of sites engraved using single laser shot (time:3 seconds, laser intensity: 12%) of diameters (a) ~71 microns (before pipetting with 1µL water), (b) ~71 microns (after pipetting with water, before heating), (c) ~90 microns (before pipetting with water), (d) ~120 microns (before pipetting with water)

Thus, from the above nucleation studies, it can be said that though the above technique of creating artificial nucleation sites using timed laser shots enabled in generating well-defined sites of distinct dimensions, the sites, largely, were not efficient enough to trap gas (or air- the exact content of bubbles being dealt with in the section 5.5). Further, for the rare cases of gas entrapments that occurred (for sites having diameters~120 microns and depths~150 microns, i.e. aspect ratios 4:5), huge bubble evolutions were observed for sites when at or in the vicinity of the water-oil (/hydrophilic-hydrophobic) interface, as with the previous nucleation studies. This hence pointed to the vulnerability of surface inhomogeneities with the above aspect ratios to serve as nucleation sites at elevated system temperatures – their probability of evolving bubbles increasing, when present in the proximity of the water-oil (/hydrophilic-hydrophobic) interface.

However, the crater like surface inhomogeneities detected by the microscopic investigations (refer surface characterization studies in the previous chapter) had diameters between 2-10 µm, inner depths between 2-4 nm, and heights (of the distinct peak like projections at their edges) in the range between 10-200 nm, making them have much larger aspect ratios (minimum 1000:1, maximum 250:1) as compared to for the sites engraved using the above technique. Thus for a detailed study of structures of much higher aspect ratios, and to investigate further the nucleation phenomenon, more sophisticated micro-fabrication techniques were employed, as discussed in the nucleation studies III and IV below.

Nucleation study III –Lithographic Etching

In order to thus generate more defined and reproducible structures, as stated above, a sophisticated technique that was next adopted was Lithography or wet etching[254-257]. Usually chemically structured surfaces being adopted for these investigations, per row of a slide surface, pits having diameters of 6,12,20, and 30 microns respectively, with their depths varying between 5-30 microns, were micro-fabricated (masks order from University of Twente, The Netherlands). Further, as with the previous nucleation studies, the structures (artificial nucleation sites) were etched on the inner hydrophilic region (holding water), on the outer hydrophobic region (holding oil), and at the inner hydrophilic-hydrophobic interface (intersected by the water-oil interface above) of the subsequent glass slides. Top and bottom view experimental investigations, using the experimental set-up's as depicted in images 5.2.15 and 5.2.16, respectively, were conducted- with minimum of ten surfaces being analyzed per case with 15 sites being tested per surface.

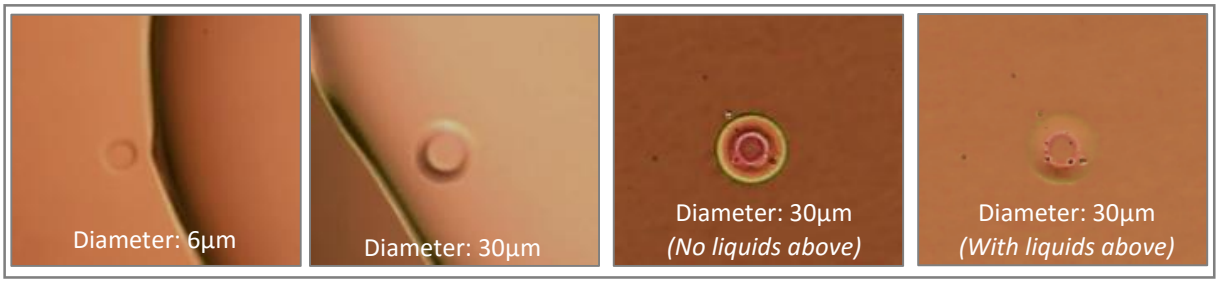

Image 5.2.20: Lithographically micro- fabricated sites having depths ~30µm

Experiments revealed sites having 30µm diameters and 30µm depths (aspect ratios 1:1) to be mostly active in terms of generating bubbles, whereas no bubble evolutions were seen from sites having lower diameters (in the range of 6-12 µm), though with equivalent depths (in the range of 5-30µm)- results as outlined in the table 5.2.1 below:

Site dimensions (diameter, depth)	Probability (%) of it being active
30µm, 25-30µm	~70%
30µm, 20-25µm	~5%
20µm, 30µm	~2%
12µm, 5-30µm	0%
6µm, 5-30µm	0%

Table 5.2.1: Probability of bubble evolutions from sites lithographically etched of varying dimensions

Additionally, as with the previous nucleation studies, greater activity was observed for the 'vulnerable' sites when present at or in close proximity to the hydrophilic-hydrophobic interface (overlapping the water-oil interface with the liquids pipetted), as compared to when present at the inner hydrophilic region (under water)- their activity being least for their occurrence when under the outer hydrophobic region holding oil.

Thus from the above nucleation studies it can be said, that the though the creation of artificial nucleation sites via wet etching gave much greater control in generating well-defined and reproducible micro-structures, not all the fabricated structures led to prominent bubble evolutions. In this regard, the probability of bubble occurrences was greater for the sites having dimeters of ~30µm and depths between 25-30µm (nearly 1:1 aspect ratios), as compared to the sites with lower diameters and lower or equivalent depths.

However, for the sites with lower dimensions, a reason for their inactivity could be the isotropic nature of the etching, typical of the lithographic micro-fabrication technique, such that the condition of gas entrapment doesn't get fulfilled and the pipetted liquid(s) fully wet the underlying structures.

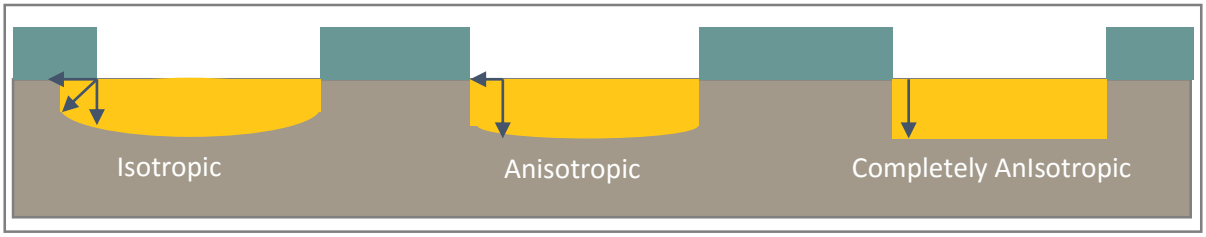

Figure 5.2.3.: Pictorial representation of isotropic, anisotropic, and completely anisotropic etching

Also, it might be that the coating (chemical structuring) of the surfaces, post-fabrication of the above structures, makes some of the etched pits dormant in nature- potentially blocking the sites especially with lower dimensions so that no gas gets trapped when liquids are dispensed above them. Hence, for further in-depth understanding of the nucleation phenomenon, and in an attempt to generate anisotropic structures, Deep Reactive Ion Etching (DRIE) was adopted as the next fabrication technique- the etched sites being tested for their activity pre and post-coating of the subsequent slide surfaces, as detailed next.

Nucleation study IV –Deep Reactive Ion Etching

As stated above, for a further analysis into the nucleation phenomena, Deep Reactive Ion Etching (DRIE)[258-261] was employed as the next micro-fabrication technique - the technique known to generate micro-structures with high aspect ratios (50 to 1), having etch depths of hundreds of microns, and nearly 90° steep vertical walls- etching rates being 3-4 times higher than the wet etching[261-262].

Employing the same mask as used for the lithographic etching, pits having varying dimensions (depths in the range of 5-30µm and diameters of 6,12,20,30 µm) were micro-fabricated (by choosing etching times of 5 min, 10 min, 20 min and 30 min, respectively) on the to be examined surfaces – the DRIE micro-fabrication being done at the Experimental Physics I Lab, University Augsburg, Germany.

For the initial studies, the structures were etched on clean, non-coated glass slides (and/or silicon wafers)- the to be investigated regions of these chemically non-structured (hydrophilic) surfaces usually surrounded by PDMS boundaries (~4mm*4mm*2mm) to confine the micro-droplets in place.

Mainly, top- view, HD, video -recording analysis being conducted in this regard (refer image 5.2.15 for the experimental set-up), various sites were examined for bubble evolutions at 95°C - comparative studies being additionally made for the sites when under water, under oil and in the vicinity of the water-oil interface, as with the previous nucleation studies.

With minimum of ten surfaces being tested per case, and around 15 sites being examined per surface, video recordings revealed, no detectable gas entrapments or bubble evolutions from any of the above micro-fabricated sites- for when present both on glass slides and/or silicon wafers. Examinations further revealed no bubble activity from any of these etched structures even for the cases when the system's temperature was raised from 95°C to 99°C.

Thus, from the above studies, it can be concluded that none of the artificial nucleation sites fabricated using the DRIE technique, irrespective of their dimensions or locations within the micro-fluidic system, and even for temperatures beyond 95°C, led to bubble evolutions. One reason to the above again could be the wetting of the sites by the dispensed liquids, i.e. the sites not fulfilling the criterion of gas entrapment say as per the crevice model of bubble nucleation. However, detailed characterization of the above etched structures (say for the

degree of their anisotropy) calls for further, advanced studies - such investigations, however, being beyond the scope of the current work.

In addition, the inability of the above structures (on non-coated surfaces) to trap gas, and lack of time and insufficient resources, questioned/hindered the conduction of similar studies on the coated (chemically structured) surfaces- such investigations nevertheless serving as another promising outlook for the detailed understanding of bubble dynamics in the micro-fluidic system as under consideration.

5.2.3 Bubble Nucleation: Summary

From the nucleation studies, it can hence be summarized:

- Surface inhomogeneities potentially act as sites for bubble formations, provided after the liquids have been dispensed atop them, conditions of gas entrapment (as per the crevice model of bubble nucleation) are fulfilled.
- The surface inhomogeneities, for which the conditions of gas entrapment get fulfilled, are found to be more active (in terms of generating prominent bubble evolutions) when under water than when under oil- the sites being most active when in the vicinity of the water-oil interface (overlapped by the hydrophilic-hydrophobic interface for the chemically structured surfaces). However, details into the exact interface (out of the many, especially overlapping interfaces occurring in the micro-fluidic system as dealt with in the current work) responsible for the bubble nucleation being dealt with in the section 5.4, and the various factors governing the growth of a nucleated bubble (for different locations of the nucleation sites within the micro-fluidic system) being dealt with in the section 5.5, the above finding nevertheless makes the surface inhomogeneities in close proximity to the water-oil (or hydrophilic-hydrophobic) interface to be the most vulnerable ones- generating bubbles, that might potentially grow big, leading to huge bursts and perhaps merging of the adjacent droplets. This, hence calls for proper characterization of the subsequent surfaces for such inhomogeneities prior to use- the detection of which necessitating the elimination of the corresponding surfaces to maintain the high efficiency of the overall micro-fluidic system due to bubble evolutions.
- Additionally, for the micro-fluidic system as under consideration, the surface inhomogeneities (if and when trapped gas) were found to emit bubbles at minimum system temperatures of ~77°C (bubbles seen evolving within approximately 40 seconds of the start of the heating)- the intensity and frequency of evolutions increasing with a further increase of the system's temperature (say up to 95°C). Besides, in analogy with the heterogeneous model of bubble nucleation, an active site keeps on emitting (a cascade of) bubbles, till the system temperatures are lowered, say below 77°C for the system as dealt with in the current work.
- Experimental studies conducted to establish the criterion of bubble nucleation (say determining the dimensions for which a site trapped gas, in analogy with the crevice

model of bubble nucleation), revealed sites having aspect ratios of 4:5 (as detected by the nucleation studies done by fabricating artificial nucleation sites via timed laser shots), and of 1:1 (as detected by nucleation studies done by fabricating artificial nucleation sites via wet etching) to be the most vulnerable ones in emitting bubbles. The surfaces, hence prior to use, must as well be characterized for surface inhomogeneities having the above aspect ratios – which if present, again necessitating the elimination of the corresponding regions/surfaces. However, the above aspect ratios filtered for the susceptible sites were much lower as compared to that for the crater like surface inhomogeneities detected in the microscopic surface investigations in the previous chapter (latter having aspect ratios of ~1000:1 and/or 250:1)- thereby calling for the fabrication and study of sites having much greater diameters as compared to their depths. Also, the spotted crater like surface inhomogeneities had distinct peaks around their edges (refer image 4.1.2), hence requiring fabrication of surfaces with not only varying depths and diameters but with varying heights (peaks) as well, and investigating them for bubble nucleations/evolutions --both pre- and post-coating of the subsequent surfaces.

5.3 Bubble growth

After nucleation, another important aspect that required understanding was the phenomena of bubble growth- for the bubbles nucleated within the microfluidic system as dealt with in the current work. Prime queries that required attention in this regard were: 'What is the mechanism of bubble growth?', 'What factors primarily govern the bubble growth phenomenon?', 'How is bubble growth influenced by the presence of the liquid-liquid interface (bi-liquid system) as compared to just a liquid-gas/air interface (single -liquid system)?', 'What is the prime transport phenomena involved in the growth of the bubbles', and, ' How is growth different for a bubble nucleated from different locations within a microfluidic system, as for the one under consideration?'.

The comprehension of the above bubble growth aspects was attempted primarily via sophisticated experimental investigations- however prior to that, a brief literature survey on the bubble growth phenomenon being put forward, as in the sub-section below.

5.3.1 Literature review

Tremendous research underwent into studying the phenomenon of bubble growth, both in macro and micro-fluidic systems, equally comprising single-liquid and bi-liquid interfaces[224-230]. As per the kind of system involved, various factors have been reported to govern the bubble growth- prime being the change in the rate of super-saturation in the concerned micro fluidic system[219]. Super-saturation, further depends on the change in the pressure or temperature of the system, where a decrease in the systems pressure or an increase in its temperature, or both, could alter the supersaturation equilibrium in any system. For instance,

a system when subjected to a change in pressure could result in the growth of the nucleated bubbles owing to the pressure difference between the medium generating the bubbles and the surrounding one, as per the Le Chatelier's principle [219,231-232]. This can be, for example, prominently seen for carbon dioxide bubbles in a beer can, where the bubbles are originally dissolved under high pressure in the liquid medium and rise/grow as the beer can is opened or the pressure released [10,220]. Researchers explained phenomena as above, by stating that as the bubble(s) travel up, the pressure of the surrounding liquid reduces such that the air inside the bubble is allowed to expand more, resulting in a visible increase in its size[219-220,233]. The acceleration with which these bubbles rise was further explained as per the Stokes law[234-235], written as:

$$F_d = 6\pi\mu RV \tag{5.3.1}$$

where 'F_d' is the frictional force (known as Stokes drag) acting on the interface between the liquid and the bubble, 'μ' is the dynamic viscosity of the liquid, 'R' is the radius of the bubble, and 'V' the flow velocity of the liquid relative to the bubble. Authors reported, that as the radius of the rising bubble in the system increases, viscous drag and thus the flow velocity increases too, making the bubbles accelerate in (say a beer) glass.

Apart from the above, another factor largely contributing to the growth of the bubbles has been reported to be the presence of density differences in the system. This can be, for instance, seen in the case of bubble(s) rising in a soft drink, owing to the lower density of the bubble in comparison to the drink itself. The growth of bubbles in this case has been reported to be governed by two major forces: the buoyant force as per the Archimedes principle which increases as the bubble grows, and the downward drag or the friction force (equation 5.3.1) the bubble experiences as it rises in the liquid which also tends to increase as the bubble grows. It was further put forward, that although these two opposing forces increase at the same time, buoyancy force increases more rapidly than the downward drag, making the bubble continuously accelerate in its ascent, leading to an increase in the spacing between the bubbles as they grow further up[215,219-220,233-237].

Nevertheless, generally for any system, there is usually a balance of various forces acting on the bubble as it grows: typically drag (F_d) and surface tension forces(F_s) tending to hinder its growth, whereas the inertial (F_i) , pressure (F_p) and buoyant (F_b) forces tending to favor its growth (refer equation 5.3.2 and subsequent figure 5.3.1)--their competition further determining the bubble's rising velocity in the system[215, 219, 238-240].

$$F_d + F_s = F_i + F_p + F_b \tag{5.3.2}$$

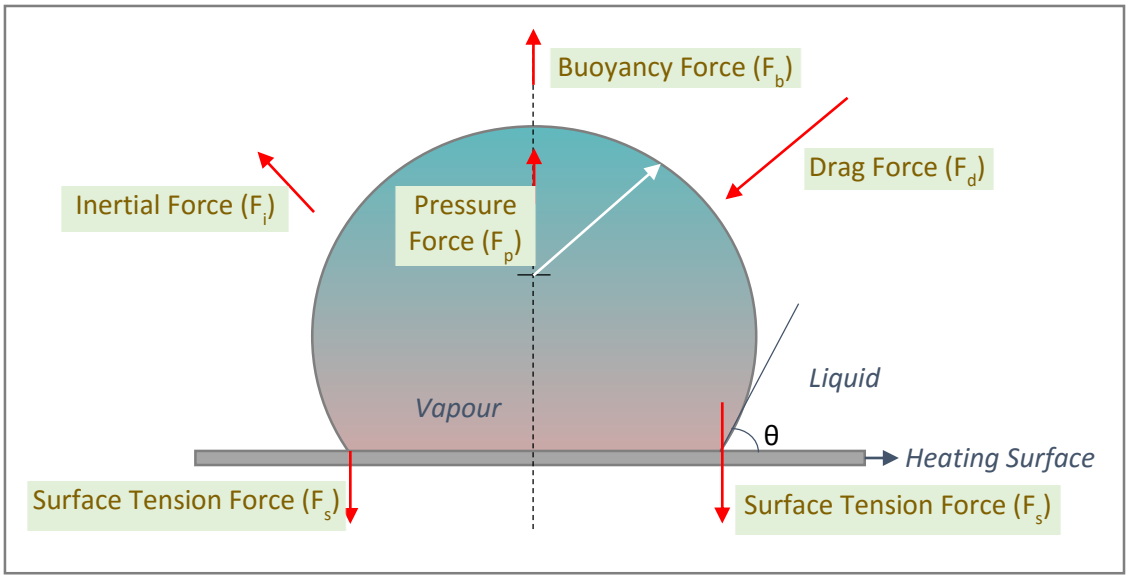

Figure 5.3.1: Various forces acting on a vapor bubble, as it grows in a liquid, on a heated surface[215,239-240]

Additionally, drag force was reported to be highly affected by the fluids viscosity and density (both of which in turn being largely temperature dependent) -altering the fluids viscosity and density alters the friction on the bubble thereby making it rise faster as the system's temperature increases. The exact relationship, however, between the size and the rate of ascent was reported to be pretty complicated to be observed owing to strong dependence of drag forces on the speed of the rising bubble. Nevertheless, for low growth rates, it was reported that the static equilibrium gets established when the following condition meets: [219, 239-240]:

$$F_s = F_p + F_b \tag{5.3.3}$$

Nonetheless, though significant factors governing the initial bubble growth seem to be unclear, the final growth was reported to be apparently governed by molecular diffusion. However, the complete description of bubble growth was stated to require consideration of many factors including diffusion of heat and gas molecules, convection, inertial, viscous and surface tension forces- requiring the coupling of various equations, chiefly being the equations of continuity, equations of motion, conservation of the diffusing species and heat and mass transfer. That said, the basic equations that control the growth of the bubbles have been reported to be primarily the diffusion equation, the Ficks equation, a mass balance equation and the Laplace equation- their solutions being dependent on the system under consideration. However, a general equation for the bubble growth was and can be given as[1]:

$$R \propto t^a \tag{5.3.4}$$

where ‘R' is the radius of the bubble and ‘t ' is the time period of its growth. The exponent factor ‘a' was found to depend on the different experimental procedures employed, how well they were conducted and on factors such as Laplace pressure, inertial and viscous forces controlling the bubble growth. For diffusion controlled growth, however, it was reported that generally a=1/2 [1,220,239-240]. Additionally, for cases where the inertial and surface tension forces are dominant, which was reported to be the most likely case in the very early stages of the bubble growth, then the time dependent bubble radius was given by the following equation [1,219-220]:

$$R(t)=At \tag{5.3.5}$$

where, A' is a constant. For cases, where the growth is determined by how rapidly material can be transported across the interface, Ficks law apply, and the calculation for the radial growth rate of the bubble (assumed spherical, or partly spherical) was performed by Scriven-- solution of the diffusion equations with appropriate boundary conditions leading to the so called Scriven equations for the bubble radius $R(t)^2$, given as [1,219-220,239-240]:

$$R(t)=2\beta\,[Dt^{1/2}] \tag{5.3.6}$$

‘β' being a constant for given conditions of system super-saturation. The above equation further shows the ‘$t^{1/2}$’ dependence of the typical diffusion controlled growth where the interfacial area grows linearly with time. However, under other constraints, for instance where direct injection of gas into the bubble is the growth mechanism, equation (5.3.7) applies [1,220] :

$$R(t)=Ct^{1/3} \tag{5.3.7}$$

‘C' being a constant for a given system. The above is an approximation, most likely a good one, keeping in mind that early in the lifetime of a bubble, its growth rate is controlled by inertia and surface tension forces that rapidly become unimportant as the bubble develops.

Besides, literature puts forward that a transition between the phases of different densities produces in the surrounding field a radial convective motion which modifies the concentration and temperature fields and hence the motion of the front. As the growth rate increases, the front moves into the concentration field producing a higher rate relative to the front, resulting in a higher gradient and hence a thinner boundary layer thickness.

Further, the growth of the bubble can as well be attributed to the Laplace law, according to which smaller bubbles having higher Laplace pressure (refer equation 4.3.6) have tendencies to merge into the larger ones having lower values of Laplace pressure, whereas on the other hand, bubbles having approximately the same sizes, tending to join and grow together in the fluidic system[193].

However, the above literature survey speaks of bubble growth in general, usually for macro-fluidic systems, involving mostly single-liquids. But when it comes to understanding the growth of bubbles in micro-fluidic systems, that too involving more than one liquids (as for the system dealt with in the current work), not much has been greatly accomplished—the experimental investigations conducted next aimed at pursuing the same.

5.3.2 Experimental investigations

As stated above, sophisticated experimental investigations were conducted to investigate the growth of bubbles in the micro-fluidic systems, as for the one considered in the current work. In this respect, in analogy with the nucleation studies, experiments were conducted to study growth rates from the nucleation sites present at different locations within the microfluidic system , say for when under water (inner liquid), under oil (outer liquid), and in the vicinity of the water-oil (liquid-liquid) interface- for the artificial nucleation sites (primarily laser engraved of 0.5mm diameters being considered in this regard) on the inner hydrophilic region, on the outer hydrophobic region, and at the (inner) hydrophilic-hydrophobic interface, respectively, for the chemically structured surfaces -AG glass slides being mainly investigated for this study.

Chiefly top down, HD, video recordings being conducted in this respect (using the experimental set-up as depicted in the image 5.2.15), minimum of ten surfaces were tested per case, with around 15 artificially engraved nucleation sites being investigated per surface. The video recordings were later evaluated using appropriate image analyzing software's as Paint.Net and Windows media player classic, and growth rates [bubble radii (average of vertical and horizontal radius, as depicted in the image 5.3.1) as a function of time] subsequently plotted via Microsoft Excel 2016.

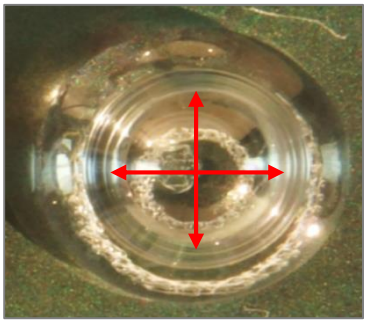

1 pixel= 4.5µm

Horizontal bubble diameter= 450 pixels= 2023.5 µm

Vertical bubble diameter= 455 pixels= 2047.5 µm

Average bubble diameter= 2036.25µm

Average bubble radius= 1018.13 µm

Image 5.3.1: Image analysis (using Paint.Net) of video recording snapshots for evaluation of bubble diameters w.r.t time

5.3.2.1 Bubble growth rate: Under inner liquid (water)

As stated in the nucleation studies, most of the artificial nucleation sites, especially the ones laser engraved (with 0.5mm diameters), though largely trapped gas, not all the nucleations led to bubble evolutions, particularly with measurable growth rates, at elevated system

temperatures. The probability of bubble evolutions (visible/measurable growths) from such sites when under water (inner hydrophilic region of chemically structured surfaces) observed to be around 80%, nucleation (II) experiments further revealed that even for the bubbles that evolved, not all grew to big enough diameters- such that their bursts cause spilling of the liquids or merging of the adjacent droplets.

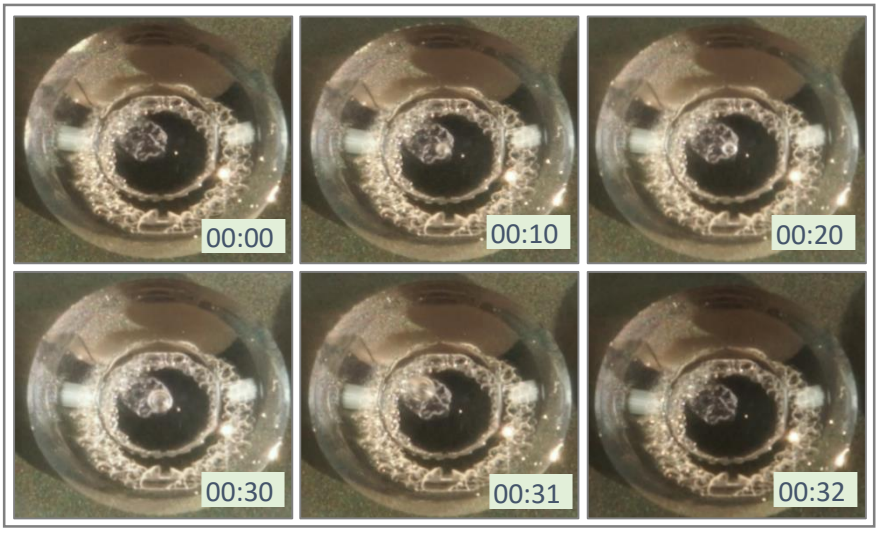

Image 5.3.2: A primary (parent) bubble in water, popping off within 32 seconds of heating (Set system temperature= 95°C) (Radius of bubble prior to burst = ~136.8 µm)

Whereas some bubbles were seen just popping off with small diameters (refer image 5.3.2), others were seen to grow to definite sizes (before their burst), as can be seen in the snapshots for the parent (initial) bubble, in the image 5.3.3 below:

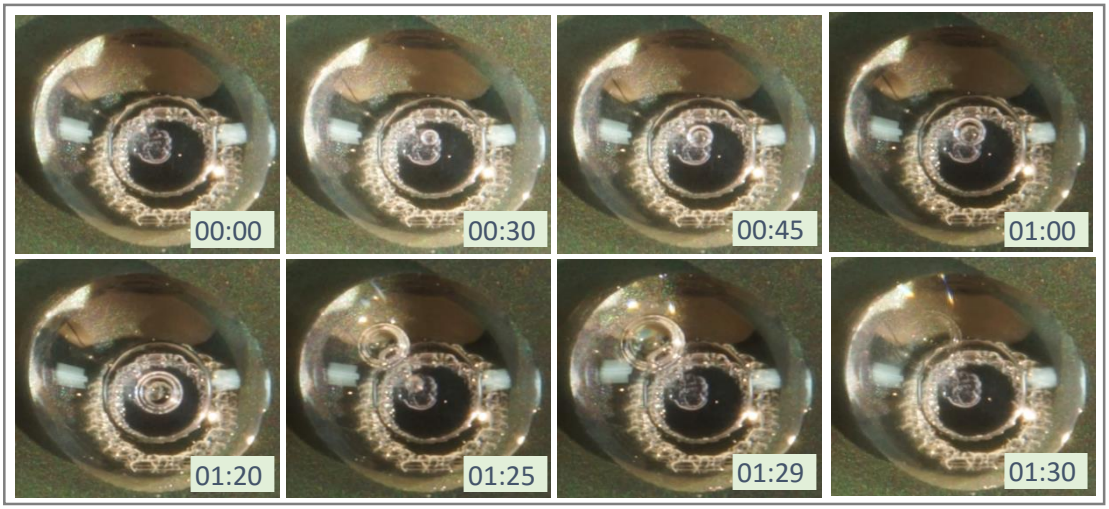

Image 5.3.3: A primary bubble in water, growing to max. radius of 380 µm, prior to its burst, (within 1 minute, 30 seconds of heating). Set system's temperature = 95°C

On the other hand, cases were observed where the nucleated bubbles were seen growing to ample diameters, at times nearly of the same size as of the reaction droplet, as can be seen in the image 5.3.4 for such a case.

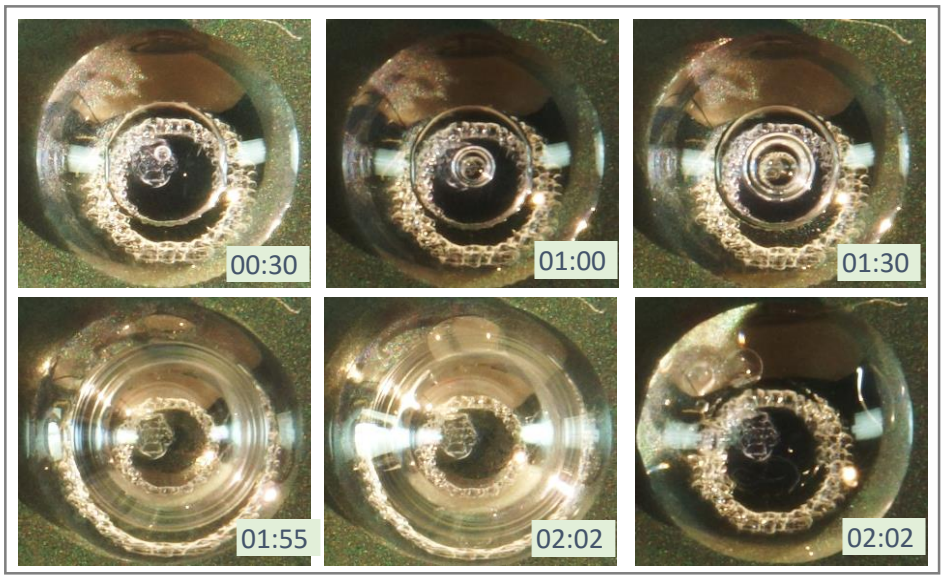

Image 5.3.4: A primary bubble in water, growing to max. radius of ~525µm prior to its burst (within 2 minutes, 2 seconds of heating). Set system's temperature=95°C

For the incidents where (parent) bubbles (evolving from the nucleation site under water) grew to sufficient diameters, their growth rate graphs (when plotted) revealed a drastic increase in the bubble radius, as it approached the water-oil interface (intersected by the hydrophilic-hydrophobic on chemically stratified surface(s), as viewed by the top down video recordings) –the growth rates as can be seen in the graph 5.3.1 below:

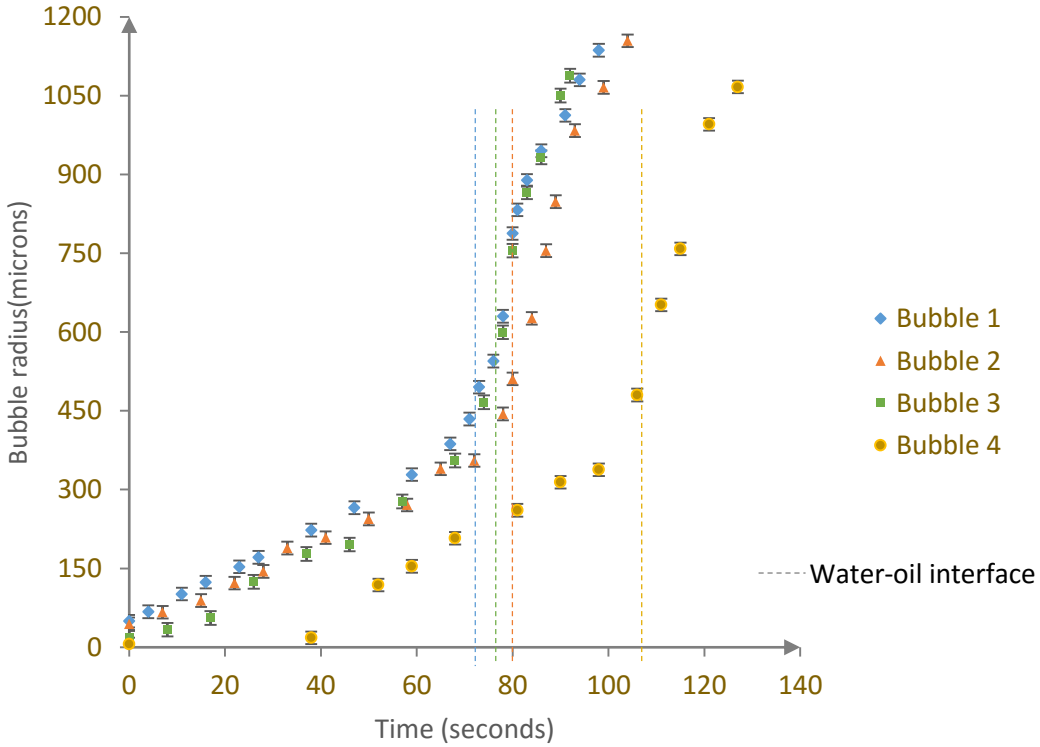

Graph 5.3.1: Growth rate of primary bubbles in water

As can be seen in the graph above, (parent) bubbles (nucleating under water) were found to have much lower initial growth rates (around 5 microns/sec), as compared to their final growth rates (around 30 microns/sec)- growths suddenly increasing as and when the bubbles approached the water-oil interface (overlapped by the hydrophilic-hydrophobic interface of the chemically structured surfaces, as previously stated).

Further, a parent bubble, usually growing to big enough diameters, after its burst, led to the generation of multiple daughter (secondary/daughter) bubbles in the system (refer image5.3.5) – the experimental observations being in analogy with the theory on bubble nucleation, that a site once active keeps on generally emitting bubbles till the temperature (and pressure) of a given system are unaltered.

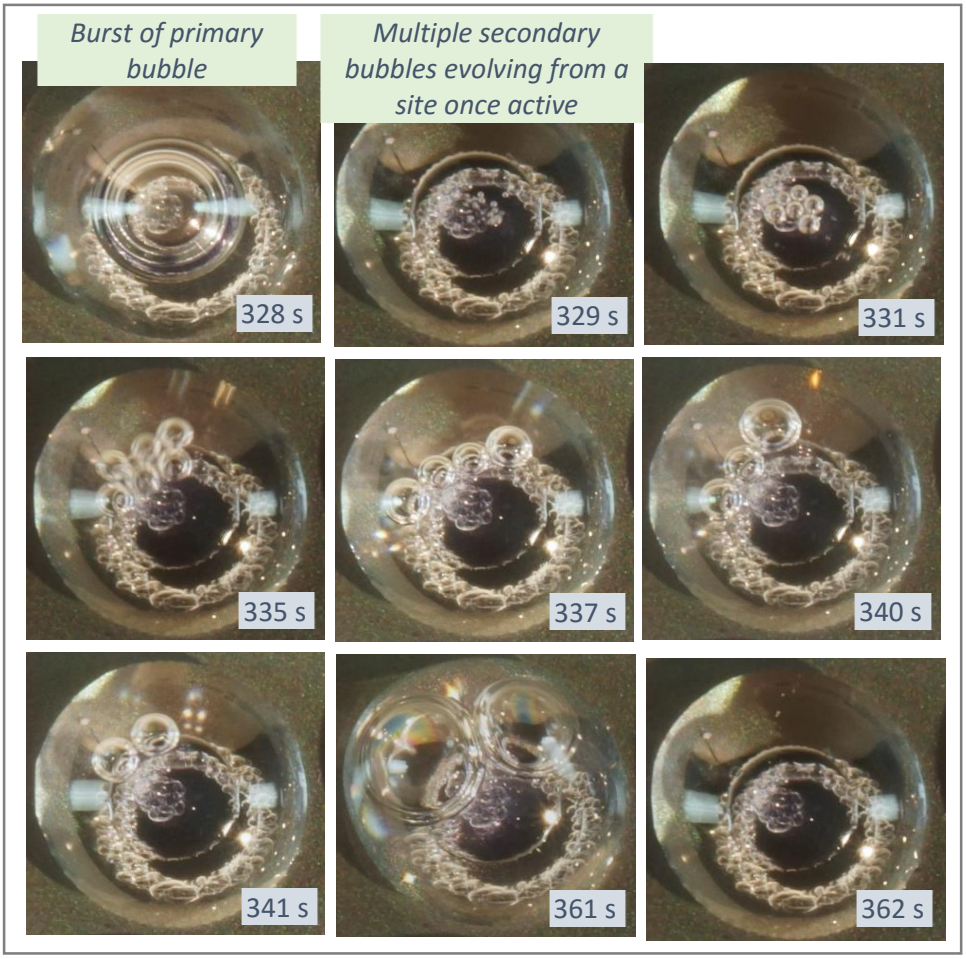

Image 5.3.5: Evolution of multiple secondary bubbles from an active nucleation site after the burst of the parent bubble (for system's temperature of 95°C)

Additionally, as can be seen in the image above, for most of the cases, multiple bubbles were seen growing/rising at a time in the system - smaller bubbles merging into bigger ones adding to the growth of the latter, whereas bubbles of comparable diameters observed to be sticking together, growing collectively within the micro-fluidic system.

Further, as for the parent bubbles, investigations revealed varying growth paths and destinies for the secondary/daughter bubbles (evolved in the system after the burst of the parent

bubble) – some just popping off, some growing to certain diameters, while others growing big enough that their bursts potentially spill the liquids, causing perhaps merging of the adjacent droplets. Also, cases were observed, where the burst of secondary bubbles generates further multiple 'grand-daughter' bubbles in the system--cascade of bubble evolutions observed from an active nucleation site for the same temperature and pressure conditions.

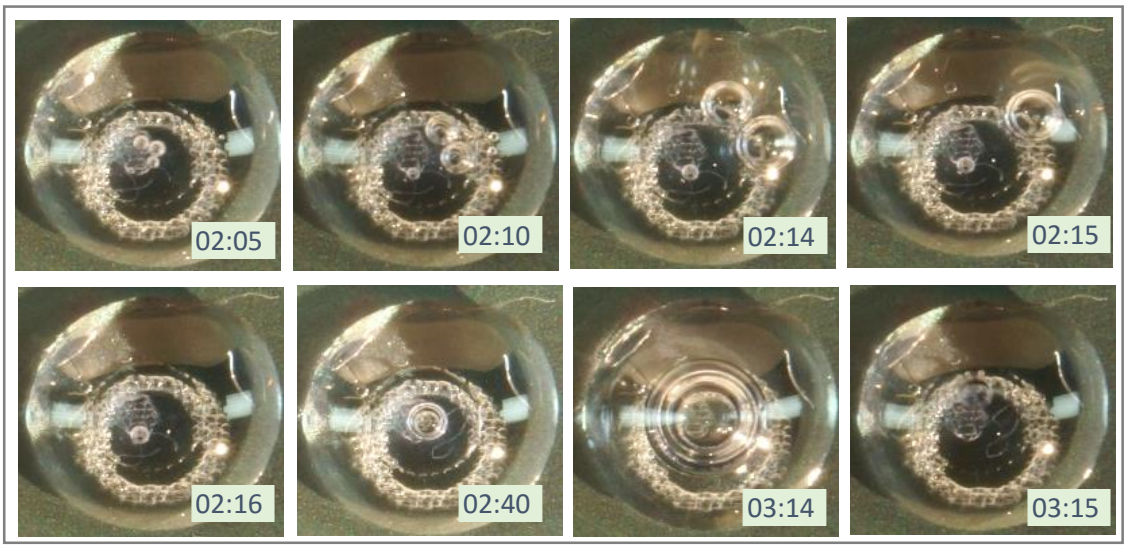

Image 5.3.6: Secondary bubble(s) growing in water at 95°C (total measuring time= 10:00 minutes)

Growth rates, when plotted in the similar fashion as the parent bubbles, especially for the (secondary) bubbles that grew to ample diameters, revealed:

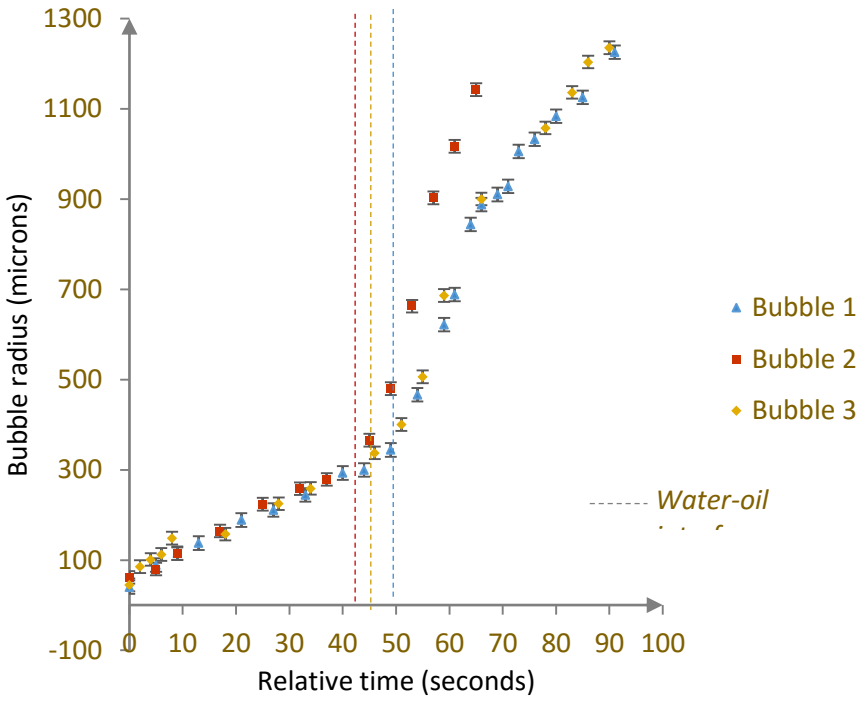

Graph 5.3.2: Growth rates of secondary bubbles in water

The behaviour of secondary bubbles, as can be seen in the graph 5.3.2, was found to be analogous to that for the primary bubbles – bubbles having slower initial growth rates (~4µm/sec), while their growths speeding up as the bubble(s) approached the liquid-liquid (/hydrophilic-hydrophobic surface) interface (growth rates ≥ 40µm/sec).

5.3.2.2 Bubble growth rate: Under outer liquid (oil)

Top-view, HD, video-recording experiments to study bubble growths revealed, no detectable growth of (especially the parent bubbles that have been initially nucleated) from the artificial nucleation sites when under oil, for the micro-fluidic system as dealt with in the current work.

However, experiments revealed, that for some cases, the burst of usually a big enough primary and/or daughter bubble, nucleated originally from a site under water, scatters multiple, additional daughter and/or grand-daughter bubbles in the system – such a bubble, now detached from its nucleation site, present independent in the micro-fluidic system. Further, for such a bubble when say present in oil, but in close proximity of the water-oil (hydrophilic/hydrophobic) interface, was seen to grow to huge diameters (refer image 5.3.7)- possibly leading to the dropout of the reaction droplet and maybe its merging with the adjacent droplets.

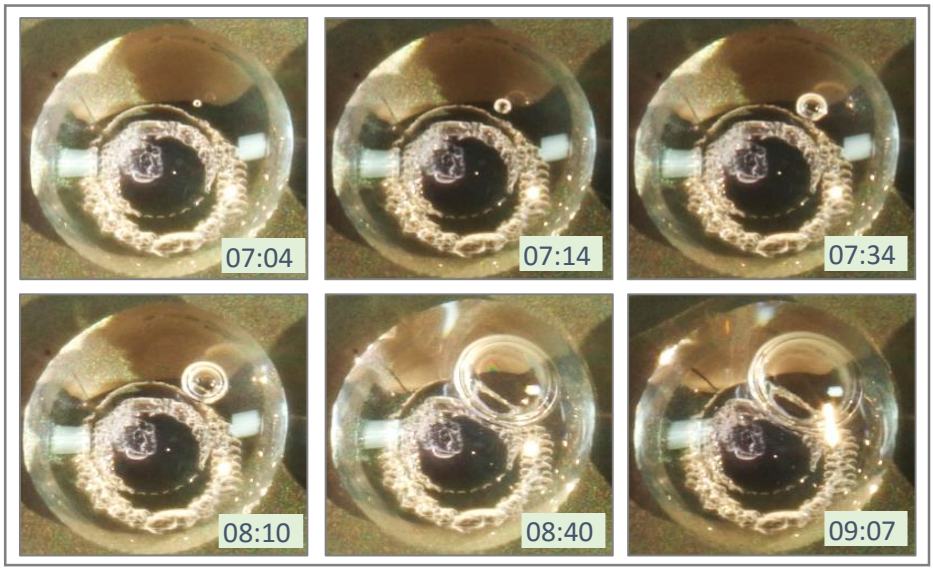

Image 5.3.7: A secondary bubble growing (at 95°C) in oil (present in vicinity of the water-oil/hydrophilic-hydrophobic interface. Total recording time =10:00 (minutes: seconds)

Also, cases were observed where the burst of secondary bubbles in oil (as for the one depicted in image 5.3.7 above), led to the generation of additional bubbles -from the same active spot in oil (the locate apparently being detached from the nucleation site on the surface and lying independently in the micro-fluidic system, as was discussed above).

Nevertheless, the presence and growth of such of secondary bubbles in oil was found to largely depend on serval factors as the initial parent bubble size(originating from the nucleation site under water), if simultaneous(other) bubble growths are taking place in the system or not, and most importantly on the position of the (scattered) secondary bubble in the oil- bubbles nearer to the water-oil (hydrophilic-hydrophobic) interface observed to grow rapidly as compared to the ones lying far away from it- unless while growing they approach the vulnerable (speedy growth responsible) region.

Thus owing to the many factors on which the growth for the secondary bubbles in oil was found to be dependent on, no two cases were similar in nature and hence could not be directly related. However, for the instances where big growths took place, growth rates of the secondary bubble in oil were plotted, as can be seen in the graph 5.3.3 below:

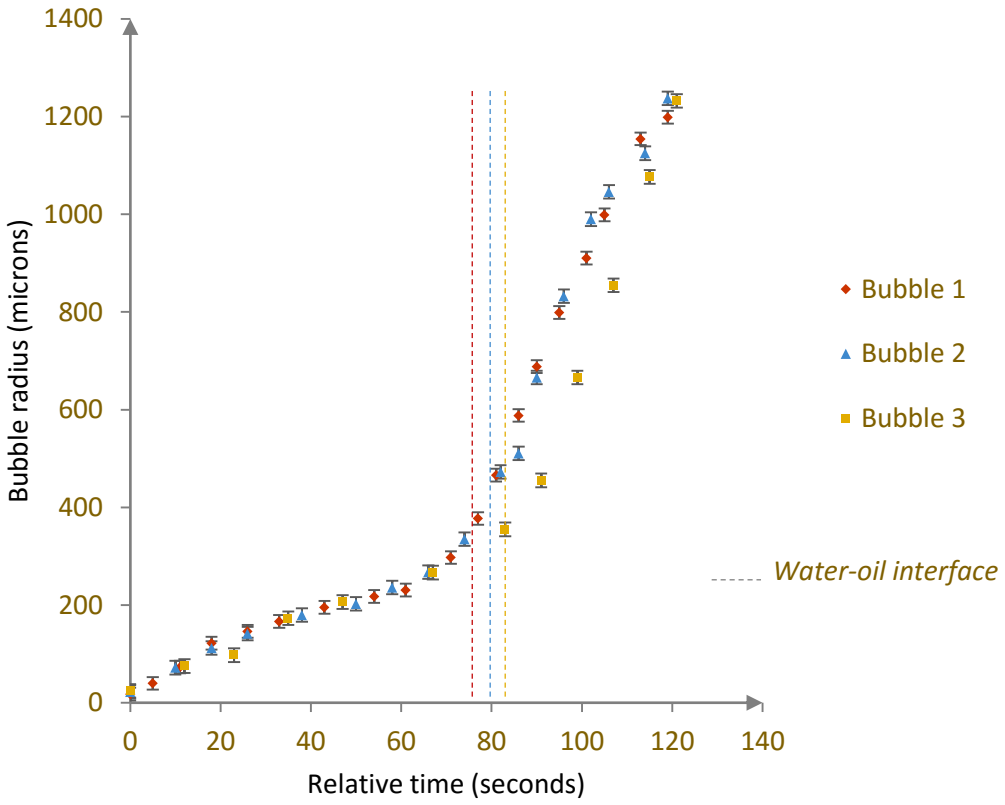

Graph 5.3.3: Growth rates of secondary bubbles in oil

As can be seen, similar behavior was observed as for the secondary bubbles growing in oil, as for the bubbles (parent/daughter) growing under water- bubbles having smaller initial growth rates as compared to their final growth rates, with them growing rapidly as and when they approached the liquid-liquid (traversing the bottom hydrophilic-hydrophobic solid) interface. However, studies revealed, the initial growth rates for the (secondary) bubbles originating in oil to be slightly lower (~2µm/sec) as compared to the initial growth rates for the (secondary) bubbles originating under water(~5µm/sec).

5.3.2.3 Bubble growth rate: In the vicinity of liquid-liquid (water-oil) interface

Growth rates were studied for the bubbles growing rapidly at the water-oil (hydrophilic-hydrophobic) interface- either originating directly from the nucleation sites at the above interface (parent bubble), or for the secondary bubbles growing in the vicinity of the above interface -as for the case depicted in image 5.3.7, and in the image 5.3.8 below:

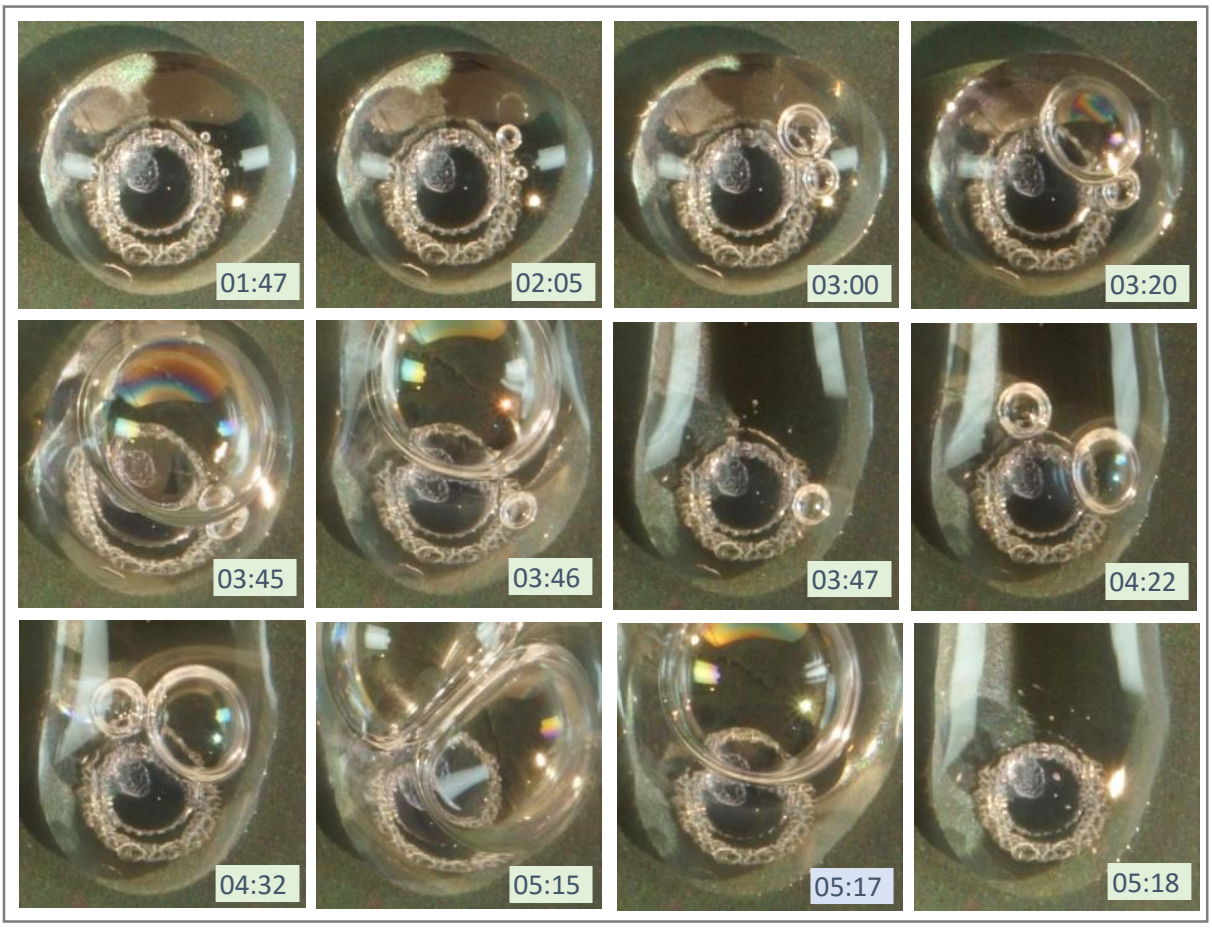

Image 5.3.8: Growth rates (at 95°C) of secondary bubbles (lying very close to the liquid-liquid interface in oil) after the rupture of primary bubble (originated from water). (Recording time units- min:sec)

Again, owing to the nature of the nucleation site, its position in the system, and topmost the position of the bubble (especially for secondary bubbles scattered after the burst of the primary bubble) in the system (as in how close it is to the liquid-liquid/ (solid-solid) interface), many cases, with no two being exactly similar in nature, were observed. However, for instances where big bubble growths were observed, leading to the dropout of the reaction drop or its merge with the adjacent ones, were considered and their growth rates analyzed.

Further, for exact understanding, it was important that cases be considered where only single bubble growing in the system was observed- as presence of other bubbles, concurrently nucleating/growing in the system might influence the growth rates of the to be examined bubble. In this respect, a promising case that was observed (bubble growing, single, independently, to ample diameters) was for a secondary bubble in oil, growing very close to

the liquid-liquid (hydrophilic-hydrophobic interface)- its growth rate as depicted in the graph 5.3.4 below:

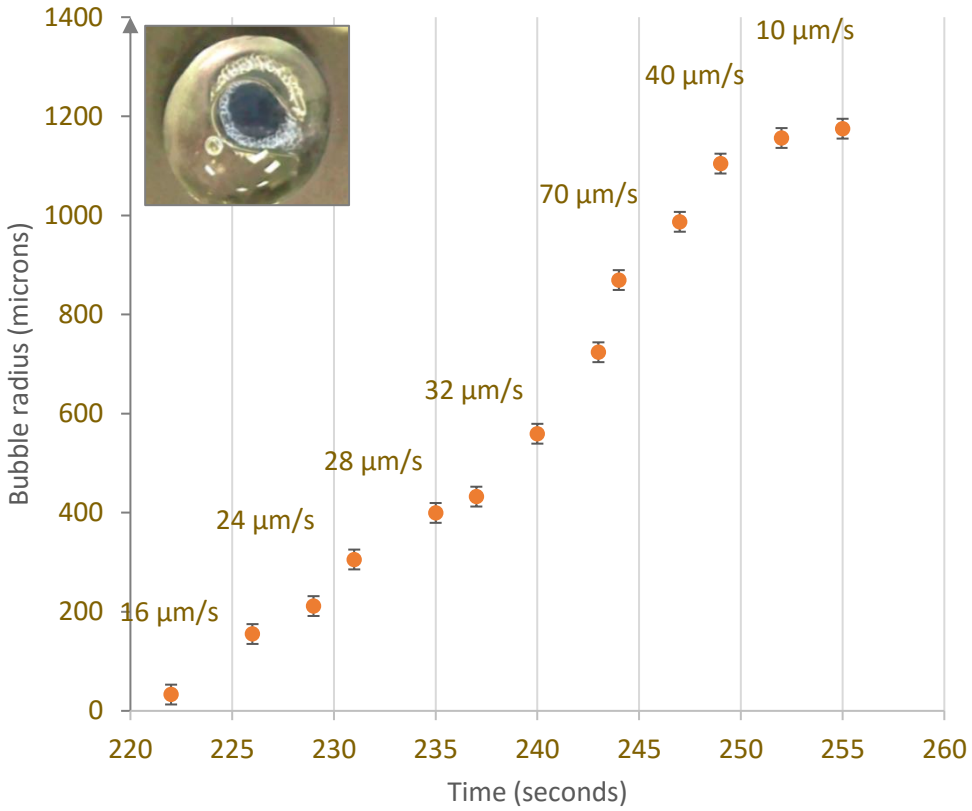

Graph 5.3.4: Growth rate of secondary bubble in oil, very close to the water-oil interface

As can be seen, the bubble was found to continuously grow when at the liquid-liquid interface, with a rapid growth rate, till the point of its burst (comparatively slower growths towards the end possibly attributed either to the curvature effect of the droplet holding it, or the fact that radius and not the volume (which might be increasing) could be evaluated and plotted as a function of time).

5.3.3 Bubble Growth: Summary

From all the above analysis, it can be hence summarized that the liquid-liquid interface (overlapped by the bottom hydrophilic-hydrophobic interface for the chemically stratified surfaces) plays an integral part in the growth of the bubbles- growth rates detected speeding up as the bubble approached the above region. A possible reason to the above could be the strong Marangoni convection [193,241-243] or the more temperature dependence thermo-capillary convection (arising at the interface of fluids having different surface tensions) [193,241-242] taking place at the water-oil interface – such a convective phenomenon probably generating local heat gradients causing rapid conversion of water into its vapor , which ,in

turn, feeds (primarily via diffusion) the bubbles, as when they approached the above mentioned interface.

The above supposition was as well supported by some experimental studies, where for the cases where multiple, continuous bubble evolutions took place (say for a surface with artificial nucleation sites), considerable low volumes of especially the inner aqueous (dummy PCR) mix was left after 10 minutes of heating at 95°C, as compared to its initial working volume (refer image 5.3.10). This hence further hinted to the possible rapid conversion of water into its vapor at the liquid-liquid interface, feeding the bubbles, such that for cases where tremendous, cascade of bubble evolutions took place, the inner aqueous droplet shrank considerably in volume at the end of the experimental run.

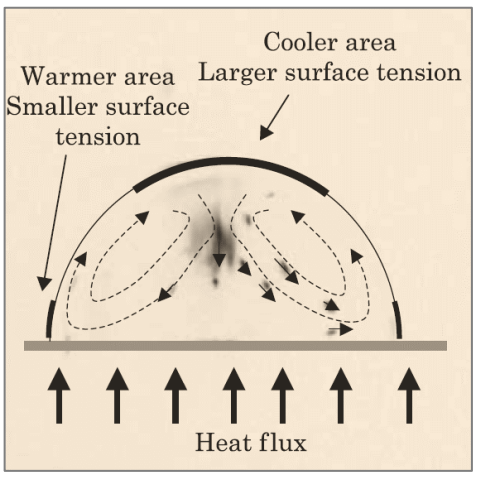

Image 5.3.9: Observation of Marangoni convection in a sessile droplet obtained by heating an ionic liquid droplet from below (photo Ph. Dubois, CEA/LETI[15]

Additionally, the almost linear initial growth rates and $R \propto t^{1/2}$ dependence later growth rates as it approached the above interface, further indicated the diffusion controlled growth of the bubbles at this region.

However, the above explanation based on Marangoni convection is just a potential hypothesis, which needs further experimental understanding, supported by well-conducted numerical analysis and/or mathematical modelling.

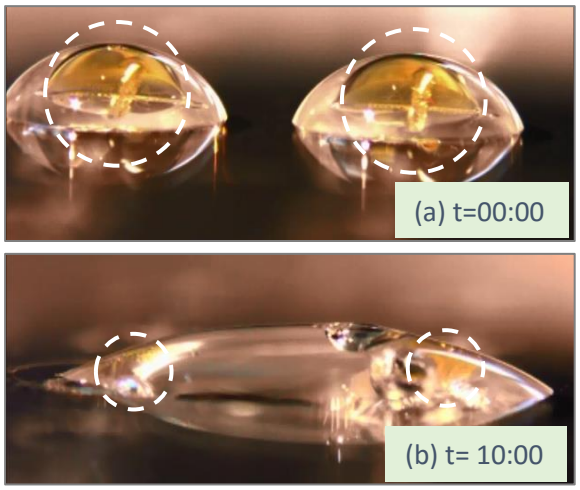

Image 5.3.10: (a) Droplets status prior to heating, (b) considerable reduction in volume, especially of the inner water based PCR mix after 10 minutes of heating (at 95°C), after multiple, huge bubbles have been evolved in the microfluidic system

Further, no prominent bubble growths for the parent bubble and comparatively lower initial growth rates for the secondary bubbles in oil (than in water) could be attributed to the high viscosity of oil[247-248] as compared to that for water (drag force on a bubble reported to be highly affected by the fluids viscosity and density, both of which in turn being largely temperature dependent - altering the fluids viscosity and density alters the friction on the bubble, thereby making it rise faster as the system's temperature increases[215,219]). Also, the major growth of the bubbles (even though initially originating from a site in water) after approaching the liquid-liquid interface taking place in oil than in water could be attributed to the lower density of oil than

water[245]- bubbles having the tendency to eventually reside in a lower density medium with lower surface tension[246].

Besides, the 'sticking' and growing together of bubbles of nearly the same diameters, and the merging of the smaller bubbles in the bigger ones, could be attributed to the Laplace law (pressure)[193,244] - bubbles with smaller diameters having higher Laplace pressure (refer equation 4.3.6) tending to merge into the bubbles with greater diameters of lower Laplace pressures.

Further the shape of the bubbles- spherical when they are small in diameters and varying unstable shapes as they grow big can be explained by the interplay of various forces acting upon them- primarily being the interfacial tension/viscous forces and the inertial forces. For the former being dominant over the latter, cases when the bubble is relatively smaller in diameters, the bubble is said to assume a spherical shape[1,263,268].

Authors have further reported that the shape of the bubbles is mostly determined by the ratio of gravity and surface forces- their rate being expressed by a dimensionless number known as the Bond number (B_o) or the Eötvös (E_O) number (small bubbles with $E_o << 0.2$ to be reported to be essentially spherical bodies). Besides, unlike drops, rising bubbles have been reported to be significantly wobbling in the system – the ellipsoidal and all geometry parameters of its projection changing as well. Two motions can be distinguishable in this case: the slow motion around the vertical axis and the harmonic wobbling around the horizontal axis. However, large bubbles with $E_O >> 30$ have been reported to have unstable shapes, mostly half spherical (with flat side oriented down). These bubbles have been reported to oscillate chaotically – being more vulnerable to break ups. For the medium sized bubbles with $0.2 < E_O < 30$, on the other hand, bubbles have been reported to be like essentially oblate ellipsoids oriented by its minor axis in the direction of the movement[263-268]. Additionally, authors have reported that the path of the rising bubbles is helical for smaller bubbles and zig-zag for the larger ones.

Thus, with large bubbles (>1mm in dimeters) the shape of the bubble is non spherical, and the path followed by such bubbles as it rises through the quiescent liquid may be spiral, or oscillatory, or chaotic. At sizes between 1mm and 1um the bubble is approximately spherical, and the rise will generally be rectilinear[263-268].

However, non-spherical particles in general have been reported to present problems more complex than those arising for a sphere- all the above calling for detailed mathematical and numerical analysis for the in-depth understanding of how the bubbles shape up during their nucleation, rising and growth stages, as function of temperature, in the system as under consideration – all the above again serving as a promising outlook!

Also, keeping in mind the various forces acting on a bubble nucleating from a site within a liquid, authors reported that the detachment of the bubble form the site is determined by the ratio of primarily surface tension, inertial, buoyancy, and gravitational forces acting on it- the first three tending to detach the bubble while the last one trying to hold it to the nucleation site. This was as well supported by the Tate's law [198,220,269], which related the

weight (W) of the detaching drop to the radius of the nucleation site (or tip) on which it its formed (r), and the surface tension(ϒ), as:

$$W=m\Delta\rho g=2\pi r\Upsilon \quad (5.3.8)$$

Additionally, some authors as well reported that the detachment is also determined by the contact angle of the bubble to the nucleation site- bubbles having smaller contact angles having greater tendencies of getting detached and vice-versa.

Nevertheless, the exact criterion and conditions for detachment for a bubble being strongly dependent on the system under consideration and the parameters being involved, the above calls for detailed investigations supported by adequate mathematical and/or numerical analysis, for the in-depth understanding of the same.

However, though the liquid-liquid interface potentially appears to be primarily contributing to the growth of the bubbles, owing to the design of the microfluidic system, the above interface is intersected by the bottom hydrophilic-hydrophobic junction on the chemically structured AG slides, which could not be very clearly distinguished in the top down video recordings. This hence calls for the study of individual interfaces, and their role in the evolution of bubbles, as will be attempted in the next section.

5.4 Separation of Interfaces

A characteristic feature of the microfluidic system, as the one dealt with in the current work, is the presence of multiple interfaces: the solid-solid (hydrophobic-hydrophilic), the solid-liquid (hydrophilic-water, hydrophobic-oil), the liquid-liquid (water-oil), and the liquid-air (oil-air) interface- the highlight owing to the design of such systems being the region where the (inner) hydrophilic/hydrophobic interface overlaps with the water-oil interface (after the liquid have been pipetted), as detailed previously in chapter 2 on system specifications.

Though the nucleation studies, via sophisticated top and bottom view HD video recordings, largely indicated the solid-liquid interface (surface inhomogeneities trapping gas if the conditions of gas entrapment are fulfilled after the liquids have been pipetted atop) to be the potential region contributing to nucleation of bubbles, growth rate studies (primarily via HD top view video recordings), however, could not essentially filter out an exact interface responsible for the prominent growth of the nucleated bubbles- the bubbles seen growing rapidly at the above discussed region where the liquid-liquid(water-oil), the solid-solid(hydrophilic-hydrophobic) and the resulting liquid-solid (water-hydrophilic, oil-hydrophobic) interfaces intersect. Hence to further put light on the exact interface responsible for the nucleation and for the growth of the bubbles, each of the above mentioned interfaces were revised individually, as dealt with in the following sub-sections:

Study of the role of the solid-solid interface

The solid-solid interface here mainly inferring to the hydrophilic-hydrophobic boundary on the chemically stratified surfaces, keeping in mind the microscopic surface characterization studies conducted in the previous chapter, where no distinct step at this interface was detected, it can be hence concluded that for homogeneous, well-coated surfaces, merely the above solid-solid interface plays no vital role in the nucleation and/or the growth of the bubbles. The finding was further supported by the heterogeneous model of bubble nucleation according to which a site acts as a nucleation or gas entrapment site only after the corresponding liquids are dispensed over it (provided the conditions of gas entrapment are fulfilled with the bubbles evolving as and when the temperature (or pressure) of the system is later altered) -- further eliminating the role of solely the solid-solid interface in the evolution of bubbles.

Study of the role of the solid-liquid interface

In accordance with the heterogeneous model of bubble nucleation, it can be hence said that for the conditions of gas entrapment being fulfilled, a site acts as bubble nucleating site once the liquids have been pipetted above it- thereby indicating the solid-liquid interface to be the potential source of bubble nucleation.

However, growth rate studies revealed no prominent growth of the bubbles nucleated from an active site within single liquids (say for the site when under water or under oil), as compared to the huge bubble growths observed in the presence of the liquid-liquid interface, hence indicating the solid-liquid interface in itself to be play no vital role in the growth of the nucleated bubbles.

Hence, it can be said that though the solid-liquid interface plays vital role in the nucleation of the bubbles (provided the conditions of gas entrapment are fulfilled), it doesn’t contribute much in the ample growths of the nucleated bubbles.

Study of the role of the liquid-liquid interface

In order to study the role of liquid-liquid interface in the nucleation of bubbles, brief experiments were conducted where freshly prepared, homogenous, and chemically non-structured (PFS) surfaces (i.e. no hydrophilic-hydrophobic or solid-solid interface present), devoid of any artificial nucleation sites were pipetted with the regular bi-liquids (water-oil) in standard volumes, and the system, minimum of six cases, analyzed for bubble nucleation’s at 95°C. Results revealed no bubble evolutions on such surfaces, thereby indicating no prime contribution of solely the liquid-liquid interface in the nucleation of the bubbles.

Further, in order to determine the role of the liquid-liquid interface in the growth of the nucleated (from the solid-liquid interface) bubbles, similar experiments as above were done where homogeneous, chemically non-structured (PFS) surfaces (i.e. with no hydrophilic-hydrophobic or solid-solid interface overlapping the liquid-liquid interface), but this time with

artificial nucleation sites (laser engraved of 0.5mm diameters) were dispensed with the regular liquids in the standard volumes, and growths of the nucleated bubbles analysed at 95°C. Results revealed, sudden increase in the bubble growth rates as and when the bubbles approached the liquid-liquid interface, hence indicating the major role of the liquid-liquid interface in the growth of the evolved bubbles.

Hence, it can be said that though the liquid-liquid interface has not much to do with the nucleation of the bubbles, it is this interface, whose presence greatly contributes to the rapid growth of bubbles, for the microfluidic system as under consideration.

Summary

Thus, from the above studies, it can be summarized that whereas the solid-liquid interface plays a major role in the nucleation of bubbles, it is the liquid-liquid interface that chiefly contributes to the rapid growth of the nucleated bubbles; the solid-solid interface in itself, on the other hand, participating not much in the occurrence of either of the above phenomenon.

Interface	Prime contribution	
	Nucleation	Growth
Solid-solid	No	No
Solid-liquid	Yes	No
Liquid-liquid	No	Yes

Table 5.4: Contribution of the respective interfaces in the nucleation and/or growth of the bubbles in the microfluidic system as under consideration

5.5 Content of bubbles

Another significant aspect of bubble dynamics that required attention was comprehending the content of the evolved bubbles- as in what nucleates in the form of bubbles and what is it that feeds them as they grow at elevated temperatures within the microfluidic system.

The apparent constituent that first comes to mind in this regard is air- either getting trapped in the (rare) surface inhomogeneities or being injected accidentally into the system during flawed pipetting/loading of the liquids- evolving as (air) bubbles at higher system temperatures. However, video recording (growth rate) experiments revealed, for most of the cases, bubbles growing to ample diameters as when they approached the liquid-liquid interface- maximum bubble diameters for the fully grown bubbles (prior to their burst) calculated to be ≥ 1600 microns, as can be seen for the cases in the image 5.5.1 below:

Image 5.5.1: Snapshots (top and side view video recordings) depicting bubbles growing to huge diameters (≥1600 microns, i.e. size of the reaction droplet itself)

Further, nucleation experiments revealed that under the same conditions of system temperature (and pressure), a site once active, keeps on emitting a cascade of daughter bubbles, growing nearly of the same size (as for the parent bubble) when in the vicinity of the liquid-liquid interface. Thus, if air be considered as the main constituent comprising the bubbles, the above findings imply that a sufficient amount of air is present within the micro-fluidic system, evolving as such huge, continuously growing bubbles.

However, the fact that the liquids have been properly degassed prior to use, and that extreme care has been taken in their loading /pipetting, questions the presence of such abundant amount of air within the microfluidic system. Further, mathematical calculations based on Henry´s law (refer Appendix E) revealed that at room temperatures, the amount of air that can get dissolved in 1µL of water and in 5µL of oil (standard volumes of regular liquids used) is nearly 0.0189 µL's and 0.5µL's respectively- the values being considerably low in volumes to generate continuous, huge bubbles, as big as max. of 1600 micron in diameter , i.e. of around 2µL in volume [assuming the bubble to be spherical in shape or conical in shape (say attached to their nucleation site on the slide surface and having height of around 0.78mm (height of the inner water drop on chemically structured surfaces as can be seen in image 4.3.1))] at a time. This hence indicates the presence of some additional component- either partially feeding the otherwise original air bubbles at some stage, or serving as the prime constituent of the evolved bubbles.

In this regard, some initial (top down) video recordings were referred to, which revealed a considerable decrease in volume, especially of the inner water based PCR solution, at the end of the biological reaction; the decrease in volume of the inner liquid observed to be largely dependent on the frequency and intensity of the bubbles evolved during the experimental run (refer image 5.3.10). One contemplated explanation to the above finding, as stated in the growth rate studies, could be the rapid conversion of water into its vapor (for working temperatures of 95°C), such a phase change predominantly occurring at the water-oil interface (conceivably attributed to higher Marangoni/thermo-capillary convection[193] at this region)- the water vapor feeding the evolved bubbles as they approach the liquid-liquid interface resulting in sudden, rapid increase in bubble sizes. Hence, even though the bubbles might be originally air bubbles, it can be interpreted that its potentially the water vapor that chiefly constitutes the bubbles (especially for the ones that grow big enough at the liquid-liquid interface) during their later(growth) stages- the prime transport phenomena being

diffusion (keeping in mind that air comprises of 2-3% of water vapor- the amount varying as per the location and its humidity[249-250]).

However, if the above holds true, the bubble should ideally shrink back with a decrease of the system´s temperature- attributed to the condensation of water vapour back to its liquid form as the temperature is lowered. To investigate this, top and bottom view video recordings were conducted (for experimental set-ups: refer images 5.2.16 and 5.2.17 respectively), by stopping the system´s (ASC) heating at a point when fully grown up bubbles were encountered (prior to their burst), and noticing any measurable/visible change in their sizes (diameters) over various time intervals (hours, days), without altering/disturbing the rest of the experimental set-up.

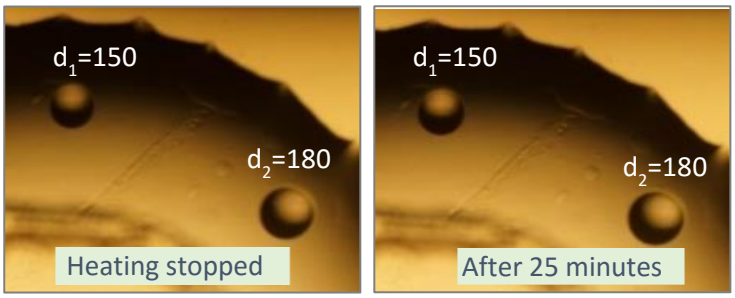

Image 5.5.2.: Bottom view analysis of bubble status: (left) immediately after the heating has been stopped, (right) 25 minutes after the heating has been stopped. (d_1, d_2= bubble diameters in microns)

Various cases being examined in this respect, observations, for one set of the instances, revealed no visible/ measurable reduction in the size (diameter) of the bubble with time, after the heating of the system has been stopped (refer image 5.5.2 and 5.5.3) (heating plate of the ASC investigated to attain room temperature (from 95°C) within 40 seconds as and when the temperature was stopped.

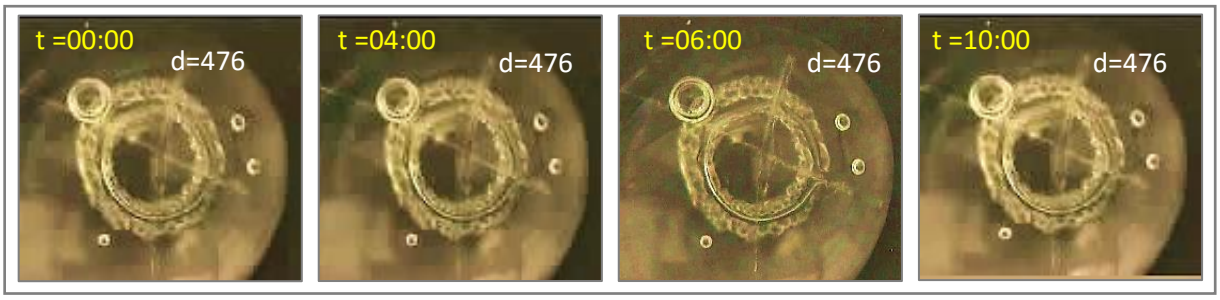

Image 5.5.3: Top-view analysis of bubble status for different time intervals (after heating of the system has been stopped) revealing no prominent change (decrease) in bubble diameter (d, in microns) with time (for 10:00 minutes)

However, for some other cases, a slight shrinkage in the bubble diameters was observed after the heating has been stopped, as can be seen in the images 5.5.4 and 5. 5.5 below:

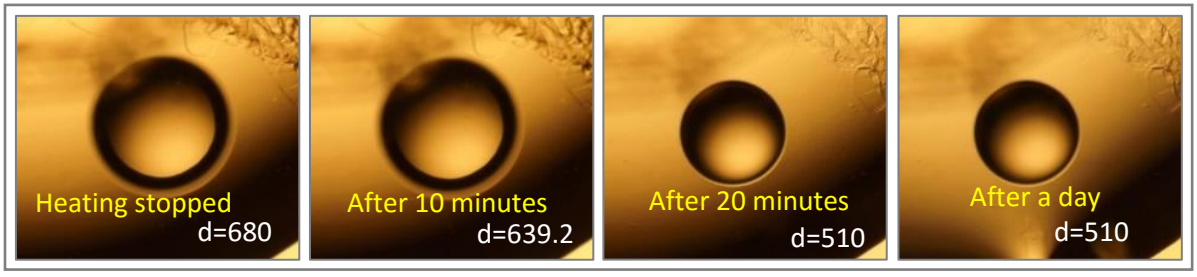

Image 5.5.4: Bottom view analysis of bubble status for various time intervals, after heating of the system has been stopped. d= bubble diameter in microns.

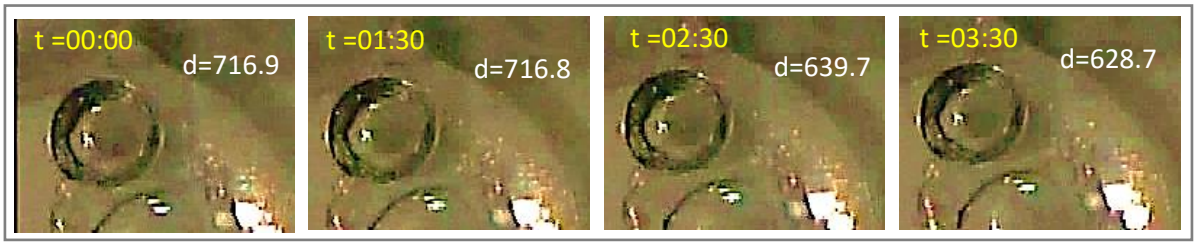

Image 5.5.5: Top-view analysis of bubble status during different time intervals (after heating of the system has been stopped) revealing little shrinkage in the bubble diameter (d, in microns) with time (within 3 minutes 30 seconds). The bubble pops off in 03:33.

A possible reason to the observed shrinkage in some cases while not in others, could be the varying amounts (percentage) of water-vapor and/or air constituting the bubbles at a given time – especially, water-vapor present below a certain value leading to not so visible/measurable condensation/ decrease in bubbles diameters. In addition, potential factors as the position of the bubble in the system, its final size (prior to burst), and probably the temperature of the surrounding medium (point at which heating was stopped), might as well determine the above – serving nevertheless as an important outlook for detailed analysis.

However, besides air and water-vapor, another possible candidate constituting (mainly or partially) the bubbles could be some additional gaseous component, evolving (degassing) as bubbles at elevated working temperatures—the detailed analysis in this regard again being an important outlook study.

5.6 Bubble burst and droplet merge

Finally, an important aspect worth comprehending was studying the phenomena of bubble burst- potentially leading to the dropout of the sample solution and the merging of the adjacent droplets, for the micro-fluidic system as dealt with in the current work.

Literature reports that a bubble, prior to its burst, is usually balanced by primarily three factors: the surface tension of the liquid in which it is contained, internal pressure applied by the air/gas/vapor inside the bubble on its surface, and the atmospheric pressure- imbalance of any of the above forces causing rupturing of the bubble[1]. As the bubble rises in the liquid(s), a stage comes where its internal pressure surpasses the surface tension forces holding it (surface tension additionally 'poked' by the comparatively cooler surroundings), that in order to attain equilibrium, the bubble pops.

Authors have as well reported that the stability of the bubble once it reaches the free liquid surface, is dependent upon the rate of the thinning of the liquid layer forming the upper surface of the bubble. For instance, a surfactant bubble in the bulk liquid has only one surface, whilst a free bubble in air has two, the excess pressures in the two extreme cases are $2\gamma/r$ and $4\gamma/r$ respectively[1]. Depending on where exactly the bubble intersects the surface, it will have an excess pressure intermediate between the above extremes (refer image 5.6.1).

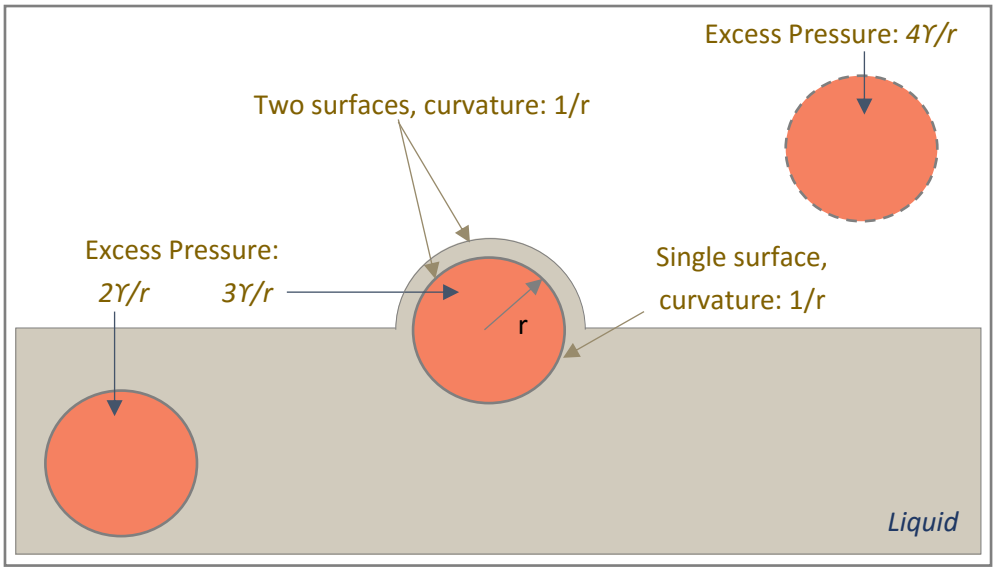

Figure 5.6.1: A (soap) bubble having completed its rise, intersects the liquid-air interface- the bubble burst being governed by the rate of thinning of the upper bubble surface[1]

However, in comparison to the behavior of the bubble in a single-liquid system, the presence bi-liquids (as for the microfluidic system dealt with in the current work), might generate additional surfaces on a (gas/air) bubble (say originating from a nucleation site under water): bubble surrounded in this case by a thin water film below a layer of oil. Nevertheless, the in-depth analysis of the exact phenomenon of bubble burst in a bi-liquid system (in analogy with the rate of thinning of the liquids surrounding it) calls for further in-depth understanding- serving as yet another promising outlook for the work under consideration.

Further, for the microfluidic system as dealt with in the current work, experimental investigations revealed various scenarios for the bubble as they burst: whereas some bubbles were seen to directly travel up, pop off and escape the microfluidic system without encountering much increase in their sizes, others were seen growing to ample diameters and rupturing big enough, leading to the dropout out of the reaction sample and perhaps merging of the adjacent droplets (the effect being highly probable when huge bubbles occur/burst simultaneously in the neighboring droplets). Bigger bubbles, in analogy with the growth rate studies, can be said to be majorly constituting of water-vapor, growing rapidly at the liquid-liquid interface (if the hypothesis of Marangoni convection holds true), such that when they burst, they spill traces of inner sample solution – the intensity of spilling further (apparently) depending on the intensity with which a bubble bursts.

Besides, after the burst of say a big enough bubble (having the tendency to cause drop out of the sample solution), the adjacent droplets may or may not merge depending primarily on the balance of surface (adhesive) forces (hydrophobic regions outside the droplets for the chemically stratified surfaces and hydrophobicity of the PFS coated glass slides repelling the liquids/holding the liquids in place), the surface tension forces (micro-droplets having a tendency of beading up), and the cohesive forces among the liquid molecules (neighboring liquids attracting each other if (after the burst) are close enough to surpass the adhesive and

surface tension forces). However, the minimum distance for which two adjacent droplets might merge, and the relation of the size of the bubble and the velocity/force with it bursts to the merging of the adjacent droplets calls for further, detailed understanding (experimental and/or numerical analysis) - serving as yet another outlook for the system as under consideration.

5.7 Elimination/control of bubbles

As stated previously, the occurrence of bubbles in microfluidic systems, as for the one under consideration, is a highly undesirable and an alarming phenomenon, potentially lowering their overall efficiency of such systems- thus calling for apposite methods for the elimination or suppression of the same.

The fundamental pre-requisite for the suppression of the bubbles at the pre-functional level was opting a system as clean and inclusion free as possible. This was attempted by careful handling of the system both during and post-production stages so as to ensure no insertion of any inhomogeneities or imperfections, which might at the operational stage, serve as 'seeds' for bubble nucleations (or aid in the growth of the nucleated bubbles). Further, it was made sure that amplification platforms having surfaces as clean, homogeneous, and freshly prepared as possible, well-calibrated and fully optimized heating cyclers, and freshly prepared and properly degassed liquids were chosen (in addition to the liquids being carefully pipetted/loaded as to ensure no carrying of any air bubbles), as to eliminate or minimize any contamination at the pre-functional stage within the microfluidic system.

However, despite of the above preventive measures, experimental investigations revealed, bubble evolutions and droplet incidences on some rare and unpredicted regions within the microfluidic system as the biological reactions proceeded- thus calling for the formulation and development of more sophisticated and reliable methods for the suppression/control of bubbles in such systems. This was attempted by checking on the evolution of bubbles at the nucleation and at the growth levels, with finally trying out methods to prevent the merging of the adjacent droplets (due to bubble bursts) – the respective experimental procedures as detailed in the sub-sections below.

5.7.1 Control of bubbles at the nucleation level

To begin with, emphasis was laid on developing methods to prevent the occurrence of bubbles at the nucleation stage itself. The most sought after way of doing so, as per literature, is either by lowering the temperature or raising the pressure of the system. The former is in accordance with Charles law[270,271], according to which for a pressure on a sample of dry gas held constant, the Kelvin temperature and the volume are directly related ($V \propto T$), indicating

that as the absolute temperature decreases, the volume of the gas as well decreases in proportion.

The latter, the effect of pressure in suppressing the nucleation of bubbles, on the other hand is in analogy with the Boyles law[270,272], which states that at a given temperature, the volume of the gas decreases as the pressure above it increases and vice-versa (PV=constant)—the phenomenon further supported by the Henry's law[273-274] according to which the solubility of gases increases with an increase in the pressure of the system($p=k_H.c$, where p is the partial pressure of the solute above the solution, c is the concentration of the solute in the solution, and k_H is the Henry laws constant having units as L··atm/mol *or* atm/(mole fraction) *or* Pa · m^3/mol).

Based on the above, sophisticated experimental investigations were conducted to study the effect of change of temperature and pressure on the evolution of bubbles in the system as under consideration, as detailed in the sub-sections below.

5.7.1.1 Effect of temperature on bubble evolution

Literature reports that higher the systems (surface) temperature, higher is the likelihood of bubble evolutions, especially in the presence of a pre-existing nucleation site. This can be attributed to the reduced Henry`s equilibrium constants and more rapid diffusion kinetics at greater system temperatures[219].

To understand the role of temperature on the evolution of bubbles in the microfluidic system as under consideration, sophisticated bottom- up HD video recording experiments were conducted, using the experimental set-up as depicted in image 5.2.17 earlier. As already stated, bubble evolution in the dealt with microfluidic system is a very rare and random phenomenon, and hence to for such investigations the surfaces were laser engraved with artificial nucleation of 0.5mm in diameter approximately in the middle of the reaction site holding the liquids, so as to enable, forced' nucleation's for the detailed and inclusive analysis. In the usual manner, once loaded with the respective liquids, the slides were placed on the heating plate of the ASC and keeping the pressure constant, the temperature of the system was raised from RT to 100°C, insteps of 5°C, and at least 10 video recording observations (10 mins 1st stage of the PCR cycle) were made per case. Additionally, comparative studies were carried out using surfaces having artificial nucleation sites and the ones devoid of them, for both chemically structured (AG) and non-structured (PFS) surfaces. The video files were documented using Windows media player classic and Paint.Net software's.

Results revealed no evolution of bubbles at any temperature for surfaces devoid of nucleation sites. Also for surfaces engraved with artificial nucleation sites, below 70°C no such evolution was observed. However, for such surfaces after 70°C bubble occurrences were witnessed, the degree and intensity of which increased as the temperature was increased beyond this point, exhibiting greater diameter bubbles, documented and as summarized in the table 5.7 below:

Temperature (°C)	Without Nucleation Sites		With Nucleation Sites			
	No. of Active Sites	No. of Merges	No. of Active Sites	No. of Merges	Min. time (min:sec) for initial bubble evolutions	Range of bubble diameters (mm)
80	0	0	20	0	00:30	0.04-0.7
85	0	0	23	0	00:27	0.04-1.06
90	0	0	24	4	00:24	0.04-2.24
95	0	0	29	6	00:20	0.04-2.9

Table 5.7: Study of bubble evolutions as function of system's temperature

The above can be attributed to the increase in system's saturation (gas dissolution) with an increase in its temperature. Thus one way to suppress/control the nucleation of bubbles could be by using lower working temperatures. However, owing to the specific temperature needs of the biological reactions as the PCR, the above approach could not be practically put to use. A detour to this could be playing with the pressure parameter, as detailed next.

5.7.1.2 Effect of pressure on bubble evolution

As mentioned, according to Henry's law, under pressurization, the solubility of the dissolved gases increases, disabling the growth in volume of the microbubbles in the PCR sample, and thereby preventing the formation of air bubbles [1-6,219]. Hence, the sealing pressurization of the PCR was reported to successfully prevent the bubble formation[33].

Based on the above, experimental investigations were conducted to study the effect of pressure on bubble formations in the microfluidic systems, as for the one dealt with in the current work. To achieve this, a pressure chamber was specially constructed, in which the dealt with microfluidic system could be placed, as can be seen in the images below:

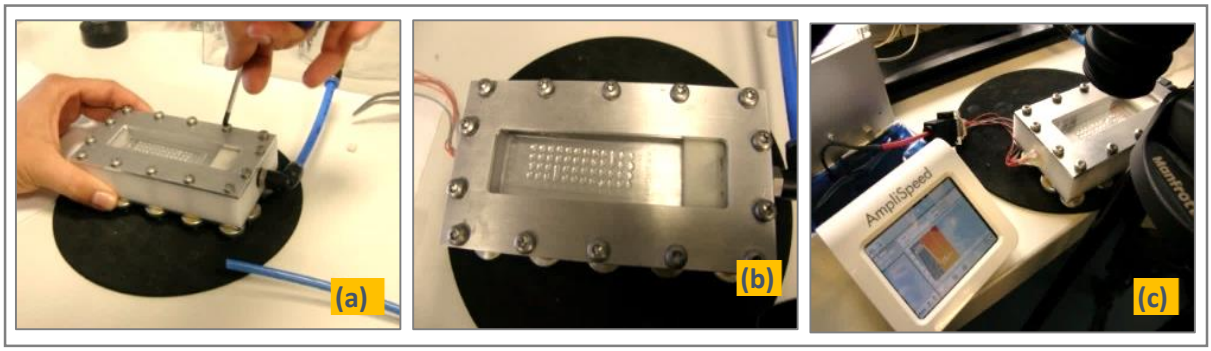

Image 5.7.1: The screws can be opened for transfer of slides (left), slide loaded with liquids carefully placed inside the pressure chamber (right). The pressure chamber attached to ASC via necessary electric connections

Having overall dimensions of approximately 100*80*35 mm (l*b*h), the chambers exterior comprised of aluminum frames- the top frame having a glass (PMMA) window to facilitate easy visualization during the experimental run. Amid the aluminum frames was further sandwiched a polymer inlet with a rectangular down cut for carrying the to be investigated surfaces (AG glass slides). The frames were coupled to this inner polymeric chamber via multiple screws- which could be unfastened for the insertion of the slide into the chamber, and fastened tightly back for an air-tight (no pressure leakage) set-up. While one end of the chamber was connected to the heating cycler (ASC) for temperature control, its other end was attached to a pressure gauge for regulating the pressure (compressed air being used for pressurization of the chamber).

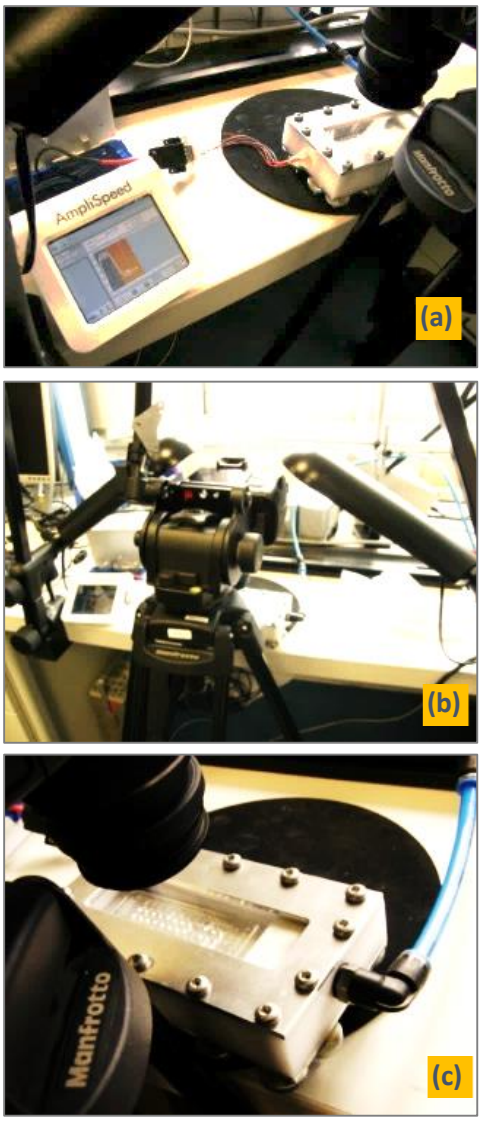

Image 5.7.2: Experimental set-up to study the effect of pressure on bubble evolutions

The system was calibrated by initially placing a dummy slide with PT100 sensors attached to it inside the chamber- all the connections being highly air tight. Numerous calibration experiments revealed that for the set temperature (ASC) of 89.5°C, within 2 minutes of heating, the temperature on the glass slide (within the chamber) was measured to be 95°C.

Next, the dummy slide was taken out and the to be examined surface: clean chemically structured (AG) glass slide with 15 reaction sites pipetted with the bi-liquid droplets in the standard manner. Owing to the rarity of the bubble evolutions otherwise, the surface was marked with artificial nucleation sites (0.5mm laser engraved on the inner hydrophilic region holding water) to study the effect of pressure on the nucleated bubbles. Further, to improve visualization of the inner (water) liquid from the outer one during the experiments, the inner liquid was colored using 0.1% Adva Blue (biocompatible coloring dye). The slide was then placed carefully inside the chamber; the system made highly air-tight and finally ready for investigations.

HD Sony camera backed with a top down Olympus microscope together with proper side lightening was adjusted directly above the pressure chamber (enclosing the slide with the bi-liquid micro-droplets) for HD video recordings- the set-up as can be seen in the image 5.7.2.

For the set temperature of 95°C (on the glass slide), and using parallel stop watch for measuring the corresponding time, the (gauge) pressure inside the chamber was varied between 0-100 kPa, and the effect of pressure on bubble formations studied. HD top down

video recordings were made and later examined via video analyzing software's as windows media player classic and Paint.Net. Minimum of six surfaces were tested in this manner, 15 reaction sites being investigated per slide selected. Additionally, comparative studies were done to determine the effect of pressure on bubble evolutions for the surfaces devoid of any artificial nucleation sites.

Results showed, as anticipated, no bubble evolutions for the surfaces devoid of any artificial nucleation sites. However, for the surfaces having the above imperfections, bubbles were seen evolving for the initial gauge pressure ~0.3 kPa - the bubbles observed shrinking/ collapsing, as the pressure inside the chamber was increased.

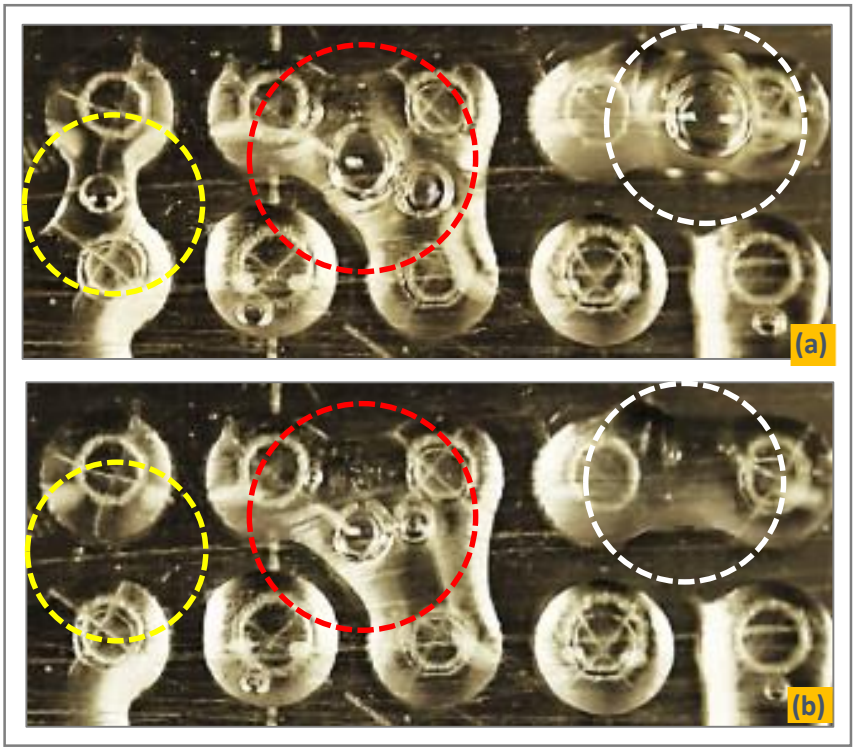

Image5.7.3: (a) Evolved bubbles for pressure=25 kPa, (b) suppression of bubbles when the pressure is raised to 100 kPa

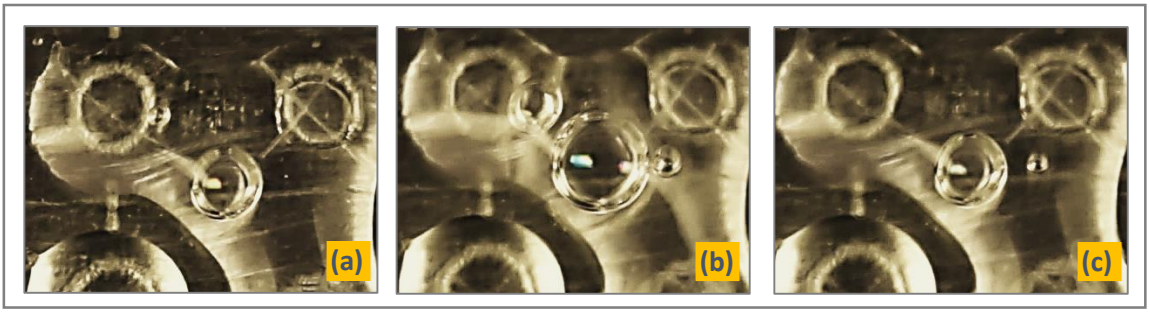

Image 5.7.4: State of bubble at pressure of (a) 100kPa, (b) at 0 kPa, and (c) at 100 kPa again

Bubbles appeared at lower temperatures, whereas shrank at higher temperatures- the minimum pressure at which the bubbles were seen shrinking, observed to be around 77kPa

(0.7bars). Thus, it can be said, that for a constant temperature (95°C), an extra pressure of 77kPa (0.7bars) applied on the system could suppress the evolution of bubbles. Hence, if the system be placed under pressure in a pressure chamber as depicted above, could suppress the occurrence of bubbles, thereby raising the efficiency of the microfluidic systems as dealt with in the current work.

However, though the above method looks highly promising, it could raise the structural complicacy of the overall microfluidic system, in addition to incurring additional costs. This hence calls for the exploration of other methods, as will be discussed next.

5.7.2 Control of bubbles at the growth level: Surfactants

The previous sections dealt with the control or suppression of bubbles at the nucleation or the root level. However, lowering of the system temperature though marks as an effective measure in achieving the above, it cannot be largely implemented to the micro-fluidic systems as dealt with in the current work owing to the ` fixed´ temperature needs of the biological reactions that such systems carried. Similarly, cumbersome experimental requirements as construction of a pressure chambers, ideally not a very cost-effective method, puts limitations as well to the otherwise successful 'decreasing the pressure of the system' attempt.

Another approach that could be however adopted could be checking the evolution of bubbles at the growth level, i.e. at the liquid-liquid interface, in order to prevent or hinder the growth of the bubbles which could not be somehow suppressed at the nucleation level, thereby minimizing big bubble bursts and the eventual undesirable merging of the adjacent droplets- hence improving the overall efficiency of the microfluidic systems.

One promising way of doing so could be by the addition of surfactants (to the concerned liquids); surfactants having the tendency of accumulating at the liquid-liquid interface, quite possibly hampering the growth of the bubbles at this 'vulnerable' region [1,246].

Based on the above, experiments were done by adding 1 vol% of Tween 20 (biocompatible surfactant) to the inner liquid (0.1% Adva blue colored 1µL water) and HD top view video recordings made (experimental set-up as depicted in the image 5.2.16), to investigate the effect of surfactants on bubble growths. As with the previous studies, examinations were made during the 1st stage of PCR cycle, i.e. at 95°C for initial 10 minutes of heating; surfaces (chemically structured AG slides) both devoid of and having artificial nucleation sites (0.5mm diameter laser engraved on inner hydrophilic region) being investigated for comparative studies- minimum of six surfaces tested per case with 15 reaction sites observed per surface.

Results revealed, as anticipated, the probability of bubble evolutions being very low, <1%, for surfaces devoid of any artificial nucleation sites. However, for the rare evolutions that occurred, major bubble activity was seen prominently within the initial 2 minutes of heating - the intensity of bubble formations nevertheless seen fading away with time. Further, multiple small bubbles were seen evolving and aggregating from the affected (exceptional) region, - as can be seen in the snapshots in image 5.7.5 below:

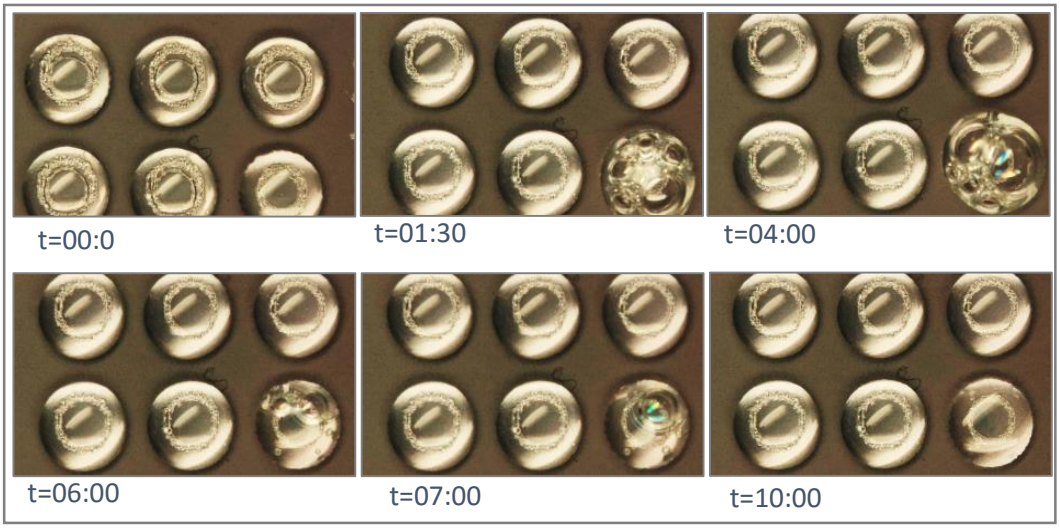

Image 5.7.5: Effect of surfactants, at 95°C, on bubble formations on surfaces devoid of artificial nucleation sites (total recording time -10:00 minutes)

However, similar phenomenon as before observed for surfaces engraved with the artificial nucleation sites- the intensity of bubble evolutions nevertheless for the latter case being much greater, with almost all of the sites being active, as can be seen in the examples cases in the image 5.7.6 below:

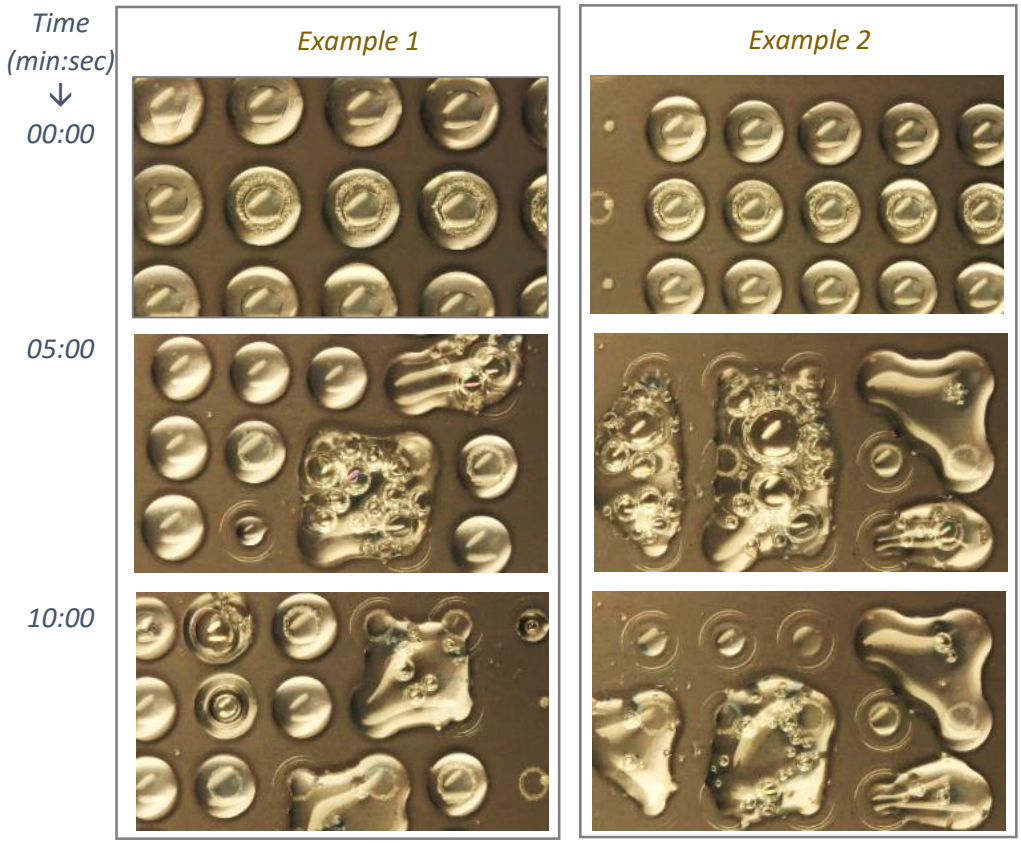

Image 5.7.6: Effect of surfactants, at 95°C, on bubble formations on surfaces with artificial nucleation sites (total measuring time -10:00 minutes)

Further, as expected, experiments revealed reduced intensity of bubble formations at lower system temperatures – multiple, small sized bubbles nevertheless seen appearing from the regions of the surfaces engraved with artificial nucleation sites, and crowding within the system, as can be seen in the snapshots in the image 5.7.7 on the right.

Thus, the addition of surfactants (1 vol % of Tween 20) was observed to have no prominent influence on the suppression of bubbles, thereby making their addition not a very promising measure in checking the growth of the bubbles, especially at the liquid-liquid interface.

However, further studies can be done in this regard where varying concentrations (as 0.1vol%) of Tween 20 and of other surfactants as Tween 80[246] could be added to the micro- droplet system (inner aqueous droplet), and experimental done to determine the effect of varying volume of different surfactants on the growth of the bubbles- the analysis serving as a promising outlook for the further analysis of the phenomenon of bubble evolution in the micro-fluidic system, as for the one under consideration.

Image 5.7.7: Effect of surfactants on bubble evolutions on surfaces engraved with artificial nucleation sites at 78.5°C (total measuring time-10:00 minutes)

5.7.3 Control of bubbles (their aftermath) at the merge level

For the bubbles, which somehow could not be filtered at the nucleation and the growth checks, the final policing was done at the merge level, in an attempt to prevent coalescence of the adjacent droplets due to big bubble bursts at elevated system temperatures, and thereby enhancing the efficiency of the overall microfluidic systems, as dealt with in the current work.

One approach that could be adopted in this regard could be by physically confining the individual droplets into isolated chambers, i.e. by positioning say a slotted plastic frame directly above and in alignment to the reactions sites on a chemically structured surface (AG glass slides), as can be seen in the image 5.7.8 on the next page.

However, for research oriented applications, on similar lines, PDMS frames could be employed, owing to the temperature resistance properties of the material, ease of preparation and low fabrication costs[278]. Experiments were done by placing the above frames on 10 randomly selected chemically structured glass slides (with laser engraved artificial nucleation sites of 0.5mm diameter in the middle of the reaction spot), to determine if they captured the merging of the adjacent droplets at high system temperatures. Naked eye observations revealed successful arrest of the merging phenomenon, thereby proving the effectiveness of the above approach in improving provisionally the efficacy of such microfluidic systems. However, owing to the 'superficial' and rudimentary nature of the above approach, more sophisticated methods were called for, as the 'virtual' compartmentalization the reaction sites using the concept of superhydrophobicity, as discussed next.

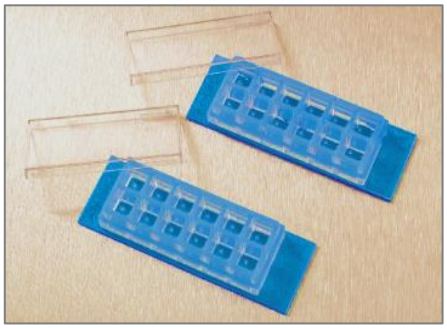

Image 5.7.8: Compartmentalized plastic frame(s) (from a biological lab) which could be placed directly above the slide surface, physically isolating the reaction sites into individual chambers[57]

Superhydrophobicity [193,196,275]

Normally speaking, a superhydrophobic surface can be said to be a surface highly hydrophobic in nature, i.e. exceptionally difficult to wet. Such surfaces have been known to exhibit extremely high CA's-values being reported to even exceed 150° for some of the cases[276-277]. The remarkably high contact angles can be explained by the Wenzel and Cassie-Baxter laws[193,196], as previously stated in dynamic CA studies, according to which, the presence of surface rigidities could alter the contact angles by increasing the hydrophobic or hydrophilic character of the respective surfaces.

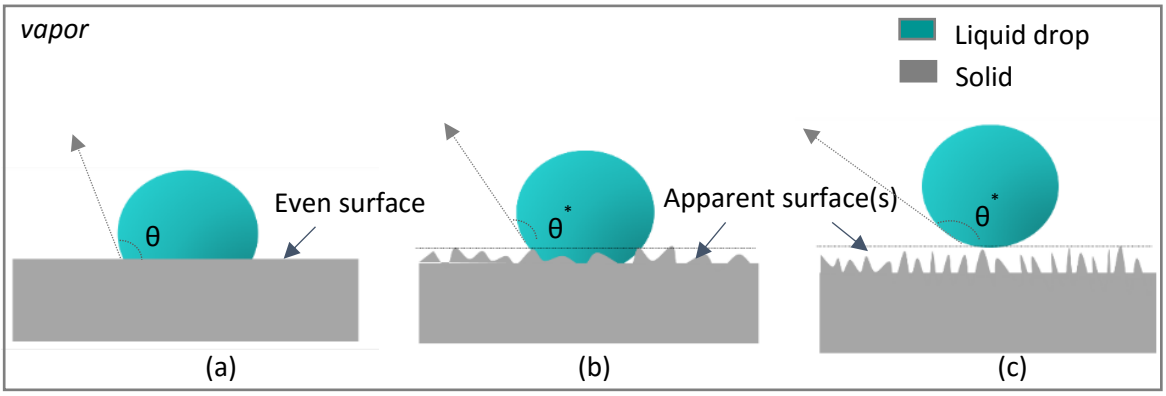

Figure 5.7.1: A liquid drop resting on (a) smooth surface with CA 'θ', (b) little rough surface (apparent surface) (Wenzel wetting state) with an apparent CA 'θ ', (c) highly rough surface (apparent surface again) (Cassie-Baxter wetting state) with an apparent CA 'θ*'*

Typically, the basic wetting state of droplets on a rough substrate can be said to be either in the Wenzel's[193] or in the Cassie-Baxter's[193,196] regime- the liquid following the surface corrugations for the former case (refer figure 5.7.1 b), whereas the liquids droplet being attached to the surface but in a position on top of the corrugations thereby allowing air pockets to be trapped under it, for the latter case (refer figure 5.7.1 c).

Mathematically (implicitly assuming the size of the roughness to be small enough such that the liquid molecules can be taken to macroscopically interact with the plane surface but microscopically with the rough surface), Wenzel law incorporated the surface roughness and modified the Young-Laplace equation as [193]:

$$\cos\theta^{*}=r\cos\theta \tag{5.7.1}$$

where, `θ´ is the intrinsic contact angle, `θ*´ the apparent CA, and 'r' the surface roughness. Taking into account r >1, the above relation attains the form:

$$|\cos\theta^{*}| > |\cos\theta| \tag{5.7.2}$$

Hence, for θ > 90° (hydrophobic contact), $\theta^{*}>\theta$, thereby increasing the hydrophobic nature of the contact due to the presence of surface roughness, whereas for θ< 90° (hydrophilic contact), $\theta^{*}<\theta$, implying enhanced hydrophilic nature of the contact. Thus, the presence of surface roughnesses can be said to enhance the wetting character of the underlying surface. Nevertheless, the surface roughnesses talked about are in the micro scale, very small compared to that of the size of the droplet, which if not, would make it difficult to achieve an axi-symmetrical and stable drop with a unique CA[193].

The Cassie-Baxter law[193,196], on the other hand, relates the intrinsic CA, the apparent CA and the topography of the roughness structure as:

$$\text{Cos}\,\theta^{*}= -1 +(1+\cos\theta)\, f \tag{5. 7. 3}$$

`f´ being the area fraction of the wet part of the solid. As f→0, θ→ 180°, indicating the role of surface rugosities in increasing the contact angle of the underlying surface.

Though both the Wenzel and the Cassie–Baxter relations have classically been used to characterize the apparent CA's with remarkable success, it has been nevertheless reported that wetting in the Cassie-Baxter's state rather than in the Wenzel state is generally a requirement for achieving superhydrophobicity[15,196].

Experimental Investigations

Based on the above, experiments were conducted by creating superhydrophobic 'virtual confinements' outside the bi-liquid micro droplet system, and observations, both naked eye and top down (for set-up refer image 5.2.16), made to determine their role in suppressing the merging of the adjacent droplets at elevated temperatures (95°C). Two types of compartmentalization were tried, as discussed in the following sub-sections:

Generation of superhydrophobic rings

The initial attempt that was made was by fabricating superhydrophobic ring outside the bi-liquid droplet system, as depicted for a chemically structured surface (AG glass slide) in the figure 5.7.2 below:

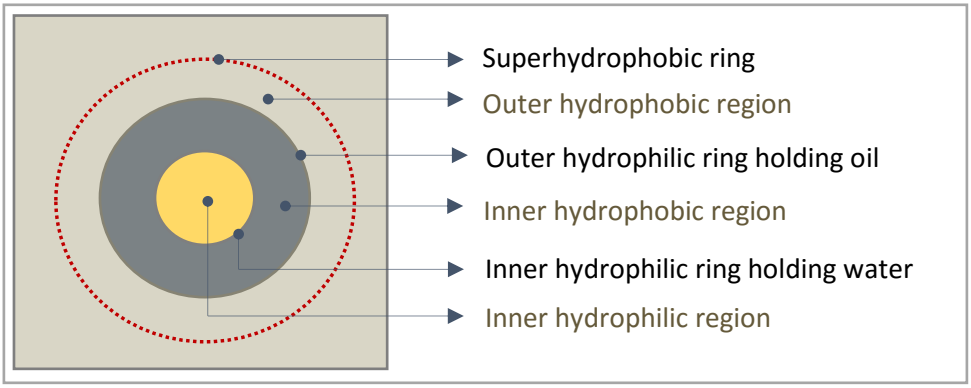

Figure 5.7.2: Pictorial representation of a superhydrophobic ring outside a reaction site on a chemically structured slide surface

As per Wenzel and Cassie-Baxter laws, superhydrophobicity in the above case was achieved by first roughening of the desired regions and then hydrophobic coating of the same. Rings of 4± 01.mm (distance measured from the center of a reaction site) were laser engraved (laser power=100, and laser velocity=10) outside the outer hydrophilic rings holding oil; the surfaces being cleaned (mild initial cleaning instead of the standard 1st cleaning as not effect much the surface roughness) and hydrophobically coated using the standard production steps as detailed in chapter 2. The surfaces were then dispensed with the customary bi-liquid system and placed on the ASC – naked eye and top down video recordings made at 95°C (10 minutes from the start of heating) to study the role of 'superhydroophic' rings in suppressing merging of the adjacent droplets after bubble bursts. Minimum of 10 slides were investigated per case, with them having artificial nucleation sites (laser engraved of 0.5mm diameters) in the middle of the inner hydrophilic ring. Comparisons were further made for surfaces without these outer 'superhydrophobic' ring like regions.

Results revealed that the superhydrophobic rings were a success in case of small bubble bursts (smaller bubbles having less liquid vapor comprising them), subduing 'moving out' of the liquid droplets by pinning their movement. However, for big bursts (big bubbles growing rapidly at the liquid-liquid interface where primarily water-vapor is feeding them via diffusion, till their surface tension is poked by lower temperature surroundings), leading to the dropout of the liquids, the strong 'spilling' and cohesive forces among the adjacent liquid droplets, were seen overpowering the 'pinning' forces provided by the superhydrophobic confinements. Additionally, not much difference was observed for surfaces without the above structures-especially for surfaces with artificial nucleation sites.

Hence from the above it can be concluded that the creation of outer superhydrophobic ring like structures was not a very successful attempt in largely suppressing the phenomenon of merging of the adjacent droplets. On similar lines, another approach that was tried out was by fabricating the entire region outside the reaction sites superhydrophobic in nature, as detailed next.

Generation of superhydrophobic regions

In the second attempt, to prevent merging of the adjacent droplets owing to big bubble bursts, instead of super hydrophobic rings, the entire region(s) outside the bi-liquids (reaction sites on chemically structured surfaces) were fabricated superhydrophobic.

Using the basic fabrication technique as before, the to be investigated regions were first laser engraved (laser power=100, laser velocity=10) and then hydrophobically coated – both mechanical and chemical coating techniques being tested to determine the degree of superhydrophicity generated.

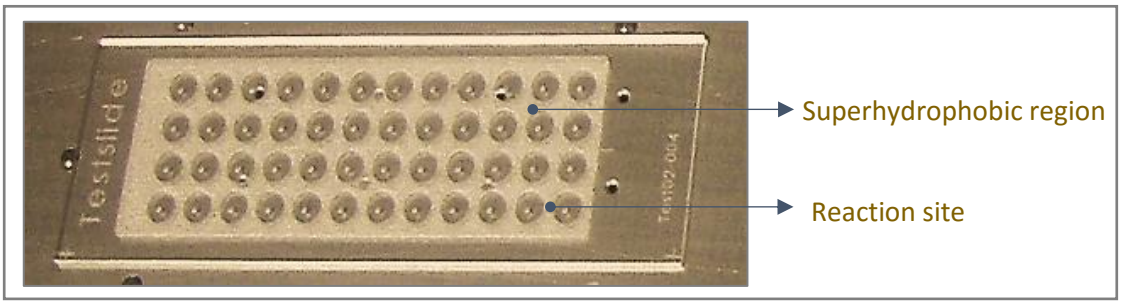

Image 5.7.9: Superhydrophobic region outside reaction sites on a chemically structured glass slide (with artificial nucleation sites in the middle of the reaction site)

Quick static and dynamic CA measurements made to determine the degree of superhydrophobicity associated with the fabricated regions, revealed:

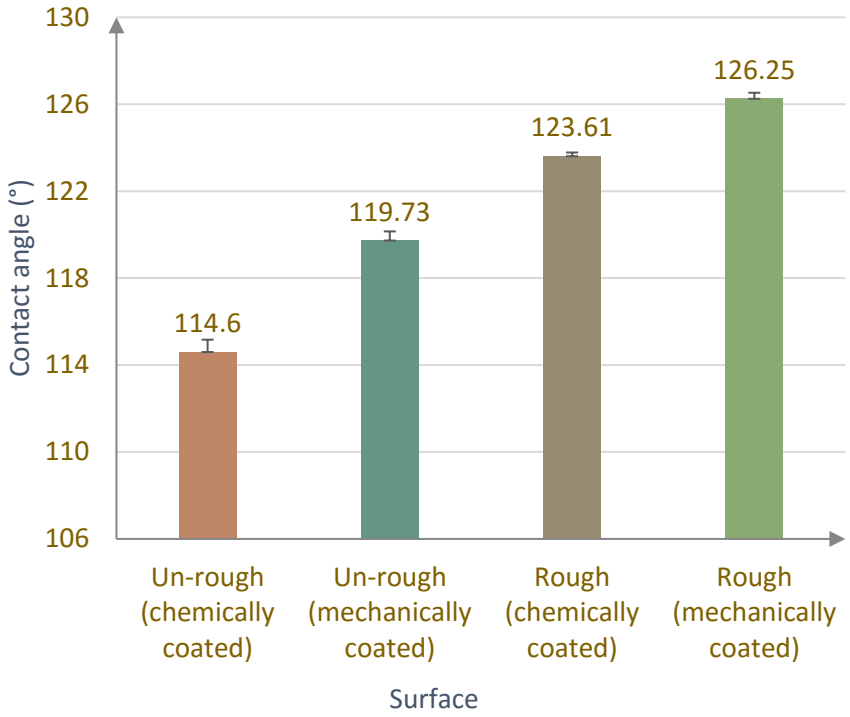

Graph 5.7.1: Comparison of static CA's (for 1µL of DI water) on un-roughened and roughened (laser engraved) surfaces -both mechanically and chemically (hydrophobically) coated

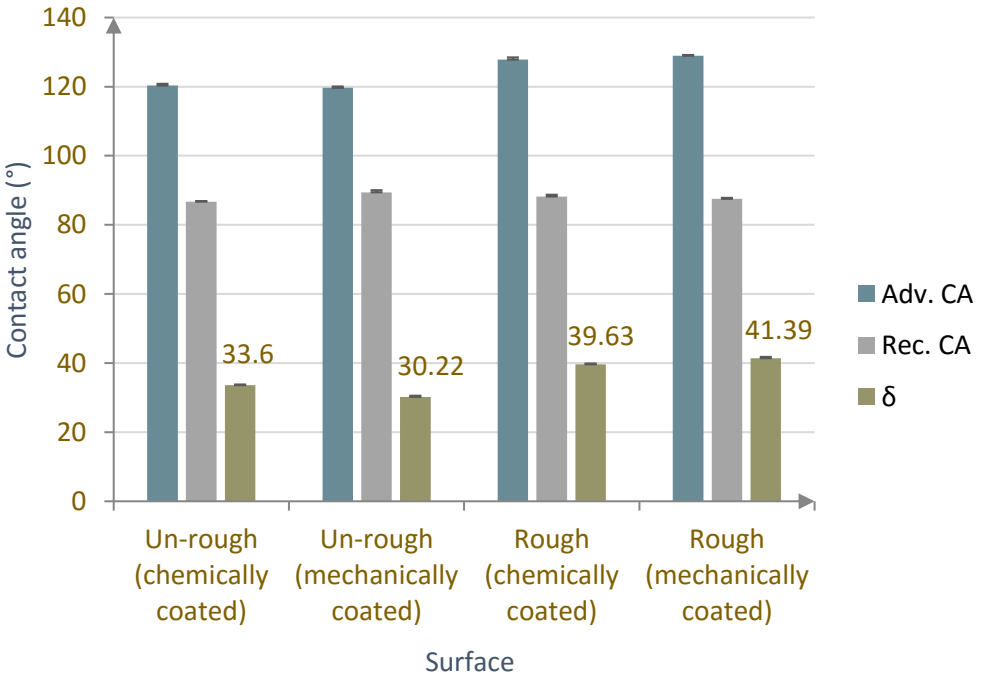

Graph 5.7.2: Comparison of dynamic CA's (measured using 1µL DI water) on (laser engraved) un-roughened and roughened surfaces -both mechanically and chemically (hydrophobically) coated

As can be seen in the graphs 5.7.1 and 5.7.2, surfaces roughened and then hydrophobically coated, particularly mechanically coated, yielded higher static CA values (~126°) and a comparatively higher dynamic CA hysteresis (~41°). This hence indicated the enhanced hydrophobic character owing to surface roughness (possibly effective in pinning the droplets motion, say while merging) associated with the fabricated regions.

Next, experiments, naked eye and HD top down video recording (refer image 5.2.16) were conducted to determine the effectiveness of the generated superhydrophobic areas in pacifying the phenomena of droplet merge at elevated temperatures (~95°C); minimum of 10 slides (chemically structured), engraved with 0.5mm (diameter) artificial nucleation sites (middle of reaction sites) being investigated per case. Additionally, relative analysis was made for surfaces without such 'virtually' confined regions.

Results revealed, no prominent suppression of the merging phenomenon by the outer 'superhydrophobic' regions, especially for huge bubble bursts leading to drop out of the liquids most likely making them spill over and merge with the adjacent droplet. As stated for the previous case, one reason to the above could be the strong cohesive forces among the liquids (adjacent droplets) initiated by big bubble bursts (sample dropouts), overpowering the pinning and superhydrophobicity provided by the fabricated surfaces.

5.7.4. Summary

Hence, from the various experiments conducted in order to eliminate/supress bubbles in the microfluidic system as dealt with in the current work, it can be summarized that a decrease in temperature or increase in pressure of the system could largely supress the bubbles at the nucleation level- bubbles not seen evolving below temperatures of 77°C (even in the presence of surface inhomogeneities/artificial nucleation sites) or when pressure of nearly 0.7 bars is applied on the system.

However, the addition of surfactants could not to a great extent control the growth of bubbles at the liquid-liquid(water-oil) interface- a crowd of multiple bubbles seen accumulating at the above interface in the presence of surfactants within the micro -droplet system.

Further, though the surfaces (generated via hydrophobic coating of the laser roughened regions) exhibited high static CA's (~126°) and a high dynamic CA hysteresis (~41°), the surfaces (or rings) exterior to the micro-drops proved not to be 'superhydrophobic' enough to prevent the merging of the adjacent droplets, especially when huge bubble bursts were encountered within the host system.

The above hence calls for more sophisticated and advanced methods say in terms of checking the growth of bubbles at the liquid-liquid interface and/or generating surfaces with much higher degrees of superhydrophobicity, as will be discussed in chapter 7 providing an outlook to the current work.

5.8 Final Conclusions

From the various aspects of bubble dynamics covered, and the many methods proposed in the control/elimination of the bubbles in the microfluidic system as under consideration, it can hence be overall concluded:

- The solid-liquid interface (surface inhomogeneities trapping gas after the liquid (s) have been pipetted atop them), among the multiple interfaces present in the dealt with microfluidic system, serves as the potential source of bubble nucleation. Nucleation studies further revealed micro sites having aspect ratios of 1:1 and 4:5 being the most vulnerable candidates in this regard- calling for the surfaces having inhomogeneities of the above dimensions to be discarded to minimize bubble evolutions in the host systems.
- Bubble growths were observed to be slower in oil than in water, possibly attributed to the high viscosity of the former liquid (exerting greater frictional/drag force on the bubble) than the latter. Further, growth rate studies filtered the liquid-liquid interface to be the susceptible region where rapid bubble growths take place- bubbles growing instantaneously to ample diameters as and when they approached the above interface. The most likely explanation to the above could be the strong Marangoni convection taking place at the liquid-liquid interface, causing local heat gradients at this region, in turn leading to rapid conversion of water into its vapor- feeding the bubbles instantaneously (via diffusion) when in the vicinity of the above interface. However, the above being just a hypothesis, though a very promising one, calls for additional experimental and/or numerical analysis/mathematical modelling to comprehend the growth of bubbles at the liquid-liquid interfaces at elevated temperatures within the microfluidic systems.
- Further, on similar lines as the above, it can be said that the major content of especially the bubbles which grow to sufficient diameters (at the liquid-liquid interface) is water-vapor, even though air being the initial constituent of the small sized (say trapped in surface inhomogeneities) bubbles.
- Bubbles growing to sufficient diameters burst with a high probability of spilling the liquids (especially the inner aqueous solution), such that for high burst velocities and if in the process of rupture, the interactions between the neighboring liquid drops overcome the surface (hydrophobic) forces separating them, the droplets merge. However, detailed analysis on the criterion for bubble merge, and study of droplet coalescence on the hydrophobic coated and chemically stratified surfaces, that too at elevated system temperatures, needs further attention, serving as a promising outlook in this regard.
- Besides opting surfaces as clean and inclusion free as possible, well-calibrated heating cyclers with homogenous heating plates, and highly degassed, accurately pipetted/loaded liquid system, studies revealed that placing the microfluidic system in say a pressure chamber, for minimum pressures of ~0.7 bars, could largely suppress

the nucleation of bubbles (from a gas trapping nucleation site). However, attempts made to suppress the growth of bubbles at the liquid-liquid interface, by addition of surfactants (Tween20) to the liquid system, yielded not very successful results, requiring hence further analysis in this regard. Also, though in order to suppress the merging of the adjacent droplets, roughened exterior (to the droplets) surfaces yielded high static CA's and corresponding dynamic CA hysteresis, the attempt served not very effective in preventing the merging of the adjacent droplets calling for more advanced surface coating techniques in this regard.

CHAPTER 6

EPILOGUE

From the various investigations done in comprehending the microfluidic system as under consideration and the phenomenon of bubble dynamics in it, it can be hence concluded that though the system is nearly flawless in its design and operation, it might yet encompass rare inhomogeneities, possibly leading to the formation of bubbles at elevated system temperatures. Though characterization of the heating platform and the bi-liquid micro-droplet system revealed no prominent imperfections /inhomogeneities, some infrequent crater like micro-structures (from microscopic investigations) were nevertheless found, primarily on the hydrophobic regions, of the chemically structured reaction slide- potentially serving as sites for bubble nucleations at elevated system temperatures. Further, the occurrence of such, again rare, defects on the hydrophobic regions of the corresponding surfaces, pointed to some missed out coating/cleaning procedures- though no exact production stage responsible for the above could be filtered out in the various microscopic and contact angle investigations conducted to characterize the dealt with surfaces.

However, various contact angle and surface tension studies successfully helped in determining the behaviour of single-liquid and bi-liquid systems, both at RT and as a function of temperature. PIV analysis, in addition, aided in estimating the flows associated within the liquids- both with and without the presence of a bubble.

Besides, various nucleation studies successfully ruled out the solid-liquid interface as the potential region responsible for bubble nucleation (in analogy with the heterogeneous and crevice model of bubble nucleations)- surface inhomogeneities trapping gas after the liquids

have been pipetted atop, provided the conditions of gas entrapment get fulfilled. Moreover, the nucleation studies revealed micro-sites with aspects ratios of 1:1 and 4:5 to be most likely candidates trapping gas – the analysis in turn calling for surfaces having imperfections of the above dimensions to be reconsidered, in order to minimize the evolution of bubbles in the associated microfluidic systems.

The growth rate studies, on the other hand, indicated the liquid-liquid interface to be the most vulnerable region where rapid bubble growths take place- such a behaviour possibly being attributed to the rapid conversion of water into its vapor at the water-oil interface (Marangoni convection/Thermo-capillary convection), feeding the bubbles primarily via diffusion. However, the above explanation, at this stage, is just a hypothesis, though a very promising one- requiring detailed experimental and/or numerical analysis/mathematical modeling for its further understanding. Additionally, growth rate studies revealed slower growth rates for the nucleated bubbles in oil than in water- the phenomenon potentially attributed to the higher viscosity of oil, exerting greater drag/frictional force on the bubble.

Various measures undertaken to suppress/eliminate the occurrence of bubbles in the microfluidic system, as for the under consideration, revealed that the bubbles get largely suppressed when the system is placed under a pressure of 0.7 bars (in a pressure chamber). Further, experiments showed that no bubbles evolve below temperatures of ~77°C (even in the presence of artificial nucleation sites on the underlying surfaces) – however, owing to the fixed temperature needs of the biological reactions (as the PCR), the latter method could not be largely implemented to control bubble evolutions in the dealt with microfluidic system. Further, though attempts were made to suppress the growth of bubbles by the addition of surfactants to the bi-liquids, and to prevent the merging of adjacent droplets (as a consequence of huge bubble bursts) by generating superhydrophobic regions/surfaces outside the micro-drops, the measures proved not highly successful in achieving what was desired- thereby calling for more advanced/sophisticated procedures in this regard.

CHAPTER 7

OUTLOOK

Though the work successfully helped in comprehending the dealt with micro-fluidic system and the various aspects of bubble dynamics for the evolved bubble in it, still many facets remained unexplored-opening ways for numerous possibilities that could be tried out not only for the betterment of such systems from an industrial perspective, but as well as pushing the envelope of academic research, in the field of microfluidics on the whole.

For instance, though the temperature dependence of contact angle studies helped gain a better insight into how the micro-fluidic system behaves as a function of temperature, interesting would be to investigate how the hydrophobicity and the hydrophilicity of the underlying substrate alters with an increase in the system's temperature, and how that would affect the profile of polar (as water) and non-polar (as oils) liquid micro-drops sitting on it.

Further, though the nucleation studies successfully confirmed the various existing models of bubble nucleation and helped in establishing the solid-liquid interface (surface inhomogeneities with the liquids atop them nucleating bubbles if the conditions of gas entrapment are fulfilled) to be majorly contributing to nucleation of bubbles, the fabricated sites, could not, however, entirely mimic the geometry of crater like (rare) surface inhomogeneities, found otherwise on the flawed regions of the slide surfaces- the latter having peak like protrusions at their edges in addition to a definite diameter and depth. This hence calls for the study of surface imperfections with peaks (of say varying heights) in the nucleation of bubbles –where structures of varying depths and heights fabricated using sophisticated micro/nano fabrication techniques as advanced lithography (Nanosphere lithography)[285-286] and RIE/DRIE [282-284], independently or coupled with each other, could be utilized.

Consequently, though the characterization of the bi-liquid system successfully explained the behaviour of the micro-droplets, both at ambient and at elevated temperatures, how and if it all would influence bubble dynamics for the rare bubbles that evolved remained nevertheless unresolved- paving thus a way for further research in this regard.

Additionally, some researchers reported the diamond shaped or rhombohedral chamber based reaction sites to be superior as compared to the typical circular chamber design in preventing the bubble formation[33], thereby calling for the study of different geometries of the reaction sites and their roles in the bubble evolution phenomenon.

Addition of temperature sensitive biocompatible dyes or beads[287-292] to determine the exact temperatures at different locations within the liquids, especially at the liquid-liquid interface- both without and in the presence of a bubble, further serves as a promising outlook for the detailed investigation of the micro-fluidic system and of bubble dynamics in the same.

Further, though the addition of surfactants (1 vol% Tween 20) did not prove to be a very successful measure in supressing the growth of bubbles at the liquid-liquid interface, other varying concentrations of equivalent biocompatible surfactants (say 0.1 and 1 vol% of Tween 80)[246] could be tested on similar lines.

Also, more sophisticated methods as electrospinning methods[293-295], wet chemical reaction[295-297], self-assembly and layer-by-layer methods[298-299], etc., can be employed in an attempt to generate highly super hydrophobic surfaces (outside the reaction drops), and such regions be tested for their effectiveness in preventing merging of the adjacent droplets due to big bubble bursts. Besides, the phenomenon of droplet merge i.e. coalescence of adjacent drops on hydrophobically coated and chemically structured surfaces, as a function of temperature, seek further investigations, that could be attempted to comprehend further the behaviour of bubbles in the microfluidic systems, as for the one dealt with in the current work.

Moreover, techniques as gas phase chromatography[306] and /or advanced acoustic and optical techniques[307] could be possibly employed to determine the exact content of bubbles – at the initial and final growth stages, and hence to decide if it's really water vapour that is feeding the bubbles at the liquid-liquid interface (Marangoni convection), thereby helping obtain a deeper insight into the dynamics of bubbles in such microfluidic systems.

Last but not the least, mathematical modelling and /or numerical simulations (computational fluid dynamics) could be attempted to further comprehend the behaviour of the micro-droplet system and the occurrence of bubbles in the same.

APPENDICES

Appendix A

Study of dependence of volume of the outer liquid (oil) on the contact angle of the inner (water) drop

For the study of the behaviour of bi-liquid micro droplet system, as for the one dealt with in the current work, an important investigation was measuring the (static) CA's of the inner (usually water) droplet(s) when beneath the outer (usually oil) liquid However, for such measurements, for the clear visualization of the inner droplets profile, it was required to place the droplet duo in a glass cuvette (referred to as the aquarium technique)- the assembly next sited on the sample stage of the CA measuring device. Further, initial experiments revealed that the standard volume of the outer oil cover, i.e. 5µL, was not sufficient enough to distinctly reveal the silhouette of the inner, usually 1µL of the water droplet, and that usually much greater volumes (minimum 900µL's) of the outer liquid needed to be dispensed in achieving the same. However, greater volumes of the outer liquid might exert additional pressure on the inner drop, probably altering its profile and hence its CA. In order to hence determine the above, experimental investigations were conducted in which varying volumes of the outer liquid (sealing solution) were pipetted above the inner liquid (1µL DI water) and its effect on the profile of the inner liquid studied by calculating the corresponding CA's (of the inner liquid). Minimum of six measurements (CA of inner drop) were made per case (volume of the outer liquid selected)- studies being made for both chemically non-structured and structured surfaces. Results revealed:

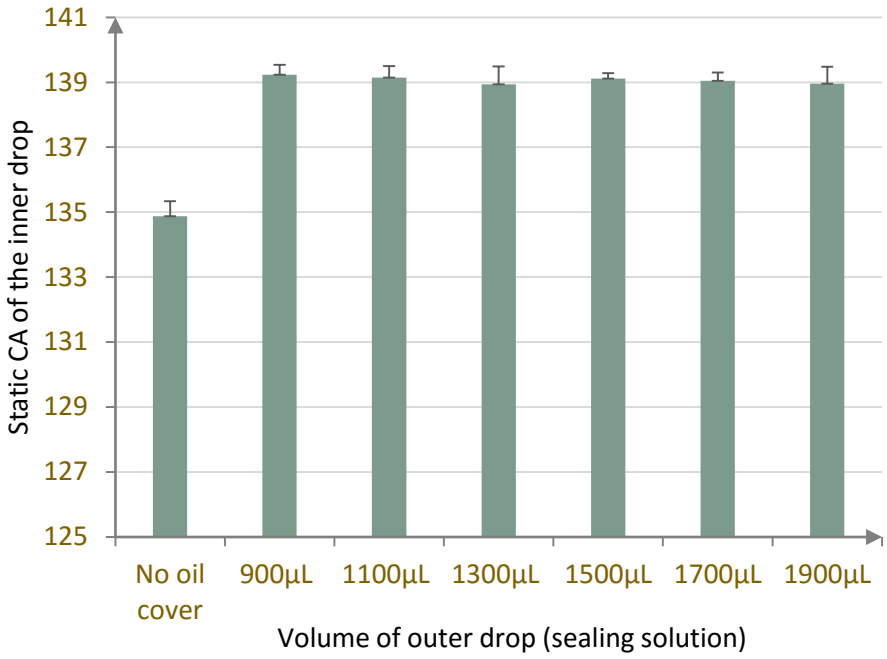

Graph A.1: Static CA of the inner liquid (1µL DI water) as function of volume of the outer liquid (sealing solution)-on chemically non-structured surfaces (PFS slides)

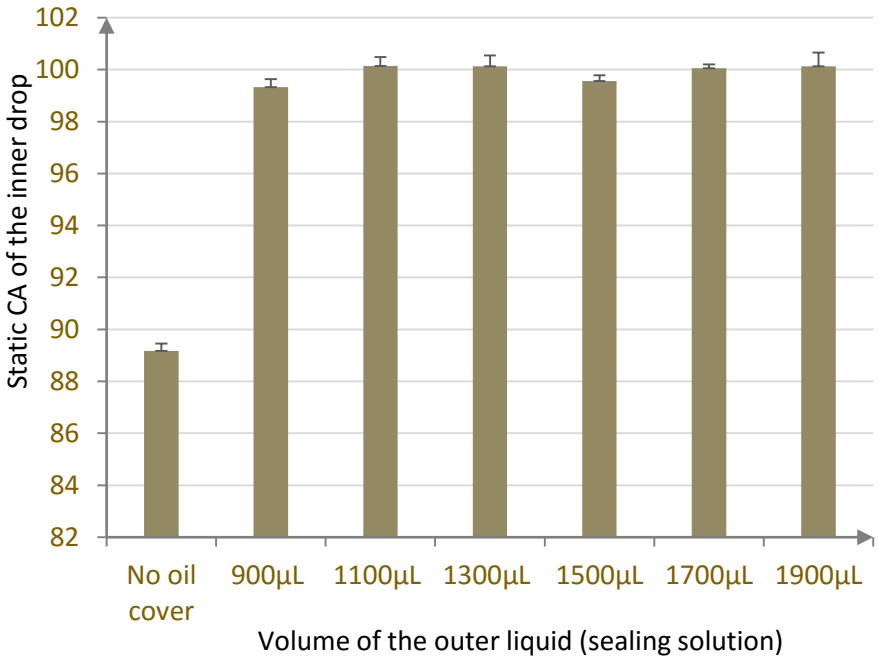

Graph A.2: Static CA of the inner liquid (1µL DI water) as function of volume of the outer liquid (sealing solution)- on chemically non-structured surfaces (reaction sites of AG slides)

As can be seen, the contact angle of the inner liquid (1µL water drop) increases when the outer liquid (oil) is pipetted above it –the value being around 25° for chemically non-

structured (PFS glass slides) surfaces and around 12° for chemically structured (AG glass slides) surfaces- the behaviour possibly attributed to the greater liquid-liquid (like molecules) interactions than the liquid-air (unlike molecules) interactions; non-structuring of the surfaces giving more room to the droplets to freely interact with each other.

Further, experiments revealed that minimum volumes of 900 μL's of the sealing solution were to be pipetted above the inner droplet to enable its profile be clearly visible in the OCA measuring window. Beyond this, as can be seen in the graphs above, the contact angle of the inner droplet was found to be independent of the height of the outer liquid pipetted – similar behaviour being observed for the liquids dispensed on both chemically structured and non-structured surfaces- thus overall pointing towards the effectiveness of the aquarium technique for bi-liquid static contact angle measurements.

Appendix B

Temperature dependence studies of density and viscosity for outer liquid (Sealing solution)*

B.1: Temperature dependence of density for Sealing solution

Literature reports decrease in density of the liquids with an increase in temperature [301-303]. However, for sealing solution, being a mixture of several oils, its density as a function of temperature was determined using Anton Paar[304] viscometer, capable of measuring density, dynamic viscosity and kinematic viscosity in a single measuring cycle on a sample volume.

Data analysis revealed, decrease in density of the sealing solution with temperature, as can be referred to in the graph B.1 below:

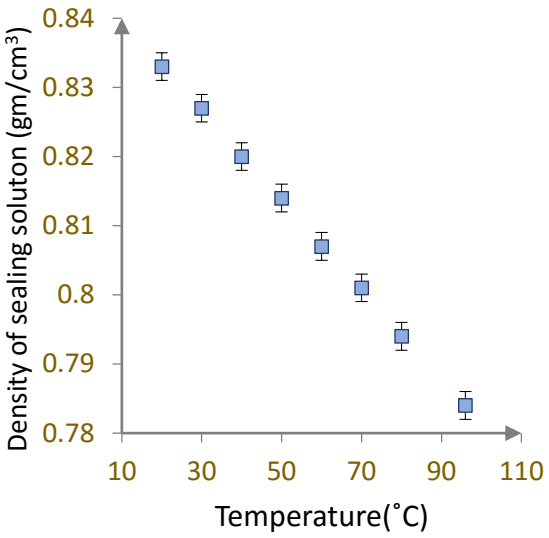

Graph B.1: Variation of density of sealing solution with temperature

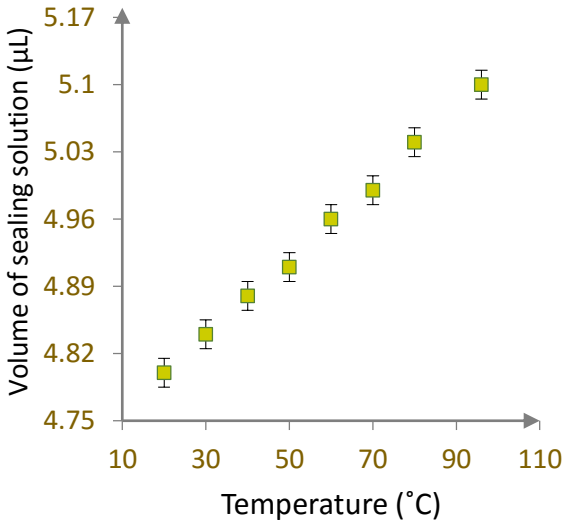

Graph B.2: Variation of volume of sealing solution with temperature

Keeping mass constant (~$4*10^{-3}$ gm), the corresponding relation between the volume (of the sealing solution) and the temperature was estimated to almost linear, as can be seen in the graph B.2 above.

* *Measurements Courtesy: Dr. Heiko Habermüller*

Temperature dependence of dynamic viscosity: sealing solution[†]

Literature reports that the shear (or bulk) viscosity of liquids decreases with temperature, as with an increase of temperature, the time of interaction between the neighbouring liquid molecules decreases owing to the increased velocities of the individual molecules. This, macroscopically, leads to a decrease in the intermolecular forces and thus the bulk(shear) viscosity[300-303]. However, the actual process can be quite complex and is typically represented by simplified mathematical or empirical models.

For water, for instance, it has been reported that its dynamic (absolute) viscosity decreases from 1.002 (Ns/m^2) $*10^3$ at 20°C to 0.315 (Ns/m^2) $*10^3$ at 90°C, and the corresponding kinematic viscosity from 1.004 (m^2/s) $*10^{-6}$ at 20°C to 0.326 (m^2/s) $*10^{-6}$ at 90°C [300-303,305].

Again, sealing solution being a mixture of several oils, the study of its viscosity with temperature was done using Anton Paar Viscometer; the results as depicted in the graph B.3.

As can be seen, the dynamic viscosity of the sealing solution decreases with temperature- in analogy with the behaviour as expected and reported for most of the liquids.

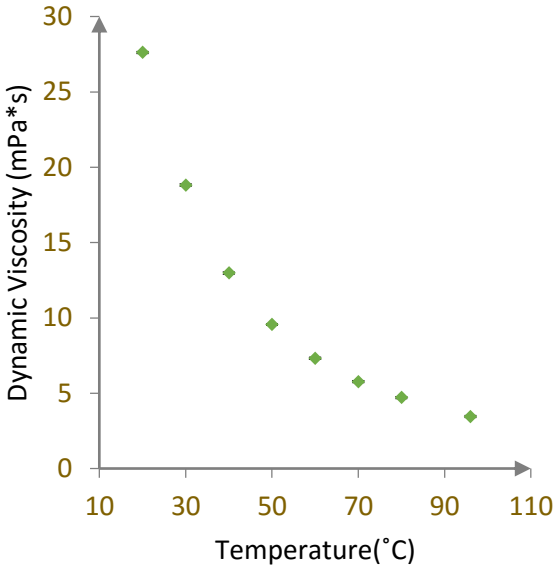

Graph B.3: Temperature dependence of dynamic viscosity for sealing solution

[†] *Measurements courtesy: Dr. Heiko Habermüller*

Appendix C

Dynamic CA measurements: Selection of Needle (diameter)

As the (tip of the) needle stays within the drop during dynamic contact angle measurements, literature reports that for accurate measurements the needle selected should not be too big in diameter [194,197 279], which might disrupt the shape of the droplets, causing false analysis. In order to verify this experimentally, dynamic contact angles were measured using needles of varying internal diameters (as 0.21mm and 0.51 mm), for different solid-liquid combinations selected.

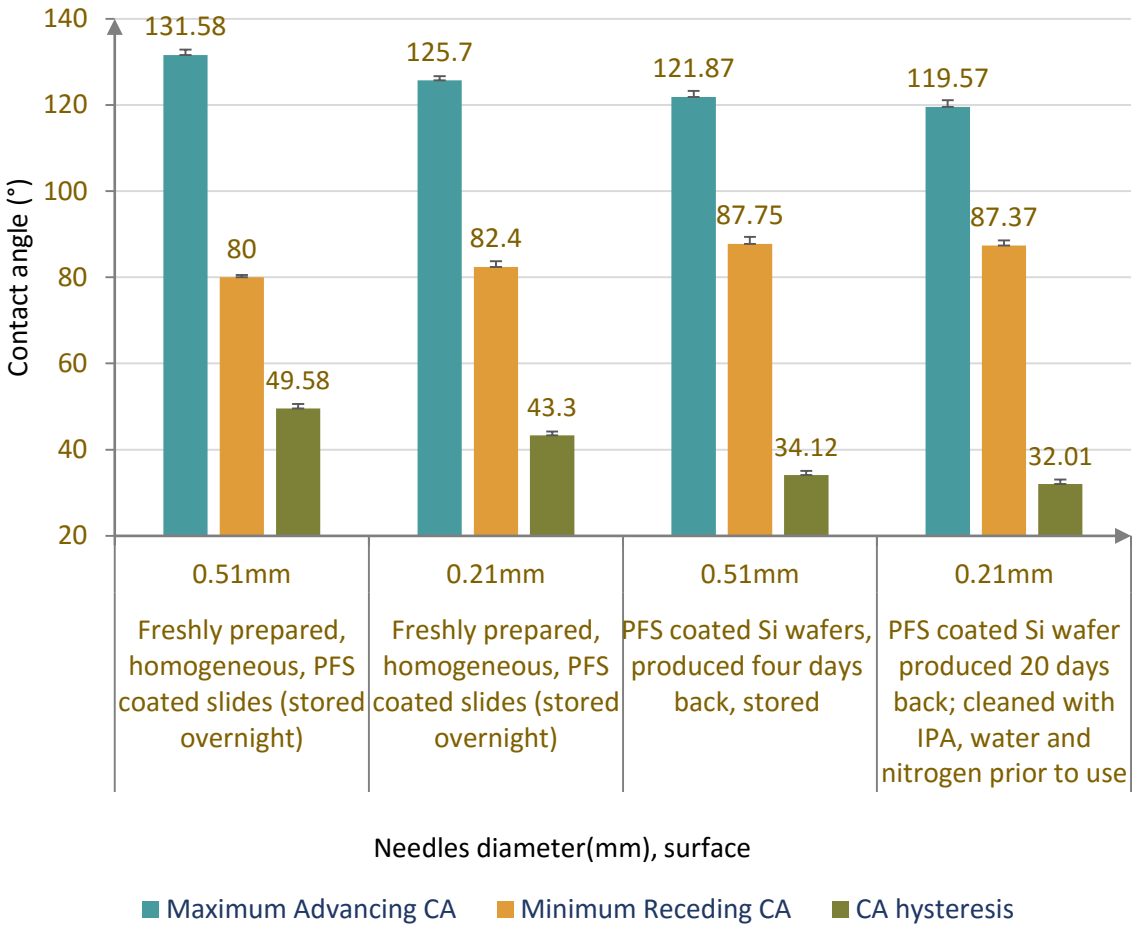

Graph C.1: Dynamic CA studies on various surfaces using dispensing needles of different diameters

Minimum of six measurements being made per case, and the data analysed using Microsoft Excel 2016, results revealed that needles with lower diameters yielded consistent and reliable dynamic contact angle values as compared to when needles with higher diameters were opted- as can be seen in the graph C.1 – thus making the needles with lower diameters preferred choice for dependable dynamic contact angle measurements.

Appendix D

Evaluation of best fitting method for static CA studies

In order to determine the method that best fits the drops profile for static CA measurements, experimental investigations were made by fitting the drops profile using various fitting methods available- primarily tested being the commonly used Y-L fitting method, Elliptical fitting, Circular fitting method and the Tangent fitting method[194,197]. Analysis was made by employing different solid-liquid combinations: chemically structured and non-structured surfaces dispensed with various test liquids as water, di-iodo-methane (DIM), and sealing solution, in the volumetric ranges of 1-5µL´s.

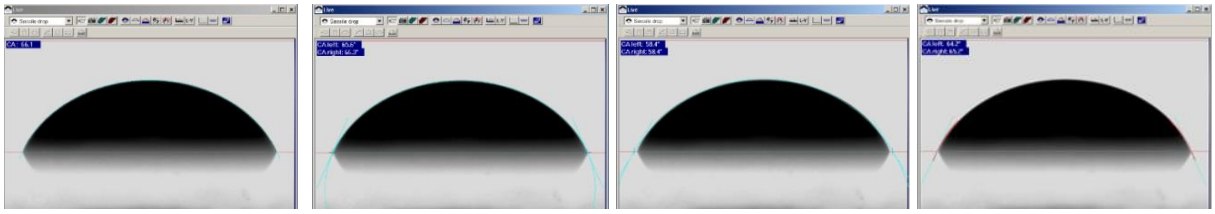

(a) L-Y fitting (b) Elliptical fitting (c) Circular fitting (d) Tangent fitting

Image D.1: Measurement of static CA from drop's profile using various fitting methods. (for ~5µL of sealing solution dispensed on the outer hydrophilic ring of the chemically structured AG slide surfaces)

With minimum of six studies being made per case, studies revealed that for around 5µL of sealing solution, suspended on the outer hydrophilic ring of the chemically structured surfaces, both Y-L and elliptical fitting methods yielded reliable and consistent static contact angle values (of nearly 60°), whereas for the same solid-liquid combination, tangent and circular fitting methods could not fit the drop's shape accurately, thereby giving inconsistent and inaccurate static CA's.

The above was in accordance with the literature data, where for the static CA's in the range of 10-100°, L-Y, Elliptical and sometimes tangent fitting methods are the best to work with- the circular fitting method whereas not at all being suited for this category. Further for drop volumes having lower and higher contact angle values than 10-100°, none of the fitting methods were found to be accurate in successfully fitting the drop's profile. However, Y-L method on the other hand can be generally used for all drop volumes, in the volumetric range

of 1-5µL making contact angles from 0-180°, as in the current study, as can be seen in the table D.1 below:

	Circle Fitting	Elliptical Fitting	Tangent Fitting	Y-L Fitting
Measuring methods				
0-20°	✓			
10-100°		✓	✓	✓
100-180°			✓	✓
Drop's weight				
Low	✓	✓	✓	✓
High		✓	✓	✓
Very High			✓	✓
Deposition				
Static	✓	✓	✓	✓
Dynamic		✓	✓	
Contour shape				
Symmetrical	✓	✓	✓	✓
Slightly symmetrical		✓	✓	
Very asymmetrical			✓	

Table D.1: Suitable static CA fitting method(s) denoted by tick mark as per the type of measurement made[194]

Experimental investigations as well revealed that for chemically non-structured surfaces as the PFS coated glass slides, for DI water as the dispensing liquid, pipetted in the volumetric range of 0.5-14µL's, Y-L fitting came out to be the most accurate fitting method. However, for low drop volumes (0.5-3µL's), nearly all the above fitting methods could be applied. Also, as the drop's volume increases, gravitational effects dominate which were found to be best compensated via the elliptical fitting method than the circular or tangent fitting methods. In this case, especially the circular fitting method ignores the gravitational effects flattening the droplet, assuming the droplet to be spherically or circularly symmetrical thereby giving inaccurate and inconsistent static CA values. Similar observations as above were made when sealing solution was taken as the test liquid on such surfaces. Further, analysis revealed, in analogy with the literature data (table D.1), that for drops having greater symmetry, all fitting methods were reliable, whereas for drops having slightly symmetrical profiles, circular fitting method was the most dependable one.

Hence, it can be concluded that on chemically structured surfaces as for the ones used in the current work, for low liquid volumes as 1µL of DI water (or dummy PCR mix) dispensed as the inner drop, and 5µL of sealing solution dispensed as the outer drop, making static CA's in the

range of ~10-160°, the best fitting method that can be adopted is the Y-L fitting method for fitting the nearly symmetrical contour shapes.

Appendix E

Calculation of the amount of air/gases dissolved in the dealt with liquids

Solubility of air in water

At standard (room) conditions of temperature and pressure, amount of gas that can be dissolved in 1µL of water can be estimated according to the following Henry´s[273,274] relation:

$$C = \frac{\rho_g}{K_H} \quad \text{(E.1)}$$

where, C= solubility of the dissolved gas, K_H= proportionality constant (dependent on the nature of the gas and the solvent) and P_g = partial pressure of the gas.

Considering oxygen and nitrogen to be the main constituents of air and that the solubility of oxygen is higher than the solubility of nitrogen[308], from equation E.1 the following relations can be further deduced:

$$k_{H,pc} = p/c \quad \text{(E.2)}$$

$$k_{H,cp} = c/p \quad \text{(E.3)}$$

where 'c' is the amount concentration of gas in solution (mol/L), and 'p' is the partial pressure of gas above the solution (in atmospheres).

From the data, that at RT (25°C), Henry´s law constants ($k_{H,pc}$) for O_2 = 756.7 atm. Liter/ mol and for N_2 = 1600 atm. Liter/ mol , molar weight of O_2= 31.9988 g/mol and for N_2 = 28.0134 g/mol, and partial fraction of O_2 ~ 0.21 and N_2 ~0.79, the amount of oxygen dissolved in water at room temperature was calculated as below :

$$C_o = \frac{(1\ \text{atm}) * 0.21 * 31.9988\ \text{g/mol}}{(756.7\ \text{atm.Liter})/\text{mol}}$$

$$= 0.0089\ \text{g/liter} \qquad \text{(E.4)}$$

On similar lines, the amount of N_2 dissolved in water at RT was calculated to be:

$$C_N = \frac{(1\ \text{atm}) * 0.79 * 28.0134\ \text{g/mol}}{(1600\ \text{atm.Liter})/\text{mol}}$$

$$=0.0138\ \text{g/liter} \qquad \text{(E.5)}$$

Thus, $C_{air} = C_O + C_N$ = (0.0089+0.0138) g/liter =0.0227 g/liter ~$2.27 * 10^{-8}$ g/µL at 25˚C. Taking density of air at sea level (~20°C) to be 1.2 Kg/m^3, at RT, in 1µL of water,

C_{air}= 0.0189 µL in 1µL of water [311] (E.6)

Solubility of air in sealing solution

For estimating solubility of air in sealing solution at RT, it was considered sealing solution to mainly comprise of mineral (90%) and silicon oil (10%).

Further, literature reports solubility of air in mineral oil (20˚C, 1 bar) = 90mL/L, and solubility of air in silicon oil = ~200mL/L .[310]

For 5µL volume of sealing solution, implying 4.5µL ($= \frac{90}{100} * 5$) of mineral oil and 0.5µL ($= \frac{10}{100} * 5$) of silicone oil, the total amount of air dissolved in it can be calculated= $4.5 * 90 * 10^{-3} + 0.5 * 200 * 10^{-3}$ =0.5 µL. Thus at RT:

C_{air}= 0.5 µL in 5µL of sealing solution (E.7)

Thus, mathematical calculations revealed that the amount of gases dissolved in the concerned liquids (1µL of water and 5µL of sealing solution) are too low in volume to generate at 95°C repeated bubbles as big as 1600 microns in diameter (i.e. max. of ~2µL in volume at a time, assuming the bubbles to be spherical in shape)- such bubbles encountered especially in the presence of artificial nucleation sites within the system.

Appendix F

Surface energy: Measuring methods

Various methods have been reported for the measurement of surface free energy (SFE), as detailed in the tables F.1 and F.2 below:

Models	Interaction components of surface energy
Fowkes	Disperse part and non-disperse part
Owens-Wendt-Rabel &Kaelble (O.W.R.K)	Disperse and polar part
Wu	Disperse and polar part
Schultz	Disperse and polar part, measurement in bulk liquid phase
Oss, Good (acid-base)	Lewis acid part and hydrogen bond part
Extended Fowkes	Disperse and polar part and hydrogen bond part
Zisman	No division into components; determination of critical surface tension
Neumann Equation of State	No division into components

Table F.1: Models for calculating the surface free energy (SFE)[194,197]

Method	Information	Min. No of fluids	Application	Examples
Zisman	Critical surface tension	2	Non-polar solids	PE, PTFE waxes
Fowkes	Disperse part of surface energy	1	Non-polar systems	PE, PTFE waxes
WORK (Owens-Wendt-Rabel and Kaelble)	Disperse and polar parts of surface free energy	2	universal	Polymers, aluminium coatings, varnishes, …
Extended Fowkes	Disperse, polar and hydrogen parts of surface free energy	3	Specific questions of surface properties	Plasma or corona treated polymers

Wu (Harmonic Mean)	Disperse and polar parts of surface free energy	2, at least one polar fluid	Low energetic systems	Organic solutions, polymers, organic pigments
Acid-Base theory	Disperse, acid and base parts of surface free energy	3	Specific questions of surface properties	Biological system
Equation of state theory	Surface free energy	1	universal	Polymers, aluminium coatings, varnishes, …
Schutz I (Polar Drop phase)	Disperse and polar parts of surface free energy	2	High energy systems	Metal, glass
Schutz 2 (Polar Bulk Phase)	Disperse and polar parts of surface free energy	2	High energy systems	Polymers, aluminium coatings, varnishes, …

Table F.2: Application examples for different surface free energy analysis methods[194,197]

Appendix G

Lithographic structuring of the surfaces: Nucleation studies III

For the fabrication of artificial nucleation sites via wet etching (nucleation studies III), the lithographic masks (having 4 rows of pits, with each row having pits of diameters 6,12,20 and 30 microns respectively with their depths varying between 5-30 microns) were ordered from the University of Twente, The Netherlands. The to be etched surfaces (after being chemically coated) were initially cleaned using Plasma cleaning in the clean room, analogous to the initial pre-baking step, where the surfaces were heated for about 10 minutes at high temperatures of around 95°C. This was done in an attempt to desorb water (remove thin monolayer of water molecules which otherwise is present everywhere on the glass surface), in order to facilitate binding of the resist to the corresponding surfaces (as at higher temperatures the OH-bonds on glass or SiO_2 decompose increasing the resist adhesion).

Post pre-baking, the surfaces were resist coated as soon as they reached room temperatures, to avoid re-adsorption of water. This was done by straightway spin coating (at a speed of 2800 rpm for 30 seconds) of the surfaces- positive resist being used for this purpose. Next, to hard bake the resist, for better resist adhesion, the surfaces were post-baked in the oven at 95°C (higher temperatures than this avoided as that could make the removal of the resist after etching difficult or almost impossible due to cross linking of the resin)- the surfaces baked for approximately 1 hour. After this, the surfaces were cooled (to room temperatures) and handled carefully as to avoid formation of any surface cracks.

Next, the lithographic machine was turned on and the lithographic mask aligned and exposed to UV light for approximately 4 seconds. The to be etched surfaces (glass slides/silicon wafers) were then placed (two at a time) and oriented as per their crystallographic axis (as for silicon wafers) below the mask. As the surfaces are coated with a positive resist, light enters through the mask via the etched structures (pits of various diameters) and removes the resist on the substrate from the exposed parts. The surfaces were next developed by dipping them in the developer solution for approximately 50 minutes, followed by a good rinse, washing under clean water and immediately drying in a machine drier (to ensure no remnant water stains).

Once done, the surfaces were tested under an upright microscope to check for the etched structures. Observations for the current case revealed that structures(pits) having greater diameters were visible (open), whereas no visibility was observed for the ones with smaller diameters. To ensure the visibility of all structures, an increase in the developing time of the surfaces post etching was attempted, where the surfaces were kept for another 30 minutes

in the developer solution. For such surfaces after being observed under the standard upright microscope, all the etched pits were visible (found open), thereby indicting the success of the lithographic etching procedure.

However, though lithography was fruitful in etching the surfaces laterally, the corresponding depths of the etched pits was achieved via HF etching- HF acid attacking only the regions uncovered by the photoresist (exposed by Lithography and then developer solution). By covering the back side of the surfaces with foil as to prevent them from getting attacked, the surfaces were kept in HF acid for about 7 minutes (rinsed gently in between), and then immediately washed nicely in a water bath and subsequently dried in a drier. In the end, the resist was removed from the surfaces via acetone or n-MP (n-Methyl Pyrodine) cleaning. The surfaces were then stored in the clean room for 2-4 days, prior to experimentations.

BIBLIOGRAPHY

[1] The Fundamentals of Bubble Evolution, *S. D. Lubetkin*, CHEMICAL SOCIETY REVIEWS, (1995)

[2] Design for mixing using bubbles in branched microfluidic channels, *Piotr Garstecki, Michael A. Fischbach, and George M. Whitesides*, Applied Physics Letters (2005)

[3] Bubble –based droplet mixers microfluidic systems, *Z.G.Li, C.D Ohl, K.Ando,J.B.Zhang and A.Q.Liu*, IEEE (2011)

[4] Dynamics of drops and bubbles in micro geometries, *Jie Xu,* Ph.D. thesis, Columbia University (2010)

[5] Formation of Micronuclei responsible for decompression sickness, *Vincent Stuart James Craig*, Journal of Colloid and Interface Science (1996)

[6] A Crevice Bubble Growth Model for the Analysis of Decompression Sickness, *Michael A. Chappell and Stephen J. Payne*, IEEE-EMBS (2005)

[7] Detection of gas emboli associated with decompression using the Doppler flowmeter, *Gillis M. F., Karagianes M. T., and Peterson P. O.,* J. Occup. Med. 11, 245 (1969)

[8] Ripples on a rising bubble through an immiscible two-liquid interface generate numerous micro-droplets, *T.Uemura, Y.Ueda and M.Iguchi*, IOP science (2010)

[9] The flow patterns in two immiscible stratified liquids induced by bubble plume, *Hassan Abdulmouti,* Fukui University, Japan, International Journal of fluid dynamics (2002)

[10] The control of bubble size in carbonated beverages, *G. S Barker, B. Jefferson and S.J. Judd*, Chemical engineering science (2002)

[11] Bubbles navigating through networks of microchannels, *Wonjae Choi, Michinao Hashimoto, Audrey K. Ellerbee,a Xin Chen, Kyle J. M. Bishop, Piotr Garstecki, Howard A. Stonec and George M. Whitesides,* Lab on a chip (2011)

[12] Control and effect of dissolved air in water during flow boiling in microchannels, *Mark E. Steinke, Satish G. Kandlikar*, International Journal of Heat and Mass Transfer (2003)

[13] Commercialization of microfluidic devices, *Lisa R. Volpatti, Ali K. Yetisen*, Trends in Biotechnology (2014)

[14] Microfluidic devices for biomedical applications, *Li, Xiujun (James), Zhou, Yu (editors),* Woodhead Publishing, ISBN 978-0-85709-697-5 (2013)

[15] Micro drops and digital microfluidics, *Jean Berthier*, ISBN 9781455725502 (2012)

[16] Introduction to Microfluidics*, P. Tabeling*, Oxford University Press. ISBN 0-19-856864-9 (2006)

[17] Droplets Formation and Merging in Two-Phase Flow Microfluidics, *Hao Gu , Michel H. G. Duits and Frieder Mugele*, International Journal of Molecular Sciences (2011)

[18] Simple 3D Printed Scaffold-Removal Method for the Fabrication of Intricate Microfluidic Devices, *Saggiomo, V., Velders, H. A.,* Advanced Science (2015)

[19] Methods in Molecular Biology - Microfluidic Diagnostics, *Gareth Jenkins & Colin D Mansfield (eds),* ISBN 978-1-62703-133-2(2012)

[20] Lab-on-a-chip: Techniques, Circuits, and Biomedical Applications, *Yehya H. Ghallab, Wael Badawy,* Artech House. p. 220. ISBN 978-1-59693-418-4 (2010)

[21] Lab-on-a-chip, *Paul Hauser*, The Berkley Science Review (2009)

[22] Polymerase Chain Reaction, *Garibyan L, Avashia N,* Journal of Investigative Dermatology (2013)

[23] The unusual origin of the polymerase chain reaction, *Kary Mullis,* Scientific American (1990)

[24] A short history of the polymerase chain reaction, *Bartlett, J. M. S., & Stirling D*, Methods in Molecular Biology (2003)

[25] PCR technology: principles and applications for DNA amplifications, *Erlich, H.A.,* Stockton Press, NY (1989)

[26] Making PCR: A Story of Biotechnology, *Rabinow, Paul,* University of Chicago Press ISBN 0-226-70146-8 (1996)

[27] DNA Amplification by the Polymerase Chain Reaction, *Gibbs, R.A*, Analytical Chemistry (1990)

[28] Polymerase Chain Reaction Strategy, *N. Arnheim, H. Erlich*, Annual Review of Biochemistry (1992)

[29] PCR Volume 1- A practical approach, *edited by M. J McPherson, P. Quirke and G.R. Taylor*, ISBN 0-190963196-4 (1991)

[30] Micro-systems in biomedical applications, *Paolo Dario, Maria Chiara Carrozza, Antonella Benvenuto and Arianna Menciassi,* J. Micromech. Microeng (2000)

[31] Microchip-based chemical and biochemical analysis systems, *Kiichi Sato, Akihide Hibara, Manabu Tokeshi, Hideaki Hisamoto, Takehiko Kitamoria,* Elsevier (Advanced drug delivery reviews) (2003)

[32] Micro-chemical system with continuous recovery and recirculation of catalyst-immobilized magnetic particles, *Chan Pil Park and Dong-Pyo Kim*, National Creative Research Center of Applied Microfluidic Chemistry, Chungnam National University, Korea (2010)

[33] Miniaturized PCR chips for nucleic acid amplification and analysis: latest advances and future trends, *Chunsun Zhang and Da Xing*, Nucleic acids research (2007)

[34] High-speed polymerase chain reaction in constant flow, *Nakano, H., Matsuda, K., Yohda, M., Nagamune, T., Endo, I. and Yamane, T*, Biosci.Biotechnol. Biochem (1994)

[35] Chemical amplification: continuous -flow PCR on a chip, *Kopp, M.U., de Mello, A.J. and Manz, A*., Science (1998)

[36] Droplet-based micro oscillating-flow PCR chip, *Wang, W., Li, Z.X., Luo, R., Lu¨, S.H., Xu, A.D. and Yang, Y.J.,* J. Micromech. Microeng. (2005)

[37] Integrated polymerase chain reaction chips utilizing digital microfluidics, *Chang, Y.H., Lee, G.B., Huang, F.C., Chen, Y.Y. and Lin, J.L*., Biomed. Microdevices (2006)

[38] Automated microdroplet platform for sample manipulation and polymerase chain reaction., *Chabert, M., Dorfman, K.D., de Cremoux, P., Roeraade, J. and Viovy, J.-L*., Anal. Chem. (2006), 78, 7722–7728.

[39] Performance characterization of a reconfigurable planar-array digital microfluidic system, *Griffith, E.J., Akella, S. and Goldberg, M.K.,* IEEE Trans. Comput. -Aided Des. Integr. Circuits Syst. 25, pp 340–352 (2006)

[40] Droplet-based micro oscillating-flow PCR chip, *Wang, W., Li, Z.X., Luo, R., Lu¨, S.H., Xu, A.D. and Yang, Y.J., J.* Micromech. Microeng. (2005), 15, 1369–1377.

[41] Microfluidic digital PCR enables multigene analysis of individual environmental bacteria, *Ottesen, E.A., Hong, J.W., Quake, S.R. and Leadbetter, J.R.,* Science (2006), 314, 1464–1467.

[42] Transcription factor profiling in individual hematopoietic progenitors by digital RT-PCR., *Warren, L., Bryder, D., Weissman, I.L. and Quake, S.R.,* Proc. Natl Acad. Sci. USA, 103, pages 17807–17812 (2006)

[43] Automated microdroplet platform for sample manipulation and polymerase chain reaction., *Chabert, M., Dorfman, K.D., de Cremoux, P., Roeraade, J. and Viovy, J.-L.,* Anal. Chem. 78, pages 7722–7728 (2006)

[44] Contamination-free continuous flow microfluidic polymerase chain reaction for quantitative and clinical applications, *Dorfman, K.D., Chabert, M., Codarbox, J.H., Rousseau, G., de Cremoux, P. and Viovy, J.L.,* Anal. Chem. 77, pages 3700–3704 (2005)

[45] Clinical evaluation of microscale chip-based PCR system for rapid detection of hepatitis B virus, *Cho, Y.K., Kim, J., Lee, Y., Kim, Y.A., Namkoong, K., Lim, H., Oh, K.W., Kim, S., Han, J. et al.,* Biosens. Bioelectron 21, pages 2161–2169 (2006)

[46] A fully integrated microfluidic genetic analysis system with sample-in–answer-out capability, *Easley, C.J., Karlinsey, J.M., Bienvenue, J.M., Legendre, L.A., Roper, M.G., Feldman, S.H., Hughes, M.A., Hewlett, E.L., Merkel, T.J. et al.,* Proc. Natl Acad. Sci. USA, 103, pages 19272–19277 (2006)

[47] A disposable microfluidic cassette for DNA amplification and detection, Wang, J., Chen, Z.Y., Corstjens, P.L.A.M., Mauk, M.G. and Bau, H.H, Lab Chip (2006), 6, 46–53.

[48] A microchipbased PCR device using flexible printed circuit technology, *Shen, K.Y, Chen, X.F., Guo, M. and Cheng, J.,* Sens. Actuators B Chem 105, pages 251–258 (2005)

[49] Microchamber array based DNA quantification and specific sequence detection from a single copy via PCR in nanoliter volumes, *Matsubara, Y., Kerman, K., Kobayashi, M., Yamanura, S., Morita, Y. and Tamiya, E,* Biosens. Bioelectron 20, pages 1482–1490 (2005)

[50] Micromachined polymerase chain reaction system for multiple DNA amplification of upper respiratory tract infectious diseases, *Liao, C.S., Lee, G.B., Wu, J.J., Chang, C.C., Hsieh, T.M., Huang, F.C. and Luo, C.H.,* Biosens. Bioelectron 20, pages 1341–1348 (2005)

[51] Nanoliter high throughput quantitative PCR, *Morrison, T., Hurley, J., Garcia, J., Yoder, K., Katz, A., Roberts, D., Cho, J., Kanigan, T., Ilyin, S.E. et al.,* Nucleic Acids Res. 34, e123 (2006)

[52] Real time PCR on disposable PDMS chip with a miniaturized thermal cycler, *Xiang, Q., Xu, B., Fu, R. and Li, D.,* Biomed. Microdevices 7, pages 273–279 (2005)

[53] A novel miniaturized PCR multi-reactor array fabricated using flip-chip bonding techniques, *Zou, Z.Q., Chen, X., Jin, Q.H., Yang, M.S. and Zhao, J.L.,* J. Micromech. Microeng. 15, pages 1476–1481 (2005)

[54] Microchamber array based DNA quantification and specific sequence detection from a single copy via PCR in nanoliter volumes, *Matsubara, Y., Kerman, K., Kobayashi, M., Yamanura, S., Morita, Y. and Tamiya, E,* Biosens. Bioelectron 20, pages 1482–1490 (2005)

[55] On-chip pressure injection for integration of infrared-mediated DNA amplification with electrophoretic separation, *Easley, C.J., Karlinsey, J.M., and Landers, J.P*, Lab Chip 6, 601–610 (2006)

[56] Planar chip device for PCR and hybridization with surface acoustic wave pump, *Zeno Guttenberg et al.,* Lab on a chip (2005)

[57] www.beckmancoulter.com

[58] Modular sub-microliter Lab-on-a-chip in forensic sciences, *Daniela Rita Woide,* Ph.D. thesis, LMU Munich *(*2010)

[59] Laser capture microdissection in forensic research: a review, *Mado Vandewoestyne and Dieter Deforce (corresponding author),* International Journal of legal medicine (2010)

[60] Preliminary trials of low volume AmpFlSTR® Profiler Plus® amplification using AmpliGrid (AG480F) slides, Runa Daniel, Adam Poy, Natalie Pederson, Roland A.H. van Oorschot, FORENSIC SCIENCE INTERNATIONAL GENETICS SUPPLEMENT SERIES 2 (2009)

[61] PCR microfluidic devices for DNA amplification, *Chunsun Zhanga, Jinliang Xua, Wenli Mac, Wenling Zhengd,* Biotechnology Advances (2006)

[62] A miniaturized silicon based device for nucleic acids electrochemical detection, *Salvatore Petraliaa, Maria Eloisa Castagnaa, Emanuele Cappellob, Fausto Puntorieroc, Emanuela Trovatoc, Antonio Gaglianod, Sabrina Conocia,* Sensing and Bio-sensing research (2015)

[63] Image data analysis in qPCR: A method for smart analysis of DNA amplification, *Massimo Orazio Spata, Maria Eloisa Castagna, Sabrina Conoci,* Bio-sensing research (2015)

[64] Electrochemical real-time DNA amplification and detection on a microchip, *T. T. Huang, J. S. Wang, Y. H. Tang, C. M. Chang*, Nano/Micro Engineered and Molecular Systems (NEMS), IEEE 10th International Conference on (2015)

[65] Lab on a chip technology: Biomolecular separation and analysis, Volume 2, *K. E. Herold, Avraham Rasooly*, pages 250-251, ISBN: 978-1-904455-47-9 (2009)

[66] Development of a Real-Time Microchip PCR System for Portable Plant Disease Diagnosis, *Chiwan Koo, Martha Malapi-Wight, Hyun Soo Kim, Osman S. Cifci, Vanessa L. Vaughn-Diaz, Bo Ma, Sungman Kim, Haron Abdel-Raziq, Kevin Ong, Young-Ki Jo, Dennis C. Gross, Won-Bo Shim, and Arum Han*, PLoS ONE 8(12): e82704. doi: 10.1371/journal.pone.0082704 (2013)

[67] An immunofluorescence-assisted microfluidic single sell quantitative reverse transcription Polymerase Chain Reaction Aanalysis of tumour cells separated from blood, *Kazunori Hoshino, HaeWon Chung, Chun-Hsien Wu, Kaarthik Rajendran, Yu-Yen Huang, Peng Chen, Konstantin V. Sokolov, Jonghwan Kim and John X.J. Zhang*, Journal of Circulating Biomarkers, ISSN 1849-4544 (2015)

[68] Micromachined polymerase chain reaction system for multiple DNA amplification of upper respiratory tract infectious diseases, *Liao CS, Lee GB, Wu JJ, Chang CC, Hsieh TM, Huang FC, et al.,* Biosens Bioelectron 20:1341–8 (2005)

[69] Advances in on-chip photodetection for applications in miniaturized genetic analysis systems, *Namasivayam V, Lin R, Johnson B, Brahmasandra S, Razzachi Z, Burke DT, et al.,* J. Micromech Microeng 14, pages 81–90 (2004)

[70] Integrated portable genetic analysis microsys- tem for pathogen/infectious disease detection, *Lagally ET, Scherer JR, Blazej RG, Toriello NM, Diep BA, Ram- chandani M, et al.,* Analytical Chemistry 76(11) (2004)

[71] Generation of Dynamic Free-Form Temperature Gradients in a Disposable Microchip, *Byung Hang Ha, Jinsoo Park, Ghulam Destgeer, Jin Ho Jung, and Hyung Jin Sung*, Analytical Chemistry, (2015)

[72] Microfluidic Chip for Single Cell Analysis of Tumor Cells Interaction with Anti-Cancer Drug Doxorubicin by AFM and Raman Microspectroscopy, *Han Zhang, Lifu Xiao, Anhong Zhou, Utah State University,* Sensors and Biosensors, Advancing Biology-Inspired Engineering, Annual Meeting (2015)

[73] Polymer microfluidic devices: an overview of fabrication Methods, *Raquel O. Rodrigues, Rui Lima, Helder T. Gomes, Adrián M. T. Silva, U.Porto ,* Journal of Engineering, ISSN 2183-6493 (2015)

[74] Polydimethylsiloxane (PDMS)-based spiral channel PCR chip, *Jia, X.Y., Niu, Z.Q., Chen, W.Y., and Zhang, W.P.,* Electron. Lett., 41, 890–891 (2005)

[75] A disposable microfluidic cassette for DNA amplification and detection, *Wang, J., Chen, Z.Y., Corstjens, P.L.A.M., Mauk, M.G. and Bau, H.H.* Lab Chip, 6, pages 46–53 (2006)

[76] Electrokinetically Synchronized Polymerase Chain Reaction Microchip Fabricated in Polycarbonate, *Chen, Jifeng; Wabuyele, Musundi; Chen, Hengwu; Patterson, Don; Hupert, Mateusz; Shadpour, Hamed; Soper, Steven A.,* Analytical Chemistry, 77(2): page 658 -666, (2005).

[77] Sacrificial polymers for nanofluidic channels in biological applications, *Wanli Li, Jonas O Tegenfeldt, Lei Chen, Robert H Austin, Stephen Y Chou, Paul A Kohl, Jeff Krotine and James C Sturm,* Nanotechnology 14, page 578–583 (2003)

[78] UV-nanoimprint lithography as a tool to develop flexible microfluidic devices for electrochemical detection, *Juhong Chen, Yiliang Zhou, Danhui Wang, Fei He, Vincent M. Rotello, Kenneth R. Carter, James J. Watkins and Sam R. Nugen,* Lab Chip (2015)

[79] A disposable laser print-cut-laminate polyester microchip for multiplexed PCR via infra-red-mediated thermal control, *Ouyang Y, Duarte GR, Poe BL, Riehl PS, dos Santos FM, Martin-Didonet CC, Carrilho E, Landers JP*, Anal Chim Acta. (2015)

[80] Analysis of multiplex PCR fragments with PMMA microchip, *Dayu Liua, Xiaomian Zhou, Runtao Zhong, Nannan Yea, Guohui Chang, Wei Xiong, Xiaodan Mei, Bingcheng Lina*, Talanta (Elsevier) (2006)

[81] A circular ferrofluid driven microchip for rapid polymerase chain reaction, *Y. Sun, Y. C. Kwoka and N. T. Nguyen*, Lab on a chip (2007)

[82] Lab-on-chips for Cellomics: Micro and Nanotechnologies for Life Science, *edited by Helene Andersson and Albert van den Berg*, (page 35-36), ISBN: 978-1-4020-6562-0 (2004)

[83] BioMEMS, *edited by Gerald Urban*, page 183, ISBN: 0-387-28731-0 (2006)

[84] Dynamic Solid Phase DNA Extraction and PCR Amplification in Polyester-Toner Based Microchip, *Gabriela R. M. Duarte, Carol W. Price, Brian H. Augustine, Emanuel Carrilho, and James P. Landers*, Analytical Chemistry (2011)

[85] Nanochromatogrophy and Nanocapillary Electrophoresis: Pharmaceutical and Environmental Analyses, *Imran Ali, HassanY. Aboul-Enein, Vinod K. Gupta*, page 37, ISBN: 978-0-470-17851-5 (2009)

[86] Performance of SU-8 Microchips as Separation Devices and Comparison with Glass Microchips, *Tiina Sikanen, Liisa Heikkilä, Santeri Tuomikoski, Tapio Kotiaho*, Analytical Chemistry 79(16) (2007)

[87] SU-8 based microdevices to study self-induced chemotaxis in 3D microenvironments, Jose *Maria Ayuso, Rosa Monge, Guillermo A. Llamazares, Marco Moreno, Maria Agirregabiria, Javier Berganzo, Manuel Doblaré, Iñaki Ochoa, and Luis J. Fernández,* Frontiers in Materials (2015)

[88] Simulation and experimental validation of a SU-8 based PCR thermocycler chip with integrated heaters and temperature sensor, *J. El-Alia, I.R. Perch-Nielsena, C.R. Poulsena, D.D. Bangb, P. Tellemana, A. Wolff*, Sensors and Actuators A: Physical, Volume 110, Issues 1–3 (2004)

[89] Surface Modification of Droplet Polymeric Microfluidic Devices for the Stable and Continuous Generation of Aqueous Droplets, *Balamurugan Subramanian, Namwon Kim, Wonbae Lee, David A Spivak, Dimitris E Nikitopoulos, Robin L. McCarley,* Research Gate (2011)

[90] Advances in Microfluidic Materials, Functions, Integration, and Applications, *Pamela N. Nge, Chad I. Rogers, and Adam T. Woolley*, Chem. Rev., 2013

[91] Advances in microfluidics for environmental analysis, *Jana C. Jokerst, Jason M. Emory and Charles S. Henry*, Analyst (2012)

[92] PCR Microchip Array Based on Polymer Bonding Technique, *Xiaomei Yu, Ting Li, Lin Hao and Dacheng Zhang*, The American society of chemical engineers (2005)

[93] A plastic microchip for nucleic acid purification, *Yuxin Liu, Nathaniel C Cady, Carl A Batt,* Biomedical Microdevices 9(5) (2007)

[94] A microchip-based PCR device using flexible printed circuit technology, *Keyue Shen, Xiaofang Chen, Min Guo, Jing Cheng,* Sensors and Actuators B 105 (2005)

[95] The low temperature co-fired ceramics (LTCC) chip for polymerase chain reaction (PCR) application, *Paweł Bembnowicz, Piotr Herbut, Małgorzata Małodobra, Anna Karpiewska, Leszek J. Golonka, Anna Jonkisz, Tadeusz Dobosz,* Optica Applicata, Vol. XLI, No. 2, 2011

[96] Dynamic passivation with BSA overcomes LTCC mediated inhibition of PCR, *Jason Besecker Kenneth A. Cornell Greg Hampikian,* Sensors and Actuators B (2012)

[97] A Novel Control System for Polymerase Chain Reaction Using a RIKEN GS384 Thermalcycler, *Nobuya Sasaki, Masakii Zawa, Masahito Shimojo, Kazuhiro Shibata, Jun-Ichi Akiyama, Masayoshi Itoh, Sumiharu Nagaoka, Piero Carninci, Yasushi Okazak,* DNA Research 4 (1997)

[98] Increased amplification efficiency of microchip-based PCR by dynamic surface passivation, *Xing Jian Lou, Nicholas J. Panaro, Peter Wilding, Paolo Fortina, and Larry J. Kricka,* BioTechniques 36, pages 248-252 (2004)

[99] Real-time PCR microfluidic devices with concurrent electrochemical detection, *Teh Huey Fanga, Naveen Ramalingama, Dong Xian-Duib, Tan Swee Nginc, Zeng Xiantingd, Annie Tan Lai Kuand, Eric Yap Peng Huate, Gong Hai-Qing,* Biosensors and Bioelectronics 24 (2009) 2131–2136

[100] DNA-based bioanalytical microsystems for handheld device applications, *Thomas Ming Hung Lee, I-Ming Hsing,* Analytica chimica acta (Impact Factor: 4.51), 556(1):26-37, (2006)

[101] Recent Progress of On-line Combination of Preconcentration Device with Microchip Electrophoresis, *Kenji Sueyoshi*, Chromatography, Vol.33 No.1 (2012)

[102] DNA amplification on a PDMS–glass hybrid microchip, *Zhi Qiang Niu, Wen Yuan Chen, Shi Yi Shao, Xiao Yu Jia and Wei Ping Zhang,* Journal of Micromechanics and Microengineering (2006)

[103] Integration of gene amplification and capillary gel electrophoresis on a polydimethylsiloxane-glass hybrid microchip, *Hong JW1, Fujii T, Seki M, Yamamoto T, Endo I., Electrophoresis* 22(2), pages 328-333 (2001)

[104] Inhibition of on-chip PCR using PDMS–glass hybrid microfluidic chips, *H. John Crabtree, Jana Lauzon, Yuen C. Morrissey, Brian J. Taylor, Tina Liang, Robert W. Johnstone, Alexander J. Stickel, Dammika P. Manage, Alexey Atrazhev, Christopher J. Backhouse, Linda M. Pilarski,* Microfluidics and Nanofluidics, Volume 13, Issue 3, pp 383-398 (2012)

[105] Polymerase chain reaction of 2-kb cyanobacterial gene and human anti-a1-chymotrypsin gene from genomic DNA on In-Check single-use microfabricated silicon chip, *Consolandi, C., Severgnini, M., Frosini, A., Caramenti, G., De Fazio, M., Ferrara, F., Zocco, A., Fischetti, A., Palmieri, M. et al.,* Anal. Biochem., 353, 191–197 (2006)

[106] Detection of a putative virulence cadF gene of campylobacter jejuni obtained from different sources using a microfabricated PCR chip, Poulsen, *C.R., El-Ali, J., Perch-Nielsen, I.R., Bang, D.D., Telleman, P. and Wolff, A*., J. Rapid Meth. Aut. Mic., 13, pages 111–126 (2005)

[107] Generation of Dynamic Free-Form Temperature Gradients in a Disposable Microchip, *Byung Hang Ha, Jinsoo Park, Ghulam Destgeer, Jin Ho Jung, and Hyung Jin Sung,* Anal. Chem., 87 (22), pp 11568–11574 (2015)

[108] A simple, valveless microfluidic sample preparation device for extraction and amplification of DNA from nanoliter-volume samples, *Legendre, L.A., Bienvenue, J.M., Roper, M.G., Ferrance, J.P. and Landers*, J.P., Anal. Chem., 78, 1444–1451 (2006)

[109] Chemical nanoprinting: a novel method for fabricating DNA microchips, *Anil Kumar and Zicai Liang,* Nucleic Acids Res. 29(2): e2 (2001)

[110] Microfluidic Techniques: Reviews and Protocols, *Shelley D. Minteer(editor*), pages 137-138, eISBN: 1-59259-997-4, ISSN: 1064-3745 (2006)

[111] Electrochemistry-Based Real-Time PCR on a Microchip, *Stephen S. W. Yeung, Thomas M. H. Lee, and I-Ming Hsing*, Anal. Chem. 80 (2), pp 363–368 (2008)

[112] Lab-on-a-Chip Technology (Vol. 1): Fabrication and Microfluidics, *Keith E. Herold and Avraham Rasooly* (editors), ISBN: 978-1-904455-46-2 (2009)

[113] Microfluidic PCR Chip Integrated with MCU controlled temperature system, *Dawoon Han, Mijung Choi, You-Cheol Jang, Kamrul Islam, Rohit Chand, Sandeep K. Jha, Sung Sik Ko, Ik-Jun Yeon, Yong-Sang Kim*, World Journal of Engineering (2010)

[114] Isolation of thermally sensitive aptamers on a microchip, *J. P. Hilton, Jinho Kim, ThaiHuu Nguyen, Mihaela Barbu, Renjun Pei, Milan Stojanovic, and Qiao Lin,* IEEE (2012)

[115] Microfluidics Meets MEMS, *Elisabeth Verpoorte and Nico F. De Rooij*, IEEE (2003)

[116] Electrokinetically Integrated Isolation and Amplification of Protein-Binding Nucleic Acids on a Microchip, *Jinho Kim, John P. Hilton, Kyung-Ae Yang, Renjun Pei, Milan Stojanovic, and Qiao Lin,* 16th International Conference on Miniaturized Systems for Chemistry and Life Sciences, Japan, October 28 - November 1 (2012)

[117] Lab on a Chip Technology: Biomolecular separation and analysis, Volume 2, *K. E. Herold, Avraham Rasooly (editors),* pages 255-256, ISBN: 978-1-904455-47-9 (2009)

[118] Effect of materials for micro-electro-mechanical systems on PCR yield, *Potrich C, Lunelli L, Forti S, Vozzi D, Pasquardini L, Vanzetti L, Panciatichi C, Anderle M, Pederzolli C.,* Eur Biophys J. 39(6), pp 979-986. doi: 10.1007/s00249-009-0466-5 (2010)

[119] Lab on a Chip Technology: Biomolecular separation and analysis, Volume 2, *K. E. Herold, Avraham Rasooly (editors),* pages 252-253, ISBN: 978-1-904455-47-9(2009)

[120] Microchip Module for Blood Sample Preparation and Nucleic Acid Amplification Reactions*, Po Ki Yuen, Larry J. Kricka, Paolo Fortina, Nicholas J. Panaro, Taku Sakazume, and Peter Wilding,* Genome Res. 11(3): pp 405–412 (2001)

[121] Microsystem Technology in Chemistry and Life Sciences, *Andreas Manz, Holger Becker(editors)*, pp 224-226, ISBN: 3-540-63424-X, ISSN: 0340-1022 (1998)

[122] Rapid Microbiological Methods in the Pharmaceutical Industry, *Martin C. Easter (editor),* pages 161-162, ISBN: 1-57491-141-4 (2005)

[123] Microreaction Technology: IMRET 5: Proceedings of the Fifth International conference on microrecation technology, *M. Matlosz, W. Ehrfeld, J.P. Baselt (editors),* ISBN: 978-3-642-62706-4 (2001)

[124] Integrated polymerase chain reaction chips utilizing digital microfluidics, *Chang, Y.H., Lee, G.B., Huang, F.C., Chen, Y.Y. and Lin, J.L.*, Biomed. Microdevices, 8, 215–225 (2006)

[125] Ultra-fast miniaturized real-time PCR: 40 cycles in less than six minutes, *Neuzil, P., Zhang, C.Y., Pipper, J., Oh, S. and Zhuo, L.*, Nucleic Acids Res., 34, e77 (2006)

[126] Lab-on-Chips for Cellomics: Micro and Nanotechnologies for Life Science, Albert *Berg, Helene Andersson,* pp 31, ISBN: 978-1-4020-6562-0 (PB), ISBN: 978-1-4020-2975-2 (e-book) (2004)

[127] Electrokinetic Phenomena: Principles and Applications in Analytical chemistry and Microchip technology, *Anurag Rathore, Andras Guttman (editors)*, pp 456-457, ISBN: 0-203-91298-5 (2004)

[128] Lab on a Chip Technology: Biomolecular separation and analysis, Volume 2, *K. E. Herold, Avraham Rasooly (editors),* pages 262-263, ISBN: 978-1-904455-47-9(2009)

[129] A Review of Heating and Temperature Control in Microfluidic Systems: Techniques and Applications, *Vincent Miralles Axel Huerre, Florent Malloggi, and Marie-Caroline Jullien,* Diagnostics 3, pp 33-67 (2013)

[130] Microfluidics: Technologies and Applications, *Bingcheng Lin*, pp 218-219, ISBN: 978-3-642-23049-3 (2011)

[131] Lab-on-Chips for Cellomics: Micro and Nanotechnologies for Life Science, *Albert Berg, Helene Andersson*, pp 30, ISBN: 978-1-4020-6562-0 (PB), ISBN: 978-1-4020-2975-2 (e-book) (2004)

[132] Integrated Microfabricated Biodevices: Advanced Technologies for Genomics, Drug discovery, Bioanalysis, and Clinical Diagnostics, *Michael J. Heller, Andras Guttman (editors*), pp 25-26, ISBN: 0-8247-0606-4 (2002)

[133] Microfluidic Lab-on-a-Chip for Chemical and Biological Analysis and Discovery, *Paul C.H. Li*, pp 295-296, ISBN-13: 978-1-4200-2745-7 (eBook-PDF) (2005)

[134] Miniaturized devices for DNA amplification and fluorescence based detection, *Sudip Mondal AND V. Venkataraman*, Journal of the Indian Institute of Science VOL 87:3 (2007)

[135] Circulating polymerase chain reaction chips utilizing multiple-membrane activation, *Chih-Hao Wang, Yi-Yu Chen, Chia-Sheng Liao, Tsung-Min Hsieh, Ching-Hsing Luo, Jiunn-Jong Wu, Huei-Huang Lee and Gwo-Bin Lee,* Journal of Micromechanics and Microengineering, Volume 17, Number 2 (2007)

[136] An inexpensive and portable microchip-based platform for integrated RT–PCR and capillary electrophoresis, *Govind V. Kaigala, Viet N. Hoang, Alex Stickel, Jana Lauzon, Dammika Manage, Linda M. Pilarski and Christopher J. Backhouse,* Analyst 133, pp 331-338 (2008)

[137] An independent, temperature-controllable microelectrode array, *Yang, H.; Choi, C. A.; Chung, K. H.; Jun, C. H.; Kim, Y. T,* Anal. Chem 76, 1537-1543 (2004)

[138] Micro-assembled, multi- chamber thermal cycler for low-cost reaction chip thermal multiplexing, *Q. Zou, Y. Miao, Y. Chen, U. Sridhar, C.S. Chong, T. Chai, Y. Tie, C.H.L. Teh, T.M. Lim, and C.K. Heng*., Sens. Actuators A, 102, pp 114–121 (2002)

[139] Microfabricated structures for integrated DNA analysis, *Burns, M. A.; Mastrangelo, C. H.; Sammarco, T. S.; Man, F. P.; Webster, J. R.; Johnson, B. N.; Foerster, B.; Jones, D.; Fields, Y.; Kaiser, A. R.; Burke, D. T.,* PNAS 93, pp 5556-5561 (1996)

[140] Micro-assembled multi-chamber thermal cycler for low-cost reaction chip thermal multiplexing, *Zou, Q. B.; Miao, Y. B.; Chen, Y.; Sridhar, U.; Chong, C. S.; Chai, T. C.; Tie, Y.; Teh, C. H. L.; Lim, T. M.; Heng, C.,* Sensor Actuat. a-Phys. 102, pp 114-121 (2002)

[141] Miniaturized, independently controllable multichamber thermal cycler, *Zou, Q. B.; Sridhar, U.; Chen, Y.; Singh, J.,* IEEE Sens. J. 3, pp 774-780 (2003)

[142] Practical integration of polymerase chain reaction amplification and electrophoretic analysis in microfluidic devices for genetic analysis, *Rodriguez, I.; Lesaicherre, M.; Tie, Y.; Zou, Q. B.; Yu, C.; Singh, J.; Meng, L. T.; Uppili, S.; Li, S. F. Y.; Gopalakrishnakone, P.; Selvanayagam, Z. E.,* Electrophoresis, 24, pp 172-178 (2003)

[143] A nanoliter rotary device for polymerase chain reaction, *J. Liu, M. Enzelberger, and S. Quake*, Electrophoresis, 23, pp 1531–1536 (2002)

[144] Disposable real-time microPCR device: lab-on-a-chip at a low cost, *P. Neuzil, J. Pipper, and T.M. Hsieh, Mol.* Biosyst., 2, 292–298 (2006)

[145] Functional integration of PCR amplification and capillary electrophoresis in a microfabricated DNA analysis device, *A.T. Woolley, D. Hadley, P. Landre, A.J. deMellow, R.A. Mathies, and M.A. Northrup*. Anal. Chem., 68, pp 4081–4086 (1996)

[146] Integrating polymerase chain reaction, valving, and electrophoresis in a plastic device for bacterial detection*, Koh, C. G.; Tan, W.; Zhao, M. Q.; Ricco, A. J.; Fan, Z. H.,* Anal. Chem. 75, pp 6379- 6379 (2003)

[147] Thermal management of BioMEMS: Temperature control for ceramic-based PCR and DNA detection devices, *Sadler, D. J.; Changrani, R.; Roberts, P.; Chou, C. F.; Zenhausern, F.,* IEEE T. Compon. Pack. T. 26, pp 309- 316 (2003)

[148] A miniaturized cyclic PCR device - modeling and experiments. Microelectron, *Chou, C. F.; Changrani, R.; Roberts, P.; Sadler, D.; Burdon, J.; Zenhausern, F.; Lin, S.; Mulholland, A.; Swami, N.; Terbrueggen, R.,* Eng. 61-2, pp 921-925 (2002)

[149] Chip elements for fast thermocycling, *Poser, S.; Schulz, T., Dillner, U.; Baier, V., Kohler, J. M., Schimkat, D., Mayer, G.; Siebert, A.,* Sensor Actuat. a-Phys. 62, pp 672-675 (1997)

[150] Miniaturized, independently controllable multi-chamber thermal cycler, *Zou, Q. B.; Sridhar, U.; Chen, Y.; Singh, J.,* IEEE Sens. J. 3, pp 774-780 (2003)

[151] A battery-powered notebook thermal cycler for rapid multiplex real time PCR analysis, *Belgrader, P., Young, S.; Yuan, B., Primeau, M., Christel, L. A., Pourahmadi, F., Northrup, M. A.,* Anal. Chem., 73, pp 286-289 (2001)

[152] A heater-integrated transparent microchannel chip for continuous-flow PCR, *Sens. K. Sun, A. Yamaguchi, Y. Ishida, S. Matsuo, and H. Misawa*. Actuators B, 84, pp 283–289 (2002)

[153] A heater integrated transparent microchannel chip for continuous-flow PCR, *Sun, K.; Yamaguchi, A.; Ishida, Y.; Matsuo, S.; Misawa, H.,* Sens. Actuator B-Chem. 84, pp 283-289 (2002)

[154] Microfabricated flow through device for DNA amplification - towards in situ gene analysis, *Fukuba, T., Yamamoto, T., Naganuma, T., Fujii, T.,* Chem. Eng. J. 101, pp 151-156 (2004)

[155] Capillary tube resistive thermal cycling, *Friedman, N. A., Meldrum, D. R.,* Anal. Chem. 70, pp 2997-3002 (1998)

[156] Integrated Modular Microfluidic System for Forensic ALU DNA Typing, *Samuel K. Njoroge,* Ph.D. thesis, pp 21-22 (2011)

[157] A miniature integrated device for automated multistep genetic assays*, Anderson, R. C.; Su, X.; Bogdan, G. J.; Fenton, J.,* Nucleic Acids Res. 28 (2000)

[158] Microchamber array based DNA quantification and specific sequence detection from a single copy via PCR in nanoliter volumes, *Matsubara, Y.; Kerman, K., Kobayashi, M., Yamamura, S., Morita, Y., Tamiya, E.,* Biosens. Bioelectron 20, pp 1482-1490 (2005)

[159] Chemical amplification: Continuous flow PCR on a chip, *Kopp, M. U.; de Mello, A. J.; Manz, A.,* Science 280, pp 1046-1048 (1998)

[160] Renewable microcolumns for automated DNA purification and flow-through amplification: from sediment samples through polymerase chain reaction, *Bruckner-Lea, C. J., Tsukuda, T., Dockendorff, B., Follansbee, J. C., Kingsley, M. T., Ocampo, C., Stults, J. R., Chandler, D. P.,* Anal. Chim. Acta 469, pp 129-140 (2002)

[161] Microfabricated device for DNA and RNA amplification by continuous-flow polymerase chain reaction and reverse transcription-polymerase chain reaction with cycle number selection, *Obeid, P. J., Christopoulos, T. K., Crabtree, H. J., Backhouse, C. J.,* Anal. Chem. 75, pp 288-295 (2003)

[162] Development of Plastic Microfluidic Devices for Sample Preparation, *Grodzinski, P., Liu, R. H., Chen, B., Blackwell, J., Liu, Y., Rhine, D., Smekal, T., Ganser, D., Romero, C., Yu, H., Chan, T., Kroutchinina, N.,* Biomed. Microdevices, 3, pp 275-283 (2001)

[163] Development of a CMOS-compatible PCR chip: comparison of design and system strategies, *Erill, I., Campoy, S., Rus, J., Fonseca, L., Ivorra, A., Navarro, Z., Plaza, J. A., Aguilo, J., Barbe, J.,* J. Micromech. Microeng 14, pp 1558-1568 (2004)

[164] Transient liquid crystal thermometry of microfabricated PCR vessel arrays, *Chaudhari, A. M.; Woudenberg, T. M.; Albin, M.; Goodson, K. E.,* J. Microelectromech. Syst. 7, pp 345-355 (1998)

[165] Automated polymerase chain reaction in capillary tubes with hot air, *C.T. Wittwer, G.C. Fillmore, and D.R. Hillyard,* Nucleic Acids Res.17, pp 4353–4357 (1989)

[166] Minimizing the time required for DNA amplification by efficient heat transfer to small samples, C.T. *Wittwer, G.C. Fillmore, and D.J. Garling.* Anal. Biochem. 186, pp 328–331 (1990)

[167] A novel real-time PCR machine with a miniature spectrometer for fluorescence sensing in a micro liter volume glass capillary, *D.S. Lee, M.H.Wu, U. Ramesh, C.W. Lin, T.M. Lee, and P.H. Chen*. Sens. Actuators B 100, pp 401–410 (2004)

[168] Integrated portable genetic analysis microsystem for pathogen/infectious disease detection, *Lagally, E. T.; Scherer, J. R.; Blazej, R. G.; Toriello, N. M.; Diep, B. A.; Ramchandani, M.; Sensabaugh, G. F.; Riley, L. W.; Mathies, R. A.,* Anal. Chem. 76, pp 3162-3170 (2004)

[169] Bulk-micromachined submicroliter-volume PCR chip with very rapid thermal response and low power consumption, *Lee, D. S.; Park, S. H.; Yang, H. S.; Chung, K. H.; Yoon, T. H.; Kim, S. J.; Kim, K.; Kim, Y. T.,* Lab Chip 4, pp 401-407 (2004)

[170] Infrared-mediated thermocycling for ultrafast polymerase chain reaction amplification of DNA, *R.P. Oda, M.A. Strausbauch, A.F.R. H¨uhmer, N. Borson, S.R. Jurrens, J. Craighead, P.J. Wettstein, B. Eckloff, B. Kline, and J.P. Landers,* Anal. Chem. 70, pp 4361–4368 (1998)

[171] Noncontact infraredmediated thermocycling for effective polymerase chain reaction amplification of DNA in nanoliter volumes, *A.F.R. H¨uhmer and J.P. Landers,* Anal. Chem. 72, pp 5507–5512 (2000)

[172] Polymerase chain reaction in polymeric microchips: DNA amplification in less than 240 seconds, *B.C. Giordano, J. Ferrance, S. Swedberg, A.F.R. Huehmer, and J.P. Landers*., Anal. Biochem. 291, pp 124–132 (2001)

[173] Non-contact photothermal control of enzyme reactions on a microchip by using a compact diode laser, *Y. Tanaka, M.N. Slyadnev, A. Hibara, M. Tokeshi, and T. Kitamori*., J. Chromatogr. A, 894, pp 45–51, (2000)

[174] Photothermal temperature control of a chemical reaction on a microchip using an infrared diode laser, *M.N. Slyadnev, Y. Tanaka, M. Tokeshi, and T. Kitamori.* Anal. Chem. 73, pp 4037–4044, (2001)

[175] Rapid amplification for the detection of Mycobacterium tuberculosis using a non-contact heating method in a silicon microreactor based thermal cycler, *Ke, C., Berney, H., Mathewson, A., Sheehan, M. M.,* Sens. Actuator BChem. 102, pp 308-314 (2004)

[176] A portable battery-operated chip thermocycler based on induction heating, *D. Pal and V. Venkataraman,* Sens. Actuators A, 102, 151–156, (2002)

[177] Microwave-assisted high-speed PCR, Fermér, *C., Nilsson, P., Larhed, M.,* Eur. J. Pharm. Sci. 18, pp 129-132 (2003)

[178] An efficient method to perform milliliter-scale PCR utilizing highly controlled microwave thermocycling, Orrling, *K.; Nilsson, P., Gullberg, M., Larhed, M.,* Chem. Commun., pp 790-791 (2004)

[179] PCR performance of the highly thermostable proof-reading Btype DNA polymerase from Pyrococcus abyssi., *Dietrich, J., Schmitt, P., Zieger, M., Preve, B., Rolland, J.-L., Chaabihi, H., Gueguen, Y.,* FEMS Microbiol. Lett. 217, pp 89-94 (2002)

[180] PCR in a Rayleigh-Bénard Convection Cell, *Krishnan, M., Ugaz, V. M., Burns, M. A.,* Science 298, pp 793 (2002)

[181] Fast temperature changes on for polymerase chain reaction on a lab-on-a-chip, *L.M.J. Nijsten,* BSc Report, University of Twente (2013)

[182] Electrokinetically controlled real-time polymerase chain reaction in microchannel using Joule heating effect, *Hu GQ, Xiang Q, Fu R, Xu B, Venditti R, Li DQ*. Anal. Chim. Acta. 557, pp146–151 (2006)

[183] Mechanical properties of materials*, Kaye and Laby Tables of Physical and Chemical Constants*, National Physical Laboratory (2008)

[184] An Introduction to Microscopy, *Suzanne Bell, Keith Morris*, ISBN 9781420084504 - CAT# 8450X (2009)

[185] Abramowitz M, Davidson MW (2007). "Introduction to Microscopy". Molecular Expressions. Retrieved 2007-08-22

[186] Fundamentals of Light Microscopy and Electronic Imaging, Douglas.B. Murphy, ISBN: 0-471-25391-X (2001)

[187] Atomic Force Microscopy: Understanding Basic Modes and Advanced Applications, Greg Haugstad, ISBN: 978-0-470-63882-8, (2012)

[188] Atomic Force Microscopy 1st Edition, Peter Eaton, Paul West, ISBN-13: 978-0199570454, ISBN-10: 0199570450 (2010)

[189] Scanning Electron Microscopy and X-ray Microanalysis, Third Edition, *Autoren: Goldstein, J., Newbury, D.E., Joy, D.C., Lyman, C.E., Echlin, P., Lifshin, E., Sawyer, L., Michael, J.R.,* ISBN 978-1-4615-0215-9 (2003)

[190] Scanning Electron Microscopy, Physics of Image Formation and Microanalysis, *Professor Dr. Ludwig Reimer,* ISBN: 978-3-642-08372-3 (1998)

[191] Filler TJ, Peuker ET (April 2000). "Reflection contrast microscopy (RCM): a forgotten technique?". The Journal of Pathology 190 (5): 635–8. doi:10.1002/(SICI)1096-9896(200004)190:5<635: AID-PATH571>3.0.CO;2-E. PMID 10727991.

[192] Interference Reflectance Microscopy, *Valarie A. Barr and Stephen C. Bunnell,* Curr Protoc Cell Biol. 2009 Dec; CHAPTER: Unit–4.23., doi: 10.1002/0471143030.cb0423s45 (2010)

[193] Micro drops and digital Micro fluids, Processing, development, and applications, *Jean Berthier*, ISBN: 978-0-8155-1544-9 (2008)

[194] http://www.kruss.de

[195] Surface Wetting, Characterization, Contact Angle, and Fundamentals, *Law, Kock-Yee, Zhao, Hong*, ISBN 978-3-319-25214-8 (2016)

[196] Surface chemistry of solid and liquid interfaces, *Professor H. Yıldırım Erbil,* ISBN-10: 1-4051-1968-3, ISBN-13: 978-1-4051-1968-9 (2006)

[197] http://www.dataphysics.de

[198] Surface Tension Measurements Using the Drop Shape Method, *Woodward, Roger P*., First Ten Angstroms (n.d.): 1-6. Web.

[199] The phenomenon of contact angle hysteresis, http://www.thass.org

[200] Surface and Interfacial Aspects of Biomedical Polymers (Vol. 1), *J. D. Andrade (editor)* Ch. 7, Pp. 249-292, Plenium Press, NY, (1985)

[201] US Geological Survey (July 2015). "Surface Tension (Water Properties) – USGS Water Science School". US Geological Survey. Retrieved November 6, 2015.

[202] MIT Lecture Notes on Surface Tension, lecture 5 (PDF), *Bush, John W. M.,* Massachusetts Institute of Technology, Retrieved (2007)

[203] Introduction to Microfluidics, *Patrick Tabeling*, ISBN-13: 978–0–19–856864–3 (2005)

[204] http://www.interactiveflows.com

[205] Fundamentals of multiphase flow (Reprint. ed.), *Brennen, Christopher E.,* Cambridge [u.a.]: Cambridge Univ. Press, ISBN 9780521848046 (2005)

[206] Springer Handbook of Experimental Fluid Mechanics, *Cameron Tropea, Alexander Yarin, John Foss (ed.),* ISBN 978-3-540-25141-5 (2007)

[207] Micro- and Nanoscale Fluid Mechanics: Transport in Microfluidic Devices, *Kirby, B.J.,* Cambridge University Press. ISBN 978-0-521-11903-0 (2010)

[208] Introduction to Fluid Mechanics, *Batchelor, G. K.,* ISBN: 0-521-66396-2 (2000)

[209] Superheating and Homogeneous Single Bubble Nucleation in a Solid-State Nanopore, *Gaku Nagashima, Edlyn V. Levine, David P. Hoogerheide, Michael M. Burns, and Jene A. Golovchenko*, Physica Review Letters 113 (2014)

[210] Bubble nucleation mechanisms of liquid droplets superheated in other liquids, *Thomas J Jarvis 1, Marc D Donohue 1, Joseph L Katz,* Volume 50, Issue 2, pp 359-368 (1975)

[211] Homogeneous bubble nucleation in liquids: The classical theory revisited, *Can F. Delale1, Jan Hruby and Frantisek Marsik*, The Journal of Chemical Physics, Vol. 118, Issue 2 (2003)

[212] A kinetic theory of homogeneous bubble nucleation, *Vincent K. Shen and Pablo G. Debenedettia*, Journal of Chemical Physics, Volume 118, Number 2 (2003)

[213] Measurement of the bubble nucleation temperature of water on a pulse-heated thin platinum film supported by a membrane using a low-noise bridge circuit, *Eric J. Ching, C. Thomas Avedisian, Michael J. Carrier, Richard C. Cavicchi, James R. Young, Bruce R. Land,* International Journal of Heat and Mass Transfer 79, pp 82–93 (2014)

[214] Active and potential bubble nucleation sites on different structured heated surfaces, *A. Luke,* Institution of Chemical Engineers Trans IChemE, Part A, Chemical Engineering Research and Design, 82(A4): pp 462–470 (2004)

[215] Cavitation and Bubble Dynamics, *Christopher Earls Brennen,* ISBN 0-19-509409-3 (1995)

[216] Nucleation and cavitation of spherical, cylindrical, and slab like droplets and bubbles in small systems, *Luis G. MacDowella, Vincent K. Shen, Jeffrey R. Errington,* The Journal of Chemical Physics 125, 034705 (2006)

[217] Microphysics of Clouds and Precipitation, *H. R. Pruppacher and J. D. Klett*, Journal of Atmospheric Chemistry, Volume 32, Issue 3, pp 420-422 (1999)

[218] Cavitation in Non-Newtonian Fluids- with biomedical and bioengineering applications, *E-A. Brujan,* 49, chapter 2-Nucleation, ISBN: 978-3-642-15343-3 (2011)

[219] Bubble nucleation from gas cavities - a review, *S.F. Jones, G.M. Evans, K.P. Galvin*, Advances in Colloid and Interface Science 80(1999) pp 27-50

[220] The fundamentals of bubble evolution, *S.D Lubetkin*, Chem. Soc. Rev.,24, pp 243-250, doi: 10.1039/CS9952400243 (1995)

[221] Surface nucleation in the freezing of gold nanoparticles, E.M-V. and R. Bowles, Eduardo Mendez-Villuendas and Richard K. Bowles, Phys. Rev. Lett. 98, 185503 – Published 3 May 2007; Erratum Phys. Rev. Lett. 99, 159901 (2007)

[222] Nucleation, Cavitation in Non-Newtonian Fluids, *E-A Brujan*, ISBN: 978-3-642-15342-3 (2011)

[223] The crevice model of bubble nucleation, *Anthony A. Atchley, Andrea Prosperetti,* J. Acoust. Sec. Am. 86 (3) (1989)

[224] Growth of bubbles in liquid, *Boris M. Smirnov and R. Stephen Berry,* Chemistry Central Journal 20159:48, doi: 10.1186/s13065-015-0127-y (2015)

[225] Bubble growth and departure trajectory under asymmetric temperature conditions, *Pruthvik A. Raghupathi, Satish G. Kandlikar*, International Journal of Heat and Mass Transfer, Volume 95, pp 824–832 (2016)

[226] Role of bubble growth dynamics on microscale heat transfer events in microchannel flow boiling process, *Sajjad Bigham and Saeed Moghaddam,* Appl. Phys. Lett. 107, 244103 (2015)

[227] On Bubble Growth Rates, *B. B. Mikic, W. M. Rohsenow, and P. Griffith*, Int.J. Heat Mass transfer, Vol 13, pp 657-666 (1969)

[228] Initiation and growth of confined vapor bubbles in micro-channels, *Wen, D.S. and Das, K.S. and Wilson, S.K. and Kenning*, 44rd European Two-Phase Flow Group Meeting, Lausanne, Switzerland (2006)

[229] Growth of a gas Bubble in a Supersaturated Liquid under the effect of variant cases of surface tension, *S. A. Mohammadein, K. G. Mohamed*, Canadian Journal of Physics 93, pp 769-775 (2015)

[230] Heterogeneous nucleation and growth of crystal bubbles in aqueous solutions and melts - thermodynamic conditions, *D. Aquilano, E. Costa, and M. Rubbo,* Cryst. Res. Technol. 40, No. 10–11, pp 1099 – 1106, / doi 10.1002/crat.200410494 (2005)

[231] The Systems Bible (3rd ed.), Gall, John, General Systemantics Press. The System always kicks back (2002)

[232] The Elements of Physical Chemistry (3rd ed.), *Atkins, P.W.,* Oxford University Press. ISBN: 978-0716723646 (1993)

[233] Bubble growth behavior in supersaturated liquid solutions, *David Robert Cyr*, Ph.D. Thesis (2001)

[234] An Introduction to Fluid Dynamics, *Batchelor, G.K.,* ISBN 0-521-66396-2 (1967)

[235] Lamb, H. (1994). Hydrodynamics (6th ed.). Cambridge University Press. ISBN 978-0-521-45868-9. Originally published in 1879, the 6th extended edition appeared first in 1932.

[236] Bubbles in a bottle of beer, Reflections on the rising, *Walker, J.,* 245, page 124 (1981)

[237] Why does champagne bubble? *Schlichting, Hans Joachim, Ucke, Christian,* Singapore: Physics & Technology Quest, Volume 2, No 1, pp 105 – 108 (1997)

[238] Heat Transfer 1994: Proceedings of the Tenth International Heat Transfer Conference *Brighton, UK, G. F. Hewitt (editor*), Volume 7, pp 479-483, (1994)

[239] https://www.thermalfluidscentral.org/encyclopedia/index.php/Bubble_Detachment

[240] Transport Phenomena in Multiphase Systems, *Amir Faghri and Yuwen Zhang*, ISBN: 978-0-12-370610-2 (2006)

[241] https://www.comsol.de/multiphysics/marangoni-effect

[242] Interfacial Phenomena and the Marangoni Effect, *M.G. Velarde, Zeytourian, K. Radyadour (Eds.),* ISBN: 978-3-7091-2550-2 (2002)

[243] http://www.physics.utoronto.ca/~nonlin/thermal.html

[244] Physics and Chemistry of Interfaces, *Hans-Jurgen Butt, Karlheinz Graf, Michael Kappl,* ISBN: 978-3-527-60640-5 (2006)

[245] http://chemistry.about.com/od/waterchemistry/f/What-Is-The-Density-Of-Water.htm

[246] Effects of interfacial forces on the evaporation of a superheated water droplet in hot immiscible oil, *F.C.H. Jongenelen, F. Groeneweg, and J. H. Gouda,* Chemical Engineering Science, Vol 33, pp 777-781, (1978)

[247] Principles of General Chemistry (1st Edition), *Martin Silberberg,* ISBN-13: 978-0073301716, ISBN-10: 007330171X, (2006)

[248] http://www.viscopedia.com/viscosity-tables/substances/water/

[249] Meteorology Today, *C. Donald Ahrens*, ISBN: 0-495-01162-2 (2007)

[250] The Science of Air: Concepts and Applications (Second Edition), *Frank R. Spellman*, pp 26-27, ISBN: 978-1-4200-7532-8 (2009)

[251] http://www.chromatography-online.org/topics/hydrophobic.php

[252] Stationary Phases in Gas Chromatography, *H. Rotzsche*, Journal of Chromatography Library-volume 48, pp 196-197, ISBN: 0-444-98733-9 (1991)

[253] Drops, Bubbles, Pearls, Waves, *P.-G. de Gennes, F. Brochard-Wyart and D. Qu´er´e*, Springer, New-York (2004)

[254] http://lnf-wiki.eecs.umich.edu/wiki/Lithography_processing

[255] http://lnf-wiki.eecs.umich.edu/wiki/Wet_etching

[256] Etch Rates for Micromachining Processing - Part II, *K.R. Williams, K. Gupta, M. Wasilik*, JMEMS vol. 12 No 6 (2003)

[257] Guide to References on III-V Semiconductor Chemical Etching, *A.R. Clawson*, Mat. Sci. Eng., vol. 31 (2001)

[258] http://lnf-wiki.eecs.umich.edu/wiki/Deep_reactive_ion_etching

[259] https://www.samcointl.com/etching/drie-systems/

[260] Deep reactive ion etching of Pyrex glass, *X. Li, T. Abe, M. Esashi*, Micro Electro Mechanical Systems, The Thirteenth Annual International Conference on, ISSN: 1084-6999 (2000)

[261] Handbook of Silicon Based MEMS Materials and Technologies (second edition), *edited by: M. Tilli, T.Motooka, V.M. Airaksinen, S.Franssila, M.P. Kroeckel, V.Lindroos*, pp 444-466, ISBN : 978-0-32329965-7 (2015)

[262] https://www.memsnet.org/mems/processes/etch.html

[263] Dynamics of an initially spherical bubble rising in quiescent liquid, *Manoj Kumar Tripathi, Kirti Chandra Sahu & Rama Govindarajan,* Nature Communications 6, Article number: 6268 (2015)

[264] The transient rise of a bubble subject to shape or volume changes, *B. Yang and A. Prosperetti, S. Takagi*, Physics of fludis, Vol.15, number 9 (2003)

[265] Oscillation of the shape of rising bubbles, Kamil Wichterle, Kateřina Smutná, Marek Večeř

[266] Experimental studies on the shape and path of small air bubbles rising in clean water, *Wu, M. and Gharib, M.,* Phys. Fluids 14, L49-L52 (2002)

[267] Bubbles, Drops and Particles, *R. Clift, J. R. Grace, and M. E. Weber*, Academic, New York, (1978)

[268] Shape Oscillations of Rising Bubbles, *Knud Lunde, Richard J. Perkins,* Applied Scientific Research, Volume 58, Issue 1, pp 387-408 (1997)

[269] Bubble and Drop Interfaces, *edited by: Miller, L. Liggieri,* page 298, ISBN: 978-90-04-17495-5 (2011)

[270] Physics Chemistry (second edition), *David W. Ball*, ISBN 13: 978-1-133-95843-7 (2015)

[271] Fullick, P. (1994), Physics, Heinemann, pp. 141–42, ISBN 0-435-57078-1

[272] Levine, Ira. N. (1978), p12 gives the original definition

[273] Experiments on the quantity of gases absorbed by water, at different temperatures, and under different pressures" *Henry, W.,* Phil. Trans. R. Soc. Lond. 93: 29–274. doi:10.1098/rstl.1803.0004 (1803)

[274] Compilation of Henry's law constants (version 4.0) for water as solvent, *R. Sander,* Atmos. Chem. Phys., 15, pp 4399–4981 (2015)

[275] Advances in Contact Angle, Wettability and Adhesion, Volume Two, *edited by K. L. Mittal*, Print ISBN: 9781118472927 (2015)

[276] Superhydrophobic Carbon Nanotube Forests, Kenneth K. S. Lau, Jose´ Bico, Kenneth B. K. Teo, Manish Chhowalla, Gehan A. J. Amaratunga, William I. Milne, Gareth H. McKinley, and Karen K. Gleason, NANO LETTERS, Vol. 3, No. 12, pp 1701-1705 (2003)

[277] Fluorinated Hydrocarbons—Advances in Research and Application: 2013 Edition, *Q. Ashton Acton*, page 305, ISBN: 978-1-481-67570-3 (2013)

[278] The mechanical properties of the rubber elastic polymer polydimethylsiloxane for sensor applications, *J.C. Loetters, W. Olthuis, P.H. Veltink and P. Bergveld*, J. Micromech. Microeng. 7 pp 145–147 (1997)

[279] Contact Angle Measurements Using the Drop Shape Method, *Roger P. Woodward,* Ph.D., First Ten Angstroms, 465 Dinwiddie Street, Portsmouth, VA 23704

[280] http://www.biocompare.com/PCR-Real-Time-PCR/22353-Real-Time-PCR-Thermal-Cyclers-Thermocyclers/

[281] Contact angle hysteresis: a review of fundamentals and applications, *H. B. Eral, D. J. C. M., 't Mannetje, J. M. Oh*, Colloid Polym Sci. (2012)

[282] Fabrication of high-aspect-ratio silicon nanopillar arrays with the conventional reactive ion etching technique, *Y.-F. Chang, Q.-R. Chou, J.-Y. Lin, C.-H. Lee*, Applied Physics A, Volume 86, Issue 2, pp 193-196 (2007)

[283] Fabrication of Periodic Silicon Nanopillars in a Two-Dimensional Hexagonal Array with Enhanced Control on Structural Dimension and Period, *Jea-Young Choi, T. L. Alford, and Christiana B. Honsberg*, Langmuir, 31 (13), pp 4018–4023 (2015)

[284] Deep reactive ion etching as a tool for nanostructure fabrication, *Y. Q. Fu, A. Colli, A. Fasoli, J. K. Luo, A. J. Flewitt, A. C. Ferrari, and W. I. Milne*, J. Vac. Sci. Technol. B 27(3) (2009)

[285] Fabrication of nanopillars by nanosphere lithography, *Cheung, C. L.; Nikolic, R. J.; Reinhardt, C. E.; Wang, T. F.,* Nanotechnology, Volume 17, Issue 5, pp. 1339-1343 (2006)

[286] Polymers in conventional and alternative lithography for the fabrication of nanostructures, *Canet Acikgoz, Mark A. Hempenius, Jurriaan Huskens, G. Julius Vancso,* European Polymer Journal Volume 47, Issue 11, Pages 2033–2052 (2011)

[287] Thermophoresis of DNA determined by microfluidic fluorescence, *S. Duhr, S. Arduini, and D. Braun*, Eur. Phys. J. E 15, 277–286 (2004)

[288] Temperature Measurement in Microfluidic Systems Using a Temperature-Dependent Fluorescent Dye, *David Ross, Michael Gaitan, and Laurie E. Locascio*, Anal. Chem., 73 (17), pp 4117–4123 (2001)

[289] Advances in Flow Analysis, *Marek Trojanowicz,* page 97, ISBN: 978-3-527-31830-8 (2008)

[290] Characterization and Optimization of Temperature-Sensitive Microbeads for Simultaneous Thermometry and Velocimetry for Fluid Dynamic Applications, *Trey Cottingham*, Master Thesis, Dept. of Science in Aeronautics & Astronautics, University of Washington (2015)

[291] Development and characterization of pressure-sensitive microbeads for simultaneous barometry and velocimetry for fluid dynamic applications, *Daniel J Lacroix*, Master's thesis, University of Washington, 2014.

[292] Characterization of multi-dye pressure-sensitive microbeads, *Daniel Lacroix, Teddy Viraye-Chevalier, Guillaume Seiter, Jonathan Howard, Dana Dabiri, Gamal E. Khalil, Younan Xia, and Cun Zhu*, Review of Scientific Instruments, 84 (2013)

[293] Electrospun Superhydrophobic Self-Cleaning Materials, *Yong Zhao, Nü Wang*, Chapter Electrospun Nanofibers for Energy and Environmental Applications (ISBN: 978-3-642-54159-9), Part of the series Nanostructure Science and Technology pp 449-472, (2014)

[294] Literature review on superhydrophobic self-cleaning surfaces produced by electrospinning, *Iurii Sas, Russell E. Gorga, Jeff A. Joines, Kristin A. Thoney*, Journal of Polymer Science, part B, Polymer Physics, Volume 50, Issue 12, pp 824–845 (2012)

[295] Recent Advances in the Methods for Designing Superhydrophobic Surfaces (chapter 11), *Harinarayanan Puliyalil, Gregor Filipič and Uroš Cvelbar*, Surface Energy, *Edited by Mahmood Aliofkhazraei*, ISBN 978-953-51-2216-6, (2015)

[296] Fabrication of superhydrophobic copper by wet chemical reaction, *Zhiguang Guo, Jian Fang, Libo Wang, Weimin Liu*, Thin Solid Films, Volume 515, Issue 18, pp 7190–7194 (2007)

[297] Recent Progress in Preparation of Superhydrophobic Surfaces: A Review, *Sanjay Subhash Latthe, Annaso Basavraj Gurav, Chavan Shridhar Maruti, Rajiv Shrikant Vhatkar,* Journal of Surface Engineered Materials and Advanced Technology, 2, 76-94 (2012)

[298] Super-hydrophobic surfaces of layer-by-layer structured film-coated electrospun nanofibrous membranes, *Tasuku Ogawa, Bin Ding, Yuji Sone and Seimei Shiratori*, Nanotechnology, Volume 18, Number 16 (2007)

[299] Superhydrophobic Thin Films Fabricated by Reactive Layer-by-Layer Assembly of Azlactone-Functionalized Polymers, *Maren E. Buck, Sarina C. Schwartz, and David M. Lynn*, Chem Mater. 22(23), pp 6319–6327 (2010)

[300] Viscosity of liquids: Theory, Estimation, Experiment, and Data, *Dabir. S.Viswanath, Tushar.K.Gosh, Dasikah.L.Prasad, Nidamarty V.K.Dutt, Kalipatnapu Y.Rani,* ISBN (13) : 978-1-4020-5482-2 (2007)

[301] Handbook of refinery desulfurization*, Nour Shafik El-Gendy, James G. Speight*, ISBN (13): 978-1-4665-9672-6 (2016)

[302] Handbook of Industrial Hydrocarbon Processes, *James Speight*, ISBN: 978-0-7506-8632-7 (2011)

[303] Handbook of hydraulic fluid technology, *George E. Totten (editor),* ISBN: 0-8247-6022-0 (2000)

[304] http://www.anton-paar.com/corp-en/products/group/viscometer/

[305] http://www.viscopedia.com/viscosity-tables/substances/water/

[306] Gas chromatographic identification of major constituents of bubbles in glass, *F.R. Bryan, J.C. Neerman,* Anal. Chem., 34 (2), pp 278–280 (1962)

[307] Handbook of Experimental Fluid Mechanics, *C. Tropea, A.L. Yarin, J.F. Foss (Eds.),* pp 981-982, ISBN: 978-3-540-25141-5 (2007)

[308] http://www.engineeringtoolbox.com/air-solubility-water-d_639.html

[309] http://www.troteclaser.com/en-US/Pages/Laser_systems.aspx

[310] A User's Guide to Vacuum Technology, Third Edition, *Joh.F. O'Hanlon*, ISBN: 978-0-471-27052-2 (2003)

[311] Gas Dissolution, Release, and Bubble Formation in Flotation Systems, *Lawrence K. Wang, Nazih K. Shammas, William A. Selke, and Donald B. Aulenbach,* Handbook of Environmental Engineering, Volume 12: Flotation Technology, ISBN-13: 978-1588294944 (2010)

ABBREVIATIONS & SYMBOLS

AG	Chemically structured (Ampli-Grid) surfaces
PFS	Chemically non-structured, hydrophobic (Per-Fluoro Silane coated) surfaces
ASC	Ampli-Speed-Cycler
CA	Contact Angle
S. T	Surface Tension
Y-L	Young-Laplace
DI	De-ionized
DIM	Di-iodo methane
δ	Dynamic contact angle hysteresis
θ	Static contact angle
θ_a	Advancing contact angle
θ_r	Receding contact angle
γ	Surface tension
γ_{lv}	Interfacial surface tension (liquid- vapor)
γ_s	Interfacial surface tension (solid-liquid)
γ_{sv}	Interfacial surface tension (solid-vapor)
k	Kinematic viscosity
ρ	Density
υ	Viscosity
R_e	Reynolds number
B_o	Bond number
l	Capillary length
E_O	Eötvös number

LIST OF IMAGES

LIST OF FIGURES

LIST OF GRAPHS

LIST OF TABLES